



**HAL**  
open science

# Orchestration of epithelial cell elimination by effector caspases

Alexis Villars

► **To cite this version:**

Alexis Villars. Orchestration of epithelial cell elimination by effector caspases. Cellular Biology. Sorbonne Université, 2022. English. NNT : 2022SORUS567 . tel-04115881

**HAL Id: tel-04115881**

**<https://theses.hal.science/tel-04115881>**

Submitted on 2 Jun 2023

**HAL** is a multi-disciplinary open access archive for the deposit and dissemination of scientific research documents, whether they are published or not. The documents may come from teaching and research institutions in France or abroad, or from public or private research centers.

L'archive ouverte pluridisciplinaire **HAL**, est destinée au dépôt et à la diffusion de documents scientifiques de niveau recherche, publiés ou non, émanant des établissements d'enseignement et de recherche français ou étrangers, des laboratoires publics ou privés.

# Sorbonne Université

École doctorale complexité du vivant

*Institut Pasteur, Département Biologie du Développement et Cellules souches, Équipe*

*Mort cellulaire et Homéostasie des épithéliums*

## Orchestration of epithelial cell elimination by effector caspases

Par Alexis Villars

Thèse de doctorat de Biologie du développement

Dirigée par Romain Levayer

Présentée et soutenue publiquement le 12 septembre 2022

Devant un jury composé de :

Magali Suzanne	Directrice de Recherche	Rapportrice
Jakub Sedzinski	Directeur de Recherche	Rapporteur
Rashmi Priya	Directrice de Recherche	Examinatrice
Michel Labouesse	Professeur Sorbonne Université	Président
Romain Levayer	Directeur de Recherche	Directeur de thèse



# Abstract

Programmed Cell death and specifically apoptosis is essential during epithelial homeostasis. Yet, cells fragment during apoptosis. Thus, cell death is a challenge for epithelial integrity. To address this issue, apoptotic cells are eliminated from epithelia through cell extrusion: a sequence of remodelling events that contract the cell while bringing its neighbours together. In the single layered *Drosophila* pupal notum epithelium, caspase activation precedes and is necessary for cell extrusion. To this date, the mechanistic relationship between caspase activation and cell extrusion is still poorly understood. Additionally, for a long time, caspase activation was seen as a point of no-return leading to apoptosis. However, recent evidence shows non-apoptotic caspase functions and transient caspase activations. Therefore, what sets the threshold between cell survival and death is unclear. In the first part of this PhD, we have demonstrated that the initiation of cell extrusion and apical constriction are surprisingly not associated with the modulation of actomyosin concentration and dynamics. Instead, cell apical constriction is initiated by the disassembly of a medio-apical mesh of microtubules driven by effector caspases. The depletion of microtubules is sufficient to bypass the requirement of caspases for cell extrusion and microtubule stabilisation strongly impairs cell extrusion. This demonstrates that microtubules disassembly by caspases is a rate-limiting step of extrusion and outlines microtubules function in epithelial cell shape stabilisation. In the second part, we showed that there is no common threshold of effector caspase leading to extrusion and that caspases levels correlate linearly with the probability to engage in extrusion. We identified parameters predictive of cell sensitivity to caspase. This is the first quantitative analysis of the engagement process in extrusion or apoptosis in vivo and at the single cell level.



## Résumé

La mort cellulaire programmée, plus particulièrement l'apoptose, est essentielle à l'homéostasie de l'épithélium. Cependant, les cellules fragmentent pendant l'apoptose. Ainsi, la mort cellulaire est un défi pour l'intégrité épithéliale. Pour pallier ce problème, les cellules apoptotiques sont éliminées des épithéliums par extrusion cellulaire : une séquence d'événements de remodelage qui contractent la cellule tout en rapprochant ses voisines. Dans l'épithélium monocouche du notum de la puppe de la drosophile, l'activation des caspases précède et est nécessaire à l'extrusion cellulaire. Pourtant, la relation entre l'activation des caspases et l'extrusion cellulaire est encore mal comprise. De plus, l'activation des caspases a longtemps été considérée comme un point de non-retour menant à l'apoptose. Cependant, des preuves récentes montrent des fonctions non apoptotiques des caspases et une activation transitoire des caspases. Par conséquent, ce qui fixe le seuil entre la survie et la mort des cellules n'est pas clair. Dans la première partie de cette thèse, nous avons démontré que l'initiation de l'extrusion cellulaire et la constriction apicale ne sont étonnamment pas associées à la modulation de la concentration et de la dynamique de l'actomyosine. Au contraire, la constriction apicale des cellules est initiée par le désassemblage d'un maillage médio-apical de microtubules induit par des caspases effectrices. La déplétion des microtubules est suffisante pour contourner l'activation des caspases pour l'extrusion cellulaire et la stabilisation des microtubules empêche fortement l'extrusion cellulaire. Ceci démontre que le désassemblage des microtubules par les caspases est une étape limitante de l'extrusion et que les microtubules jouent un rôle prépondérant pour stabiliser la forme des cellules épithéliales. Dans la deuxième partie, nous avons montré qu'il n'y a pas de seuil commun de caspase effectrice menant à l'extrusion. Au contraire, les niveaux de caspases sont corrélés linéairement avec la probabilité de s'engager dans l'extrusion. Par ailleurs, nous avons identifié des paramètres prédictifs de la sensibilité des cellules aux caspases. Il s'agit de la première analyse quantitative du processus d'engagement dans l'extrusion ou l'apoptose in vivo et au niveau de la cellule unique.



# Remerciements

I would like to start by thanking the member of my thesis jury and my reviewer. Thank you for accepting kindly my invitation to review my work.

This PhD manuscript concludes 4 years of work that I have not conducted alone. It is, therefore, necessary to start by thanking everyone who has helped me achieve this. My first words go to the members of the *cdeh* lab. Tout d'abord, merci à toi Romain. Merci d'avoir cru en moi en m'offrant l'opportunité de rejoindre ton labo au début de mon stage de Master. Il est difficile d'exprimer en quelques mots ma reconnaissance. J'ai énormément appris pendant cette thèse au travers des multiples discussions avec toi. Tu as fait du laboratoire un environnement idéal d'un point de vue professionnel en poussant toujours pour le partage dans la science mais aussi sur le plan personnel. Je me dois aussi de remercier ceux qui ont eu à me supporter le plus longtemps dans le laboratoire : Léo et Florence. Florence, je n'oublierai jamais la quantité d'expressions françaises que j'ai appris grâce à toi. Je suis constamment impressionné par tes talents en biologie moléculaire. Merci de m'avoir aidé des dilutions jusqu'à l'établissement des mutants pour l'article. Léo je ne peux pas écrire de remerciements au labo sans souligner tes blagues... (toujours déconcertante dirons-nous). Merci également pour toutes les discussions sur les codes et tout le soutien pendant la thèse. Merci à vous Alexis et Rali pour le duo que vous formez derrière moi au bureau. Vos discussions constantes n'ont de cesse de me faire pouffer de rire. Alexis merci aussi pour ton aide avec le modèle dans l'article. Rali merci d'avoir soignée mon PhD belly avec les gaufrettes. Fabiana, merci d'avoir réussi à me supporter pendant 3 ans à ma droite. Merci pour les moments qu'on a partagé en regardant ensemble twitter sur mon ordi. Tom, I enjoyed collaborating with you. Thanks for constantly upgrading my English. I loved sharing about music and stand-ups with you. J'aimerais aussi remercier Anne, j'ai beaucoup apprécié encadrer ton stage et les données obtenues ont permis de lancer ce qui est devenu mon projet annexe.

More generally my acknowledgements need to go to all the members of the Department of Developmental and Stem Cells Biology at the Institut Pasteur. With its nice dynamics, it has largely contributed to creating a nice environment for me to work in. More specifically, I must acknowledge the best floor of the Monod Building: the 5<sup>th</sup> floor. All these colleagues I now consider friends. Thank you for always making my day worth enjoying. Thank you Loan and Miri for relentlessly offering beer hours. Thanks, Miri, for complaining with me about the administrative problems throughout the PhD. Merci



Loan d'avoir la patience de venir me demander tous les jours pour le café pour me sortir devant mon écran, ça m'aura offert une bouffée d'air continue. Merci David pour tous les échanges sur l'escalade et les mangas. I also need to thank the new ones: Névé and Arantxa you have made the last retreat excellent!

Sur un plan plus personnel, je me dois de remercier également toutes les personnes qui m'entourent pour le soutien qu'elles m'ont apportées pendant cette thèse. D'abord merci à Matthieu. Je n'aurais pas vraiment pensé qu'une thèse était possible pour moi quand on s'est rencontré. Merci à toi mon frère d'avoir constamment poussé le feignant qui est en moi. Merci aussi à toi Élodie pour le soutien sans faille que tu m'apportes depuis toutes ses années. Erwan, mon frère tu es toujours là depuis toutes ces années je ne sais pas comment te remercier. Merci entre autres de m'avoir offert une bouffée d'air en jouant avec moi en ligne pendant le covid.

Papa et maman merci d'avoir toujours poussé Mathis et moi à faire ce qui nous plais dans la vie. A vos manières vous êtes tous les deux des soutiens sans faille et bien évidemment je n'aurais pas été jusque-là sans vous. Mon petit frère Mathis merci pour ton franc parler tu me permets de garder les pieds sur terre ! Finalement je conclurais par remercier celle avec qui je partage ma vie depuis presque six ans. Justine, c'est impossible de mettre en quelque ligne tout ce que tu m'apportes depuis que je te connais. Tu m'auras permis de maintenir un équilibre sain pendant l'ensemble de cette thèse y compris pendant les confinements. Surtout, tu me fais rire sans relâche. Tu sais toujours trouver le moyen de me calmer et tu fais tous les jours de moi une meilleure personne. Je t'aime.

## **Table of contents**

<b>Abstract .....</b>	<b>3</b>
<b>Résumé .....</b>	<b>5</b>
<b>Remerciements.....</b>	<b>7</b>
<b>General introduction.....</b>	<b>11</b>
<b><u>Chapter I: MORPHOGENESIS .....</u></b>	<b>15</b>
<b>1. Introduction .....</b>	<b>19</b>
<b>2. Morphogenesis of an Epithelium.....</b>	<b>20</b>
2.1. What is an epithelium?.....	20
2.2. Some shape changes of epithelia .....	23
<b>3. Morphogenesis: a cell-centred view .....</b>	<b>31</b>
3.1. Cortical tension.....	32
3.2. Adhesion: the role of E-cadherin.....	48
3.3. Microtubules and mechanics .....	54
<b><u>Chapter II: HOW TO ELIMINATE A CELL? .....</u></b>	<b>67</b>
<b>1. Introduction: Cell deaths.....</b>	<b>70</b>
<b>2. Apoptosis.....</b>	<b>72</b>
2.1. Apoptosis during development .....	72
2.2. Caspases .....	76
2.3. Caspases targets and cellular demolition.....	85
<b>3. How to protect coherent tissue from cell death: cell extrusion .....</b>	<b>89</b>
3.1. What is cell extrusion? .....	89
3.2. What drives cell extrusion? .....	89
3.3. Remodelling events .....	94
3.4. The role of caspases .....	100
<b>4. Results: Paper: Microtubule disassembly by caspase is the rate-limiting step of cell extrusion     108</b>	
<b><u>Chapter III: DECISION-MAKING.....</u></b>	<b>128</b>
<b>1. Decision making &amp; apoptosis: non-apoptotic functions of caspases.....</b>	<b>132</b>
1.1. Survival to caspase activation during development: non-apoptotic function in physiological contexts 134	
1.2. Role in cancer .....	142

1.3.	Mechanism of caspase regulation for non-apoptotic functions .....	143
<b>2.</b>	<b><i>Results: Decision-making in cell extrusion</i></b> .....	<b>152</b>
	<b><u>Chapter IV: DETECTION OF EXTRUSION</u></b> .....	<b>162</b>
<b>1.</b>	<b><i>Introduction</i></b> .....	<b>166</b>
<b>2.</b>	<b><i>Machine Learning</i></b> .....	<b>167</b>
2.1.	The case of linear regression .....	168
2.2.	Logistic regression: classification problem .....	170
2.3.	Neural networks .....	173
2.4.	Sequential models. ....	176
<b>3.</b>	<b><i>Results: Dextrusion: Machine-Learning enhanced tool for epithelial event detection</i></b> .....	<b>177</b>
	<b><u>Chapter V: DISCUSSION &amp; PERSPECTIVES</u></b> .....	<b>188</b>
<b>1.</b>	<b><i>Remodelling during extrusion</i></b> .....	<b>192</b>
1.1.	Putative mechanisms for MT depletion by caspases .....	192
1.2.	Tensegrity .....	195
1.3.	Cell shape stabilisation .....	197
1.4.	Sensitivity to compression.....	200
1.5.	Cell insertion.....	204
<b>2.</b>	<b><i>Decision making</i></b> .....	<b>206</b>
2.1.	Parameters influencing the caspase threshold .....	207
2.2.	Microtubule depletion: a decision step?.....	210
<b>3.</b>	<b><i>Prediction of cell death</i></b> .....	<b>211</b>
3.1.	Can we harvest the model to find predictive features of extrusion?.....	211
3.2.	How to use the model for something else? .....	213
	<b><i>Table of Illustrations</i></b> .....	<b>214</b>
	<b><i>References</i></b> .....	<b>216</b>
	<b><i>Appendix-1: paper supplementary material</i></b> .....	<b>246</b>
	<b><i>Appendix-2: review</i></b> .....	<b>264</b>
	<b><i>Appendix-3: dispatch</i></b> .....	<b>272</b>

# General introduction

Epithelia are certainly the most represented tissue type in metazoans. They are made of cells that are tightly adherent to each other through which they act as a barrier. This allows them to protect the different organs they encase. The development of an embryo entails numerous deformations of epithelia. For instance, they can extend, retract, or fold. This process, called morphogenesis, gives rise to complex forms necessary to organ functions. Cell division, cell death, cell rearrangements, cell shape changes but also extracellular volume changes contribute to morphogenesis. Ultimately, cell shape changes mainly rely on the cell's cytoskeleton. The actomyosin cortex is located just below the plasma membrane and produces contractile forces. Actin is assembled in filaments arranged in a complex network which serves as a substrate for myosin motors. Myosin pulls on the Actin network which produces contractile forces. The number of produced forces can be tuned by the architecture of the network by crosslinkers or the turnover of different proteins which compose that network. These forces will tend to reduce the apical cell area and are resisted by adhesion or other cytoskeletal components. Accordingly, adhesion mediated by E-cadherins will tend to expand the contact area between cells. Moreover, E-cad adhesive forces are increased upon pulling by the cortex. They also actively help shaping the actomyosin network. Finally, Microtubules are also instrumental regulators of morphogenesis. First, they can interact with the actomyosin network to modulate contractility. Second, they can directly influence contractility by their ability to resist compressive forces or to actively exert pushing forces on the cortex. Overall, these elements self-organise to mediate apical cell shape changes to influence morphogenesis.

On the other hand, apoptosis is another potent regulator of morphogenesis. This mode of cell death leads to the irreversible destruction of vital cell functions. The cell condenses and fragments while keeping most of the intracellular components enclosed within membranes. This cell death process helps to sculpt epithelia by removing specific cells. Apoptosis can be permissive for tissue movement as it leads to tissue fluidization. It can also actively produce local deformation necessary for epithelial morphogenesis. Additionally, it buffers variations during development by removing damaged or less fit cells which help to regulate tissue size. Finally, the balance of apoptosis with cell division maintains a constant number of cells in adult tissue in a process called tissue homeostasis.

The molecular regulation of apoptosis relies on caspases. This family of proteases can cleave hundreds of substrates in epithelial cells to ensure their collapse. Interestingly they are expressed in all cells and are therefore tightly regulated to prevent spurious activation and non-desired cell death. Apoptotic stimuli induce the activation of pro-apoptotic proteins which antagonise inhibitors of caspase. This double negative regulation ensures fast activation of caspase upon pro-apoptotic stimuli. Initiator caspases then activate effector caspases which cleave all substrates needed. Caspase activation was long considered a point of no return leading to the irreversible engagement in apoptosis. Yet, it appears that multiple cells survive caspase activation during development. Moreover, caspases actively regulate different processes such as cell proliferation, cell differentiation or cell remodelling in a non-apoptotic manner. To mediate these functions, epithelial cells modulate intracellular levels, dynamics or location of both caspases and their inhibitor. This ensures that caspase activation is maintained at a sub-lethal level and in restricted subcellular region. Thus, it has led to the idea that the irreversible commitment of a cell into apoptosis depends on a caspase threshold. Below that threshold the cell survives but dies when caspase activity exceeds that limit.

Cell extrusion is at the crossroad between cell shape changes and apoptosis. It is a sequence of remodelling steps which allows to constrict a cell while bringing closer its neighbours. This process allows to eliminate a cell from an epithelium while maintaining tissue sealing. As such it can remove apoptotic cells but also less fit or pre-tumoral cells. It can also happen in response to overcrowding to remove numerous cells and maintain homeostasis. Hence, it is an instrumental process in the maintenance of epithelial integrity. The study of cell extrusion has mainly focused on actin and myosin because of their ability to induce cell shape changes. The cell fated to die becomes hypercontractile through the formation of an internal actomyosin ring. This pulls on neighbours through E-cadherin adhesion and leads to the reorganisation of the actomyosin network in the neighbours. These cells then form a supracellular actomyosin ring which allows to expel the cell out of the epithelium. Alternatively, actomyosin pulses can also induce apical constriction and cell extrusion. During the morphogenesis of the *Drosophila* pupal notum, a single layer epithelium, numerous cell extrusions happen stochastically within a reproducible pattern in the midline and in posterior regions. Previous results from the lab have demonstrated that caspase activation precedes and is necessary for cell extrusion in the notum. This demonstrates that caspase activation orchestrates cell extrusion in the notum.

My PhD started in this background. Caspases can cleave multiple substrates in epithelial cells. Yet, most of these substrates were not functionally analysed. There was no clear mechanistic link between caspase activation and cellular remodelling. Moreover, there was no clear characterisation of the extrusion process in the notum. What are the substrates that are cleaved by caspases which mediate the cell shape changes leading to extrusion? What are the key stages of extrusion influenced by caspase activity? Moreover, the idea of a caspase threshold can be found in several instances in the literature. Yet it is unclear what this caspase threshold is. What set the balance between cell survival and the irreversible commitment to extrusion and apoptosis? Is this threshold value unique across a given cell population? Finally, what are the parameters which modulate this threshold?

In this manuscript, I will introduce the concept of morphogenesis and how it emerges in part from apical cell shape changes and apoptosis. I will further detail the contribution of actin, myosin, E-cadherin and microtubule to the regulation of apical epithelial cell shape changes. I will emphasise how they self-organise with their regulators to induce deformation. Then I will focus on apoptosis during development. I will provide a description of the different layers of regulation converging to the activation of caspases and the cleavage of substrates. Moving forward, I will present the concept of cell extrusion and the different cell shape changes leading to cell elimination. I will then discuss the necessity for caspase activation to induce cell extrusion. At this point, I will describe the main result of my PhD. We have demonstrated that the initiation of cell extrusion in the notum is not associated with changes in actomyosin levels or dynamics. Rather, it requires the disassembly of a medio-apical pool of Microtubules driven by caspases. Microtubule disassembly is sufficient to bypass the need for caspase and the stabilisation of Microtubules slows down cell extrusion. This shows that Microtubule disassembly is a rate-limiting step for extrusion and highlights the role of microtubules in apical cell shape stabilisation. I will then present the non-apoptotic functions of caspases and how epithelial cells modulate intracellular levels, dynamics, or location of caspases. Afterwards, I will detail my second PhD project. We have demonstrated that there is no common threshold, and that caspase activity scales with the probability to irreversibly commit to extrusion. We also identified parameters predictive of the cell sensitivity to caspase. Finally, cell extrusions are stochastic events and their manual recognition in microscopy movies is painstaking. Machine Learning has now emerged as a remarkable tool to recognise patterns of sequential events. I will therefore present some

Machine Learning concepts. This will allow me to introduce the concept needed for my last PhD project in which we have developed a Machine Learning enhanced tool. This tool automatically recognises sequential events such as extrusion in epithelial tissue and allows for faster analysis of large number of extrusions.

CHAPTER  
**MORPHOGENESIS**

**1**

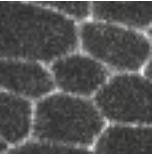






## **Table of contents**

<b>1. Introduction.....</b>	<b>19</b>
<b>2. Morphogenesis of an Epithelium.....</b>	<b>20</b>
<b>2.1. What is an epithelium?.....</b>	<b>20</b>
2.1.1. The ubiquity of epithelium .....	20
2.1.2. Apicobasal polarity and junctions.....	20
<b>2.2. Some shape changes of epithelia .....</b>	<b>23</b>
2.2.1. In-plane deformation: tissue shrinkage and extension .....	25
2.2.2. Out-of-plane deformations: Folding.....	27
<b>3. Morphogenesis: a cell-centred view .....</b>	<b>31</b>
<b>3.1. Cortical tension .....</b>	<b>32</b>
3.1.1. The role of Actin .....	32
3.1.2. Myosin motors.....	41
3.1.3. Different organisations of actomyosin .....	42
<b>3.2. Adhesion: the role of E-cadherin.....</b>	<b>48</b>
3.2.1. E-cad structure .....	48
3.2.2. E-cad dynamics & interactions with the actomyosin cortex .....	49
3.2.3. Role in morphogenesis (apical contraction mainly) .....	50
<b>3.3. Microtubules and mechanics .....</b>	<b>54</b>
3.3.1. Microtubules dynamics and polymerisation .....	54
3.3.2. Interaction with the actomyosin cortex .....	57
3.3.3. Force production and response to forces .....	60



# 1. Introduction

One clear defining feature of life might be the complex forms it encounters. These complex shapes are present at all scales from single cells to more complex multicellular organisms. How these forms emerge from smaller units has been a long-lasting question in biology. It goes back at least to the 18<sup>th</sup> century when the philosopher Goethe coined the term *morphogenesis* to describe the study of the generation of morphology <sup>(1)</sup>. As a botanist, Goethe was most likely referring to the rule governing the emergence of shape in plants.

Indeed, historically the study of shape in biology was focused on multicellular organisms, and particularly, one group has drawn much attention: Metazoans. The reasons for that are numerous ranging from the will to understand the making of humans, to the ease of access to members of this group. One hallmark of the architecture of metazoans is the presence of epithelia which may account partly for the complex forms of metazoans. These ordered arrays of tightly joined cells are at the basis of form emergence during development. They form sheets in their most simple form but can fold and invaginate to form tubes or even branches.

This chapter will be focused on morphogenesis, first at the tissue scale and secondly at the cellular scale. In its first part, I will describe what makes an epithelium and briefly illustrate a few epithelial shape changes. As the focus of this manuscript lies at the cellular scale, I will then explain how most of these shape changes emerge from force generation at the single-cell level. In addition, cell death is an important driver of epithelium morphogenesis. Thus, I will emphasise its role for in-plane and out-of-plane deformations. I will describe how cellular actors produce tension and adhesion. Finally, I will spend some time on other cellular factors: microtubules. I will detail their dynamics and how they may respond or produce forces either directly or indirectly. I will introduce in this chapter key elements for the understanding of the following manuscript.

---

<sup>1</sup> *morpho* - shape, form, *genesis* - origin, production

## 2. Morphogenesis of an Epithelium

### 2.1. What is an epithelium?

#### 2.1.1. *The ubiquity of epithelium*

The development of an embryo from one cell to birth entails drastic deformations of the tissues it is composed of. These tissues are of two main types: epithelial and mesenchymal. Of the two, epithelia are most represented throughout metazoans and are thought to be the default states of cells in metazoans. They are so ubiquitous that they are a defining feature of that group<sup>1</sup>. Even more generally, recent studies have provided evidence of epithelium-like structures in *Sphaeroforma arctica* a unicellular holozoan (monophyletic group encompassing animals<sup>2</sup>). Therefore, these examples place the epithelial structures at the root of opisthokonts or even Unikonts. So, what are epithelia, what are they made of and what makes them so ubiquitous?

Epithelia are made of one or several layers of tightly adherent cells. These adhesions result in a continuous array of cells which act as a mechanical barrier providing support to the organs they encase (**Figure 1a**). Additionally, they have an apical-to-basal polarity<sup>3</sup> leading to a selective barrier function in between the different compartments they separate (**Figure 1b**). For instance, the mammalian gut separates the lumen (outside environment) and the interior of the body<sup>4</sup>. They come in different shapes and sizes from flat to cuboidal or even columnar. Finally, they are highly dynamic and demonstrate high rates of turnover through cell division and cell death<sup>4</sup>.

#### 2.1.2. *Apicobasal polarity and junctions*

Epithelial cells have an apicobasal polarity that leads to different morphologies and specific functions along the apical to the basal axis. For instance, the two domains differ in membrane composition or adhesion<sup>3</sup>. Pioneering work regarding the establishment of polarity has been conducted in *D. melanogaster* during cellularization (a process leading to the formation of the membrane surrounding previously syncytial nuclei<sup>5</sup>). Therefore, I will first focus on insect polarity and its establishment and then highlight some differences with vertebrates.

The apicobasal polarization depends on the mutual exclusion of different complexes. The Bazooka (Baz) and Crumbs (Crb) complexes are apical while the Discs-Large (Dlg) complex is basolateral. First, Cadherin-Catenin clusters are recruited laterally in a Par3/Baz dependent manner<sup>6</sup>. Cadherin-Catenin will coalesce and form the adherent-

Junctions (AJs) also called the zonula-adherens (ZA)<sup>3</sup>. Apical Baz then apically recruits the Crb complex which will displace the Dlg complex basolaterally through their mutual antagonist interaction<sup>6,7</sup>. In  $\beta$ -catenin mutants, Crb is apically recruited by apical Baz but fails to exclude Dlg. This emphasizes the key role of AJs in the establishment of different polarity domains and their maintenance<sup>8</sup>.

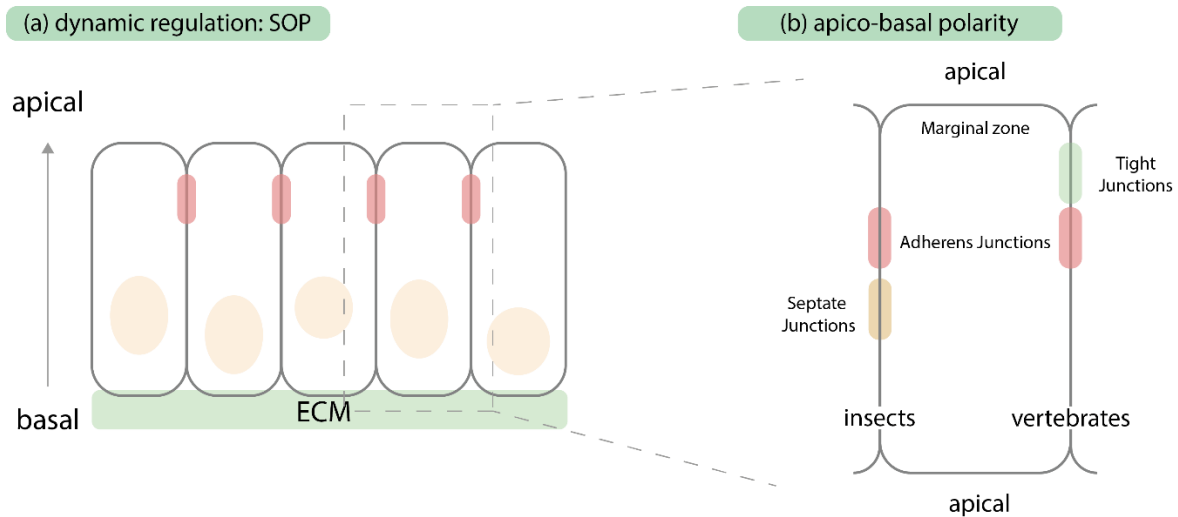


**Figure 1** - Epithelial organization. **(a)** Side view of a schematic epithelial layer. The apical side is up and the basal side is down next to the Extracellular Matrix (ECM) **(b)** The different domains of the apicobasal polarity. (Adapted from<sup>3</sup>). On the left it represents the organization of insects' junctions. Adherens Junctions (red) are apical and mediate adhesion between cells. Below are Septate junctions (yellow) which mediate sealing. This is reversed in vertebrates where Tight Junctions (green) which mediate sealing are more apical than Adherens junctions (right of the figure)

The positions of the resulting domains (**Figure 1b**) are mostly conserved throughout animals. However, some differences can be highlighted between insects and chordates. From apical to basal:

Beneath the apical plasma membrane, the cortex is a dynamic network made of actin filaments interacting with myosin<sup>9</sup>. Its dynamic confers epithelial cells their mechanical properties such as contractility and elasticity<sup>10</sup>. This contractile network together with adhesion controls cell shape<sup>10</sup>.

AJs (or ZA) are mediated by transmembrane proteins called cadherins, specifically E-cadherin (E-cad) in Epithelia<sup>11</sup>. Their homophilic interactions with other cadherins at the surface of neighbouring cells provide adhesion. Through their intracellular domains, E-cad interacts with  $\beta$ -catenin itself linked to  $\alpha$ -catenin<sup>3</sup>. This allows AJs to interact with the cytoskeleton. This coupling provides mechanical coordination across many cells and is one of the key properties for the emergence of tissue shapes.

Tight junctions (TJ) are likewise, made of transmembrane proteins: Claudins and Occludins<sup>12</sup>. Like for AJs they form homophilic interaction with neighbouring cells and form adhesion to seal the gap between cells<sup>13</sup>. However, no tight junction has been observed in *Drosophila*. Their function is supported by septate junctions (SJ) which have a different molecular and structural organisation<sup>3</sup>. While TJs are found apically in vertebrates, SJs are situated below AJs.

Apart from cell-to-cell adhesions, epithelia are attached to the Extracellular Matrix (ECM). This is provided by hemidesmosomes in vertebrates or hemi-adherens junctions in insects through transmembrane proteins like integrin<sup>14</sup>. Integrins also interact with actin in a similar principle to AJs.

Overall, these interfaces are the main relays between extracellular forces and intracellular forces generated by actomyosin at specific locations in the cells established by polarity. Together, these active stresses are the main driving forces for tissue morphogenesis<sup>15</sup>.

## 2.2. Some shape changes of epithelia

The development of a complex organism ultimately leads to the formation of specified structures or organs which need to acquire a stereotypical shape to perform their function. Several mechanical models have been put together to try to understand tissue shapes. For instance, the concept of surface tension has proven to be useful to describe the organization of one or a group of cells<sup>16</sup>. It explains that if two different classes of particles with different properties are put in contact, their interface will take a shape that minimizes the surface of contact between them. This is like the organisation of oil-water emulsions. In these emulsions, water will form round-shaped bubbles. This is because interactions between water molecules are stronger than the interactions between water and oil. Therefore, at equilibrium, these water-oil interactions will be minimized leading to the water droplet taking a round shape. This framework allows to recapitulate single cell or epithelial cell organization. For instance, an individual cell in a medium will tend to form a sphere<sup>17</sup>. In an epithelium, cells will arrange in a way that minimizes their surface of interaction which often results in a hexagonal packing<sup>16</sup>.

This framework is based on the balance of cortical tension and cell-cell adhesions. Cortical tension favours a decrease in surface area which is resisted by an opposing cell osmotic pressure<sup>17-19</sup>. On the other hand, intercellular adhesion favours expansion of the surface area.

Therefore, morphogenesis can be seen as a sequence of deformations of the contacts between cells. These deformations rely on feedbacks between cellular processes and global tissue properties or geometry<sup>15,20</sup>. Cell division, cell death, cell rearrangements, cell shape changes and to a lesser extent extracellular volume changes are the main contributors to tissue size and shapes<sup>21,22</sup>. Hereafter, I will succinctly cover tissue morphogenesis emerging mainly from cell shape changes and cell death. As tissue shape changes are numerous, I will illustrate the role of cell mechanics-driven processes in tissue extension and tissue bending. Precise molecular details regarding the regulation of cytoskeleton dynamics and the contractile machinery will be covered thoroughly in **part 3** of the current chapter. Finally, the understanding of morphogenesis partly relies on a mechanical framework. I send the reader to **Box 1** for the definition of key mechanical parameters that will be useful for the rest of the chapter.



### Box 1: Mechanical definitions

Tension: Constraint of a linear material when submitting to two pulling forces at each of its ends. It is expressed in Newtons (N).

Stress: Force per unit area. It is a measure of the internal forces in a material. If we apply a force  $F$  on a material of length  $L$  it will deform by a length  $d$ . Once  $d$  and  $F$  are normalized by the object dimension the stress is obtained as  $\sigma = \frac{F}{A}$ , where  $A$  is the cross-sectional area.

See **Figure 2**

Strain: It is a measure of the deformation of a material in response to a force. relative to an initial length. It is expressed as  $\epsilon = \frac{d}{L}$ . See **Figure 2**

Elastic material: Material inducing a constant deformation when subjected to constant stress over some time due to its capacity to store energy. See **Figure 2**

Viscous material: Material in which the strain (deformation) is proportional to the duration of the stress application due to its capacity to dissipate energy. See **Figure 2**

Viscoelastic material: Material able to store and dissipate energy during the time of stress application. See **Figure 2**.

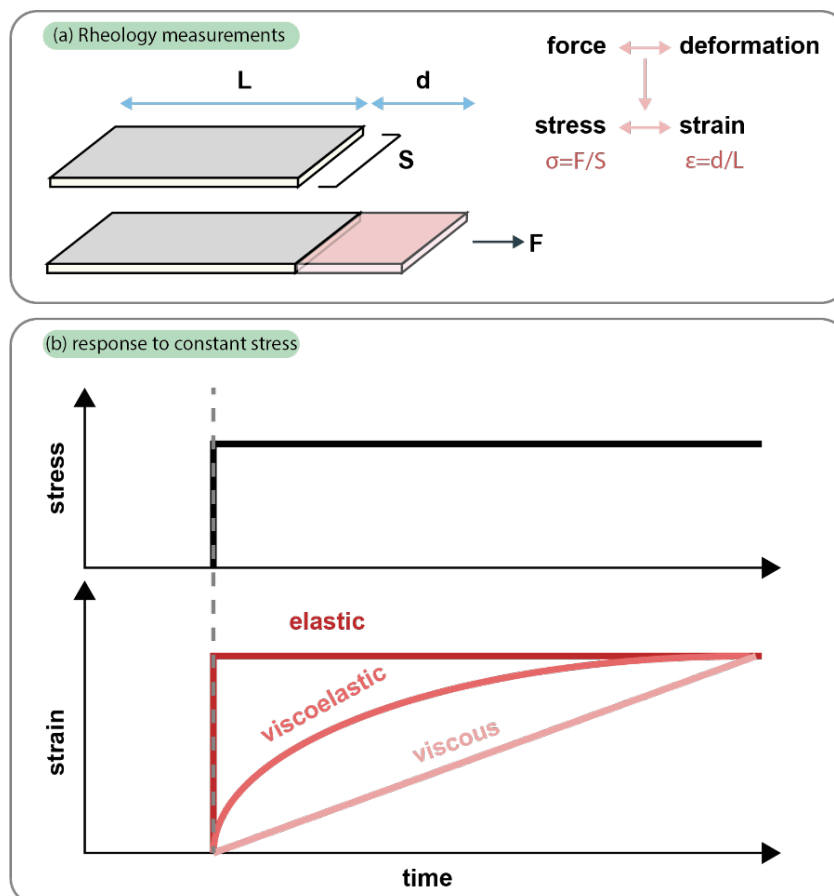


**Figure 2** - Mechanical parameters. (a) Deformation of a material under force leads to a stress and a strain. (b) Constant stress application (top) leads to different material response (bottom). Adapted from<sup>18</sup>. See Box1 for definitions

### 2.2.1. In-plane deformation: tissue shrinkage and extension

Body axis extension is one of the main in-plane tissue movements during development. It consists of a preferential extension in one direction associated with a convergent of the tangential axis in a movement called convergence and extension (CE). For instance, during neural tube closure in vertebrates, the neural plate undergoes CE<sup>23-25</sup>. It extends anteroposteriorly and converges mediolaterally toward the medial fold in a movement thought to promote tube closure<sup>26</sup>. Similarly, CE are observed during primitive streak formation in chick<sup>27</sup> or during germband extension in *D. melanogaster*<sup>28-30</sup>. Classically, cell intercalation was thought to mediate such movement either through lateral protrusion<sup>31,32</sup>, through orientated junction contraction<sup>28-30</sup>, or both<sup>33</sup>.

Similarly, convergence extension can be achieved through cell shape changes only, like in the case of abdomen morphogenesis in *Drosophila*. In this tissue, a set of Larval Epithelial Cells (LEC) is replaced by histoblast cells that come together in segments forming the epidermis (**Figure 3a**). Once the segments are formed, epidermal cells drastically change their orientation. Cells oriented in the initial anteroposterior axis reorient toward the mediolateral axis<sup>34</sup>. This is mediated by atypical cadherins Dachous/Fat. These cadherins are expressed in opposing gradients which generate directional information. This process called planar cell polarity (PCP) drives the orientation of cell shape changes (**Figure 3a**). Tissue elongation can also be regulated by changes in tissue thickness (**Figure 3b**). For instance, tissue flattening leads to tissue expansion as in the case of limb elongation in *Drosophila*. Wings and legs elongate by reducing their cell height and expanding cell width in a. First PCP drives polarized recruitment of MyoII which drives anisotropic elongation through convergence extension. Then a columnar-to-cuboidal transition follows convergence extension in the proximal-distal axis. More specifically, MyoII is recruited and constricts lateral junctions which drive tissue flattening and subsequent elongation<sup>35</sup>.

Interestingly, the opposite cell shape changes can drive the opposite tissue shape change (**Figure 3c**). Early on during larval development, all wing disc cells are cuboidal and later become columnar in the wing pouch. In this case, Rho (a MyoII activator) and

MyoII are excluded from the lateral junctions by Decapentaplegic (Dpp). Accordingly, lateral domains expand and lead to a cuboidal-to-columnar transition<sup>36</sup>.

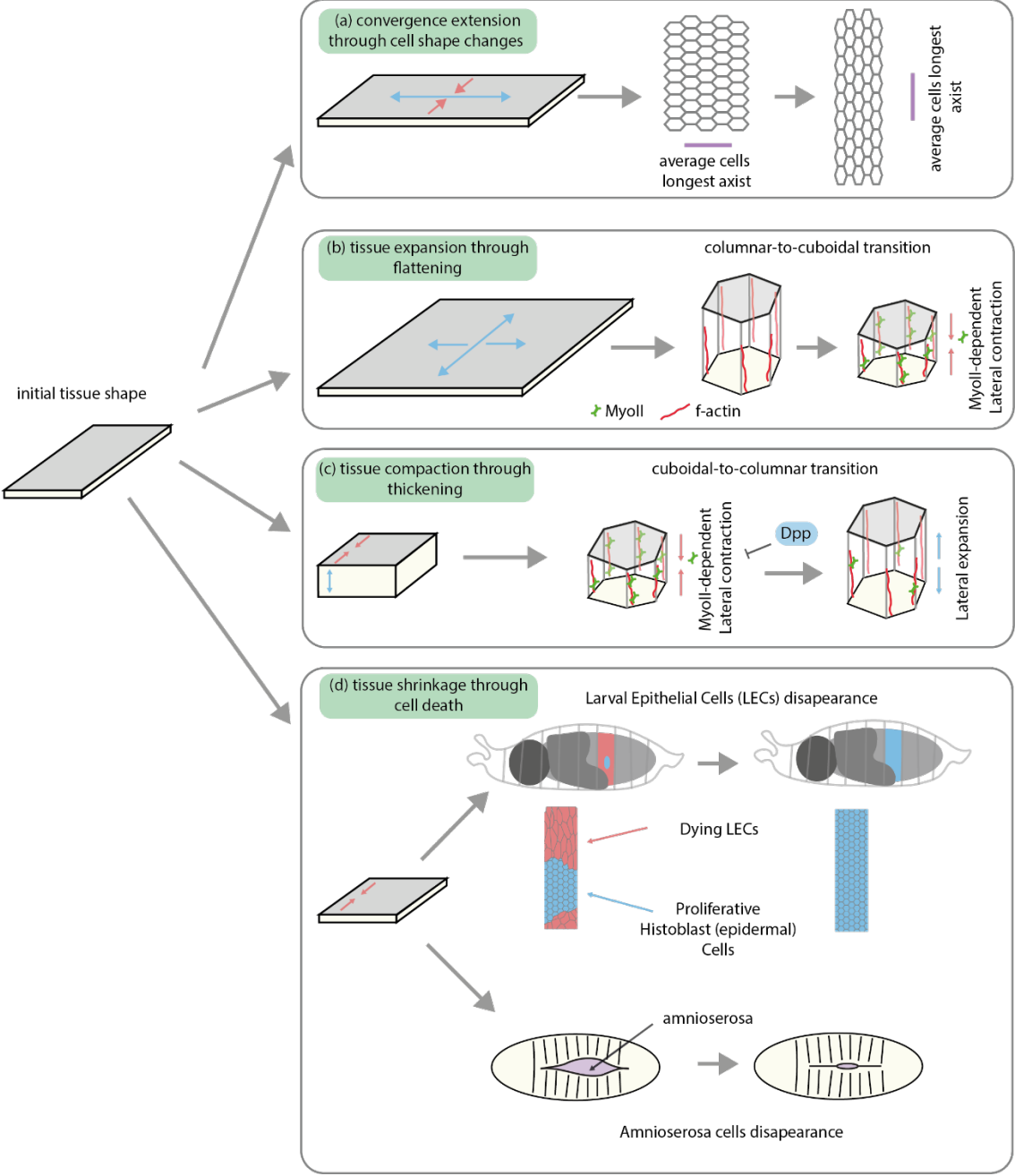


**Figure 3** - In-plane tissue deformation through cell death and cell shape changes. (a) Convergent extension through cell shape changes. Changes in the orientation of cells drives convergence extension during the morphogenesis of *Drosophila* abdomen. Purple shows the average cell orientation in the tissue (b) Cell shape changes drive tissue flattening leading to tissue expansion. Myosin (green) and F-actin (red) localisation to the lateral junctions lead to their constriction and cell flattening. (c) Cell shape changes from cuboidal cells to columnar cells drives tissue thickening and therefore tissue compaction. (d) In-plane tissue shrinkage can be driven by the disappearance of cells through cell death. For instance, the death of LECs (red) drives the extension of neighbouring histoblasts (blue). Similarly, death of amnioserosa cell leads to its disappearance and dorsal closure.

Finally, the epithelial planar surface can be reduced through cell death (**Figure 3d**). During abdominal morphogenesis, LECs are eliminated by apoptosis, a form of cell death, for the benefit of the expanding epidermal cells<sup>37</sup>. Similarly, early on *Drosophila* embryos go through a step of dorsal closure. During this process, the amnioserosa (an extra-embryonic tissue) undergoes a drastic reduction in size through cell death which contributes to its elimination<sup>38</sup>. To summarise these examples, highlight how cell shape changes and cell death are re-used in different conditions to drive in-plane morphogenesis. Epithelia also can undergo more complex 3D deformation through the same processes.

### 2.2.2. Out-of-plane deformations: Folding

Tissue folding or invagination is one way to produce out-of-plane deformations. They are widely observed throughout animals<sup>39-41</sup>. One reason is that invagination allows to separate a new and independent germ layer from the original epithelium. We find examples in insects with mesoderm invagination<sup>39,42</sup>, or amongst vertebrates with the formation of the 3 layers: neurectoderm<sup>40,41</sup>, mesoderm, and endoderm<sup>43</sup> (**Figure 4**). Strikingly, the mechanisms leading to such folding seem to be conserved and rely on a similar set of cellular factors. A subset of cells undertakes apical constriction leading these cells to acquire a bottle shape along their apicobasal axis. Then, a step of lateral contraction followed by basal expansion allows to stabilise this wedge shape (**Figure 4a**).

During mesoderm invagination in *Drosophila*, *twist* and *snail* are expressed in a band of cells on the ventral side of the embryo, therefore, restricting apical constriction to this domain<sup>39</sup> (**Figure 4b. 1**). Contrary to what is observed in other systems, there, apical constriction is not driven by a junctional actomyosin purse-string<sup>40,44</sup>. Rather, contraction happens through a sequence of contractile myosin pulses and stabilisation. These medio-apical Non-Muscle Myosin-II (MyoII) pulses pull AJs inward each time, resulting in an incremental decrease of the apical area (**Figure 4b. 2 and 3**)<sup>42</sup>. Interestingly, optogenetic activation of MyoII at the basal side of these cells inhibits basal expansion, cell shortening & subsequent tissue bending. This suggests that basal relaxation through MyoII depletion is necessary for proper folding<sup>45</sup>. Although under different genetic controls, overall, this mechanism seems to hold across animals. For instance, *shroom* is necessary and sufficient to drive apical constriction through MyoII during neural tube closure in mice or chickens (**Figure 4**). and gut formation in *Xenopus laevis*<sup>43,46</sup>. This results in cells adopting very similar shapes to the one just described (**Figure 4**).

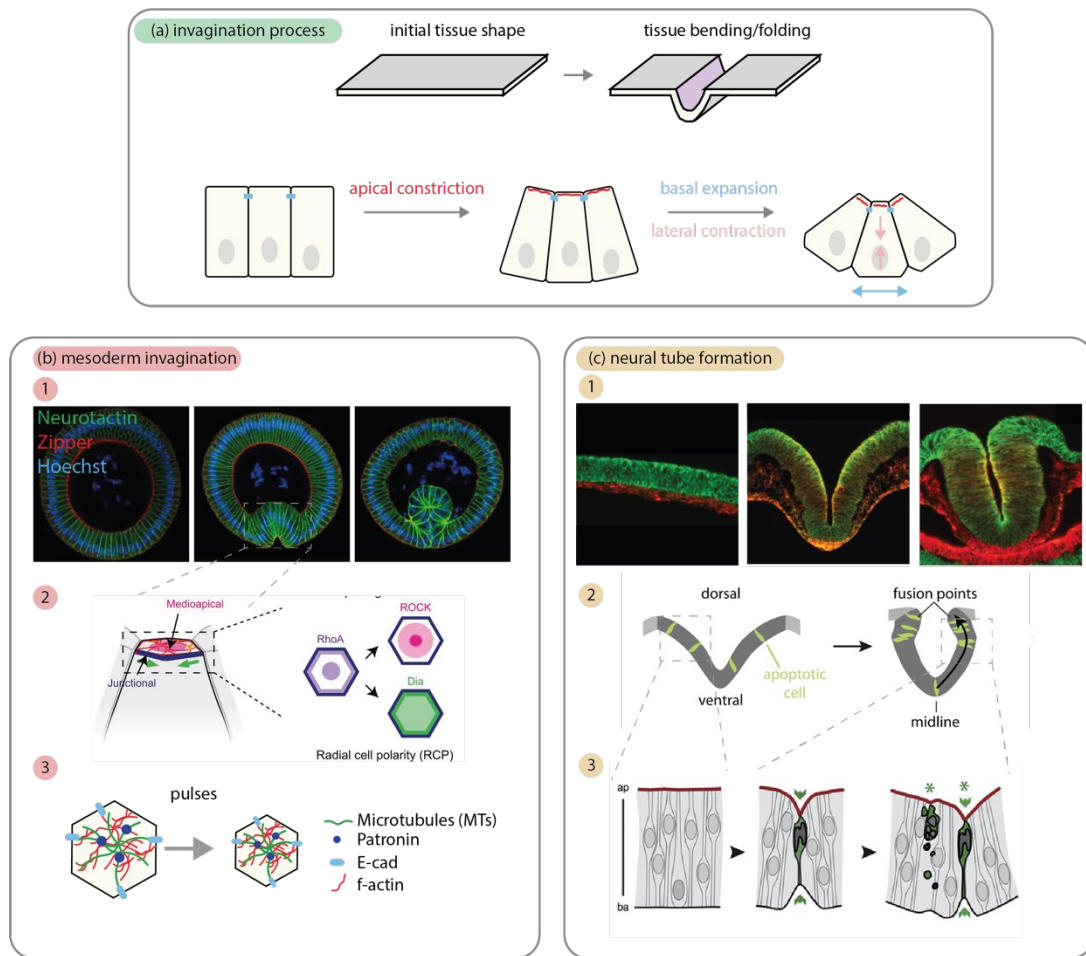


**Figure 4** - Out-of-plane tissue deformations through cell death and cell shape changes. (a) Tissue folding happens through a common mechanism. First apical constriction leads the cells to take a bottled shape. Then cells take a wedge shape basal expansion and lateral contraction. Through adhesion, this transfer forces leading to tissue bending. (b) Example of invagination due to apical constriction. (1) Actin and myosin organise in the medioapical area through a process of radial cell polarity (2). RhoA forms a focus at the centre of the cell and activates ROCK in the centre of the cell. However, ROCK is excluded from the junctions. Therefore, actomyosin pulses only take place in the medioapical region of the cell (3). Through their interaction with AJs, they transmit forces which bend the tissue. (c) Example of invagination through both apical constriction and apoptotic forces (1). Cell death (green) localises at the top of the newly formed fold and is necessary to mediate secondary bending and fusion of the neural tube (2). Indeed, the cell triggers the formation of an apicobasal MyoII cable which produces force perpendicular to the tissue plane (3). This leads to increased tension and tissue bending. Adapted from <sup>15,47,48</sup>.

AJs are instrumental during folding because they allow contraction happening on the apical sides of cells to be transmitted across several cells to ultimately lead to bending<sup>49</sup>. For instance, during mesoderm invagination in *Drosophila*, it is only when the actomyosin cortex is linked to E-cad that contractile pulses effectively lead to tissue buckling<sup>49-51</sup>. Alternatively, AJs can modulate epithelial bending and apical contraction independently of their interaction with the actomyosin cortex. In the context of dorsal fold formation, the levels of actomyosin remain homogeneous and low. However, AJs

slide basally resulting in a two-fold effect. First, this drives the basal shift of Microtubule arrays which are thought to exert pushing forces on the apical side which results in apical constriction. Secondly, only the cells in the fold shift their AJs basally while the neighbours remain at the same position which forces tissue bending<sup>52</sup>.

However, these mechanisms are not sufficient to fully explain all folding events. Briefly, depending on the timescale considered, epithelial tissues can be considered elastic materials. Put under compressive loads these materials can buckle to relieve these compressive stresses (think of a sheet of paper you would compress by bringing your hands together). This happens in vivo when growth is somehow constrained like during gut vilification, or when two adjacent tissues have differential growth rates as during brain vilification<sup>15</sup>.

Finally, cell death can also be an important mediator of tissue bending and folding (**Figure 4c**). The *Drosophila* embryo is divided into segments which form under the control of homeotic genes (*hox* genes). For instance, *deformed* (*dfd*) regulates the formation of mandibular segments and *abdominal-B* (*abd-B*) regulates part of the abdominal segments. Both regulate the expression of the pro-apoptotic gene *reaper* (*rpr*) at the interface between consecutive segments. This drives apoptosis which is necessary and sufficient for groove formation that separates segments<sup>53</sup>. Similarly, apoptosis takes place during the second step of neural tube closure & inhibiting cell death impairs closure. This depends on the formation of a contractile actomyosin cable along the apico-basal axis of the cell. This cable produces forces which lead to tissue bending and accelerate closure<sup>47</sup>. Such apico-basal forces mediated by apoptotic cells were previously shown to drive folding during leg segment formation in *Drosophila*<sup>54</sup>. Likewise, in this system apoptotic cell form an apico-basal MyoII-cable which pulls on the surface and increase tension in the neighbouring cells ultimately inducing epithelial folding.

*Conclusion: Take-home messages.*

So far, I described how epithelial tissues are prevalent in animals. I exemplified how the strong adhesion, so important for the coherence and barrier function of these tissues, arises from the establishment of apicobasal polarity. The resulting subcellular domains allow to spatially orchestrate the cellular machinery such as contractility through the actomyosin cortex. I then illustrated how some of the epithelial shape changes emerge from these two concepts: the spatially regulated activation of the contractility and the mechanical coupling between cells allowing the propagation of such forces at the tissue scale. Finally, I described how cell death also contributes to morphogenesis either through the simple elimination of cells or through active apoptotic forces.

During this part, I voluntarily left aside the molecular mechanisms leading to the regulation of the cytoskeleton. However, understanding the factors controlling cytoskeleton dynamics is key to appreciate how forces are produced and how these can be spatially regulated in the cell. Therefore, the next part of that chapter will focus on the molecular regulators of cell morphogenesis.

### 3. Morphogenesis: a cell-centred view

We demonstrated in the previous part how cell shape changes are important during development through the formation of complex organs. These cell shape changes arise mainly from the generation of forces from the cell's cytoskeleton. Understanding cell mechanics requires to consider the dynamics and interactions between the cytoskeleton constituents. Therefore, I will address in this part the molecular basis of force generation.

In the previous chapter, we introduced how surface tension is a very adequate framework to describe cell and epithelial shapes. It arises from interactions between molecules generating cortical tension (mainly actomyosin), intercellular adhesions (mainly E-cad). However, surface tension is not able to describe the interaction with other cytoskeleton elements (Microtubules and/or intermediate filaments). Microtubules, however, appear as essential regulators of cell mechanics, could it be on their own or through their crosstalk with the actin and myosin or E-cad<sup>55,56</sup>. Consequently, while debated, some models like tensegrity have tried to incorporate them. They highlight how these regulators might also intervene in morphogenesis <sup>57,58</sup>.

In this part of the chapter, I will put together these three elements in the context of force generation mainly regarding cell apical constriction. First, I will explain how cortical tension results from myosin pulling on the actin network. I will emphasize how the network's architecture and dynamics influence contractility. Then, I will describe some adhesion molecules and how their dynamics and interactions with actomyosin contribute to cell shape. Finally, I will focus on an underestimated actor in apical cell mechanics: microtubules. I will describe their dynamics, how they produce and respond to forces and finally highlight their interaction with the actomyosin cortex.



### 3.1. Cortical tension

Cortical tension is generated in the cortex: a layer of actin, myosin and very diverse interactors that sits just below the plasma membrane. The cortex spans the apical surface of most epithelial cells. It is built from actin filaments embedded in a network by crosslinkers that serve as a substrate for myosin constriction<sup>59</sup>. Therefore, it can be physically described as an active polymer network (or active viscous material)<sup>60</sup>. This network is highly dynamic and plastic. This is due to protein turnovers, changes in its molecular components or rearrangement due to myosin contractility. All these lead to changes in cortex mechanics. As such, to understand cortical mechanics, we need to understand the length and dynamics of actin filaments and the way they are arranged relative to each other.

#### 3.1.1. The role of Actin

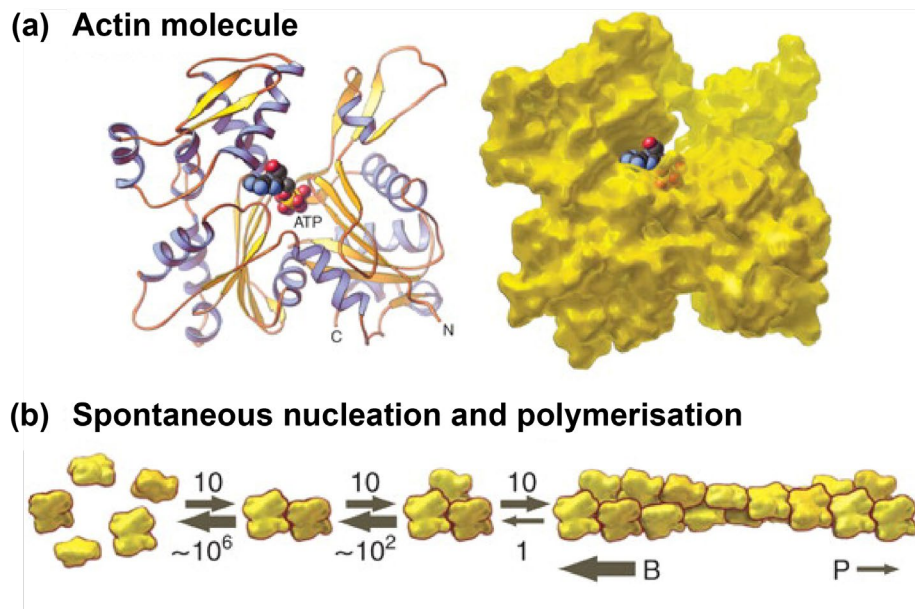


**Figure 5** - Globular actin, filamentous actin, polymerisation. (a) Structure of the actin molecule and highlight of the ATP cleft. (b) Spontaneous nucleation and polymerisation. Spontaneous nucleation is unlikely (left) however once a trimer is form barbed end polymerisation becomes favourable. Adapted from<sup>59</sup>.

Actin is a very abundant and conserved protein amongst animal cells. It exists in two forms: the monomeric or Globular-Actin (G-actin) and the Filamentous actin (F-actin, **Figure 5**)<sup>61,62</sup>. It is an ATPase whose structure is composed of two major domains each subdivided into two sub-domains. Once folded these domains form a cleft which binds ATP. Spontaneous hydrolysis of ATP by this cleft, catalyses the transition between G-actin and F-actin in a process called polymerisation. Because of this internal asymmetry, the polymerised filament is itself polarized into a barbed (+) end and a pointed (-) end.

The cleft binding ATP is exposed on the barbed end leading to favourable kinetics towards the association of new monomers at this end compared to the pointed end (**Figure 5**)<sup>62,63</sup>. Once added, ATP is then hydrolysed from the new monomer. However, this happens with a delay. Thus, it results in a region toward the barbed end rich in ATP followed by a gradient of ATP to ADP along the filament<sup>63</sup>. This gradient leads to the accumulation of hydrolysis-dependent conformational changes along the filament which results in a loss of stability toward the pointed end. Therefore, monomers are preferentially added at the barbed end and dissociated more from the pointed end. This process is called treadmilling. This phenomenon is key to the dynamics of actin networks and seems to be sufficient by itself to generate forces<sup>63</sup>.

While the affinity of free G-actin monomers to a filament is very high, the dissociation constant of a simple G-actin dimer is also very high. This makes it unlikely to observe any spontaneous polymerisation in physiological conditions<sup>61,63</sup>. It is also partly due to the association of some Actin Binding Protein (ABPs) with actin monomers preventing *de novo* nucleation. Therefore, *de novo* actin polymerisation & actin dynamics are under multiple layers of regulation (**Figure 6**). Ultimately, three parameters are key for the function of the actin network:

- (a) Filament length — is regulated by the balance between polymerisation (see **3.1.1.1**) and depolymerisation (see **3.1.1.2**)
- (b) Filament flexural rigidity — regulated by actin crosslinking (see **3.1.1.3**)
- (c) Network activation — regulated by GTPases. (see **3.1.1.4**)

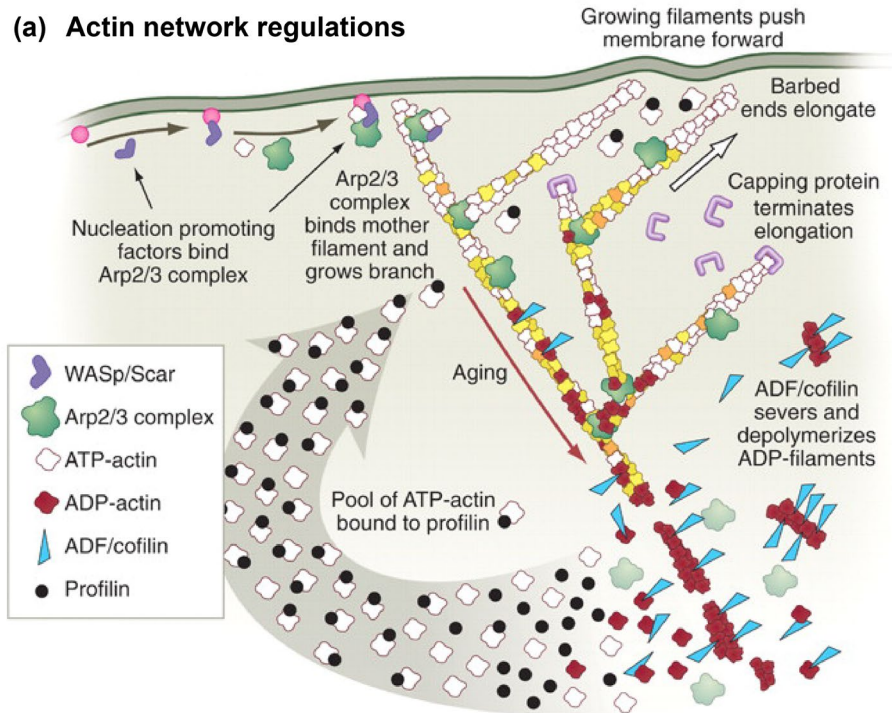


**Figure 6** - Diversity in the regulation of the actin network. Filament length is regulated by nucleation factors (top left), capping (top right) and severing (cofilin lower right). Network organization in branches is regulated by nucleation factors (Arp2/3, middle). Adapted from<sup>59</sup>.

### 3.1.1.1. Polymerisation: Nucleation & elongation

The nucleation step corresponds to the initiation of actin polymerisation from free monomers. Because it is unlikely to happen spontaneously in cells, it needs to be regulated by ABPs. Some ABPs like Profilin tend to positively regulate actin polymerisation by monomer binding. Profilin prevents the addition of G-actin to the pointed end, but profilin-G-actin dimers are added to the barbed end at a similar rate compared to free monomers<sup>63</sup>. This results in a net increase in polymerisation (**Figure 7a**). Two main classes of nucleators exist and result in very different actin network organisation.

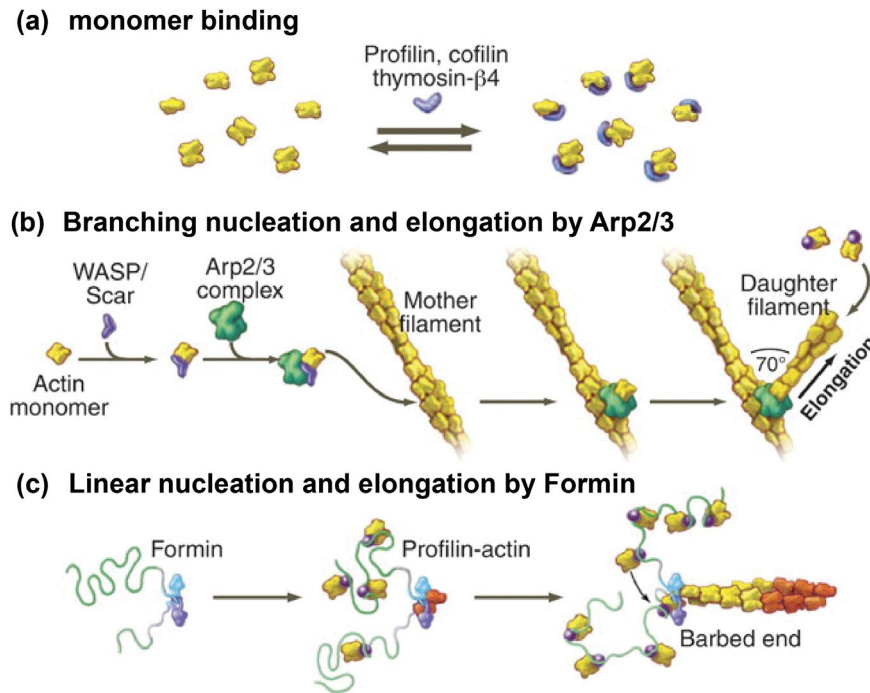


**Figure 7** - Regulation of polymerisation. (a) Regulation of polymerisation through monomer binding. (b) Regulation of polymerisation in branches by Arp2/3 nucleation. (c) Regulation of polymerisation in linear filaments by Formins. Adapted from<sup>59</sup>.

First, branched actin networks are key in cortical actin organisation and actin-dependent mechanisms. Their formation is mainly mediated by the Arp2/3 complex. For instance, *Drosophila* mutants for Arp2/3 show defects in embryonic actin structures and lethality<sup>64</sup>. Moreover, Arp2/3-mediated networks support morphogenetic events. For instance, Arp2/3 is necessary to ensure force-channelling during the folding of *Drosophila* leg segments which ensures robustness in the position of these segments<sup>65</sup>. This complex is composed of 7 proteins: Arp2 & 3 and from ARPC1 to ARPC5. They crosslink F-actin into a Y-branched array of filaments all separated from 70° (**Figure 7b**)<sup>63,66</sup>. Interestingly, Arp2/3 only has low activity on its own. To efficiently branch actin, it needs to be activated by some Nucleation Promoting Factors (NPFs). NPFs are a very diverse protein family that vary in size and sequence. However, they all present 3 important domains. The W domain (WASP Homology domain — WH2), the C domain (Connexion) and the A domain (acidic). Depending on the class of the NPF, the activation of Arp2/3 happens either upon the formation of a ternary complex with Arp2/3-NPF-G-actin (**Figure 7b**) or Arp2/3-NPF & a mother filament. In either case, the activation is mediated by the CA domains and WH2 mediates actin binding<sup>62,67</sup>.

The second mode of nucleation and elongation leads to the formation of unbranched F-actin and is mainly mediated by Formins. This drives the assembly of structures like

actomyosin rings. For instance, the Formin Diaphanous (Dia) in *Drosophila* is necessary for cell contractility<sup>68</sup>. Accordingly, *dia* mutants that reduce its activity led to junction destabilisation and inhibition of actomyosin ring contractility. Contrary to Arp2/3 complexes, it seems that Formins can nucleate de novo actin without pre-existing filaments (**Figure 7c**). They form dimers whose function relies on 4 domains. Their FH1 domain can tether multiple profilin-bound actin monomers. This allows to increase monomer concentration locally toward the barbed end. Their FH2 domain on the other hand, is involved in accelerating de novo nucleation, and elongation. It binds to the fast-growing barbed end and moves processively with it, therefore, preventing barbed-end capping by other capping proteins (**Figure 7c**)<sup>69,70</sup>.

#### 3.1.1.2. Depolymerisation: capping and severing

The efficiency of contractility is partly dependent on actin filament length. Filament length is a result of the equilibrium between polymerisation & depolymerisation. Depolymerisation is regulated by capping and severing proteins (**Figure 8**). The former can inhibit/terminate actin polymerisation. Such activity can be mediated by proteins such as Gelsolin or Tensin. Barbed end binding by these proteins leads to the inhibition of the addition of new G-actin. This consequently favours depolymerisation from the pointed end. However, it needs to be contrasted. Indeed, releasing of G-actin from the pointed end is thought to locally increase free G-actin concentration consequently promoting locally polymerisation in a process called “Funnelling treadmilling”<sup>71</sup>. Additionally, some regulators like ADF/Cofilin (**Figure 6**) prevent actin polymerisation through their binding to actin monomer by slowing down hydrolysis<sup>67</sup>. By directly binding to actin lateral sides, Cofilin also mediates direct cleavage of actin through its severing action<sup>66</sup>. This cuts actin filaments which also reduces filament size. Alternatively, cofilin also promotes debranching in the dendritic actin network, therefore, realising free G-actin and reducing mean filament sizes<sup>63,67</sup>.

### (a) depolymerisation

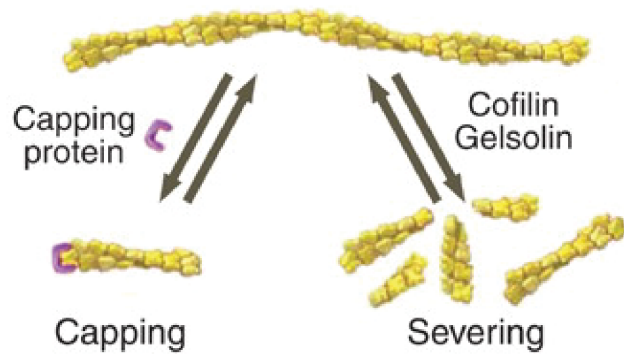


**Figure 8** - Depolymerisation mechanisms: depolymerisation through capping (left) or through direct cleavage called severing (right). Adapted from<sup>59</sup>.

#### 3.1.1.3. Crosslinking

Single actin filaments are mostly semi-flexible inside the cell. They have a persistence length of  $\sim 10\mu\text{m}$  under which they are rigid and above which they are more flexible<sup>72</sup>. Therefore, they are likely to be bent above that length. Accordingly, gliding *in vitro* assays demonstrated that actin buckles when its pointed end is attached, and its barbed end polymerises under a constrained distance<sup>73</sup>. Similarly, *in vitro* models recapitulating cortical networks demonstrated that single actin filaments buckle upon MyoII contraction<sup>72-74</sup>. Indeed, upon the action of MyoII, tension builds up between actin ends which leads to an increase of compressive stresses on the filament and breakage. Interestingly both observations can be modelled showing that the force exerted by a single MyoII filament is sufficient to induce such breakage. Therefore, alone they are unlikely to be able to bear the mechanical load produced in the cortex. Thus, by increasing the number of bridges between actin filaments, Actin crosslinking increases flexural rigidity. So, it is a very important modulator of network contraction upon the action of MyoII.

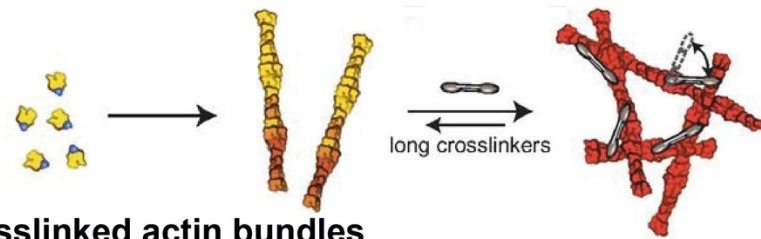
In the cell, F-actin is embedded in a network with proteins bridging different filaments together called crosslinkers. This results in a net increase in network stiffness<sup>75,76</sup>. Two main network architectures exist depending on the size of the crosslinkers because it influences the bridging distance between filaments<sup>77,78</sup>. Filamins have the largest crosslink distance with about 160nm (**Figure 9**)<sup>78</sup>. They mainly form branched actin networks leading to the formation of actin gels. It forms Y-shaped dimers in which the actin-

binding domains are at the N-ter of both ends of the Y. This allows filamin to bind orthogonal actin filaments and to form X, T or Y-shaped branches<sup>78</sup>. Such networks are the basis of apical constriction during mesoderm invagination in *Drosophila*. In this system, a medio-apical branched actin network support pulses of MyoII leading to cell apical constriction<sup>42</sup>. Accordingly, increasing the number of filaments in the network by lowering actin turnover impairs constriction<sup>79</sup>. Similarly, downregulating Ableton kinase leads to an increase in the formation of actin bundles which no longer support apical constriction<sup>80</sup>.

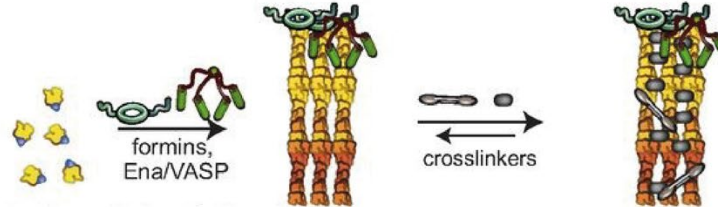
On the other end of the spectrum, we find crosslinkers with smaller typical bridge distances of about 10nm (**Figure 9**)<sup>77</sup>. This group contains for instance Fimbrins/ $\alpha$ -actinin family which are mainly found in bundles. The main reason for that is that they present two tandem ABD (Actin Binding Domains) in very close proximity, therefore, bridging actin filament closer. While actin bundles can be made of actin filament aligned in parallel, Fimbrins/ $\alpha$ -actinin are thought to mainly mediate these anti-parallel conformations<sup>81</sup>. Such network architectures are more likely to be found in contractile structures<sup>72</sup>. In vitro, reconstituted networks on micropatterns showed that anti-parallel bundles are preferentially targeted by MyoII<sup>82</sup>. Moreover, they produce faster contraction than branched networks<sup>82</sup>.

To a large extent, the orientation and the architecture of the network modulate MyoII motor activity. One other major parameter is the level of connectivity by crosslinks (**Figure 9**). Maximal level of contractility happens with intermediate levels of crosslinking<sup>82-85</sup> (reviewed in<sup>17,75</sup>). In reconstituted networks, below a certain threshold of connectivity, MyoII-driven stresses are not propagated to the network and only small clusters form<sup>85</sup>. Similarly, high levels of connectivity limit the remodelling of the network upon MyoII-mediated stresses and therefore impairs tension generation (**Figure 9d**)<sup>19</sup>.

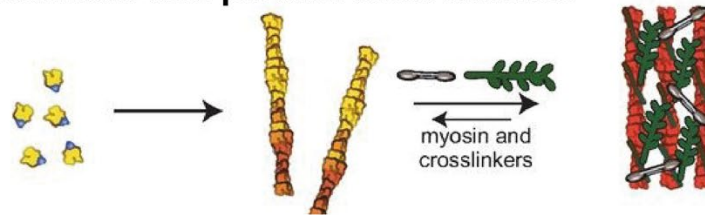
**(a) crosslinked actin networks**



**(b) crosslinked actin bundles**



**(c) crosslinked anti-parallel actin bundles**



**(d) efficiency of contractility depending on connectivity**

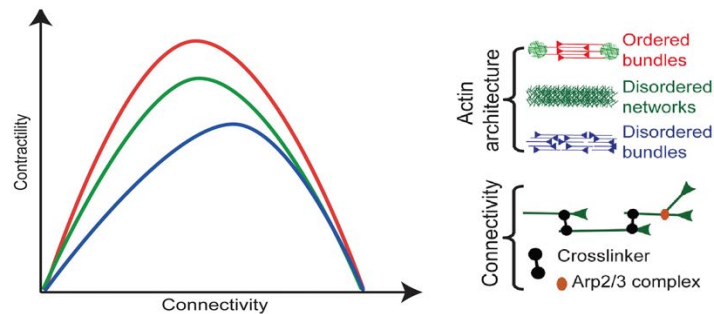


**Figure 9** - crosslinking. (a) Crosslinking in branched networks. (b) Crosslinking in actin bundles. (c) Crosslinking in anti-parallel actin bundles. (d) Efficiency depending on connectivity in the network. Network with intermediate levels of connectivity is the most contractile. This is increased in ordered bundle networks. Adapted from <sup>72</sup>& from <sup>85</sup>.

Finally, for the cortical forces to deform the cell, the cortex needs to be attached to the membrane<sup>17</sup>. This happens mainly through Spectrins and ERM proteins (Ezrin, Radixin & Moesin). Albeit through different mechanisms, both types bind cytoplasmic regions of membranous proteins (for instance through FERM domains for ERM)<sup>86</sup>. Therefore, part of their function is to crosslink the actomyosin cortex, which results in increased rigidity and the other part is to transmit deformations to the membrane.<sup>86</sup>

3.1.1.4. Rho-GTPases



So far, I have shown how the regulation of the actin network emerges from ABPs and their interaction/activation by NPFs. Both are also under Spatio-temporal regulation by a small set of G-proteins: GTPases (**Figure 10**). In their ‘active’ state they bind to GTP. This allows them to recognize their targets and to provide function until hydrolysis of GTP to GDP and to return to an ‘inactive’, GDP-bound state. This cycle is in turn regulated by two sets of proteins: GEFs (Guanine nucleotide exchange factors) and GAPs (GTPase-activating proteins). On one hand, GEFs are mediating the activation of Rho-GTPase by promoting nucleotide exchanges. On the other hand, GAPs promotes GTP hydrolysis which favours the inactivation of Rho-GTPases (**Figure 10**, reviewed in <sup>87</sup>). Of that family Rho, Cdc42 and Rac are the best characterized.

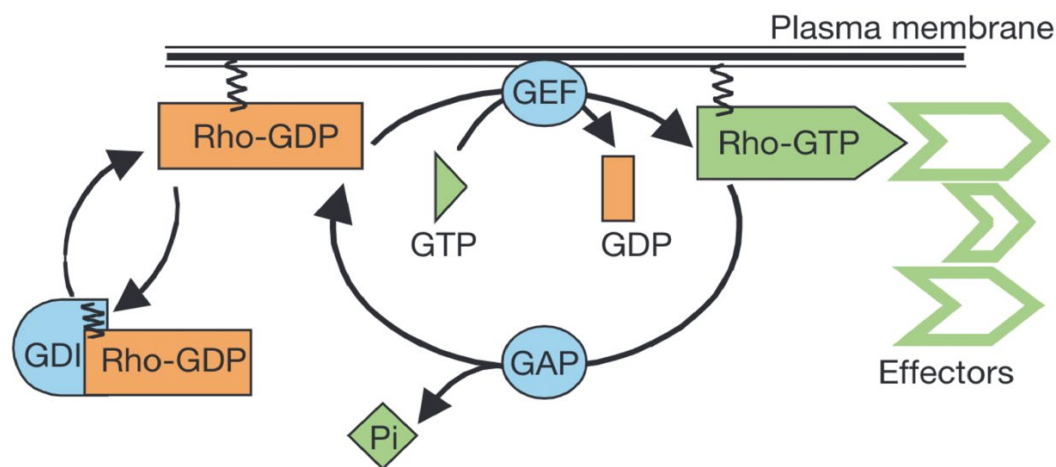


**Figure 10** - Rho-GTPases cycle. RhoGEF promote GTP binding leading to the activation of Rho-GTPases which in turn activate effectors. On the other end, RhoGAP promote hydrolysis of GTP in GDP+Pi which inactivates Rho-GTPases. Adapted from.

Usually, NPFs are found in an inactive closed state through internal inhibition<sup>62,63</sup>. For instance, the Rho-GTPase Cdc42 binds to WASP an activator of Arp2/3. This leads to a conformational change from a closed to an open and activated state. This in turn leads to Arp2/3 activation and nucleation.

Alternatively, Rho can bind directly to Formin-like protein and triggers their activation through a similar switch between their close (inactive) and open (active) forms. The DID (Diaphanous Inhibitory Domain) and the DAD (Diaphanous Autoregulatory Domain) are reciprocally located on the N-ter and C-ter of the protein. Thus, they surround the FH1 and FH2 domains necessary for Formin polymerising function. Both domains' internal interaction leads to a close and inactivated conformation which becomes active only upon the binding of G-protein to the GBD (G-protein Binding Domain)<sup>63,69</sup>. Additionally, Rho-GTPases can modulate actin depolymerisation through

the control of actin severing protein activation. Rho activates ROCK (Rho-associated coiled coil-containing kinase) which phosphorylates LIMK (LIM kinase). Cofilin phosphorylation by LIMK reduces its actin-binding activity. This ultimately reduces its severing activity and filament cleavage<sup>62</sup>. Finally, ROCK, amongst other kinases, also phosphorylates and activates MyoII leading to its contractile activity<sup>75,88</sup>. This shows how Rho and its regulators are potent modulators of MyoII contractility.

I will now review the mechanisms of Myosin activation and force production specifically in the context of apical constriction.

### *3.1.2. Myosin motors*

#### 3.1.2.1. How do they produce tension with actin?

Myosins are a family of actin-dependent molecular motors<sup>89</sup>. While the family contains several isoforms, I will only focus on non-Muscle Myosin II (MyoII or NMII) as it is the most prevalent in providing constriction during morphogenesis events<sup>90</sup>. MyoII comprises 3 pairs of peptides: 2 heavy chains (MHCs), 2 regulatory light chains (RLCs) responsible for the regulation of MyoII activity & essential light chains (ELCs) (**Figure 11**). These fold into a hexamer with head, neck, and tail domains. The globular head contains the ATP & actin-binding sites which are essential to provide the motor function. ATP binding allows MyoII to bind actin filaments. When ATP is hydrolysed, the release of the Phosphate (Pi) triggers a conformational change leading to actin sliding. The neck region allows the amplification of head rotation upon Pi release (**Figure 11**). Then ADP is discharged which leads to the dissociation of MyoII from actin. Finally, the tail is made of a coiled-coil domain forming a helix and is necessary for the formation of dimers which form MyoII motors (**Figure 11**)<sup>91</sup>. This tail region is also necessary to form bipolar myosin filaments<sup>92</sup>. Indeed, single MyoII motors produce very little force on their own. Because of their opposite polarity, bipolar filaments are more processive than single dimers when pulling on antiparallel actin filaments<sup>93</sup>.

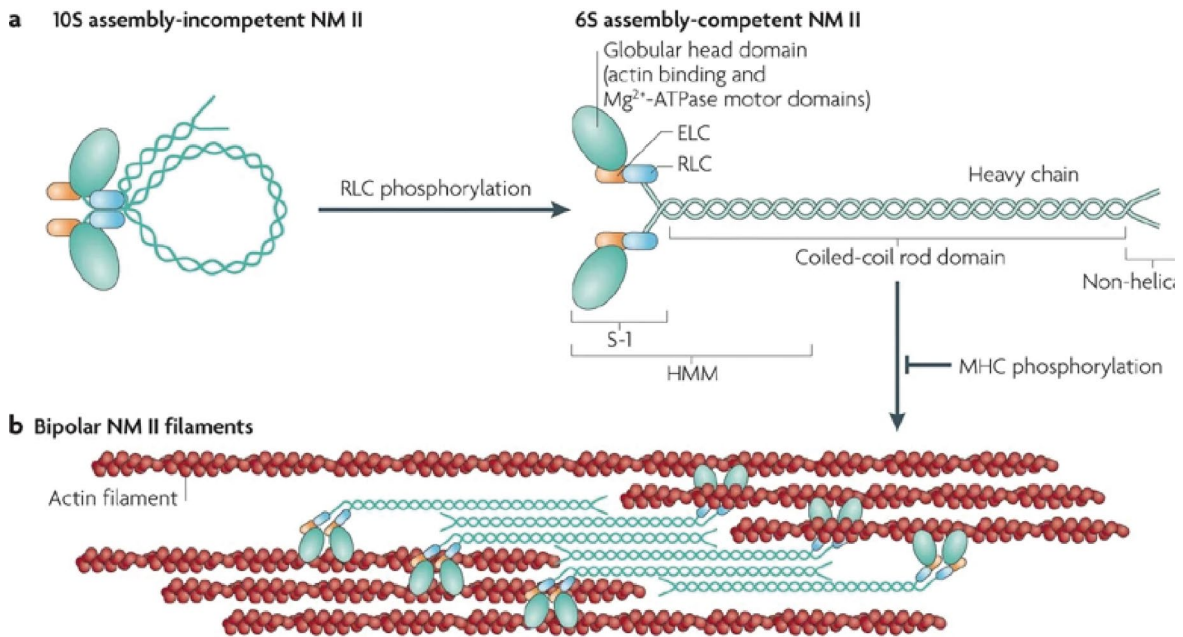


**Figure 11** - Myosin motors. (a) closed and inhibited MyoII conformation. (b) Phosphorylation leads to the opening of MyoII in a form competent to assemble in MyoII mini filaments. (c). MyoII can assemble in bipolar MyoII mini filaments which are more efficient for contraction than MyoII single filaments. Adapted from<sup>92</sup>.

MyoII functions together with actin to form a contractile network. The viscoelasticity of that network is an emerging property of the interactions between motors, actin and crosslinkers. MyoII increases fluidity when the network is weakly crosslinked. Conversely, crosslinking rigidifies the system by reducing the degrees of freedom in the network<sup>94</sup>. MyoII pulling on such a network will only increase its stiffness. As a result, elasticity dominates upon fast deformations while on longer time scales, the network's remodelling and turnover result in a more viscous behaviour<sup>75,83,89</sup>. This is key to the understanding of apical contractility as the stiffness and organization of the network together with the length scale of deformations lead to different contractile dynamics: pulses or rings of actomyosin.

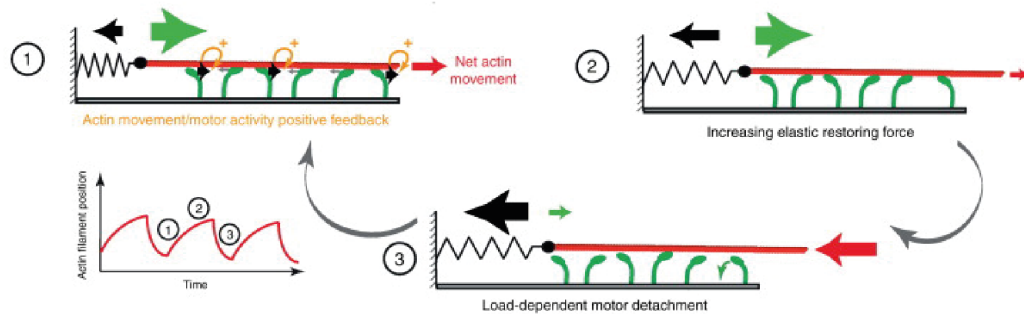
### 3.1.3. Different organisations of actomyosin

#### 3.1.3.1. Pulses & flows

Actomyosin networks exhibit very complex dynamics which can engender flows in the network<sup>95,96</sup>. The formation of cortical flows depends on the number of crosslinkers in the network and the turnover of the network's constituents. Moreover, they require the presence of a gradient of contractile activity. For example, the entry of sperm into the zygote of *Caenorhabditis elegans* locally inhibits contractility. This locally destabilises

the actomyosin network. This asymmetry then leads to a gradient of tensions that initiates actomyosin flow toward the anterior side<sup>97</sup>. Such flow can be sustained through tension-dependent mechanisms. For instance, self-organized *in vitro* actomyosin networks show examples of contraction-dependent actin turnover<sup>98</sup>. F-actin depolymerisation is locally promoted and supplies a constant G-actin pool and subsequent repolymerisation, therefore, enforcing the tension gradient (**Figure 12**).

**(a) pulse generation from elastic feedbacks**



**(b) MyoII-dependent actin depolymerisation**

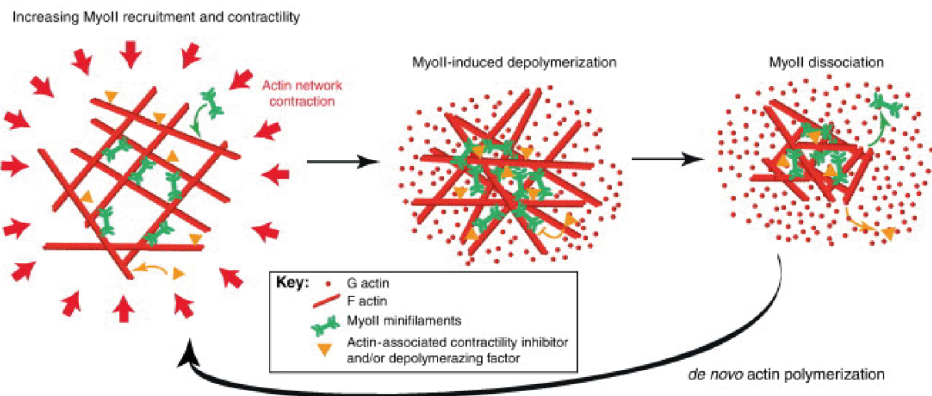


**Figure 12** - Mechanisms of pulse generation. (a). Several MyoII motors (green) bind F-actin (red) and pull on it (Green arrow is the force generated by multiple motors pulling on actin - 1). The actin filament is stabilised thus MyoII pulling generates an elastic force constraining the movement (2). This elastic force (black arrow) acts as negative feedback and the motors detach from the filament which therefore moves backward (3) (b). MyoII is recruited to an actin network and reorients actin resulting in positive feedback. Contractility increases generating an inward flow of MyoII. This increase together with tension increase in turn leads to MyoII-induced depolymerisation and subsequent MyoII dissociation (negative feedback). New actin monomers allow the process to repeat. Adapted from<sup>75</sup>.

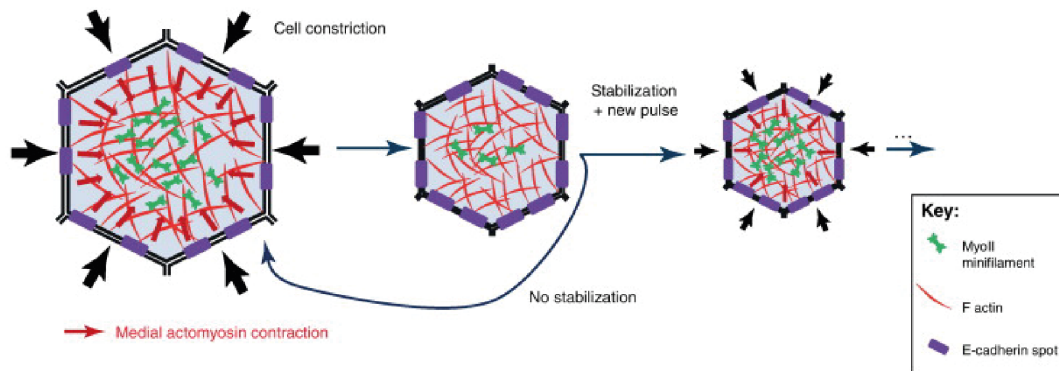
However, how contraction flows are initiated in branched networks is unclear. It seems that the polarity is not necessary for contraction<sup>99</sup>. Thus, less ordered/polarised actomyosin networks could generate cortical tension upon the action of myosin motors. Local heterogeneities could be enough to drive the initiation of myosin foci surrounded

by F-actin. This would then be sustained as flow themselves promote actin bundling and polarization of the network<sup>100</sup>.

Such flows can happen in distinct pulses and have been reported in many cases to drive apical constriction<sup>42,101–103</sup>. Apical constriction during mesoderm invagination in *Drosophila* happens through a sequence of medio-apical pulses of myosin separated by stabilisation periods (**Figure 13**)<sup>42,104,105</sup>. Reducing F-actin turnover impairs these pulses. This enforces how F-actin turnover is important for pulses/flows generation<sup>79</sup>. These pulses are organized by a medio-apical radial polarity pathway in which we find foci of RhoA and ROCK at the centre of the cell (**Figure 4**). Conversely, ROCK is excluded from the AJs and therefore drives specific activation of MyoII at the centre of the cell. On the other end, Diaphanous, which drives actin polymerisation, is localised at the AJs<sup>104,105</sup>. This seems to be important for coupling the cortex with the junctions to drive deformations. Interestingly, these cells seem to exhibit cortical actomyosin flows prior to deformation. Similarly, during *C. elegans* gastrulation cells exhibit constitutive inward-directed flows. However, they don't produce deformation unless it is coupled to AJs<sup>96,106</sup>. The transition from a continuous signal to a pulsed signal often results from negative feedback. These can be diverse. In the case of pulsed contractions in the early *C. elegans* embryo, RhoA begins to accumulate in foci before actin and MyoII. Actin accumulation in turn recruits with a delay RGA-3/4 a Rho-GAP. This inactivates RhoA and results in negative feedback that terminates the pulse.

Actomyosin pulses can also emerge from the collective activity of motors on an elastic material. In this case, the negative feedback can emerge from tension-dependent mechanisms resulting from the material being elastically coupled to its environment (**Figure 12**)<sup>107–109</sup>. For instance, in *Drosophila* follicles, strengthening actomyosin attachment to the extracellular matrix provides increased tension in the network. This results in an increased delay between pulses during Follicle elongation<sup>101</sup>. Similarly, during dorsal closure, a supracellular actomyosin ring surrounds the amnioserosa. This provides resistance to the pulsatile amnioserosa cells necessary for the closure<sup>103,110</sup>. Finally, such pulses were recently thought to promote cell extrusion in epithelial tissues in zebrafish or during neuroblast formation in *Drosophila*<sup>111,112</sup>.

### (a) actomyosin pulses during mesoderm invagination



### (b) ratchet mechanism

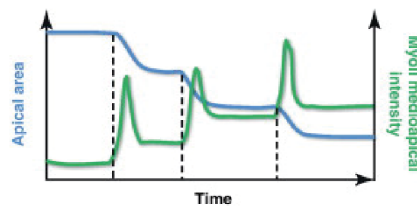


**Figure 13** - Actomyosin pulses during endoderm invagination. (a). A branch actin network (red) supports the formation of actomyosin pulses (MyoII in green). These pulses precede the changes in the apical area. Once they are attached to the junctions through E-cad, these pulses produce deformation. A sequence of contraction through actomyosin pulses and relaxation leads to a stepwise reduction of cell apical area leading to tissue bending and mesoderm invagination. (b) Schematic evolution of apical area over time due to the sequence of MyoII pulses and relaxation. Overtime average MyoII medioapical intensity tends to increase. Adapted from<sup>75</sup>.

#### 3.1.3.2. Rings & belts

Very often the actomyosin pulses and ring co-exist in epithelial cells<sup>42,113</sup>. Such rings (**Figure 14**), rely on bundled networks of antiparallel actin filaments as in the case of cytokinesis<sup>95,114</sup>. Indeed, such bundled networks are thought to be more efficient to drive constriction<sup>102</sup>, although such architecture is not necessarily required. Classical studies of neural tube closure in vertebrates highlight the role of actomyosin junctional rings<sup>35</sup>. Myosin pulls on antiparallel actin filaments, therefore, reducing the distance between them. This led to the purse-string model. Indeed, isotropic constriction resembles the closure of a purse-string (**Figure 14b**)<sup>35</sup>.

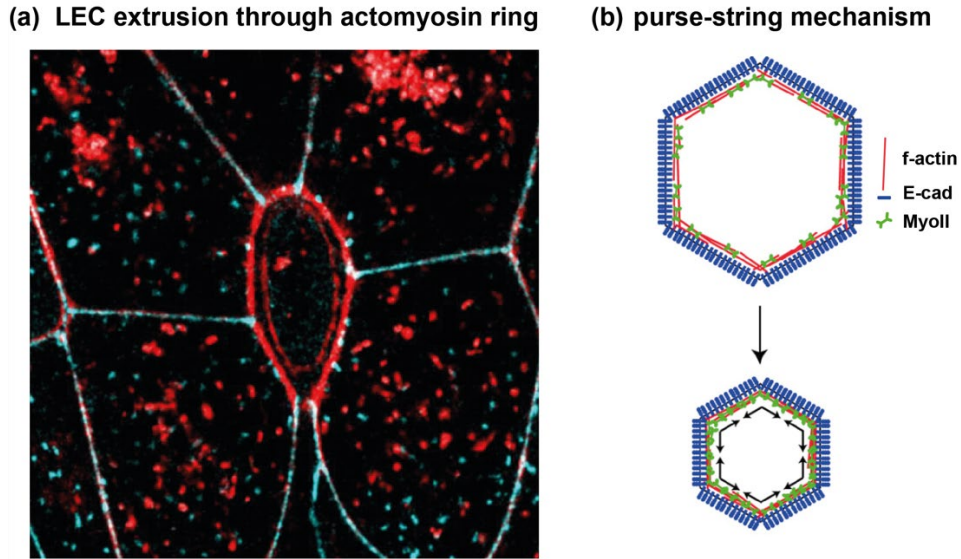


**Figure 14** - actomyosin ring. (a) Internal and external actomyosin ring drive LEC extrusion during abdominal morphogenesis in *Drosophila*. These rings constrict the cell following a purse-string mechanism. (b) The purse-string mechanism leads to the shrinkage of the cell through the progressive constriction of actomyosin belt/ring at the AJs. Adapted from <sup>37</sup>& from<sup>48</sup>.

As in the case of apical pulses formation, the location of upstream actomyosin activators is important to localise the ring to the AJs. In the case of vertebrate neural tube closure, Shroom3 targets actomyosin to the apical cell circumference in a Rho-dependent manner<sup>19,41,103</sup>. Both Shroom3 and RhoA bind ROCK (although their exact cooperation is unclear<sup>103</sup>), which in turn activate MyoII at the AJs leading to cell apical constriction. Finally, as for pulses, more examples of such purse-string mechanisms were shown to be leading to the extrusion of cells from epithelial tissue in *Drosophila* Larval Epithelial Cells or epithelial MDCK cultures<sup>104,105</sup>.

**Conclusion: Take-home messages.**

Cell apical constriction results from very complex and dynamic layers of regulations of the actomyosin cortex, which are not fully understood and to some extent still debated. However, one clear emerging property is the viscoelasticity of this network, which is key to its function. On rapid deformations, it is elastic because it stores energy due to the many entanglements and absence of turnover. Conversely, when stresses are applied for several minutes, viscosity in the network appears dominant because of the turnover of its components. To make it clear to the reader, one can explain the emergence of this property through the following:

- Effect of filament size: short filaments are rigid while long filaments bend more. As a result, they move less leading to a stiffer network.
- Effect of turnover: The more turnover, the more fluid and plastic the network is leading to deformations.
- Effect of network density & connexion: the more crosslinker there are, the stiffer the network is. Bundles are actin filaments crosslinked in fibres. Meshes are actin filaments crosslinked in branches.
- Effect of MyoII: MyoII is a motor which brings together fibres leading to constriction. This activity increases fluidity on a lowly crosslinked network but stiffens more crosslinked networks.



## 3.2. Adhesion: the role of E-cadherin

Ultimately, epithelial morphogenesis relies on the modulation of cell-cell junctions. To produce deformations, specifically during apical contractility, the actomyosin cortex needs to be linked to AJs. Indeed, it is their remodelling upon stress production by the actomyosin cortex which leads to cell apical shrinkage<sup>106</sup>. As we have discussed in the first part of this chapter, epithelial cells are tightly linked to each other through the role of many adhesion molecules. In the following section, I will only cover the role of E-cadherin (E-cad) adhesions. The reasons are two folds. First, we focus on apical contractility and as such, we exclude the role of non-apical adhesion molecules. Although they certainly have a role during morphogenesis. Second, AJs are the most prevalent apical junctions and force transducer in epithelia.

### 3.2.1. E-cad structure

Cadherins are a superfamily of glycoprotein mediating adhesion in most animal cells. E-cad is considered a “classical” member of that family. It was discovered in epithelial cells and is the most represented cadherin in that type of tissue. It is a transmembrane protein, and its extracellular part is made of 5 EC (Extracellular Cadherin) domains conserved amongst cadherin<sup>115</sup>. EC domains are separated by linkers which bind  $\text{Ca}^{2+}$ <sup>107</sup>.  $\text{Ca}^{2+}$  binding induces conformational changes and results in a typical angle between EC domains. This rigidifies E-cad curvature into a crescent shape (**Figure 15**). The resulting angle between EC1 and EC5 is about  $90^\circ$  and is key to the *trans* interactions<sup>108</sup>. Indeed, these domains then form *trans* heterodimers from the surface of two juxtaposed cells which mediates adhesion.

What triggers the formation of mature AJs remains unclear. Two conflicting models are possible. The first one proposes that *trans* heterodimers form through the binding of their most distal EC1 domains. This model requires the formation of additional *cis* interactions between E-cad ectodomains which were never observed in solution. The second one proposes that they interact in *trans* through the entirety of their EC domains. It is based on the observation of multiple adhesive states *in vitro* which doesn't fit with the first model<sup>109</sup>. Nonetheless, in its final conformation, E-cad is found to form both *cis* and *trans* interactions in AJs. Indeed, *cis* oligomerization has been shown to mediate the lateral assembly of already formed *trans* dimers. This could account for the multiple adhesive states previously observed and resolve the discrepancies between these two models<sup>116,117</sup>. Finally, in non-mature epithelia, E-cads are found in punctate junctions

which later resolve into linear junctions at the circumference of the cells. It is not clear if the latter emerges from a continuous array of E-cad junctions or from an ensemble of punctate junctions<sup>116</sup>.

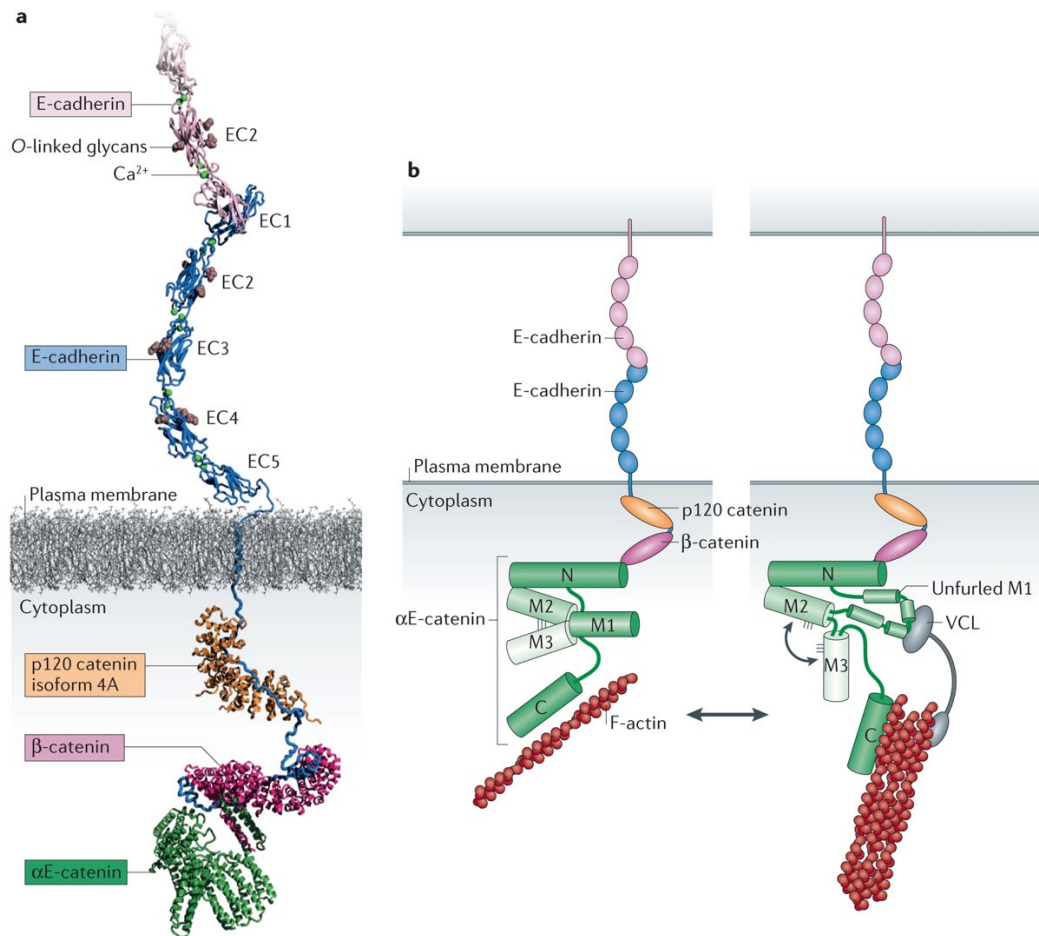


**Figure 15** - Ecad structure and adhesion. (a) E-cad structure represents the 5 EC domains and intracellular binding to the CCC complex. Note the curved extracellular domain due to the binding of  $Ca^{2+}$ . (b) E-cad association with the actomyosin network.  $\alpha$ -catenin can bind actin through its C-Ter domain (left). Upon tension on  $\alpha$ -catenin, cryptic domains are exposed which allows binding of VCL. VCL in turn binds to actin. This interaction increases adhesion upon tension. Adapted from<sup>117</sup>.

### 3.2.2. *E-cad dynamics & interactions with the actomyosin cortex*

The generation of forces by the actomyosin cortex would tend to weaken or disrupt E-cad adhesion. Indeed, mature forms of E-cad adhesions, present in AJs, are thought to show slip-bound behaviour when put under stress<sup>118</sup>. This suggests that some mechanisms strengthen adhesion in response to contractility. This may emerge from the fact that in cells, E-cad is part of a complex and doesn't mediate adhesions on its own (**Figure 15**). E-cad cytoplasmic domain binds to p120-Catenin and  $\beta$ -catenin which in turn binds  $\alpha$ -catenin. This forms the Catenin Core Complex (CCC) which is essential to mediate its interaction with actomyosin.  $\alpha$ -catenin, by its C-Ter domain can bind F-actin<sup>119</sup>. This

binding favours the formation of unbranched actin bundles and contributes to the organisation of AJs. Moreover, this interaction is key to increase adhesion strength upon stress. However,  $\alpha$ -catenin doesn't function alone and the CCC is thought to interact with actin filament through Vinculin instead of  $\alpha$ -catenin.  $\alpha$ -catenin uses its M1 domain to bind Vinculin which in turn binds to actin filaments.<sup>120</sup> The M1 domain is a cryptic domain which is hidden in the absence of forces. Tensile forces pull  $\alpha$ -catenin C-Ter and open  $\alpha$ -catenin which enables its binding to VCL<sup>121</sup>. This process is called a catch-bond as tension leads to stronger adhesions. Furthermore, this complex also reinforces AJs in response to forces through the stabilisation of E-cad and the formation of E-cad clusters in a Rho-dependent manner<sup>122</sup>. Taken together, this shows how adhesion-cortex interaction can modulate both the cortex dynamics and adhesion strength.

AJs stability is also modulated by E-cad turnover. p120-catenin is thought to be one of the main mediators of E-cad turnover (**Figure 15**). Inhibition of p120 increases the internalization of E-cad in a Clathrin-dependent manner. Therefore, p120 inhibits E-cad internalization/turnover. Counterintuitively, this endocytosis is key for the function of E-cad. First, inhibiting turnover inhibits the formation of new AJs. Second, this dynamic process of turnover leads to enhanced plasticity of Ecad and subsequent contractility. Ultimately, the binding of the cortex to cadherin allows forces emerging at the cell level to be transformed into supracellular forces.

### *3.2.3. Role in morphogenesis*

As mentioned in the first part of this chapter, E-cad is a key component during folding as it allows the transmission of forces across multiple cells like during mesoderm invagination<sup>49-51</sup>. Indeed, it is only when E-cad is coupled to internal actomyosin pulses that these pulses become efficient to apically constrict cells and lead to mesoderm invagination. More generally, E-cad and MyoII mutual regulations are key in shaping cell apical area in morphogenetic processes. First this interaction is fundamental during the biogenesis of the junction. In MCF-7 cells, the recruitment of MyoII at the junction is an E-cad-dependent process that requires E-cad activity. Conversely, inhibiting of MyoII activity by blebbistatin lowers E-cad recruitment at the junction. This results in lower adhesion in these cells. Therefore, MyoII is required to concentrate E-cad at the junctions while E-cad is necessary to localise MyoII at the junctions<sup>122</sup>. Ultimately, this may depend on the ability of E-cad to localise modulators of MyoII activity such as ROCK, RhoGEF or RhoGAP. Indeed, still in MCF-7 cells,  $\alpha$ -catenin through its

interaction with centralspindlin recruits a RhoGEF to the AJs.<sup>123</sup> This ultimately supports E-cad stability by modulating MyoII activity through Rho. This seems to be a general mechanism in epithelial cells because Rho is similarly increased at the AJs of MDCK-II cells<sup>124</sup>. Conversely, centralspindlin also excludes Rho such as RhoGAP from the AJs<sup>123</sup>. Thus, AJs through E-cad act as a platform for Rho modulators. The balance between activators and inhibitors ensures correct MyoII contractility which may ultimately influence apical constriction. The regulation of MyoII at the junction is mediated by Rho Kinases. In MCF-7 cells, the inhibition of ROCK phenocopies the inhibition of MyoII activity and lowers E-cad concentration at the junctions<sup>122</sup>. Finally, neural tube formation relies on the localisation of Shroom3 to the apical side of neuroepithelial cells. Shroom3 in turn recruits ROCK to the AJs which induces MyoII contractility<sup>23</sup>. Ultimately this apical recruitment may be regulated by p120-catenin. Indeed, it has been shown to localise both Shroom3 and ROCK at the AJs<sup>125</sup>.

Alternatively, MyoII affects the stabilisation of E-cad which equally affects morphogenesis. Germband elongation in *Drosophila* is a process that relies on convergence-extension through the radial intercalation of cells. Junctions in the dorso-ventral (DV) axis are predominantly shrunk which biases the direction of elongation<sup>126</sup>. E-cad levels regulates actomyosin contractility in this process. Therefore, initial asymmetries of E-cad levels in DV junctions leads to the formation of MyoII flows toward regions of enriched E-cad. E-cad levels then fluctuate between the two facing DV junctions because of E-cad endocytosis. Interestingly, this is enhanced by MyoII flows which induce E-cad disassembly<sup>126</sup>. Interestingly, the effect of MyoII on E-cad stability depends on the direction of applied MyoII stresses on E-cad<sup>127,128</sup>. Indeed, medio-apical MyoII contractility applies tensile stresses on E-cad which leads to its stabilisation. Conversely, junctional MyoII contractility exerts shear forces because of its uneven distribution between different junctions which ultimately leads to E-cad disassembly<sup>128</sup>. This was recently tested in caco-2 cells<sup>129</sup>. RhoA activation in a gradient through optogenetics led to asymmetric junction constriction. RhoA increased friction through E-cad recruitment and stabilisation where it was the most enriched. At the opposite of the gradient, E-cad was destabilised, and the vertex could constrict thus leading to uneven junction contraction.

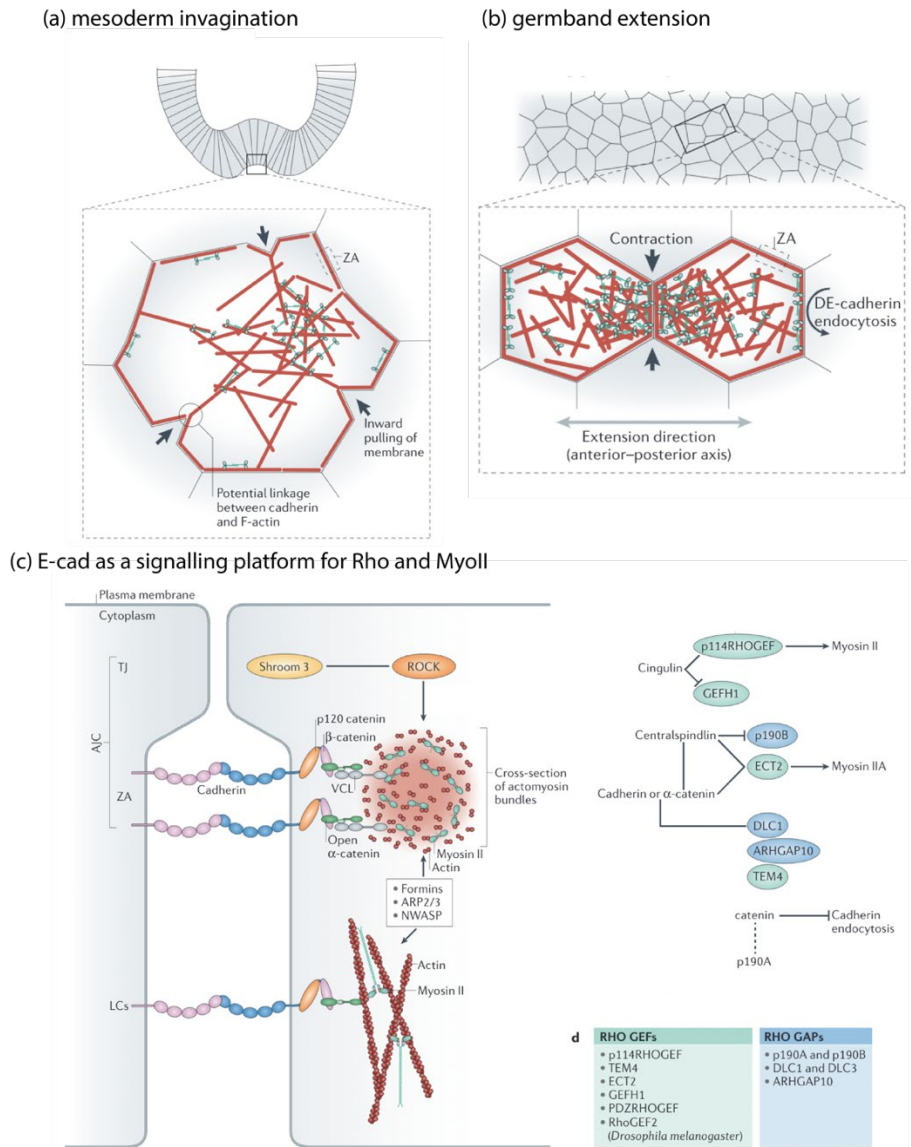


**Figure 16 - E-cad influence on morphogenesis.** (a) MyoII internal pulling forces are coupled to E-cad which ultimately drives apical constriction. The coupling between cells leads to the transmission of forces which ultimately induces tissue bending (not shown). (b) Local instability in E-cad levels drives actomyosin flows toward the junction with highest E-cad levels. This induces junction contraction along a preferred axis and drives convergence extension. (c) E-cad as a platform for Rho localisation and signalling. P120 localise apically both Shroom3 and ROCK. Shroom3 is also key to localise ROCK apically which leads to RhoA activation and localised myoII contractility necessary to drives neural tube formation. Right: blue is all RhoGAP localised at E-cad junctions and Green is all RhoGEF at E-cad junctions. Many examples are not explicated in the text and are here for illustrational purposes. Adapted from <sup>117</sup>

Finally, during cell extrusion, E-cad is necessary to mediate mechanotransduction. For instance, during cell extrusion: a remodelling process leading to cell elimination from an epithelium. Indeed, first, the extruding cell becomes highly contractile. This generates forces which are transmitted to its neighbours through E-cad. This in turn leads to RhoA activation in the neighbours to further proceed to the expulsion of the extruding cell<sup>130</sup>.

This process is regulated by the E-cad-dependent recruitment of S1P which is necessary to modulate the F-actin network<sup>131-133</sup>.

**Conclusion: Take-home messages.**

E-cad is an instrumental modulator of cell shape changes. On one hand, it mediates cell adhesions between juxtaposed cells which tends to increase the contact area and resists contractile forces. On the other hand, through these adhesions, E-cad allows force transmission to neighbouring cells to transform individual cell deformations into tissue-wide forces. Such adhesions are then actively reinforced through E-cad interactions with the cortex or through E-cad clustering. Finally, in turn, E-cad regulates the stability of the actomyosin network by modulating its polymerisation and activation. Together this modulates epithelial cell shape changes.

### 3.3. Microtubules and mechanics

In the previous part I have describe how actomyosin networks have emerged in the literature as the main drivers of cell shape changes. Microtubules (MTs) on the other hand, are cytoskeletal elements which were initially thought to be implicated in functions such as chromosome separation during cytokinesis, transport & cilia formation<sup>134</sup>. Recently, however, MTs have increasingly raised attention regarding shape regulation<sup>55,56</sup>. They show multiple crosstalks with actin, like crosslinks, anchoring & mechanical support. Here I will describe microtubule dynamics and I will illustrate their role in morphogenesis either through their interaction with the actomyosin cortex or through what appears to be autonomous activity.

#### *3.3.1. Microtubules dynamics and polymerisation*

Microtubules (MTs) are made of protofilaments, themselves constructed by the polymerisation of  $\alpha\beta$ -tubulin heterodimers (**Figure 17**)<sup>134-136</sup>. Their polymerisation is regulated by the hydrolysis of GTP and results in a polarized protofilament with  $\beta$ -tubulin exposed on one side (+ end), and  $\alpha$ -tubulin exposed on the other end (- end). 13 protofilaments are then arranged in a hollowed helix and held together through lateral interactions in a structure called the microtubule<sup>134</sup>. Because of its crystal-like structure and by analogy with metals it is often referred to as MTs 'lattice' (**Figure 17**). In a process akin to the polymerisation of actin, the GTP hydrolysis is delayed in time during polymerisation. Therefore, the internal asymmetry is transposed at the level of the MT. The GTP-cap is close to the +tip and the GDP-island is found toward the minus end. GTP hydrolysis leads to conformational changes of  $\alpha$ -tubulin and allosteric changes in the lattice affecting lateral interactions. This produces a gradient of stability from the plus-end to the minus-end. The latter is thus associated with less stable GDP-bound tubulin responsible for MT dynamics instability. While MTs treadmilling and dynamic instabilities were initially debated<sup>137</sup>, treadmilling has emerged as a consensus mechanism for the description of MT dynamics. Indeed, in the presence of the GTP-cap, MTs polymerise. However, when it's lost it leads to shrinkage and repolymerisation events called catastrophe and rescue (**Figure 17**). Additionally, while both ends can grow, the minus-end grows slower and seem to undergo less catastrophe<sup>134,135,138</sup>.

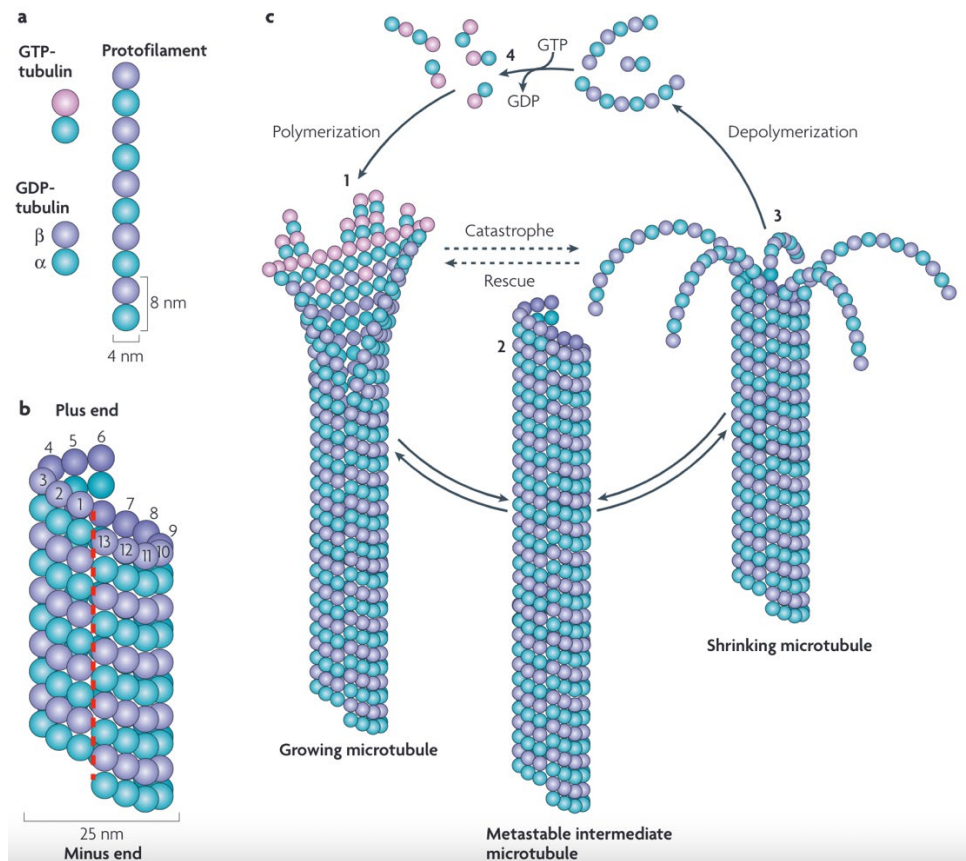


**Figure 17** - Microtubule structure and dynamics. (a).  $\alpha$  &  $\beta$ -tubulin assemble in heterodimers that are the basis of Microtubules (MTs). Heterodimers then assemble in protofilaments. These protofilaments are asymmetric with one end preferentially associated with GTP and the other with GDP (b) 13 protofilaments assembled into MTs in a helical shape. MTs are also asymmetric with a plus end and a minus-end (c) Dynamic instabilities of MTs. New dimers preferentially associate with MT plus end because of its GTP cap (1) and result in metastable MTs (2). Loss of the GTP cap leads to depolymerisation (3). GDP is replaced by GTP (4) and new dimers become potent to assemble in MT in a process called rescue. Adapted from<sup>135</sup>.

To follow the analogy with actin networks, MTs are embedded in a network with multiple Microtubule Associated Proteins (MAPs) in arrays emerging from Microtubules Organizing Centres (MTOC). Moreover, they also interact with their own motors (Dyneins & kinesins). Therefore, MT dynamics and stability is regulated by proteins that convey similar function to that described previously for actin<sup>136,138</sup>. I will therefore quickly describe 4 types of MAPs: +tips binding, EB (End-Binding protein), motors, and minus-end bindings proteins (**Figure 18**).

First, we find protein binding specifically to the +tips of MTs. Among them XMAP215 or CLASPS promote polymerisation (**Figure 18a**). XMAP215 are polymerases, they function in a way like Formins on actin. They move processively with MTs and locally recruit tubulin dimers thus increasing tubulin addition<sup>139</sup>. CLASPs (Clip Associated Proteins) achieve similar results by suppressing catastrophe. They also bind



to +tips and promote MTs growth by recruiting tubulin dimers. Together they help to promote MT polymerisation.

End-Binding proteins are very potent regulators of MT polymerisation due to their binding to both growing MTs ends. They mostly tend to depolymerise MT in vitro (certainly due to their capping function)<sup>140</sup>. However, they result in a mild increase in polymerisation rates in vivo. This is certainly because they inhibit the binding of kinesins that are more potent depolymerases (**Figure 18b**)<sup>141,142</sup>. For instance, Kinesin 8 removes terminal subunits from MT ends by walking to the + end which destabilises the GTP-cap. Other motors like Dyneins are minus-end directed motors. However, they can also bind to the plus-end and exert pulling forces which ultimately reduces MT polymerisation. Of note, there are severing proteins like Katanin and Spastin which can directly cut the MT lattice<sup>143</sup>.

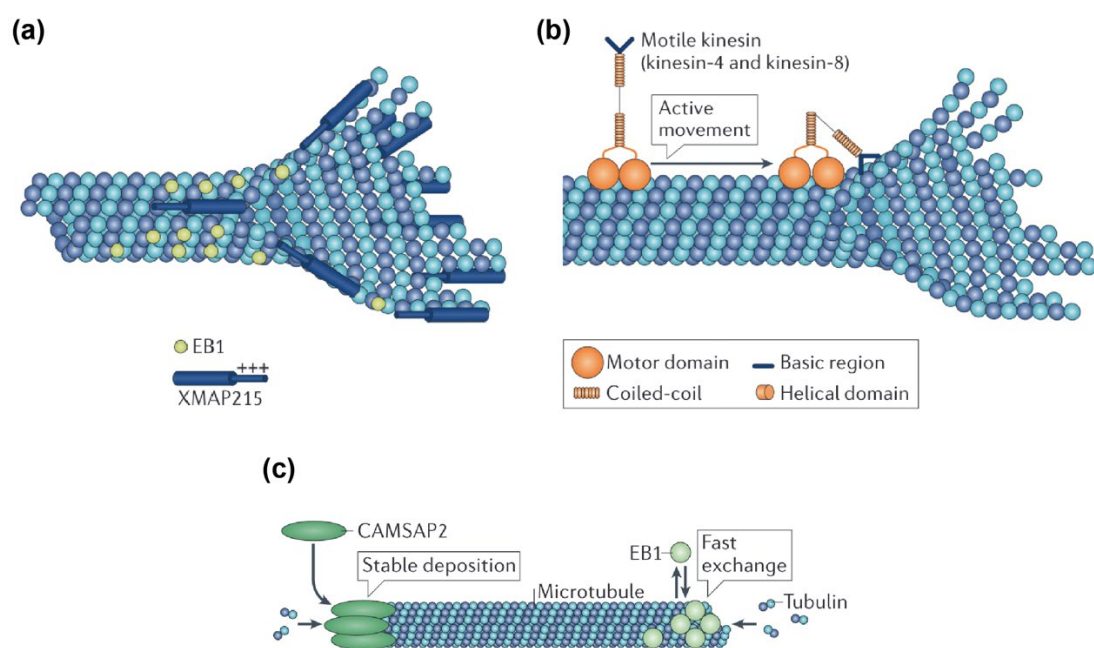


**Figure 18** - Microtubule interactors. (a). Plus-tip associated proteins tend to favour polymerisation by protecting MT plus end (b). MTs motors. MTs motors like kinesin-8 can remove dimers by walking on MTs. (c). End-associated proteins. CAMSAP is a minus-end binding protein that promotes polymerisation by stabilising GDP associated minus-end. EB1 is a plus-end binding protein that promotes polymerisation. Adapted from<sup>135</sup>.

MTs don't polymerise alone, they are embedded in a network. Therefore, On the other hand of the spectrum are MTs minus-end binding factors (**Figure 18c**). Such factors are key in the organization of MTs. As such, they have often been termed Microtubule Organizing centres (MTOC). The main known minus-end factor is the  $\gamma$ -tubulin ring

complex ( $\gamma$ -TURC<sup>144</sup>). It mostly nucleates MTs and caps the minus-end of preformed MTs. It lies at the core of the nucleation complex leading to the centrosome formation (the most prevalent MTOC). Additionally, the  $\gamma$ -TURC complex can be recruited to the MT lattice by Augmin. This leads to crosslinking and results in the formation of branched MT sarrays<sup>145</sup>. Alternatively, CAMSAP or Patronin in *Drosophila* binds MT minus-end independently of  $\gamma$ -tubulin (**Figure 18c**). This binding stabilises MT in non-centrosomal organizing centres<sup>143,146-148</sup>. Interestingly, both non-centrosomal MTOC and centrosomes can be localised apically in epithelial cells. For instance, Ninein binds  $\gamma$ -TURC and re-localises the centrosome at the apical sides of epithelial<sup>149</sup>. On the other hand, Patronin-protected MTs can be localised to AJs<sup>150</sup>. This highly suggests that they might play a role in epithelial shape regulation or that they define the polarity and AJ position of the cell<sup>8</sup>.

Therefore, the balance between microtubule polymerisation and depolymerisation is precisely regulated. The function of these proteins is reminiscent of those that regulate actin. Similarly, microtubules are nested in a network whose architecture affects their function in morphogenesis. Thus, I will now describe their function in morphogenesis, starting with their interaction with the cortex.

### 3.3.2. Interaction with the actomyosin cortex

One way for MTs to mediate cell shape changes is through their interactions with the actomyosin cortex<sup>151,152</sup>. Some crosslinkers like Spectraplakins or GAS2 allow MTs to bind actin directly through actin-binding domains hence resulting in a co-alignment directing MTs growth (**Figure 19a**)<sup>153</sup>. A similar outcome is achieved through Myosin motors. For instance, Myosin-V transports MTs plus end along actin in an EB1-dependent manner which leads to co-alignment<sup>135</sup>. Additionally, actin-binding proteins such as mDia stabilise MTs during cell migration by binding directly to microtubules (**Figure 19b**)<sup>154</sup>. Therefore, MTs plus ends interact with the cell cortex in very diverse manners. In turn, MTs can respond to the cortex. The local force exerted by retrograde actomyosin flow can lead to MT catastrophe at the cortex (**Figure 19c**). This blocks local MT polymerisation at the edge of the cell<sup>137</sup>. However, this seems to be context dependent. Indeed, conversely, Dynein bind MT + end leading to force generation and consequent MT network positioning<sup>155</sup>.

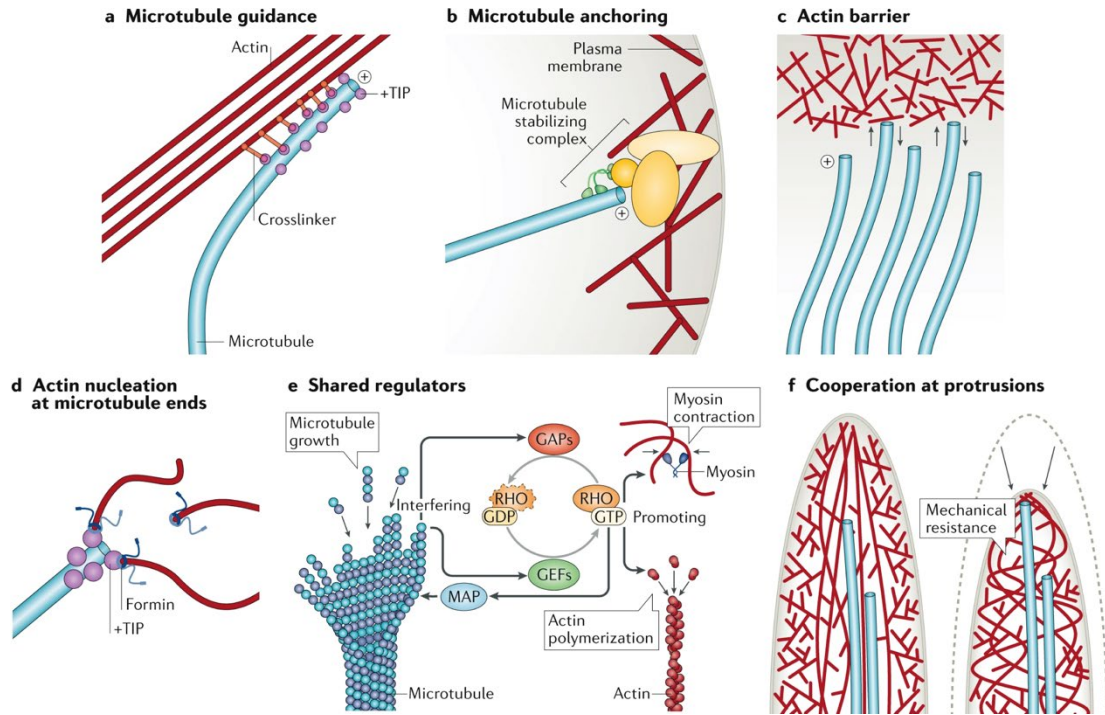


**Figure 19-** MT affects cell morphogenesis through interactions with the actomyosin cortex. (a) The actin network provides a guidance for MT growth through the action of common crosslinkers such as spektraplakin. (b) the actomyosin cortex can form stabilising complexes. (c) The actin and myosin cortex can also exert retrograde flows. In this case, MT respond to the interaction with the cortex which triggers local depolymerisation of MTs. (d) The minus-end can impact the actin network by the interaction with actin nucleators at MT ends. (e) Microtubules and actomyosin share common regulators. (f) These mechanisms can be used in different ways to produce forces. At lamellipodia ends MT provide mechanical resistance that promote the growth of lamellipodia. Adapted from<sup>151</sup>.

Such interactions can be co-opted in various manners to generate forces and modulate epithelial cell morphogenesis. In epithelial cells, MTs minus ends can be localised apically through the means of non-centrosomal MTOC<sup>156,157</sup>. Spectraplakins complexes, or in fly the Short Stop (Shot) and Patronin complexes stabilise MTs minus-end<sup>157-161</sup>. This results in MTs that span the apicobasal axis of the cell. Such a MT pool is necessary for apical constriction in various epithelial cells like in the primordium of the *Drosophila* placode or during neural tube formation<sup>40,44</sup>. Disrupting Patronin in the salivary gland placode cells inhibits actomyosin pulsatility and subsequent cell wedging<sup>162</sup>. Similar results are obtained in cells undergoing mesoderm invagination in *Drosophila*<sup>51</sup>. In these cells, Patronin mediates the connexion between the medioapical actomyosin pulses and AJs. Therefore, inhibiting Patronin results in the alteration of mesoderm invagination. Although in that case it doesn't affect apical contractility directly. Furthermore, in *Xenopus*, depolymerisation of apicobasal MTs through nocodazole inhibits apical constriction and bottle cell morphogenesis<sup>163</sup>. MTs are also critical during subcellular wound healing in *Xenopus*. They are transported by actin flows toward the wound and

form a radial array around it. At the wound edge, MTs buckle and break due to high actomyosin contraction whereas MTs away from the wound polymerise toward it<sup>164</sup>. Interestingly, this interaction with actin is reciprocal. Inhibiting MTs before wounding impairs purse-string formation. Conversely, disrupting MT after the formation of the actomyosin ring accelerates purse-string contraction<sup>165</sup>. These observations were reproduced in reconstituted actin-myosin-MT networks, in which MTs enable self-organization of the system's contractile activity<sup>166</sup>. MT provide flexural rigidity to the network by its connexion with actin which reduces constriction. Accordingly, networks without MTs undergo more efficient contraction compared to similar networks containing MTs.

The other way for MTs to interact with the actomyosin cortex is through shared regulators (**Figure 19e**). MTs tips concentrate Rho-GTPases, GEFs and other kinases which also regulate actin polymerisation and MyoII activation. The binding of EB1, Rho-GEFs and a neuron-specific protein can lead to neurites extension or to push on the membrane to produce protrusions<sup>151</sup>. Yet, the interactions of MTs with GEFs are incompletely understood. In the case of cytokinesis, contractile ring formation is promoted by MTs, but astral MTs suppress Rho everywhere else<sup>155</sup>. Similar regulation of junction contraction happens during germband extension and mesoderm invagination where specific Rho-GEFs regulate MyoII under the control of MTs. Indeed, EB1 binds RhoGEF2 at the plus tips of medioapical MTs leading to its sequestration from the AJs. In normal conditions, the peptide Fog binds to the GPCR Mist. This activates Concertina which in turn recruits T48. Through its PDZ domain, T48 releases RhoGEF2 from MTs (reviewed here<sup>15</sup> & here<sup>20</sup>). This specifically activates Rho1 (and therefore MyoII) at the medioapical domain but not at AJs. Indeed, another Rho-GEF (Dp114RhoGEF) is localised at AJs where it activates Rho1 signalling. Accordingly, Colcemid-dependent MTs depletion leads to RhoGEF2 ectopic release. This triggers MyoII activation in the medioapical region, MyoII inhibition at the AJs and subsequent germband extension defects<sup>167</sup>.

Furthermore, during cell extrusion, neighbouring cells exhibit a directional MTs polymerisation toward the extruding cell in response to its constriction. This allows the release of p115 RhoGEF at the junction with the extruding cell and consequently mediates the formation of a supracellular actomyosin ring<sup>168</sup>. Ultimately, the basal or apical orientation of MTs in this context decides the direction of extrusion. Taken

together, these results highlight how MTs can physically interact with the actomyosin cortex or modulate actomyosin regulators to change force distribution and epithelial cell shape changes.

### 3.3.3. Force production and response to forces

Microtubules can directly mediate cell shape changes by their ability to produce or respond to forces (**Figure 19c and f**). During development, microtubule alignment and cell elongation occur simultaneously<sup>169</sup>. Recent experiments show that microtubule alignment follows cell shape and is guided by geometrical cues<sup>169</sup>. Nevertheless, other examples demonstrate a role for MT polarization along the longest axis of the cell in controlling cell length homeostasis (**Figure 20**)<sup>170</sup>. Experiments with HeLa cells on micropatterns show that dynamic polarized microtubules mediate cell extension independently of cell size, pattern width or actomyosin cortex. This seems to be due to their local interaction with cell borders and is conserved in zebrafish neural tubes or *Drosophila* cells<sup>170</sup>. Along the same line, a polarized array of MTs regulates the mechanical autonomy of cells during wing development in *Drosophila* (**Figure 20e**). This non-centrosomal array of MTs bears compressive forces & exerts pushing forces along the longest axis of the cell. Therefore, its depletion leads to cell shortening along the main axis of the cell<sup>171</sup>. MTs are also able to modulate amnioserosa morphogenesis in flies through MTs-base pushing forces (**Figure 20d**). The amnioserosa is an extraembryonic tissue in flies. First, epithelial cells in the amnioserosa are initially columnar cells. Interestingly, they flatten & elongate through an MT-dependent mechanism the author called “rotary cell elongation”. In this process, growing MTs rotate and actively push against the cortex to induce cell flattening and cell elongation<sup>172</sup>. Additionally, dorsal closure (the process leading to the fusion of embryonic tissue over the amnioserosa) involves a step of seaming dependent on the formation of cellular protrusion based on MTs. Interestingly, this process is conserved in other fly species<sup>173</sup>. Finally, changes in MT-dependent force generation drive apical folding independently of MyoII during *Drosophila* gastrulation (**Figure 20f**)<sup>174</sup>. Indeed, the formation of the *Drosophila* dorsal fold appears to occur despite any localised MyoII changes. Instead, the Patronin-organised network is shifted basally weakening the level of forces exerted on the apical side of the cell. This leads to cell shortening necessary for dorsal fold formation. Taken together, these results suggest that microtubules may play a prevalent role in morphogenesis independently of their interaction with the cortex.

These observations could be explained partly by the ability of MT to bear compressive forces (**Figure 20g**)<sup>73</sup>. The persistence length of microtubules is of the order of a millimetre compared to that of actin which is around  $10\mu\text{m}$ <sup>72</sup>. For the same size, it would therefore require more energy to bend a MT than an actin filament. Thus, MTs are more resistant to compression. Yet, MTs can still bend with sufficient force. If they do not have a defect in the lattice, then they recover elastically<sup>175</sup>. However, MTs regularly show defects in their structure which leads to their softening. Moreover, subjecting microtubules to repeated folding cycles also leads to the accumulation of defects in their lattice and to their softening. Nevertheless, providing free dimers rescues MT stiffening and enhanced their stability<sup>176,177</sup>. Because defect repair leads to MT stabilisation and longer lifespans, it may also be a mechanism to further resist compression. Accordingly, in cells, MTs are often bent or curved. For instance, in newt lung epithelial cells, contraction, and retrograde flow of the actomyosin cortex can lead to bending in MT lattice<sup>137</sup>. Yet, it is unclear if this is due to repair machinery or directly to stress.

It seems that CLASP proteins recognize bent MTs conformations and improve the recruitment of free tubulin and therefore promote repair. Indeed, sequences of compression of cells lead to bending and stabilisation of MTs in a CLASP2-dependent manner<sup>178</sup>. As a result, MTs are more stabilised and resist nocodazole-induced MT depolymerisation. Alternatively, migration through confinement leads to compressive forces and similar MT response<sup>179</sup>. This highly suggests an emerging conserved mechanism for MT stabilisation and resistance under compressive load. This is in good agreement with experiments conducted on muscles. In cardiomyocytes, detyrosinated MTs are attached to sarcomeres and resist actomyosin contractile forces by buckling. Their detachment from the sarcomere leads to less resistance during cardiomyocyte contraction<sup>180</sup>. This supports older experiments that have shown that the buckling wavelength of MT was reduced upon lateral reinforcement allowing MT to bear extensive compressive load<sup>181</sup>.

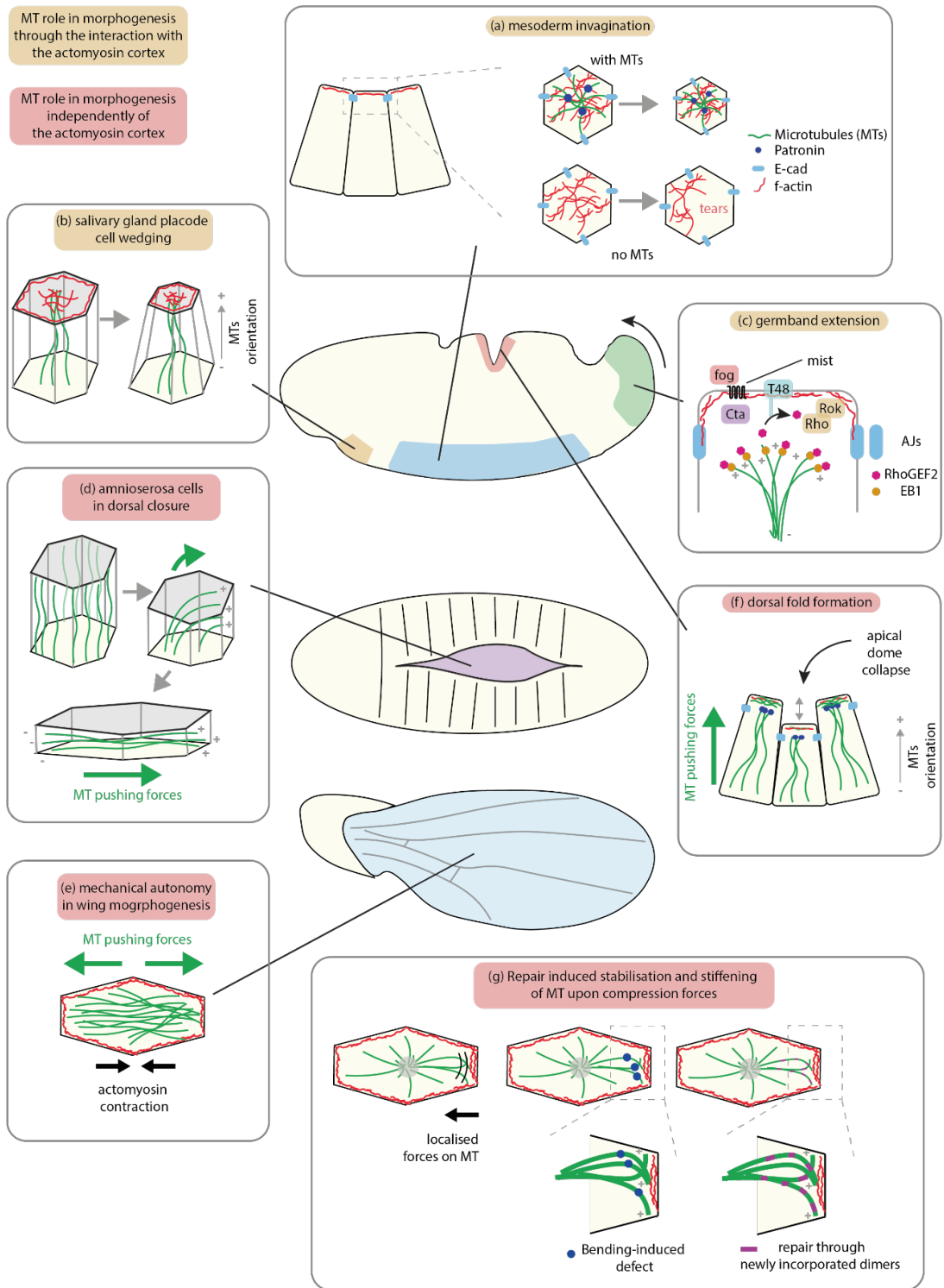


**Figure 20** - Roles of MT in morphogenesis. Orange boxes highlight roles of MT through the interaction with the cortex, red boxes highlight direct roles of MT in morphogenesis. (a) Patronin organise an apical MT array necessary for apical constriction during mesoderm invagination. (b) Apicobasal MTs are necessary for apical constriction in placode cells. (c) MTs regulate different pool of RhoGEFs during germband extension. (d) MT pushing forces mediate columnar-to-squamous transition necessary for dorsal closure. (e) MT pushing forces stabilise cell shape during pupal wing morphogenesis. (f) Basal shift of Patronin deplete pushing forces from the apical side leading to bending in the dorsal fold. (g) MT resistance to compressive forces is increased through repair mechanisms.

Finally, inhibiting MT nucleation or depolymerizing MT leads to a fluidification of the cytoplasm necessary for cell division, independently of actin<sup>182</sup>. They can equally modulate tissue softening separately of the actomyosin cortex during early *Drosophila* morphogenesis<sup>183</sup>. Taken together, this would point to a mechanism by which MTs resist compressive load and modulate cell pressure/area elasticity. Such forces could be induced either by intracellular machinery or by extracellular forces. Therefore, modulating MTs in that context could be a major mechanism leading to cell and tissue shape changes.



**Conclusion: Take-home messages.**

Microtubules are dynamic cytoplasm components. Like actin, they arrange in a network with capping proteins, polymerisation regulators, severing proteins and crosslinker. They can be organized in centrosomal organizing centres or non-centrosomal ones like in epithelial cells. They have long been seen as bearing only housekeeping functions in cells. However, they now emerge as clear regulators of cell and tissue morphogenesis through their role in force generation (**Figure 20**). They seem to provide such function & affect cell shape through two main routes:

- Interaction with the actomyosin cortex: In this first case they can interact directly with the cortex through crosslinkers. This modulates their direction of polymerisation, or they can affect the contraction yield by reducing the flexural rigidity of the cortex. Secondly, they can interact with the cortex through the sequestration of common regulators like Rho-GEFs.
- Independent force generation and force response: In this second case they affect cell shape through their pushing forces, through their ability to resist compressive forces or by modulating cytoplasm fluidity.

## CHAPTER CONCLUSION

The cytoskeleton should be understood as a unified system. Each of its parts has individual roles but they are co-regulating each other in a self-organized manner to ensure correct spatiotemporal positioning and therefore function. One of these functions is to mediate cell shape changes during development. From the actomyosin cortex emerge contractile forces which tend to reduce the apical area. These forces are produced by the action of myosin motors on actin network. Actin regulators like crosslinkers mediate the formation of networks with different structures which are differently localised in cells and have different properties. Branched network in the medioapical area often result in actomyosin contractile pulses. Conversely, antiparallel actin bundles are organised in belts localised close to the AJs and mediate contractility in a purse-string manner.

Ultimately the apical constriction of cells is the result of a shift in the equilibrium between contractile forces that tend to reduce the apical area and resisting forces. These are mediated by adhesion molecules or other cytoskeletal components like microtubules. Adhesion, mainly mediated by E-cad in epithelia tends to increase the contact area between adjacent cells. In addition, E-cad at Adherent Junctions also interacts with the underlying actomyosin cortex. For instance, the adhesion strength is increased upon force production by the cortex. Conversely, on longer time scales, E-cad contributes to active stresses through the regulation of the cortex. Finally, both need to be linked in order to trigger cell apical constriction. Lastly, Microtubules influence cell mechanics through their interaction with the actomyosin cortex. This modulates cortical properties actively by influencing the polymerisation of actin or MyoII activation but also indirectly by reducing the flexural rigidity of the cortex and subsequent contraction. Additionally, Microtubules may influence cell shape directly by exerting pushing forces on the membrane or by their ability to bear compressive forces. This would resist the contractile forces produced by the cortex and would make microtubules a very potent modulator of cell shape during morphogenesis.

In the following chapter, I will cover the mechanisms leading to caspase activation and apoptosis. I will describe how apoptotic cells are removed from epithelia while maintaining the sealing through a process called cell extrusion. All parameters presented in the current chapter are key to understanding the forces produced during apical constriction leading to cell extrusion and could be affected upon caspase activation preceding cell extrusion and apoptosis.



CHAPTER  
**HOW TO ELIMINATE A CELL?**

**2**

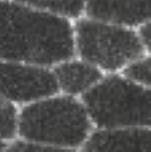




## **Table of contents**

<b>1. Introduction: Cell deaths</b>	<b>70</b>
<b>2. Apoptosis</b>	<b>72</b>
<b>2.1. Apoptosis during development</b>	<b>72</b>
2.1.1. Deterministic elimination of cell lineages	72
2.1.2. Force generation through apoptosis	73
2.1.3. Apoptosis in permissive for tissue deformation and tissue fluidification	74
2.1.4. Apoptosis for error correction and size regulation	75
<b>2.2. Caspases</b>	<b>76</b>
2.2.1. Caspase structure and activation	76
2.2.2. Caspase negative regulation	78
2.2.3. Extrinsic & Intrinsic pathways lead to mitochondrial permeabilization	81
<b>2.3. Caspases targets and cellular demolition</b>	<b>85</b>
2.3.1. Substrate structure & Conservation of the pathway for cleavage	85
2.3.2. Caspases substrates: Nodes of cellular demolition	86
<b>3. How to protect coherent tissue from cell death: cell extrusion</b>	<b>89</b>
<b>3.1. What is cell extrusion?</b>	<b>89</b>
<b>3.2. What drives cell extrusion?</b>	<b>89</b>
3.2.1. Extrusion during epithelial homeostasis	89
3.2.2. Extrusion, cell competition & tumorigenesis	90
3.2.1. Extrusion as a defence against pathogens	92
<b>3.3. Remodelling events</b>	<b>94</b>
3.3.1. Cell constriction at the core of extrusion	94
3.3.2. Maintenance of cell-cell adhesion and mechanotransduction	96
3.3.3. Signalling for extrusion: the role of S1P	97
3.3.4. Apical or basal? Which way to go?	98
3.3.5. Collective roles	99
<b>3.4. The role of caspases</b>	<b>100</b>
<b>4. Results: Paper: Microtubule disassembly by caspase is the rate-limiting step of cell extrusion</b>	<b>108</b>

## 1. Introduction: Cell deaths

Cell death is inherent to cellular life. It can be defined as the irreversible collapse of housekeeping cellular functions which results in the loss of cellular integrity either through cell fragmentation or membrane permeabilization<sup>184</sup>. By its very nature, which involves the elimination of cells that die, it has long been difficult to analyse the mechanisms leading to death. Indeed, scientists have been noticing for a while the disappearance of certain organs or structures during the development of embryos. However, developmental cell death was only discovered during the 19<sup>th</sup> century after the use of the microscope became prevalent. It was first noticed in the notochord of the amphibian midwife toad by Vogt (1842)<sup>185</sup>, and later during the metamorphosis of insects by Weismann (1864)<sup>185</sup>. Yet, it is only through the work of Kerr (1972) that the term apoptosis was coined to distinguish it from necrosis based on morphological differences<sup>186</sup>. In the case of necrosis, the dying cell swells and its membrane ruptures to release its intracellular content which leads to inflammation. On the other hand, apoptotic cells condense and fracture while keeping their intracellular components enclosed, inside intact membranes. It would only be after Robert Horwitz joined the effort led by Sydney Brenner and John Sultson (1974) to trace cell lineages in *C. elegans* that the idea of apoptosis as a form of programmed cell death (PCD) surfaced<sup>187</sup>. *C. elegans* has a determined cell lineages which generate a fixed number of cells with specific fates in the adult<sup>188</sup>. Mutants affecting *ced-3* or *ced-4* genes accordingly result in a transformation of fates in cells that would have normally disappeared through cell death<sup>189,190</sup>. From that point on it was clear that PCD is a regulated process.

While animals were fundamental to understand these regulations, regulated cell death seems to be a common feature throughout different phyla although mediated by different molecular systems. In the green algae *volvox*, PCD of somatic cells is necessary to prepare the algae for subsequent reproduction rounds<sup>191</sup>. More generally, examples of PCD were observed in *Dictyostelium discoideum* or yeast making it a widespread mechanism<sup>192,193</sup>. Moreover, diversity in the modes of death can be observed even within the animal cells themselves. Although death is regulated, it can take place through drastically different mechanisms. These are mainly classified based on their morphological differences as we described in the case of apoptosis and necrosis (**Figure 21**)<sup>194</sup>. To mention only a few ones, death can also be mediated by the loss of adhesion with the matrix through anoikis,

by cytoplasmic oxidative perturbation like in ferroptosis or even through the internalization of a cell by another one in a process called entosis<sup>194</sup>.

This chapter will solely focus on apoptosis. I will describe the two main pathways leading to apoptosis and emphasize the role of caspases as the main mediator of apoptosis. In the previous chapter, I highlighted how epithelial tissues are essential during the development of animals. I illustrated how their barrier function relies on the adhesion between epithelial cells. Consequently, apoptosis imposes an important challenge on epithelial integrity as it may rupture tissue sealing through the fragmentation of cells. Therefore, I will illustrate in the following parts how epithelia eliminate cells while maintaining tissue sealing through a process called cell extrusion. I will demonstrate how cell extrusion co-opts the cytoskeletal machinery described in the first chapter to mediate cell shape changes. I will finally explain how these remodelling events emerge cell-autonomously and from interaction with neighbouring cells and how these can lead to tissue morphogenesis. These will introduce all the concepts necessary for the understanding of the first part of my PhD project which will represent the final part of this chapter.

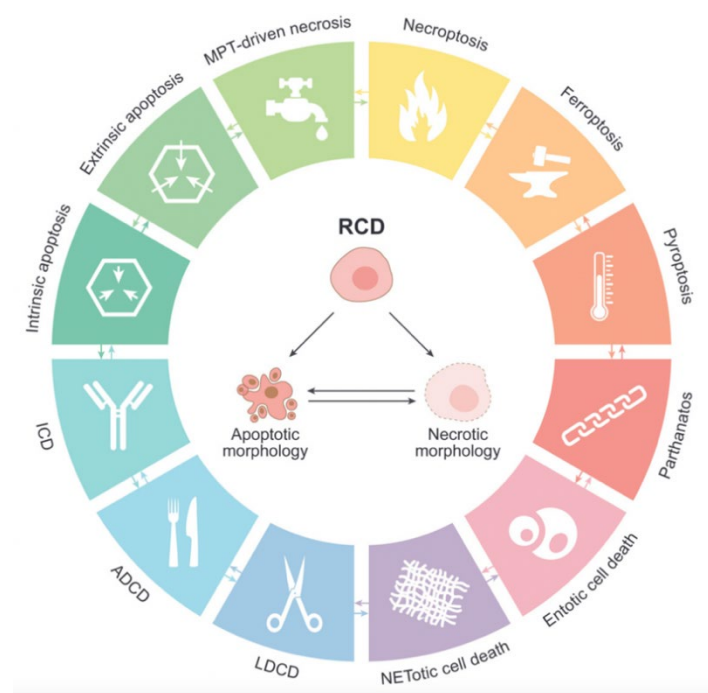


**Figure 21** - death diversity. Cell exposed to perturbation or programmed to die undergo one of these Regulated Cell Death (RCD) pathways. These pathways are defined by the morphological and molecular signature they exhibit. (ICD) Immunogenic cell death, (ADCD) autophagy-dependent cell death, (LDCD) lysosome-dependent cell death. (MPT) mitochondrial permeability transition. Adapted from<sup>194</sup>.



## 2. Apoptosis

### 2.1. Apoptosis during development

Apoptosis is the most prevalent and certainly the most studied form of PCD in animal cells. It is a conserved process which results in an irreversible demolition of the cell. First, the cell undergoes nuclear and cytoplasmic condensation. The cell then fragments into several membrane-bound and preserved fragments called apoptotic bodies. These are finally endocytosed by neighbouring cells or phagocytes<sup>186</sup>. In epithelia, this sequence of events is preceded by a step of cell extrusion which allows the removal of the dying cell from the epithelial layer while bringing its neighbours together. As such, it expels the cell while maintaining tissue sealing. I send the reader to the next part of that chapter for an in-depth cover of that process. Because it removes cells from tissues, apoptosis is instrumental in many developmental processes. I will now review some of the developmental functions of apoptosis.

#### 2.1.1. Deterministic elimination of cell lineages

First, apoptosis has been shown to be required to shape cell lineages in order to keep only cells important for the final function of the organ. A classic example of this is the elimination of cells in *C. elegans*. *C. elegans* has a determined cell lineage in which a set of 131 cells normally die in WT animals. However, these cells survived in *ced-3* and *ced-4* mosaic animals. Indeed, these genes respectively encode caspase-9 and Apaf1 homologues which are keys in the apoptotic pathways. The *Drosophila* adult is covered with sensory hair called macrochaetes or macrochaetes. These emerge from Sensory Organ Progenitors (SOPs). SOPs undergo a sequence of asymmetric division necessary to produce all the differentiated cells essential for the function of the sensory organ<sup>195</sup>. It first divides in pIIa and pIIb. pIIa then divides giving rise to a shaft cell and a socket cells. On the other hand, pIIb will generate a neuron and its associated sheath cell together with a glial cell. Interestingly, this glial cell is always fated to die<sup>196</sup>. Forcing the survival of this cell leads to axonal outgrowth. On the other hand, this cell still dies upon transformation of its fate suggesting that it undergoes PCD<sup>197</sup>. This deterministic elimination of cell by apoptosis is key in sculpting structures during organogenesis both in mammals and invertebrates. The most classical example of such a mechanism is the formation of digits in vertebrates. Initially, digits are held together by epithelial tissues. Apoptosis is specifically induced in interdigital tissues and leads to their removal resulting in perfectly separated digits<sup>198</sup>. Accordingly, *bak* (a pro-apoptotic gene) mutant mice

have palmed paws. Taken together it shows how apoptosis is required for the deterministic elimination of certain cells in a lineage. This removes cells whose functions are primarily to support other cells in the lineage during development.

### 2.1.2. Force generation through apoptosis

Secondly, apoptosis has been shown on several occasions to be important for force production during development. I send the reader to the first chapter where, I highlighted how they can regulate in-plane morphogenesis. Briefly, during the *Drosophila* dorsal closure, cells from the amnioserosa die from apoptosis which induces surface reduction and ultimately closure<sup>38</sup>. By their extrusion, these cells pull on neighbouring cells and drive their elongation. These forces can effectively extend to several cell rows and account for close to 30% of the net forces driving dorsal closure<sup>199</sup>. Additionally, the elimination of LECs in the thorax seems to be necessary for thorax closure during pupae formation. These cells activate caspase and undergo cell extrusion by which they produce forces necessary for *Drosophila* thorax closure. However, the relative contribution of these forces compared to active cell migration from the two hemithorax hasn't been assessed. Similarly, I have briefly covered some of the role of apoptosis for out-of-plane epithelial morphogenesis in the first chapter. Generally, apoptosis seems to be important in the formation of folds. For instance, localised expression of *reaper* and *hid* (two pro-apoptotic genes) in ring-like pattern of the presumptive *Drosophila* leg drives fold formation. These genes trigger apoptosis which precedes and is detected during fold formation<sup>53,54</sup>. When these cells extrude, they form an apico basal actomyosin cable. This cable induces apical deformation of the cells<sup>54</sup>. Because of its adhesion with the neighbours the forces are transmitted and drive tissue bending. Accordingly, the inhibition of apoptosis or MyoII block the process. Interestingly, the induction of apoptosis in a restricted domain is sufficient to drive bending of other epithelia such as the *Drosophila* wing disc<sup>54,200,201</sup>. Furthermore, the extrusion of these apoptotic cells induces myosin accumulation in the neighbours and highlights the non-autonomous effect of apoptosis. Accordingly, driving inhibition of MyoII in the apoptotic cells inhibits the accumulation<sup>54</sup>. Additionally, recent evidence show that a similar mechanism regulates neural tube invagination, bending and fusion (see **Out-of-plane deformations: Folding**)<sup>47</sup>. Taken together, this demonstrates the role of apoptosis in producing forces necessary for tissue morphogenesis.

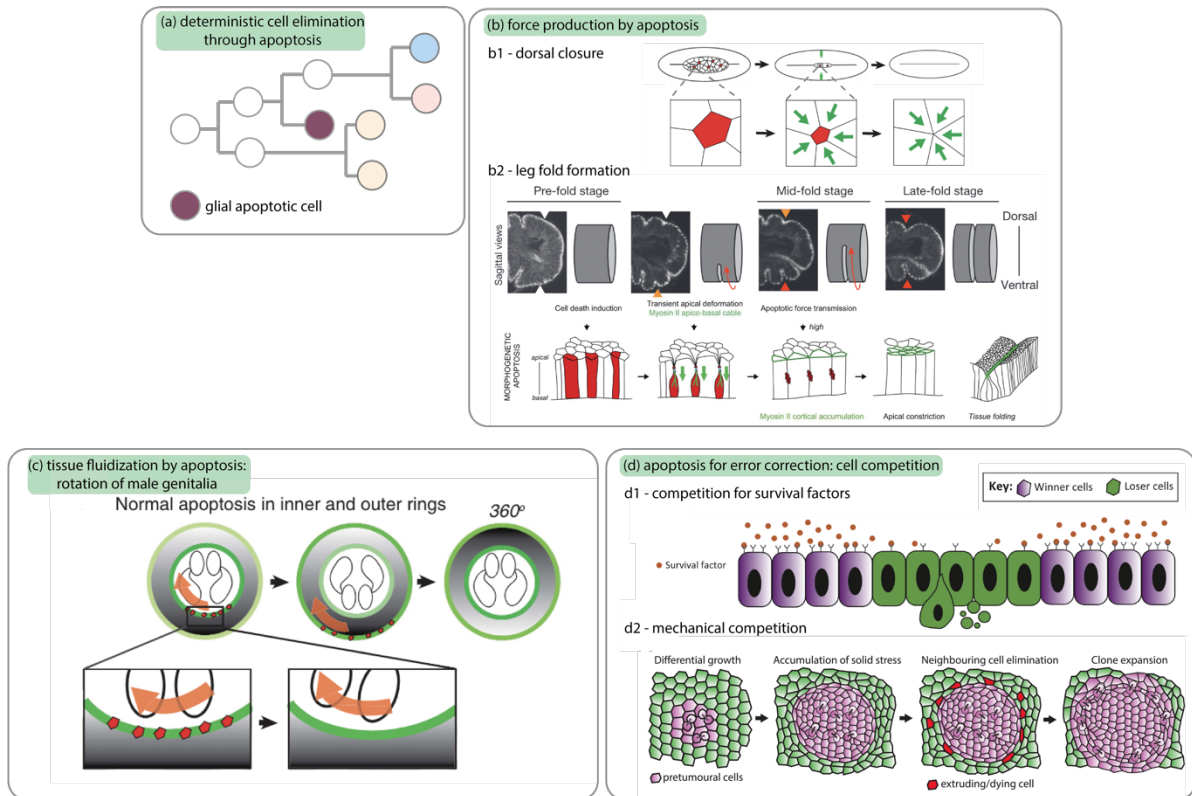


**Figure 22** - Role of apoptosis during development. (a) apoptosis induces the stereotypical elimination of certain cells in certain lineages. This allows to remove specific support cells which are important for development but not for the adult structure. The example here is the SOP formation. The glial cell in red is always eliminated. (b) Apoptosis mediates forces production during morphogenesis. (b1) Apoptotic extruding cells (red) in the amnioserosa drives forces productions by pulling on neighbours (green arrows). This force expands several rows away and account for one third of the forces driving dorsal closure. (b2) Apoptotic extrusion drives fold formation. Spatially localised expression of *reaper* and *hid* induces apoptosis (red) in specific domain of the presumptive leg. These cells extrude before and during fold formation. They drive the folding by the formation of an apicobasal actomyosin cable (green) that pulls on the apical area which drives folding. (c) Apoptosis is permissive for tissue fluidization. Apoptosis (red) acts a brake-release by removing cells which normally limit male genitalia rotation (orange arrow). (d) Apoptosis is important to buffer variation during development or to eliminate damaged or less fit cells. This process is known as cell competition. (d1) cell competition can be mediated by the competition for survival factors. Their lower concentration in one population induces its apoptosis. (d2) Mechanical cell competition can be driven by the expansion of one cell population faster than the other one (here pretumoral cells (purple compared to wt cells green). This differential growth drives the compaction of the other population (WT cells here) which induces its apoptosis (red) at the boundary.

### 2.1.3. Apoptosis in permissive for tissue deformation and tissue fluidification

On top of its ability to actively produce forces, apoptosis is also permissive for tissue deformation and tissue fluidization. Indeed, in silico work using continuum models of tissue dynamics showed that division and apoptosis promote tissue viscoelasticity and liquid-like behaviour. Conversely, without apoptosis, the tissue behaves as an elastic solid. This is because apoptosis and division induce local anisotropic stresses<sup>202</sup>. This is well exemplified by the role of apoptosis in regulating male genitalia rotation in *Drosophila*.

This tissue is made of two rings that each rotates 180° for a total 360° rotation. Apoptosis happens at the ring boundaries and remove cells that normally act as a brake. Therefore, it seems to be permissive for the rotation. Accordingly, blocking apoptosis through the inhibition of caspases (main apoptotic effectors) drastically reduced the rotation speed of male genitalia in *Drosophila*<sup>203,204</sup>. Taken together these demonstrate how apoptosis can drive morphogenesis through its ability to increase tissue fluidization.

#### 2.1.4. Apoptosis for error correction and size regulation

Additionally, apoptosis can also affect adult tissue size and shape through finer roles. Indeed, apoptosis is thought to refine or fine-tune adult organs' size by regulating cell numbers. Internal monitoring in the tissue allows buffering for variation during growth and increases the robustness of the final organ<sup>205</sup>. For instance, cells that proliferate slower are eliminated by a population of faster dividing cells. For instance, cells mutant for *minute* (a ribosomal gene) proliferates slower than their WT counterpart and are eliminated in presence of WT cells<sup>206,207</sup>. This process is called cell competition and is a context-dependent elimination of one cell population for the benefit of the expansion of another one. Indeed, *minutes* mutant flies develop correctly and show very minor defects on their own<sup>206</sup>. Additionally, multiple scenarios of cell competition exist in which cells compete for a limiting amount of survival signals<sup>208</sup>. For instance, cells that have reduced ability to process survival factors like Dpp are extruded from the tissue<sup>208</sup>. Alternatively, death can be induced by the contact between the two populations<sup>209</sup>, or by mechanical stress<sup>210,211</sup>. This is the case for the extrusion of clone of polarity mutants like *scribble*, *disc-large* lethal giant etc..<sup>6,212</sup>. In these contexts, the contact with WT neighbouring cells triggers the activation of c-Jun N-terminal kinase (JNK) only in the first row of loser cells which then drives cell death. Similarly, cells expressing low levels of the transcription factor *myc* are eliminated by apoptosis in a contact-dependent manner in the *Drosophila* pupal *notum*<sup>213</sup>, or mouse epiblast<sup>214</sup>. This further shows how the probability of a single cell dying is set both internally and through its environment. It also demonstrates how apoptosis is able to buffer for developmental fluctuations which may ultimately affect tissue size.

The role of death in the growth of an organ was long neglected. Indeed, the growth pattern is considered to depend mainly on the distribution of divisions and their orientation<sup>215</sup>. However, the pattern of death can modulate locally and quantitatively the

local growth of tissue<sup>216</sup>. Work from our lab recently showed that apoptosis is spatially biased in the anterior and dorsal compartment of the growing wing disc. This a negative effect on local growth and may ultimately the size and shape of these compartments in adult wings. Alternatively, apoptosis has also been shown to regulate cell proliferation and growth through compensatory proliferation. Yet, this has been mainly studied in context of undead cells<sup>217</sup>, or massive death induction either through irradiation or upon the genetic ablation of large domain<sup>218</sup>. Therefore, it is unlikely to have a role in physiological contexts.

Taken together this demonstrates the instrumental roles of apoptosis during development. All these different functions are possible because all the components necessary for apoptosis like caspases are expressed in all cells. This ensures that upon the correct signal, nearly any cell type can be eliminated in a fast and irreversible manner. Because of this, apoptosis needs to be tightly regulated to prevent spurious activation of the pathway. Thus, I will now review the processes of apoptotic regulation. Caspases & apoptotic regulation

## 2.2. Caspases

### 2.2.1. Caspase structure and activation

Caspases (**C**ystein **a**spartate-specific protein**a**ses) are the main effectors of apoptosis. They are a set of proteases that cleave their substrate after an Asp residue<sup>219</sup>. This proteolysis reaction is irreversible which makes them very potent remodelling enzymes. In addition, they cleave numerous substrates that they recognized with high fidelity. This polyspecificity makes them highly efficient as the main effectors of apoptosis. They can be classified into 3 groups (**Figure 23**) depending on their role in the caspase cascade<sup>220</sup>. Here, I will only focus on groups II and III which are found more broadly in evolution compared to group I which is specific to vertebrates. In addition, the group I only mediates inflammation pathways and is, therefore, less relevant regarding apoptosis.

Group II contains initiator caspases like Dronc (and Dredd) in *Drosophila* and mainly caspases 9-12 in mammals. Group III are executioner caspases mainly Drice and Dcp-1, in *Drosophila* (also Decay & Damm) and mainly caspase 3 and 7 in mammals (**Figure 23**). Caspases are present in all cells as inactive precursors called zymogens (or pro-caspases). Indeed, all caspases contain 3 important domains. A large subunit, a small subunit, and an N-ter pro-domain. These domains are highly conserved amongst the

caspase family and are key for the regulation of caspases. Indeed, the cleavage of pro-domains and of the long and short subunits allows the folding of pro-caspases into heterotetramers (**Figure 26**). This folding triggers the formation of an active site which is necessary for the recognition of the caspase's substrates.

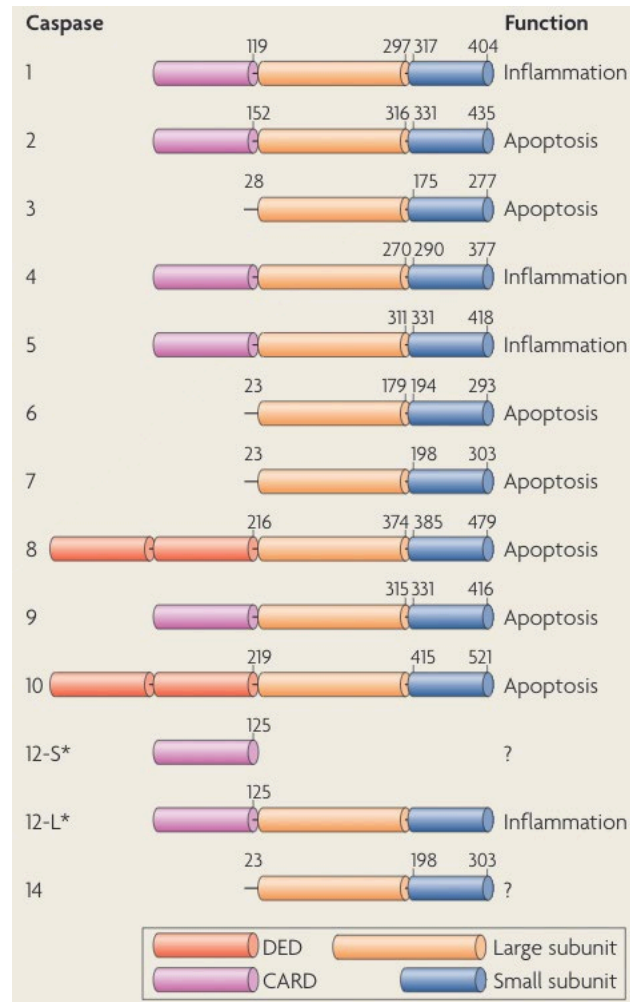


**Figure 23** - Caspases family. The caspase family can be divided in 3 groups. The first one includes caspases which are involved in inflammation (1, 4, 5, 12). Groupe II and III are involved in apoptosis. Group II are initiator such as 8, 9, 10. They are composed of a CARD pro-domain compared to group III that contains effector caspases like 3, 6, 7 and 14, that are devoid of CARD domains. Adapted from<sup>220</sup>.

The difference between both groups lies in the fact that initiator caspases contain longer Pro-domains with a Caspase-recruitment domain (CARD, pink in **Figure 23**). The CARD is highly important for binding upstream scaffolds such as APAF1<sup>221</sup>, or Dark (*Drosophila* APAF1 Related Kinase<sup>222</sup>). Upon death stimuli, Cytochrome-C is released through mitochondrial permeabilization which promotes the assembly of the apoptosome. This complex made of 7 APAF1 molecules allows the clustering of initiator pro-Caspase 9 and favours its auto-processing and activation into Caspase-9<sup>221</sup>. In *Drosophila*, this function is mediated by Dark but the necessity for Cytochrome-C release is not clear<sup>223</sup>.

Initially, the apoptosome was thought to be required for Caspase-9 activation<sup>224</sup>. However, it seems that it amplifies rather than initiates caspase activation<sup>225</sup>. Indeed, in S2 *Drosophila* cells Dronc undergoes a basal level of autoprocessing<sup>226</sup>. This would explain why *dronc* mutants for the CARD domain don't completely block cell death (debated in<sup>227</sup>). Alternatively, it suggests that effector caspases can be activated independently of *dronc*.

Finally, once Caspase-9 is activated it cleaves effector pro-caspase like Caspase-3/ Caspase-7 or Drice/Dcp-1 (*Drosophila* ICE) which induce their subsequent activation. These effector caspases execute apoptosis through the cleavage of multiple targets which leads to cell remodelling. Accordingly, *Drosophila* mutants inhibiting Drice function rescue phenotypes triggered by the overexpression of pro-apoptotic genes (*hid*, *grim* and *reaper*)<sup>227</sup>. Interestingly, this rescue is only partial which suggests overlapping function with other effector caspases. Indeed, Drice has overlapping functions with Dcp-1<sup>227</sup>. Equally, Decay, another effector caspase has been shown to be involved in *hid*-mediated cell death. However, *Drosophila* mutants for *decay* show that death occurs normally which suggests that it may be redundant as well<sup>228</sup>. Finally, Damm on the other hand seems to only sensitise cells to apoptosis<sup>229</sup>. This is in good agreement with mice mutants for single pro-apoptotic genes showing a very mild effect due to redundancy<sup>198</sup>. Alternatively, mice mutants for only Caspase-3 or only Caspase-7 showed normal appearance and organ morphology due to their redundancy. Accordingly, only double Knock-Out show apoptosis defect and embryonic death<sup>230,231</sup>. Taken together this highlight how essential caspases are in mediating cleavage leading to cell death. This may explain why high redundancy is needed in the pathway to ensure fast and errorless apoptosis.

### 2.2.2. Caspase negative regulation

Caspases are expressed ubiquitously in cells. Therefore, their activation needs to be tightly regulated to prevent any unwanted initiation of the caspase cascade. Thus, negative regulation of caspase is the first layer of regulation preventing the apoptotic cascade. It is mediated by a family of Inhibitors of Apoptosis (IAP) such as Diap1 (*Drosophila* IAP) in *Drosophila* or XIAP (X-linked IAP) and cIAP in mammals (**Figure 24**)<sup>232</sup>. They were identified through infection by a virus lacking the p35 sequence to identify other regulators of apoptosis in baculovirus<sup>233</sup>. Indeed, p35 is a baculovirus protein which inhibits effector caspase activation. IAP are known to contain BIR

(Baculovirus IAP repeat) and RING (Really Interesting New Gene) domains. On one hand, through their BIR domains, IAPs can bind both initiator and effector caspases which removes their apoptotic activity (**Figure 24**, light blue)<sup>234</sup>. On the other hand, the RING domain functions as an E3 ubiquitin ligase and mediates caspases ubiquitylation leading to their direct inhibition or inhibition through their degradation by the proteasome. Accordingly, Diap1 inhibition induces early embryonic cell death<sup>235</sup>. Conversely, XIAP deficient mice seemed normal, certainly due to the compensation of the lack of XIAP by cIAP<sup>236</sup>. This shows that here again there is high redundancy in the pathway.

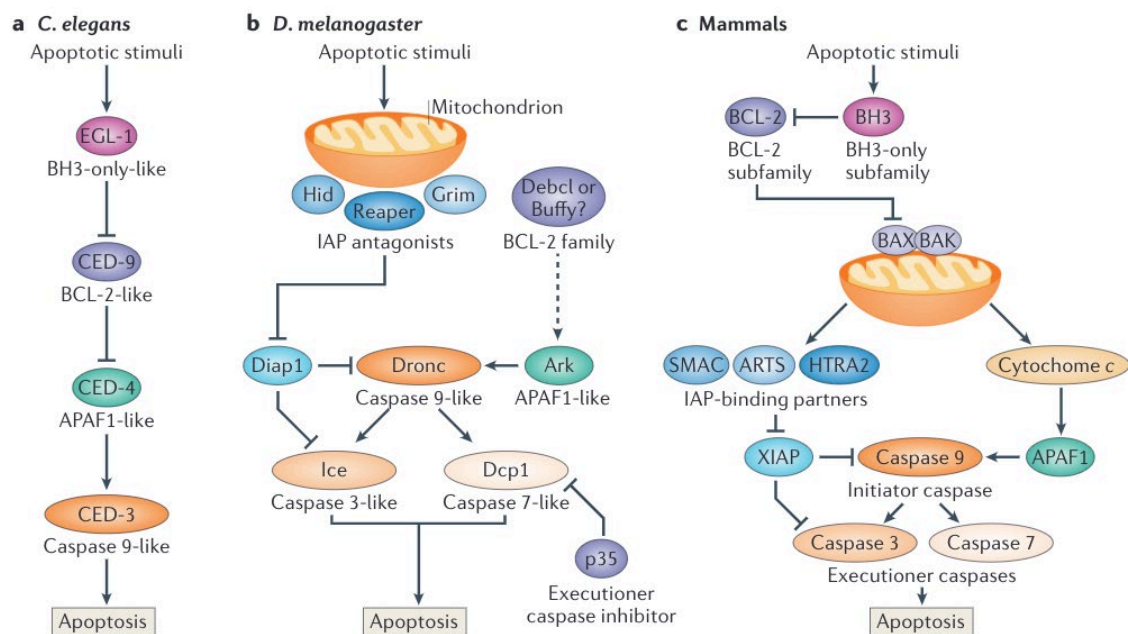


**Figure 24** - conservation of the apoptosis pathway between (a) *C. elegans*, (b) *D. melanogaster* and (c) mammals. Adapted from<sup>220</sup>.

Alternatively, the BIR domain also mediates the regulation of IAPs through IAP antagonists (**Figure 24**, blue). Such antagonistic function is mediated by Reaper, Hid (Head-Involution Defective) and Grimm (RHG) in *Drosophila* (**Figure 24**)<sup>237</sup>. They present an N-ter IAP-Binding Motif (IBM) which is conserved between flies and mammals<sup>238</sup>. This IBM motif allows IAP antagonists to bind the BIR domain of IAP and disrupts the binding of IAP to Caspases-3 or -9 which induces cell death<sup>232,235</sup>.

Additionally, the IBM motif favours the recruitment and oligomerization of RHG at the mitochondrial membrane leading to apoptosis activation<sup>239</sup>. In mammals, IAP inhibition is mediated by SMAC/DIABLO, ARTS or HTRA2. For instance, although ARTS doesn't have IBM it localises to the outer mitochondrial membrane similarly to



RHG. This allows ARTS to target XIAP to degradation<sup>240,241</sup>. Other data for mammal IAP antagonists are scarce. Indeed, while they are thought to be involved in promoting apoptosis, the high level of redundancy in the mammalian pathway has made their analysis difficult.

Hence, as expected, the loss-of-function of Diap1 fails to block RHG induced death. On the other hand, single point mutations which reduce the binding of RHG to Diap1 lead to gain-of-functions of Diap1 and therefore suppress RHG death<sup>242,243</sup>. Taken together this shows how IAP act downstream of IAP-antagonist to inhibit caspase activation. However, this is to be nuanced. Indeed, BIR domains also mediate the binding from Diap1 to RHG. This may allow Diap1 to titrate RHG away from its targets. This would inhibit cell death in addition to their role in the direct binding of caspase<sup>235</sup>. Thus, it would provide a supplementary safeguard to prevent any spurious activation of the caspase cascade unless the balance is shifted toward death through the overactivation of RHG.

However, when death signals are received and caspases are activated, the pathway presents sufficient levels of redundancy to ensure fast and irreversible cellular destruction. Indeed, upon their activation, caspases cleave IAPs. For instance, caspases cleave XIAP in Jurkat cells<sup>226</sup>. In *Drosophila*, Drice and Dcp-1 or even Dronc can cleave Diap1<sup>226,244</sup>. This acts as a positive feedback loop by reducing Dronc levels and its ability to protect S2 cells against apoptosis. Interestingly, the cleavage of Diap1 by Dronc only affects Diap1 interactions with the processed form Dronc not with pro-Dronc. Alternatively, Drice can also regulate its own inhibition. Drice cleaves and activates Diap1 which in turn targets Drice to nondegradative polyubiquitylation. This polyubiquitylation inhibits Drice activity. This negative feedback loop thus neutralises apoptosis<sup>245</sup>.

To summarize, IAP are the first layer of regulation of caspases (**Figure 24**). They inactivate caspase directly through binding or indirectly by directing them to the degradation pathway or through polyubiquitylation. IAP are downstream of IAP antagonists which disrupt IAP binding to caspase. This double negative regulation allows for fast activation of the caspase cascade upon death signals. The cascade of activation shows a high level of redundancy (mostly in mammals) and positive feedback loops. This ensures fast and irreversible apoptosis upon death signals which prevent the survival of damaged cells which could jeopardize further the tissue. Finally, these layers of regulation are themselves under upstream regulators responding to death signals.

### 2.2.3. Extrinsic & Intrinsic pathways lead to mitochondrial permeabilization

The top layer of apoptotic regulation relies on the extrinsic and intrinsic pathways (**Figure 25**). They depend, as their name indicates, reciprocally on extrinsic signals and intrinsic signals. For instance, wing disc cells compete for Dpp survival factors to prevent apoptosis<sup>208</sup>. Their withdrawal therefore leads to apoptosis. Alternatively, intrinsic signals such as the accumulation of DNA damages lead to the activation of the intrinsic pathway. For instance, replication stresses like s-phase arrest promote cell extrusion and apoptosis in *C. elegans*<sup>246</sup>. While they might be induced by different signals, they nevertheless, both culminate in the activation of caspases.

The extrinsic pathway is itself mainly mediated in two ways: The Granzyme-B-Perforin pathway and the TNF $\alpha$ /FasL-Death receptor-FADD pathways (**Figure 25**). The granzyme-B and Perforin are contained in granules secreted by immune cells. Perforin leads to membrane permeabilization which allows the entrance of the granzyme. This can further activate apoptosis through the cleavage of BID or through its binding to downstream caspases. Additionally, Granzymes also are proteases, like Caspases, which cleave their substrates after Asp residues<sup>247</sup>. BID is also a common target to the other main extrinsic pathway (**Figure 25**). Indeed, the binding of Fas Ligand or TNF $\alpha$  (Tumour Necrosis Factor  $\alpha$ ) to death receptors leads to the recruitment of FADD (Fas-Activated Death Domain)<sup>248</sup>. This in turn recruits Caspase-8 and leads to its autoactivation. Ultimately, Caspase-8 processes BID (BH3-interacting domain death agonist) into its truncated form t-BID. This makes t-BID competent to bind pro-apoptotic members of the BCL-2 (B-Cell Lymphoma-2) family and to further activate the apoptotic pathway.

On the other hand, internal signals like DNA damage, lead to the activation of the intrinsic pathway. Interestingly, this pathway crosstalks with the extrinsic pathway through the mean of BCL-2 family members. These proteins were mainly characterised in mammals by the presence of BH domains. These domains mediate their interactions at the surface of the mitochondrial membrane<sup>220,249,250</sup>. The BCL-2 family is divided into 3 groups based on their function (**Figure 25**).

- (1) Anti-apoptotic like BCL-2 or BCL-XL
- (2) Pro-apoptotic like BAD or BID
- (3) Pro-apoptotic pore formers containing only the BH3 domain as BAX and BAK.

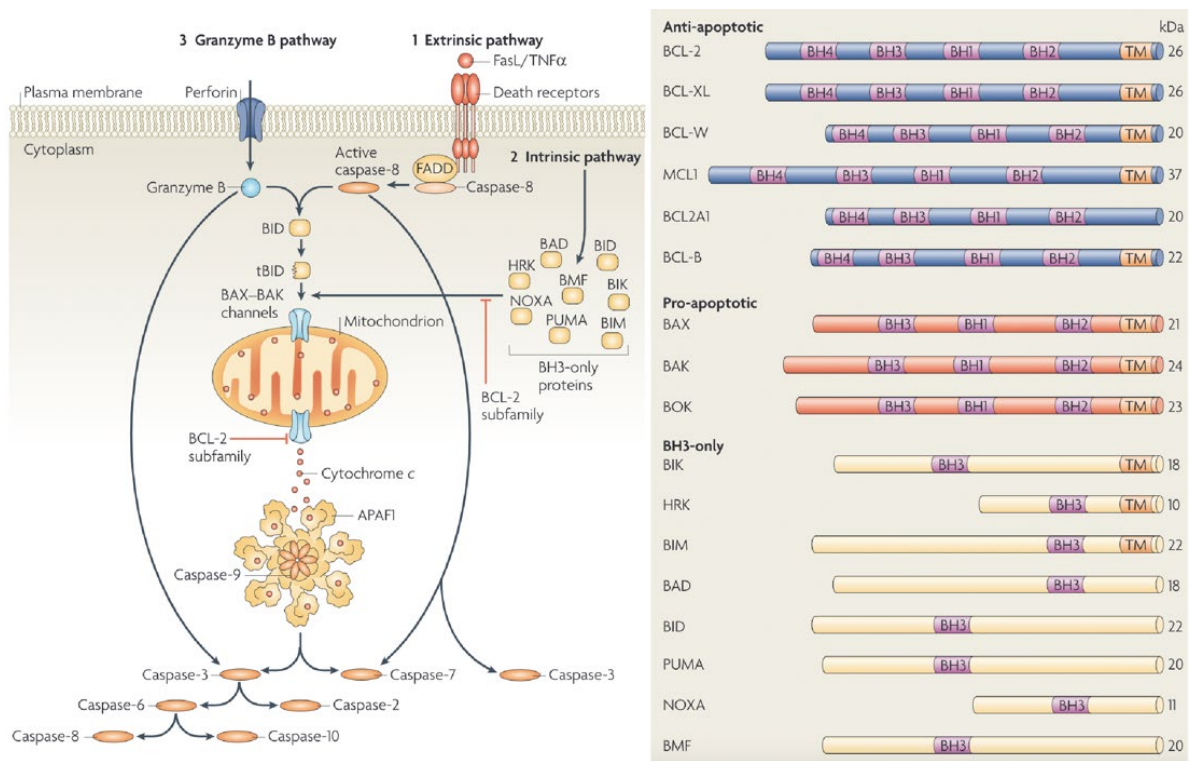


**Figure 25** - BCL2 superfamily. Left: The Extrinsic pathway. Fas Ligand or  $TNF\alpha$  bind death receptor. This activates Caspase-8 in a FADD dependent manner which will cleave BID in t-BID (1). Alternatively, Granzyme-B can enter the cell through Perforin and cleave BID as well (3). On the other hand, the intrinsic pathway (2) can also activate cell death by shifting the balance between anti-apoptotic and pro-apoptotic BCL-2 family members. This will lead to mitochondria permeabilization and Cytochrome-C release which ultimately triggers the caspase cascade. Right: The BCL-2 superfamily is made of anti-apoptotic members such as BCL-2, pro-apoptotic members such as the couple BAX-BAK which drives mitochondria permeabilization and BH3-only members which tend to be pro-apoptotic as well. Adapted from<sup>220</sup>.

As for the case of more downstream actors of the pathway, the BCL-2 family shows high levels of redundancy inside each group. All these three groups interact with each other and the balance between these members shifts the equilibrium toward pro-apoptosis or anti-apoptosis (**Figure 25**). For instance, cells deficient for all BH3-only members resist most apoptotic stimuli<sup>220</sup>. However, removing anti-apoptotic members like BCL-XL leads to apoptosis in these cells. This shows how essential anti-apoptotic BCL2 members are<sup>251</sup>. Indeed, BCL-XL seems to be directly binding to pro-apoptotic BAX inhibiting its oligomerization with BAK (both BH3-only). Accordingly, point mutations affecting the BAX-binding domain of BCL-XL prevent their association in Mouse embryonic fibroblasts<sup>250</sup>. This leads to BAX-BAK oligomerisation triggering mitochondrial outer membrane permeabilization and Cytochrome-C release. In *Drosophila*, these actors are less represented. Their homologues Debel or Buffy lack mechanistic proof.



*Conclusion: Take-home messages.*

So far, I have described the necessary functions of caspases during cell death. Because *Drosophila* and mice have been instrumental in the dissection of the apoptotic pathway, I have mainly focused on data from these organisms. I emphasized the multiple layers of regulation of this pathway. The reason for the need for such regulation is twofold. First, caspases are expressed as inactive zymogens in virtually all cell types. Therefore, their activation needs to be tightly regulated to prevent any spurious activation of the pathway which would lead to unwanted cell death. Second, once the pathway is activated and the decision for the cell to die is taken, caspase will cleave different targets and damage the cells. Therefore, multiple positive feedback ensures that once the cell commits to apoptosis, its destruction is fast and irreversible. This prevents the survival of damaged cells that would be deleterious to the tissues they are in. That regulation is provided by the following actors:

- The extrinsic and intrinsic pathways sense the state of the cell and lead to the activation of apoptosis. They converge to the permeabilization of the mitochondria through the regulation of BCL-2 family members.
- The activation of pro-apoptotic genes or IAP antagonists inhibits IAP which leads to caspase activation
- IAPs inhibit Caspase activation by direct binding or ubiquitination and degradation.
- Once inhibition is released effector caspases cluster. This allows the cleavage of their pro-domain and subsequent activation. This in turn activates effector caspase as well through the cleavage of their pro-domains. These effector caspases finally mediate substrate cleavage and cellular remodelling.

I will now cover how caspases recognise their targets and how this leads to essential cellular remodelling.

## 2.3. Caspases targets and cellular demolition

### 2.3.1. Substrate structure & Conservation of the pathway for cleavage

Apoptosis culminates in caspases irreversibly cutting cellular substrate which eventually mediate cell shape changes. Many caspase substrates were identified in different mammalian species, flies, or *C. elegans*. To put it in perspective, some studies report a list of nearly 400 proteins cleaved by caspases in mammals<sup>252</sup>. Other, more recent, datasets present an overwhelming number of 1444 caspases substrates in humans<sup>253</sup>. It seems very unlikely that all these substrates play equally major roles in this process. One proposed approach to identify meaningful targets could be to check for conservation of this target in other species. However, this might be difficult. Indeed, pathways, rather than substrates or cleavage sites seem to be conserved over evolutionary distances (**Figure 26**)<sup>253</sup>. More precisely, caspases recognise their substrate through the recognition of a consensus DEVD (or DEVDG) sequence. These positions are called P4 to P1 and the cleavage takes place at P1 position (after the D, **Figure 26**). There is an absolute requirement for the P1 position with an exception for Dronc which can cleave also after glutamate (E). In addition, the secondary and ternary structures also affect substrate recognition by caspases (reviewed in <sup>219</sup>). On short evolutionary distances (humans to mice), caspase tends to recognize and cleave these motifs on ortholog proteins. However, on longer evolutionary distances (humans to *Drosophila*), the level of conservation shifts to the protein level or to the pathway level. Overall, what seems to be conserved is the targeting of common cellular functions or compartments rather than specific proteins.

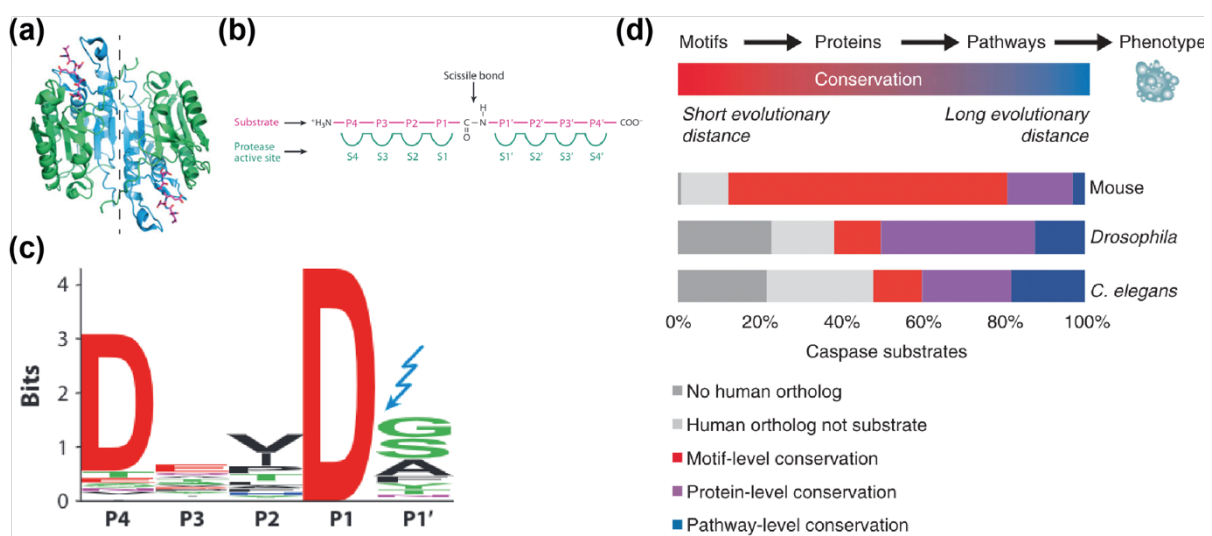


**Figure 26** - Caspase substrate specificity and conservation. (a) Caspase structure. It is made from two sub-units folded into heterotetramers. The dotted lines show where the two dimers meet. (b) Caspase substrate interaction. Pink shows the substrates and green the caspase catalytic sites. P1 to P4 represent the nomenclature for the

conserved domains. Substrates will be cleaved after the P1. (c) Primary structure specificity for the cut, the size of the letter is proportional to the probability to cut in the domain. Thus, it shows how the cut is specific for Asp (D) residues and specifically the one at the P1 position. (d) Levels of cleavage conservation. It shows how caspase target specific cellular function rather than particular substrates. The colour represent at which level the cleavage is conserved between human and the given specie. Dark gray: no ortholog, light gray: the ortholog is not cut. Red: The motif inside the protein is conserved and cut. Purple: the cleavage is conserved at the level of the protein. Blue: The cleavage is conserved at the level of the pathway. Adapted from<sup>219,253</sup>.

Accordingly, to this date, only very few caspase substrates were functionally analysed. However, their functional analysis led to the identification of key cellular nodes that seem to be targeted by caspase for apoptosis.

### *2.3.2 Caspases substrates: Nodes of cellular demolition*

Amongst the few caspase substrates functionally analysed, we find members of the apoptotic cascade. I already have covered, in the previous part, how their cleavage upon caspase activation results in positive feedback loops leading to death. Amongst the other cellular functions and compartments targeted are DNA<sup>254</sup>, nuclear membrane, mitochondria, cell membrane and finally adhesion and cytoskeletal components. Here I will only cover some examples of adhesion and cytoskeletal targets. Indeed, as I have illustrated in the precedent chapter, they are the main drivers of cell shape changes. Thus, they are crucial in the remodelling leading to apoptotic cell extrusion.

Apoptosis in cardiomyocytes apparently results in the cleavage of actin and actinin which leads to impaired force production<sup>255</sup>. Yet, cleavage of these proteins was only assessed in vitro which may not reflect real caspase concentration. Similar results were obtained in T-lymphocytes (Jurkat Cells or neutrophils). Exposure of these cells to Fas or Granzyme-B led to the cleavage of actin and actin-binding proteins like Filamin<sup>256</sup>, Fodrin<sup>257</sup>, Vimentin, Spectin<sup>258</sup>, Gelsolin<sup>259</sup>, but also activators of actomyosin like Rho. We can expect these cleavages to influence cell morphology and contractility. Yet, the functional relevance of these cleavages regarding cellular remodelling was only assessed in a few cases. For instance, the expression of the cleaved form of gelsolin leads to neutrophils rounding<sup>259</sup>. Filamin relocalised from the membrane to the cytoplasm and correlate with cell changes upon apoptotic stimuli but wasn't directly tested<sup>256</sup>. The only thorough analysis for a cytoskeletal component was conducted on ROCK1 by two independent studies on Jurkat cells and fibroblasts<sup>260,261</sup>. In both cell types, activation of caspase 3 leads to ROCK1 cleavage. This truncated form increased MyoII light chain phosphorylation and lead to increased contractility and cell blebbing. Interestingly, this cleavage and over-phosphorylation are inhibited when caspases are blocked.

In epithelial tissues, while cell-cell adhesions are key for the sealing of the tissue, they need to be removed to allow the cell to round up and be expelled during apoptosis. Accordingly, in MDCK (Madin-Darby canine kidney) cells, E-cad is directly cleaved upon apoptosis induced by staurosporine (a kinase inhibitor). This cleavage is dependent on caspase as it can be partially inhibited by caspase-3 inhibitors<sup>262</sup>. Additionally, E-cad binding to the cytoskeleton is also affected upon caspase activation in MDCK cells.  $\beta$ -catenin is cleaved by caspase-3 and loses its ability to bind  $\alpha$ -catenin. As a result, cells lose contact, and the actin network is remodelled<sup>263</sup>. This cleavage is conserved in *Drosophila* epithelia. Indeed, in DIAP1 mutant embryos, both Armadillo (Arm, the *Drosophila*  $\beta$ -catenin) and E-cad are removed from the junctions. Indeed, Drice cleaves Arm at its N-Ter end. Mutations of its cleavage sites blocks Arm cleavage both in vitro and in *Drosophila* embryos<sup>264</sup>. Interestingly this mutation delays the removal of E-cad from the junctions. Therefore, the cleavage of Arm is necessary to deplete E-cad from the junction. Yet, the overexpression of a form of Arm lacking its N-ter is able to mediate adhesion in *Arm* null background. This suggests that the cleavage doesn't impair Arm ability build junctions but rather affects the stability of the junctional complex otherwise. Interestingly, this happens without any cleavage of E-cad. This was later confirmed in both Diap1 null embryos and embryos overexpressing the pro-apoptotic gene *reaper*<sup>265</sup>. This triggered caspase activation which altered both E-cad and MyoII localisation. This was mediated through the cleavage of Bazooka (Baz, fly homologue of Par3) and Disc Large (Dlg) during early steps of apoptosis independently of any cleavage of E-cad<sup>265</sup>.

Finally, MT-related proteins and  $\alpha$ -tubulin were found to be cleaved in neurons<sup>266</sup>, or Jurkat cells<sup>258</sup>. Similarly, in HeLa cells, protein forming MTOC (Microtubules Organizing Centers) are cleaved upon caspase activation<sup>267</sup>. This seems to be required for the formation of the AMN (Apoptotic Microtubule Network). Indeed, early upon apoptosis induction, MT reorganise in an AMN. This network sits at the cortex which protects cortical components from the access and cleavage by caspases. However, how this network forms is still unclear<sup>268</sup>. Finally, microtubules reorganisation upon caspase activation seems necessary for the formation of apoptotic bodies<sup>269</sup>.

### **Conclusion: Take-home messages.**

Apoptosis is a cell death event that has been characterised by its morphological changes. Cytoskeletal components are essential to mediate such cell shape changes. Yet, taken together these results demonstrate how caspase substrates in the cytoskeleton have



been overlooked. Only a limited number of data supports functional evidence of caspases substrate affecting cell shape changes. Moreover, these studies don't provide any temporal information. Furthermore, studies have mainly focused on cell cultures, because of that we lack an understanding of what happens in epithelial contexts where cells are tightly adherent to each other. Indeed, in epithelia, apoptotic cells are eliminated by cell extrusion. In that context, drastic cellular remodelling events, like cell fragmentation, are preceded by constriction events expelling the cell out of the epithelial layer. In the *Drosophila* pupal notum, caspase activation is necessary and precedes all extrusion events. However, we currently do not know which steps of extrusion are regulated by caspases or how effector caspase activation initiates and orchestrates epithelial cell extrusion. This was the first problematic of my PhD. Before I can describe this part of my work, I need to introduce the concept of cell extrusion in further details. Hence, the following part will be focused on the cellular remodelling leading to cell extrusion.

### 3. How to protect coherent tissue from cell death: cell extrusion

#### 3.1. What is cell extrusion?

Cell extrusion is a process that leads to the expulsion of a cell from an epithelium. It is characterised by a sequence of remodelling steps preceding that elimination. First, the extruding cell constricts. Because of its adhesion with neighbouring cells, this pulls on the neighbours and ensures constant contact throughout the process. Therefore, it expels the cell while maintaining constant sealing throughout the process. It is a very powerful mechanism as it allows the accommodation of the elimination of nearly 40% of cells in a tissue while maintaining a constant barrier<sup>270</sup>. This mechanism is used throughout metazoans from sponges<sup>271,272</sup>, nematodes<sup>246</sup>, insects<sup>210,273</sup>, and vertebrates<sup>111,274</sup>. Interestingly, this process is also conserved in epithelia from different embryonic origins. Indeed, cells can be expelled from endothelia which are epithelia derived from mesodermal origins. Accordingly, endothelial cells are extruded from the dorsal aorta in zebrafish in a process producing hematopoietic stem cells<sup>275</sup>. Finally, more recently, examples of apoptotic extrusion were found in zebrafish common cardinal veins<sup>276</sup>. But what drives cell extrusion?

#### 3.2. What drives cell extrusion?

##### *3.2.1. Extrusion during epithelial homeostasis*

Numerous processes lead to and require cell extrusion. First, cell extrusion is instrumental in maintaining epithelial homeostasis. This process refers to the balance of cell division and cell death that results in the epithelium having a constant number of cells. This dynamic equilibrium therefore ensures that the tissue preserves its size and shape and therefore its functions. This is well illustrated by the turnover in the small intestine (**Figure 27a**)<sup>277</sup>. This tissue is folded in crypts and villi which allows the increase of surface area for nutrient exchange. The bottom of the crypts is made of highly proliferative stem cells which then migrate up the villi and are finally expelled in an extrusion zone at the top of the villi (**Figure 27a**)<sup>278</sup>. Extrusion is necessary for the removal of approximately  $10^{10}$  intestinal cells per day. Accordingly, reduced shedding shifts the balance and leads to inflammation<sup>279</sup>. What drives the elimination of these cells is still unclear. One proposed mechanism is that cells compete for space. Indeed, in vivo cells were observed to extrude in region of high crowding in human intestine, zebrafish epidermis or in the fly notum<sup>274,280,281</sup>. Additionally, inducing overcrowding leads to increased cell extrusion<sup>274</sup>. The reason for that might be that overcrowding results in a

local increase in compressive stresses. Accordingly, in MDCK cultures, 70% of extrusions happen in region of high compressive stresses. Similarly, defects in the nematic alignment of cells were found to be associated with higher probability of extrusion as a result of local increase in compressive stresses<sup>282</sup>.

### 3.2.2. *Extrusion, cell competition & tumorigenesis*

More generally, cell extrusion mediates the elimination of cells during various cell competition scenario. As I previously mentioned, cell competition is a context-dependent elimination of cells. Cell populations with competitive disadvantages are extruded in presence of other cell population which drive the expansion of that second population. I illustrated in part **2.1.4** how the WT population drives the extrusion of the looser mutant cells. However, the opposite scenario may be true. Overexpression of *myc* in clones usually drives the expansion of that population at the expense of the WT population in a process called supercompetition<sup>214,283</sup>. Similar overexpression of other oncogenes like active Ras (Ras<sup>V12</sup>) or Yorkie (Yki) also leads to supercompetition. Activation of Ras in the pupal notum leads to overproliferation and inhibition of apoptosis through the inhibition of *hid*. This compresses the WT cells near the clone which downregulates ERK and leads to cell extrusion and apoptosis<sup>210,273,284</sup>. This mechanism is thought to replicate field cancerisation.

Interestingly, cell extrusion may be a mechanism to protect epithelia against expansion of transformed cell population. Indeed, it has also been shown to be involved in the elimination of tumoral cells in a process called Epithelial Defence Against Cancer (EDAC, **Figure 27b**)<sup>285</sup>. This may seem counterintuitive as I have just described how transformed cell populations can outcompete their WT neighbours. Yet, this just reflect another competition scenario. For instance, cells mutant for *dCsk* overactivated the pro-oncogene *Src*. In the wing disc these cells would promote proliferation and overgrowth when surrounded by other *dCsk* cells<sup>286,287</sup>. However, *dCsk* cells are eliminated at the interface with WT neighbours. Similarly, MDCK cells transformed with v-*Src* temperature sensitive mutant extrude when they are surrounded by WT cells<sup>288</sup>. It was proposed that *src* relax adherens junction and that permissive tension at the interface with WT cells<sup>289,290</sup>, together with filamin accumulation at the boundary allows the extrusion of transformed v-*src* cells<sup>291,292</sup>. Similar results were obtained in cells transformed with active Ras<sup>V12</sup> in MDCK cells or in mouse intestine<sup>293,294</sup>. Ephrin signalling was proposed to mediate the recognition of Ras<sup>V12</sup> and increase their contractility and extrusion both in

MDCK cells or wing imaginal discs (**Figure 27b**)<sup>293</sup>. Alternatively, scribble polarity mutant can co-operate with Ras to drive tumorigenesis<sup>212</sup>. However, on their own scribble mutant clones are extruded through cell competition in the wing disc. SAS accumulates in the WT cells at the boundary with scribble cells accumulating PTP10D. This leads to the transactivation of PTP10D in the scribble cells, downregulation of EGFR signalling and upregulation of JNK<sup>209</sup>. JNK in turn leads to extrusion by Slit-robo repulsive signalling and downstream activation of Ena (an actin polymerisation protein)<sup>295</sup>.

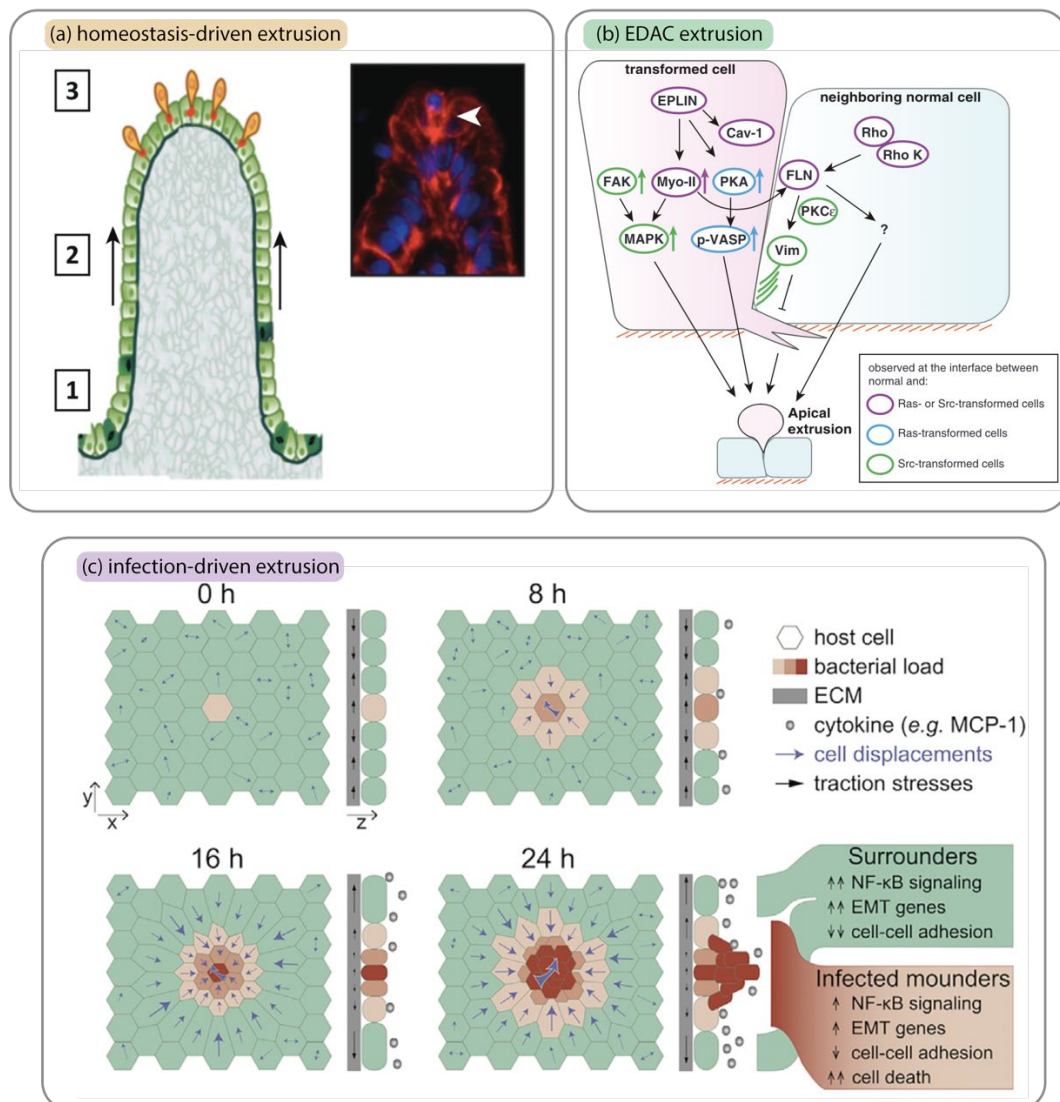


**Figure 27** - Some drivers of extrusion. (a) Extrusion driven by homeostasis turnover of cells in the gut. As the cell go up the villus the cell density increases which triggers compaction and cell extrusion. Adapted from<sup>296</sup>. (b) Comparison of extrusion of different transformed cells through Epithelial Defense Against Cancer (EDAC). Adapted From<sup>285</sup>. (c) Extrusion happening upon cell infection. The neighbours WT cells migrate toward the infected cells which leads to cell extrusion by mechanical competition and subsequently to cell death. Adapted from<sup>297</sup>.

On the other hand, extrusion can also be hijacked to promote tumorigenesis upon the activation of certain form of Ras (k-Ras<sup>V12</sup>). Indeed, k-Ras<sup>V12</sup> promotes basal cell extrusion

both in MDCK cells<sup>298</sup>, and zebrafish epidermis<sup>299</sup>. Cell-autonomous degradation of S1P through autophagy (a determinant for apical extrusion) or failure in apical signalling led to basal extrusion and is thought to increase tumorigenesis and tumour aggressiveness<sup>298,300,301</sup>. However, this is to be contrasted as it was shown that only cells with supplementary mutation in p53 survive after basal extrusion<sup>299</sup>. What sets the balance between supercompetition/tumorigenesis and EDAC is unclear.

### 3.2.1. Extrusion as a defence against pathogens

Finally, extrusion is also a very efficient way to protect epithelial tissue against pathogens infection (**Figure 27c**)<sup>302,303</sup>. *Erwinia carotovora carotovora 15* infection leads to infected cell extrusion in the *Drosophila* gut through the downregulation of the EGFR pathway<sup>304</sup>. Additionally, MDCK cells infected with *Listeria monocytogenes* or *Rickettsia parkeri* are also extruded. These cells drive the activation of NF- $\kappa$ B which reduces their intracellular stiffness. This together with directed migration of the neighbours toward the infected cells lead to their extrusion (**Figure 27c**)<sup>297</sup>. More generally, extrusion in the gut is a first protection layer against diverse pathogens infections like *Neisseria gonorrhoeae*. In a parallel with what I described earlier for the dissemination of cancer cells, extrusion can also be harnessed by bacteria to promote their dispersal. Rodent Gut cells loaded with *Salmonella enterica* are expelled toward the lumen through cell extrusion. This consequently spread bacteria primed for subsequent infection<sup>305</sup>. On the opposite, *Neisseria gonorrhoeae* increases adhesion in infected rodent gut cells which prevents their extrusion and promote bacterial spreading. Finally, while extrusion is clearly a defence mechanism against infection it can also be exploited as a weakness by bacteria. Indeed, E-cad is transiently exposed to the luminal surface of gut cells during and after cell extrusion. This transient event is necessary to remove adhesion to finally expel the extruding cell. However, *Listeria monocytogenes* takes advantage of that remodelling to cross the epithelial barrier<sup>306</sup>.

*Conclusion: Take-home messages.*

Taken together these results demonstrate the essential role of cell extrusion in preserving the epithelial barrier function. It regulates epithelial homeostasis by removing supernumerary cells or dying cells. Additionally, it participates in the elimination of unfit or transformed cells during cell competition. Finally, it is also the first layer of defence against bacterial infection. In different cases however, that process can be hijacked and misused leading to the deregulation of epithelial structure and function. But how exactly is the cell expelled from the epithelium to preserve its function? In the next part, I will review the mechanisms leading to the remodelling steps of extrusion.

### 3.3. Remodelling events

The sequence of remodelling events leading to extrusion mainly relies on the cytoskeletal components I have presented in the first chapter of this manuscript (**Morphogenesis: a cell-centred view**): adhesion, actomyosin contractility and microtubules. Because the extruding cell is embedded in an epithelium, the extrusion is therefore by definition a multicellular process. Thus, I will highlight the cell-autonomous and non-autonomous mechanisms leading to cell extrusion. Finally, I will cover the role of caspases in cell extrusion.

#### 3.3.1. Cell constriction at the core of extrusion

The contraction of the cell is at the basis of cell extrusion. It mediates the remodelling leading to the removal of the cell. Interestingly, cell extrusion has been shown to happen mainly toward the apical side in vertebrates and epithelial cell culture systems (**Figure 28a and d**). Conversely, cell preferentially extrude basally in *Drosophila* in a process often referred to as basal extrusion or delamination (**Figure 28b and c**). Here I will first focus on the event leading to cell constriction regardless of the direction of extrusion. Mechanisms leading to apical or basal extrusion will be detailed after. Accordingly, seminal work regarding cell extrusion has been conducted in MDCK cells specifically focusing on the role of the actomyosin contraction<sup>270</sup>. Irradiation of MDCK led to the caspase activation and apoptotic extrusion of 10% of cells. An actomyosin ring was detected both in the extruding cells and in the neighbours. First the extruding cell constrict which is followed by the formation and contraction of an actomyosin ring in the neighbours (similar to the one in **Figure 28a**). Injection of Rho-kinase inhibitor Y-27362 or inhibition of MyoII light chain kinase through ML-9 blocked cell extrusion and demonstrates the absolute requirement for actomyosin contractility in that process<sup>270</sup>. Interestingly, specifically inhibiting RhoA in the extruding cell didn't block extrusion. Likewise, inhibiting the cleavage of downstream ROCK1 by caspase inhibitor didn't block extrusion. Both results suggest that contraction through this pathway is therefore dispensable for cell extrusion<sup>270</sup>. Interestingly, microtubule inhibition in these cells disrupts MyoII localisation and activation. Indeed, microtubules associate with p115Rho-GEF (a Rho activator) and target it to the basolateral surface both in the extruding cell and its neighbours. This activates RhoA basolaterally and leads to constriction which promotes apical extrusion<sup>168,307</sup>. This seems to be a general mechanism for cell extrusion as it has been replicated in different other cell culture systems. For instance, in caco-2

cultures, apoptotic cells become highly contractile which leads to pulling on neighbours and formation of a supracellular actomyosin ring in the neighbours. This reorganisation is triggered by the localisation of coronin-1B to the cortex of neighbours (**Figure 28a**)<sup>132</sup>. Similarly, the formation of such supracellular actomyosin ring was also observed in the case of extrusion of transformed Ras or Src cells or upon crowding-induced cell extrusion<sup>274,289,298</sup>. Comparably, apoptotic extrusion in *Drosophila* Larval epithelial cells is also governed by the formation of both an intracellular and supracellular actomyosin cables (**Figure 28b**)<sup>37</sup>. Examples of extrusion in the *Drosophila* pupal notum also showed late-stage formation of an actomyosin ring although less characterised<sup>280</sup>.

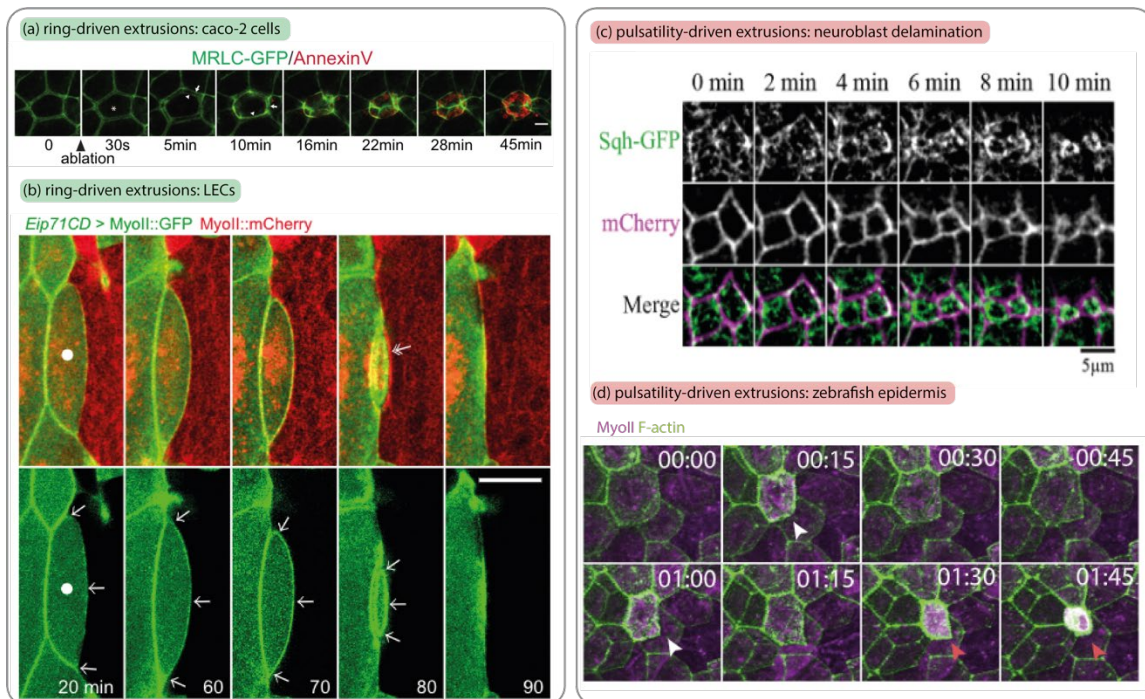


**Figure 28** - contraction during cell extrusion. (a-b) contraction of extruding cell through the formation of internal and supracellular actomyosin rings. (a) Extrusion in caco-2 cell cultures driven by ablation triggers the formation of an internal actomyosin ring. This increases contractility in the extruding cell (white arrowhead) and drives the formation of a supracellular ring (larger arrow). Green is myosin regulatory light chain and red is annexin V a marker of apoptosis. (b) Extrusion of Larval Epithelial Cells driven by the formation of an internal actomyosin ring (green MyoII::GFP, simple arrows on the bottom panel) and then the formation of a supracellular ring (red MyoII::mCherry, note the accumulation next to the extruding cell pointed by double headed arrow). (c-d) extrusions driven by medio-apical actomyosin pulses. (c) Pulses of medio-apical myosin (green sqh-GFP a myoII marker) driven the delamination of neuroblasts. (d) Pulses of myosin (purple, pointed by white arrowhead) drive the extrusion of cells in the zebrafish epidermis upon induction of cellular damages. Adapted from<sup>37,111,132,308</sup>.

Interestingly, a sub-population of larval cells in the dorsal midline seems to extrude independently of the formation of such rings. Instead, these cells exhibit contractility through medioapical myosin pulses like what has been described for mesoderm invagination in the *Drosophila* embryo<sup>309</sup>. For instance, pulsatile constrictions precede



and drive the extrusion of zebrafish epidermis cells upon cellular damages (**Figure 28d**)<sup>111</sup>. Comparably, contractile actomyosin pulses also drives apical constriction leading to the live delamination of *Drosophila* neuroblast (**Figure 28c**)<sup>308</sup>. Why cells undergo cell extrusion through pulsatile contractility rather than ring formation is unclear. One explanation could be that pulses allows cells to overcome high local tension. Indeed, in the zebrafish epidermis, pulses are driven by local tension increase. Likewise, dorsal midline Larval Epithelial Cells are extruded by actomyosin pulses which are correlated with a developmental time where mechanical tension is higher<sup>309</sup>.

### 3.3.2. Maintenance of cell-cell adhesion and mechanotransduction

Adhesion between epithelial cells during cell extrusion needs to be maintained throughout extrusion to ensure permanent tissue sealing. Indeed, E-cad adhesion allow force transmission which leads to the elongation of neighbouring cells to close the gap left by the extruding cell. Accordingly, E-cad KD leads to failure in elongation and compromised epithelial barrier function<sup>310</sup>. More than that, cell-cell adhesions are crucial to the formation of the actomyosin ring. Indeed, in caco2 cell cultures, once the extruding cell becomes hyper-contractile, it produces forces that are transmitted to the neighbours through E-cad adhesion. This recruits Coronin-1B to the adherens junction which remodels the actomyosin network in the neighbours. The network reorganises in F-actin bundles in a ring with a sarcomeric organisation of MyoII which produce higher tension and contractility necessary for cell extrusion (**Figure 28a**)<sup>132</sup>. Similarly, in MCF7 cells, hyper contractility of the extruding cells leads to RhoA activation in the neighbours through E-cad-dependent mechanotransduction<sup>130,133</sup>. Tension exerted on E-cad by the extruding cells relocalised Myosin-VI which activate RhoA through p115-RhoGEF. Accordingly, Myosin-VI KD cells fails to mediates this mechanotransduction. Similarly, both in caco2 and MCF7 cells, inhibiting apoptotic constriction of the extruding cell or E-cad failed to reorganise and activate the actomyosin ring in the neighbours<sup>130-132,311</sup>.

The maintenance of cell junctions during cell extrusion is crucial in maintaining the sealing of the tissue. However, for the extruding cell to leave the tissue, it must at some point abolish its adhesion with its neighbours. Accordingly, extruding LECs deplete E-cad adhesions up to 15min prior to the completion of extrusion<sup>37</sup>. Similarly, cells expressing active form of cdc42 or Ras (cdc42<sup>V12</sup> or Ras<sup>V12</sup>) display E-cad depletion. Cdc42<sup>V12</sup> overactivates MEK which induces the activation of metalloproteases and the cleavage of E-cad. The cleavage of E-cad was sufficient to drive cell extrusion<sup>312</sup>. This is

counterintuitive given the role of E-cad in regulating tension and mechanotransduction. One potential explanation is that fast E-cad cleavage leads to fast tension release. However, while local tension release was shown otherwise to be necessary in the neighbours during extrusion, it was not shown to be sufficient to drive cell extrusion<sup>289</sup>.

Finally, while E-cad is depleted prior to the completion of extrusion, adhesion still needs to be maintained until the cell is fully out of the tissue and that new adhesions are built between remaining cells. This is thought to be mediated by desmosomes and tight junctions. First, during enterocyte extrusion in the gut, tight junctions exhibit a basolateral movement following a zipper model to ensure constant sealing<sup>279</sup>. Similarly, in MDCK cells, desmosomes remain intact throughout extrusion. Additionally, neighbouring non-dying cells, form new desmosomes below the extruding cell ensuring constant sealing<sup>313</sup>. Of note, caspase activation has been shown to be required for the remodelling of tight junctions in enterocytes and desmosomes are cleaved by Caspase-3<sup>314</sup>. Inhibition of caspase-mediated processing of desmosomes or desmosomes KD leads to extrusion inhibition<sup>313,314</sup>. Finally, the formation of new desmosomes is mediated by the formation of basal lamellipodia protrusion. These lamellipodia help positioning the apical myosin ring but also contribute to cell extrusion. Both structures thus cooperate which makes cell extrusion more efficient than using a single mode<sup>130,315</sup>. Additionally, whether the cell decides to use a mode rather to the other depends on the cell density within the epithelium. Weakly packed epithelia seem to rather choose extrusion using lamellipodia compared to highly dense epithelium which extrude cells through actomyosin ring mechanisms<sup>316</sup>.

### *3.3.3. Signalling for extrusion: the role of S1P*

The lipid Sphingosine 1 Phosphate (S1P) has been shown in different instances to be important for cell extrusion (**Figure 29a**). However how exactly S1P regulate extrusion is still debated. Initially, it was proposed that S1P is secreted by the extruding cell and binds the G-protein-coupled receptor Sphingosine 1 Phosphate receptor 2 (S1P2) in the neighbouring cells. This would then in turn activate Rho-mediate contractility (**Figure 29a**)<sup>317</sup>. Accordingly, decreased S1P2 leads to accumulation of epithelial masses in zebrafish and MDCK cells due to lower extrusion rates. Similar results were obtained for the extrusion of MDCK Ras<sup>V12</sup> cells. However, in this case S1P is not specifically secreted by the extruding cell but is rather present in the whole culture medium certainly secreted by all the cells. Similarly, cellular damage in the zebrafish epidermis leads to caspase

activation which triggers secretion of S1P. S1P then in turn promotes increased tension which leads to pulsatile contractility and extrusion. However, here again that secretion is homogeneous rather than localised<sup>111</sup>. Finally, S1P was similarly shown to be necessary for priming MDCK cells for mechanotransduction but was not secreted locally<sup>130</sup>.

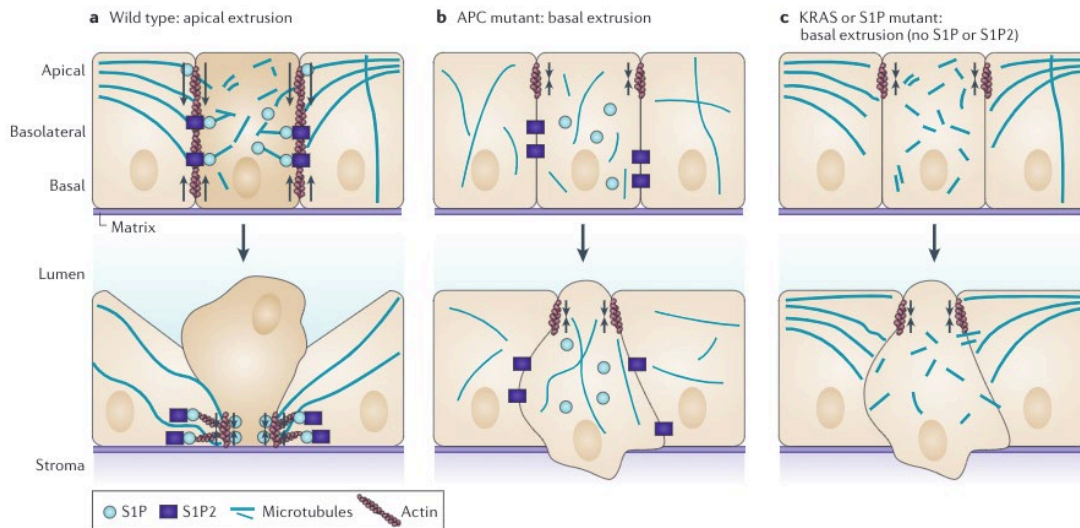


**Figure 29** - Apical or basal & the role of S1P signalling. (a) WT apical extrusion. Both the extruding cells and its neighbours reorient their microtubules toward the basal side of the cell. This is supposed to restrict S1P to the basal side and gives important cues for the apical extrusion. Additionally, Microtubules reorientation in the neighbours leads to Rho increase at the basal side and increase actomyosin contraction leading to apical extrusion. (b) APC is an important microtubule regulator. Its mutation disrupts microtubules dynamics and drives basal cell extrusion. This only affects the cells bearing the mutation hence, cell-autonomous MT dynamics in the extruding cell might be prevalent in setting the orientation of cell extrusion. (c) Constitutive activation of Kras drives the downregulation of S1P and S1P2 by autophagy. This removes the necessary cues to extrude apically and drives basal cell extrusion. This can be replicated by S1P mutants. In both (b) and (c), the junctional actomyosin network drives the basal cell extrusion through apical constriction. Adapted from<sup>301</sup>.

### 3.3.4. Apical or basal? Which way to go?

As I mentioned previously, cells mainly extruded apically in vertebrate systems but rather basally in flies (**Figure 29a**). Additionally, basal extrusion is also a hallmark of aggressiveness for transformed cell<sup>299</sup>. So, how is the direction of extrusion chosen? Ras<sup>V12</sup> cells delaminate basally due to higher rates of autophagy which downregulates S1P (**Figure 29c**)<sup>298</sup>. Alternatively, it seems that microtubules play an important role in that decision by localising p115-RhoGEF. Upon normal extrusion, neighbouring cells relocalised p115-RhoGEF basally which leads to apical extrusion (**Figure 29a**)<sup>168</sup>. Affecting the microtubule regulator APC in clones led to basal cell extrusion suggesting that APC also regulate MTs localisation in the extruding cells (**Figure 29b**)<sup>307</sup>. How both system crosstalk to dictate the direction of extrusion is unclear. In addition to the

localisation of p115-RhoGEF, it seems that MTs could help localising S1P at the apical or basal side. This would reconcile both views and would help to ensure robust decision regarding the direction of extrusion.

### *3.3.5. Collective roles*

As it appears, cell extrusion is a multicellular process. On one hand, it depends on the intracellular constriction of extruding cells. On the other hand, the interactions between extruding cells and their neighbours are key to ensuring correct extrusion. For instance, adhesions between extruding cells and their neighbours mediate force transmission which leads to the remodelling of the actomyosin cortex in neighbouring cells. More generally, the fine coordination between the extruding and its neighbours ensures the maintenance of tissue sealing. I have covered extensively the collective effects in cell death and cell extrusion in a review and through the highlight of back-to-back papers on these issues. I invite the reader to find this review and the dispatch in the appendix of this manuscript (*Appendix-2: review*, *Appendix-3: dispatch*)

### 3.4. The role of caspases

So far, I have covered the different remodelling steps leading to apoptotic cell extrusion. As I highlighted in the first part of this chapter, caspases are the main effector of apoptosis and are therefore likely to be involved in the remodelling steps leading to apoptotic extrusion. Accordingly, both the intrinsic and extrinsic pathway have been shown to induce caspase activation upstream of cell extrusion in both MDCK and HBE cell lines<sup>318</sup>. When caspases were inhibited using pan caspase inhibitor zVAD-FMK cells were becoming necrotic and were not eliminated through cell extrusion. Similarly, caspase activation precedes cell extrusion in different systems. Cell shedding in the mammalian gut is associated with caspase activation and apoptosis. However, it is unclear if caspase activation is the driver of cell extrusion in that context. Indeed, recently, Caspase-3 and -7 double knockout mice in intestinal epithelial cells (IECs) had very minor effects on the shedding process. They elicited no morphological difference or inflammation in the gut. Therefore, Caspase-3 or -7 dependent apoptosis might be dispensable for the homeostatic turnover of IECs<sup>319</sup>. Therefore, it is unclear if cell extrusion is indeed dependent on effector caspase activation.

In Larval Epithelial Cells, the overexpression of the baculovirus caspase inhibitor p35 led to a reduction of about 90% of the number of extruding cells. This led to a consequent delay in the expansion of the neighbouring histoblast tissues. However, extrusion still occurred in p35-positive cells certainly because of pushing forces exerted by the neighbouring histoblasts<sup>37</sup>. In this case, it was not accompanied by MyoII accumulation or E-cad depletion. This is coherent with the role of caspases which cleave ROCK1, E-Cad or  $\beta$ -catenin. This further emphasises the role of caspases in favouring apoptotic cell extrusion but suggests that they may not be entirely necessary for the process. Nevertheless, several examples in *Drosophila* point for a requirement for caspase activation in cell extrusion. During dorsal closure, cells are eliminated through apoptotic cell extrusion. Accordingly, overexpression of p35 in these cells reduces the rate of extrusion and similarly induces delay in dorsal closure<sup>199</sup>. In the developing *Drosophila* legs, Dpp is found to form a gradient. A sharp boundary in that gradient induces Jnk and *reaper*-dependent apoptotic extrusion<sup>200</sup>. As I have described previously, this apoptotic extrusion leads to the formation of an apicobasal actomyosin cable which produces apicobasal forces necessary for fold formation<sup>54</sup>. Accordingly, inducing *reaper* expression ectopically in the wing disc leads to ectopic fold formation. All this is abolished

when cell death is inhibited through the overexpression of p35 in the corresponding domains or through the deletion of the region containing the three apoptotic genes *hid*, *grim* and *reaper* (H99)<sup>200</sup>. Similar process takes places during avian neural tube bending and likewise inhibition of caspase led to impaired bending<sup>47</sup>. Taken together, this enforces the role of caspase activation in cell extrusion.

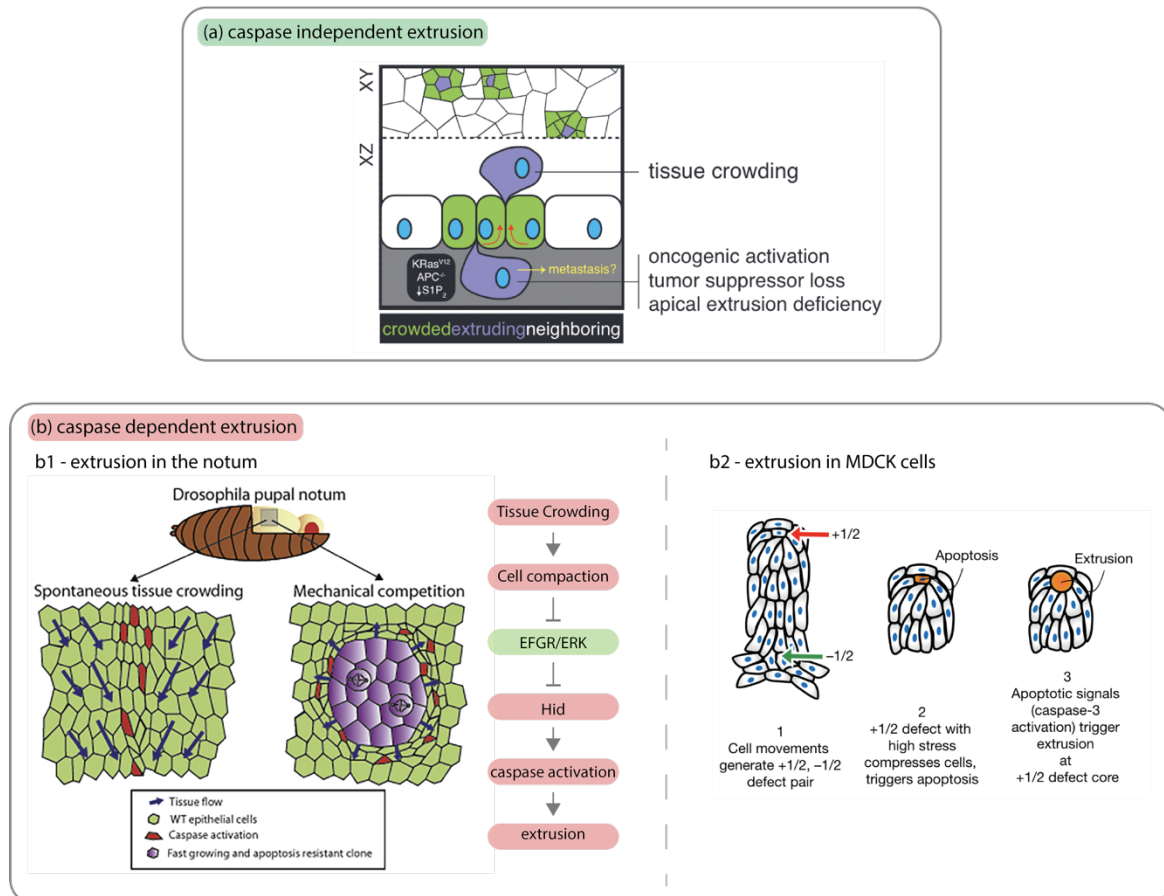


**Figure 30** - Caspases and extrusion. (a) caspase independent cell extrusion. Local tissue crowding promotes cell extrusion in MDCK cells and zebrafish epidermis predominantly without caspase activation. (b) Caspase dependent extrusion. (b1) In the notum, spontaneous tissue crowding, or mechanical competition drives local cell compaction. This downregulates EGFR/ERF. Because EGFR/ERK inhibits the pro-apoptotic gene *hid*, the downregulation of EGFR leads to caspase activation. This ultimately triggers cell extrusion. Interestingly, tissue stretching can activate EGFR/ERK and promote survival. The inhibition of caspase activation by diverse means leads to the inhibition of cell extrusion. Conversely, activation of Dronc by optogenetics leads to caspase activation and cell extrusion. (b2) topological defects in the cell alignment drives local compressive stresses which lead to caspase activation and caspase dependent cell extrusion.

However, puzzling results contrast this view. For instance, earlier results show that caspase inhibition of MDCK layers through zVAD-FMK didn't block cell extrusion<sup>270</sup>. Correspondingly, *C. elegans* cells which normally die through a caspase mediated process are extruded in *C. elegans* mutant embryos lacking all the caspases genes<sup>187</sup>. The implication of caspase during that process seems to depend on the signal leading to cell

extrusion. Accordingly, crowding-induced cell extrusion seems to be variability associated with caspase activation in human colon, zebrafish epidermis and MDCK cell culture (**Figure 30a**)<sup>274</sup>. Indeed, in these contexts, using Cleaved Caspase-3 staining, they found predominantly caspase-negative extrusions ranging from 67% of the extrusions in MDCK culture up to 88% in the zebrafish epidermis. By contrast, epidermis treated with geneticin drove mainly apoptotic extrusions. The extrusions not associated with caspase activation were observed in regions of higher cell density (**Figure 30a, Figure 27a**). To replicate crowding artificially they plated cells on a stretched substrate that was then relaxed. This led to compaction and crowding. Upon this overcrowding condition, the number of cells extruding without any noticeable caspase activation was similar to the homeostasis condition. Once replated these extruding cells were able to proliferate again to confluent layers. Similar results were obtained by using nucview to label caspase activation. Inhibition of BCL-2 didn't block live extrusion but reduced the number of apoptotic extrusions. Similar results were obtained by blocking JNK. This suggests that crowding induced extrusion are independent of caspase activation. Conversely, inhibiting the stretched activated channel Piezo led to a reduction of live extrusion suggesting that it is necessary for live extrusion. Finally, live extrusions share similar mechanisms to the apoptotic extrusion because the inhibition of ROCK or S1P which are necessary to apoptotic extrusion also inhibited live extrusion. Therefore, in the context of overcrowding in these tissues it seems that part of the extrusions happens independently of caspase activation.

Similar results were initially obtained in the *Drosophila* pupal notum upon crowding<sup>280</sup>. Cells mainly extrude in the midline: a region of higher crowding. Accordingly, increased extrusion was observed in the midline upon the induction of growth through overexpression of p110 or PTEN under the control of pnr-Gal4 (a driver expressed throughout the notum). The inhibition of growth on the other hand reduced cell extrusion in the midline arguing for a crowding induced extrusion process in the notum. Extrusion in the midline were different than the one induced after UV irradiation. They extruded by progressively losing neighbours and by staying anisotropic compared to UV treated cells which abruptly lost neighbours. This suggested that they are triggered by different mechanisms. When caspase activation was inhibited by the overexpression of Diap1 in the notum under the control of npr-Gal4, this resulted only in a mild and non-significant decrease of the number of extrusions in that context. Thus, the authors argued for those extrusions in the midline are non-apoptotic extrusion induced by local overcrowding.

However, these results were never reproduced in the notum. First, previous results in the lab demonstrate that caspase activation precedes cell extrusion (**Figure 30b1**). These observations were made using different caspase reporters such as *apoliner* or the fret sensor *scat3*. Both reporters yielded similar results and showed that caspases were activated with various lag time from 60 to 420min prior to termination of extrusion. Likewise, we monitored caspase activation using the GC3Ai caspase reporter which showed that caspases exponentially accumulate prior to cell extrusion. Finally, the lab developed an optogenetic tool to drive Dronc activation. Blue-light-induced clustering of Dronc led to its trans-activation activation which was sufficient to drive cell extrusion in the notum. Therefore, caspase activation precedes and is sufficient for cell extrusion in the notum.

Initial results by the lab showed that constitutive overexpression of the caspase inhibitor Diap1 under the control of act-Gal4 nearly abolished all extrusions both in the midline and outside extrusion<sup>281</sup>. Similarly, extrusion was nearly abolished in Flip-out clones expressing Diap1 or the effector caspase inhibitor p35 or in mitotic clones with a homozygous deletion covering all pro-apoptotic genes (H99). Additionally, overexpression of Diap1 specifically in the midline under the control of Dad-Gal4 led to a substantial thickening of the midline arguing again for an inhibition of cell extrusion. Similar results were obtained by driving Diap1 under the control of pnr-Gal4 across the whole notum. More recent results from our lab show that death in the notum is dependent on the pro-apoptotic gene *hid* and not *rpr*. Indeed, RNAi knockdown against *hid* but not *rpr* led to an increase of midline thickness when driven across the whole notum. Similarly, *hid*-RNAi clones displayed nearly no extrusion compared to control clones. This is also supported by the observation that *hid* is enriched in the midline. Additionally, inhibiting EGFR led to smaller nota because of an increased probability of cell extrusion while overexpression of EGFR reduced the probability to extrude (**Figure 30b1**). This was rescued by *hid* downregulation. Therefore, EGFR promotes cell survival in the notum by downregulating *hid*. Interestingly, EGFR/ERK levels are downregulated by tissue compaction which mediates crowding induced cell extrusion in the notum.

Finally, these results were also confirmed by other labs. First, the Miura group showed that delimitation in the midline were drastically reduced upon RNAi against *hid*, *grim* and *repear* or only *hid*. Moreover, they showed that Dark-RNAi (*apaf-1* homologue) or Dronc-RNAi achieved similar results. Furthermore, they also overexpressed Diap1 or p35



under the control of pnr-Gal4 which equally resulted in nearly total inhibition of extrusion. These data further emphasise that caspase activation is necessary for cell extrusion in the notum. Secondly, compression-dependent cell extrusion in MDCK layers may also be triggered by caspases activation. Indeed, the Ladoux group showed that topological defects in the alignment of cell in MDCK layers lead to local high compressive stresses (**Figure 30b2**). These stresses occurred 100min before caspase-3 activation and drive caspase-3 activation, as monitored by the use of nucview. This ultimately leads to cell extrusion. Accordingly, inhibiting caspase-3 activation largely inhibited cell extrusion in MDCK layers without affecting the number of defects. This show that compression-driven cell extrusion may also be driven by caspase-3 activation in MDCK layers.

Therefore, caspase activation preceding extrusion is debated and may depend on the system used. However, it is clear that in the notum caspase activation precedes cell extrusion. It is also necessary and sufficient for cell extrusion in the notum. Alternatively, the process of extrusion and apoptosis may be considered as a separated part. As it was suggested before<sup>318</sup>, the extrusion step may be seen as a non-apoptotic process in which caspase may be involved or not through their non-apoptotic functions.

**Conclusion: Take-home messages.**

The extrusion involves the constriction through the actomyosin cortex and cell-cell adhesion mainly through E-cad adherens junctions similarly to diverse cell shape changes. The mode of constriction may differ depending on the extrusion system and may involve actomyosin contractile pulses, purse-string contraction, or a mix between purse-string contractility and basal lamellipodia. Similarly, the direction of extrusion depends on the system. In either case, the E-cad adhesion are key in transmitting forces and remodelling the F-actin network in neighbouring cells. Thus, by definition, cell extrusion is a multicellular process that involves coordination between the extruding cell and its direct neighbours or even larger cellular population (see review). The necessity for caspase may be debated depending on the context. However, it clearly emerges that caspase activation is necessary for cell extrusion in *Drosophila* and particularly in the *Drosophila* pupal notum.

## CHAPTER CONCLUSION: PhD problematic.

I have illustrated how epithelial morphogenesis arises from cell shape changes and apoptosis. I first showed how the actomyosin cortex, E-cad adhesions, and microtubules crosstalk in cell shape regulation. The first chapter was focused on their role in cell shape changes during tissue morphogenesis. The amount of F-actin, the length of filaments, the rate of polymerisation together with the density of crosslinkers modulate to a large extent the ability of the network to constrict upon MyoII activity. This motor is able to exert forces by sliding F-actin filaments. Its activity can be modulated by kinases whose function is regulated by a balance of activators like RhoGEF or inhibitors like RhoGAP. Taken together, this complex network exhibits complex architectures and dynamics such as belts or pulses. These different dynamics are key in producing forces necessary to deform epithelial apical area and to drives morphogenesis. In order to do so however, the pulling forces exerted by the actomyosin network need to be coupled to the cell boundary by E-cad-mediated adhesion. This allows the remodelling of apical area by contractile forces and, because cells are coupled to each other, it allows the transmission of forces necessary to bend tissues. These forces are balanced by the ability of the cell to resist compression which may be driven by microtubules. Their dynamics and long persistence length makes them able to exert pushing forces or bear considerable compressive loads. Moreover, they interact highly with the actomyosin cortex. Taken together, this emphasises how MTs can be important to modulate epithelial cell shape changes.

In the second chapter, I have then described how apoptosis can be a mediator of tissue morphogenesis and how it is itself mediated by caspases. Moreover, in epithelia, apoptotic cells are removed through the process of cell extrusion. This process is a sequence of remodelling steps that involves the constriction of the extruding cell together with coordinated remodelling in its neighbours. This ensures the removal of cells from epithelial layers without impairing the sealing property of these tissue. So far, studies on cell extrusion have mainly focused on the role of actin, myosin and E-cad given their ability to modulate cell shape changes. Effector caspases have hundreds of substrates in epithelial cells. Interestingly, some of the previously mentioned cell shape regulators are cleaved by effector caspases to trigger cell shape changes during apoptosis. However, it appears that very few of these substrates were functionally analysed in the context of epithelial tissue. While it can be debated in other systems, I showed how cell extrusion is always preceded by caspase activation in the notum and how caspase activation is



necessary and sufficient to drives cell extrusion in this single layer epithelium. This clearly demonstrates that caspase activation orchestrates cell extrusion in the notum. Yet, no clear characterisation of cell extrusion in the notum was performed to this date. Additionally, virtually nothing is known on how caspase activity may orchestrate cell extrusion and what are the substrates cleaved by caspases which mediate the cell shape changes necessary to push a cell out of the epithelium. My PhD emerged from these observations and aimed at answering the following question:

**Which steps of extrusion are regulated by caspases or how effector caspase activation initiates and orchestrates epithelial cell extrusion?**

#### **4. Results: Paper: Microtubule disassembly by caspase is the rate-limiting step of cell extrusion**

Hereafter the reader will find the results of the main part of my PhD. Additionally, the reader can find all the supplementary material of this paper in the first appendix of this PhD manuscript ([Appendix-1: paper supplementary material](#))

# Microtubule disassembly by caspases is an important rate-limiting step of cell extrusion

Alexis Villars <sup>1,2</sup>, Alexis Matamoro-Vidal<sup>1</sup>, Florence Levillayer<sup>1</sup> & Romain Levayer <sup>1</sup>✉

The expulsion of dying epithelial cells requires well-orchestrated remodelling steps to maintain tissue sealing. This process, named cell extrusion, has been mostly analysed through the study of actomyosin regulation. Yet, the mechanistic relationship between caspase activation and cell extrusion is still poorly understood. Using the *Drosophila* pupal notum, a single layer epithelium where extrusions are caspase-dependent, we showed that the initiation of cell extrusion and apical constriction are surprisingly not associated with the modulation of actomyosin concentration and dynamics. Instead, cell apical constriction is initiated by the disassembly of a medio-apical mesh of microtubules which is driven by effector caspases. Importantly, the depletion of microtubules is sufficient to bypass the requirement of caspases for cell extrusion, while microtubule stabilisation strongly impairs cell extrusion. This study shows that microtubules disassembly by caspases is a key rate-limiting step of extrusion, and outlines a more general function of microtubules in epithelial cell shape stabilisation.

<sup>1</sup>Department of Developmental and Stem Cell Biology, Institut Pasteur, Université de Paris Cité, CNRS UMR 3738, 25 rue du Dr. Roux, 75015 Paris, France.

<sup>2</sup>Sorbonne Université, Collège Doctoral, F75005 Paris, France. ✉email: [romain.levayer@pasteur.fr](mailto:romain.levayer@pasteur.fr)

How epithelia maintain their physical and chemical barrier functions despite their inherent dynamics due to cell proliferation and cell death is a central question of epithelial biology. Cell extrusion, a sequence of coordinated remodelling steps leading to cell expulsion, is an essential process to conciliate high rates of apoptosis and cell elimination while preserving tissue sealing<sup>1,2</sup>. This process is essential for tissue homeostasis and its perturbation can lead to chronic inflammation or contribute to tumoural cell dissemination<sup>2,3</sup>. Yet much remains unknown about extrusion regulation and orchestration.

Studies in the last decade have demonstrated that the remodelling steps of extrusions are mainly dependent on actomyosin contraction and mechanical coupling through E-cadherin (E-cad) adhesion. First, an actomyosin ring forms in the extruding cell driving cell-autonomous constriction<sup>4–6</sup>. This ring pulls on neighbouring cells through E-cad anchorage, resulting in force transmission which promotes the recruitment of actomyosin in the neighbouring cells and the formation of a supracellular actomyosin cable<sup>1,4–7</sup>. Eventually, the constriction of the cable combined with E-cad disassembly<sup>6,8</sup> leads to cell expulsion either on the apical or the basal side of the tissue. Meanwhile, neighbouring basal protrusions also contribute to cell detachment<sup>9,10</sup>. Alternatively, pulses of contractile medio-apical actomyosin can also contribute to cell expulsion<sup>11,12</sup>. Interestingly, while a lot of emphases has been given to actomyosin and E-cad regulation, we only have a limited understanding of the contribution of other cellular factors and cytoskeleton components to cell extrusion (see ref. <sup>13</sup> for one exception). Apoptosis is one of the main mode of programmed cell death which is essential for tissue homeostasis and morphogenesis<sup>14</sup>. It is driven by the activation of caspases which through the cleavage of thousands of proteins orchestrate cell deconstruction<sup>15</sup>. While caspase activation is an important mode of epithelial cell elimination<sup>14</sup>, how caspases orchestrate the key steps of extrusion remain poorly understood. Accordingly, only a handful of caspase targets relevant for cell extrusion have been identified so far<sup>16</sup>.

The morphogenesis of the *Drosophila* pupal notum, a single-layer epithelium located in the back of the thorax, is an ideal system to study the regulation of apoptosis and cell extrusion. High rates of cell extrusion in reproducible patterns are observed in the midline and posterior region of the notum<sup>17–21</sup>. Interestingly, the majority of cell extrusion events in the pupal notum are effector caspase-dependent. Accordingly, caspase activation always precedes cell extrusion and inhibition of caspase in clones or throughout the tissue dramatically reduces the rate of cell extrusion<sup>18,20–22</sup>. However, we currently do not know which steps of extrusion are regulated by caspases or how effector caspase activation initiates and orchestrates epithelial cell extrusion.

Here, we performed the quantitative phenomenology of cell extrusion in the midline of the pupal notum. Surprisingly, while we observed the formation of a supracellular actomyosin ring in the late phase of extrusion, the initiation of cell apical constriction was not associated with any change in the dynamics and concentration of actomyosin and Rho. Accordingly, comparison with the behaviour of extruding cells in a vertex model suggested that cell extrusion in the notum is not initiated by a change of line tension. Moreover, the speed of extrusion is poorly affected by the reduction of MyoII activation. Instead, we found that cell extrusion initiation is concomitant with the disassembly of an apical mesh of microtubules (MTs). This disassembly is effector caspase-dependent and is required for cell extrusion. More importantly, the requirement of caspase activation for extrusion can be bypassed by MT disassembly, and MTs stabilisation strongly impairs cell extrusion, suggesting that the remodelling of MTs by caspases is an important rate-limiting step of cell extrusion. This work also emphasises the need to study the

contribution of microtubules to epithelial cell shape regulation independently of actomyosin regulation.

## Results

**Actomyosin modulation is not responsible for extrusion initiation.** We focused on the *Drosophila* pupal notum midline (Fig. 1a, b), a region showing high rates of cell death and cell extrusion<sup>17–20</sup>. To better characterise the process of cell extrusion, we first quantified the evolution over time of the main regulators of cell–cell adhesion (E-cad) and cortical tension (non-muscle MyosinII, MyoII) by averaging and temporally aligning several extruding cells (one extrusion event lasting ~30 min). Contrary to other tissues<sup>6,8</sup>, we did not observe a depletion of E-cad at the junctions during the constriction process, but rather a progressive increase of its concentration (Fig. 1c, d and Supplementary Movie 1). More strikingly, the onset of cell extrusion (defined by the inflexion of the apical perimeter, see “Methods”) was not associated with a clear increase of MyoII levels (looking at myosin regulatory light chain, MRLC, Fig. 1e, f, Supplementary Movie 2), either at the junctional pool or in the medio-apical region (Supplementary Fig. 1a). Instead, a clear accumulation of MyoII forming a supracellular cable was observed during the last 10 min of cell extrusion (Fig. 1e, f and Supplementary Fig. 1a). Similar to extrusion in other systems<sup>1,4,6,7</sup>, both the dying cells and its neighbours contribute to the late accumulation of MyoII, the cell-autonomous accumulation slightly preceding the accumulation in the neighbours (Supplementary Fig. 1b). Similarly, F-actin starts to accumulate only in the late phase of extrusion concomitantly with the formation of the supracellular cable (Fig. 1g, h, Supplementary Fig. 1h, i and Supplementary Movie 3), similar to the dynamics we observed for Rho1, a central regulator of F-actin, MyoII activity and pulsatility<sup>23</sup> (Supplementary Fig. 1j–l and Supplementary Movie 4).

Pulsatile actomyosin recruitment is observed during a wide variety of morphogenetic processes<sup>24–26</sup>. We also observed fluctuating levels of MyoII (Fig. 1i and Supplementary Fig. 1c) with pulses correlating with transient constriction of the cell apical perimeter (Supplementary Fig. 1c, d). The amplitude, duration and/or frequency of MyoII pulses can affect the efficiency of cell constriction<sup>27</sup>. However, we did not observe any significant change of these parameters before and after the onset of cell extrusion (Supplementary Fig. 1e–g). Finally, to better characterise the link between perimeter constriction and MyoII dynamics, we calculated a contraction yield (the ratio of constriction rate over the intensity of MyoII). We observed a significant increase in the contraction yield at the onset of cell extrusion (Fig. 1j, k), suggesting that similar MyoII pulses lead to more deformation after the onset of extrusion.

Altogether, we found that the initiation of cell extrusion and apical constriction is not associated with a significant change of actin, MyoII and Rho dynamics/levels. Their enrichment appears during the last 10 min of extrusion and is associated with the formation of a supracellular actomyosin cable. This suggests that MyoII activation/recruitment and dynamics are not sufficient to explain the initiation of extrusion and that MyoII activation is unlikely to be the rate-limiting step that initiates cell extrusion. Accordingly, we observed a significant increase of MyoII levels upon inhibition of caspase activity (by depleting Hid, a proapoptotic gene, Supplementary Fig. 1m, n), a condition that almost completely abolishes cell extrusion<sup>20</sup>, suggesting once again that MyoII recruitment is not the main rate-limiting step of extrusion downstream of caspases.

**Cell extrusion in the midline is not driven by increased line tension.** To get a better understanding of the mechanical

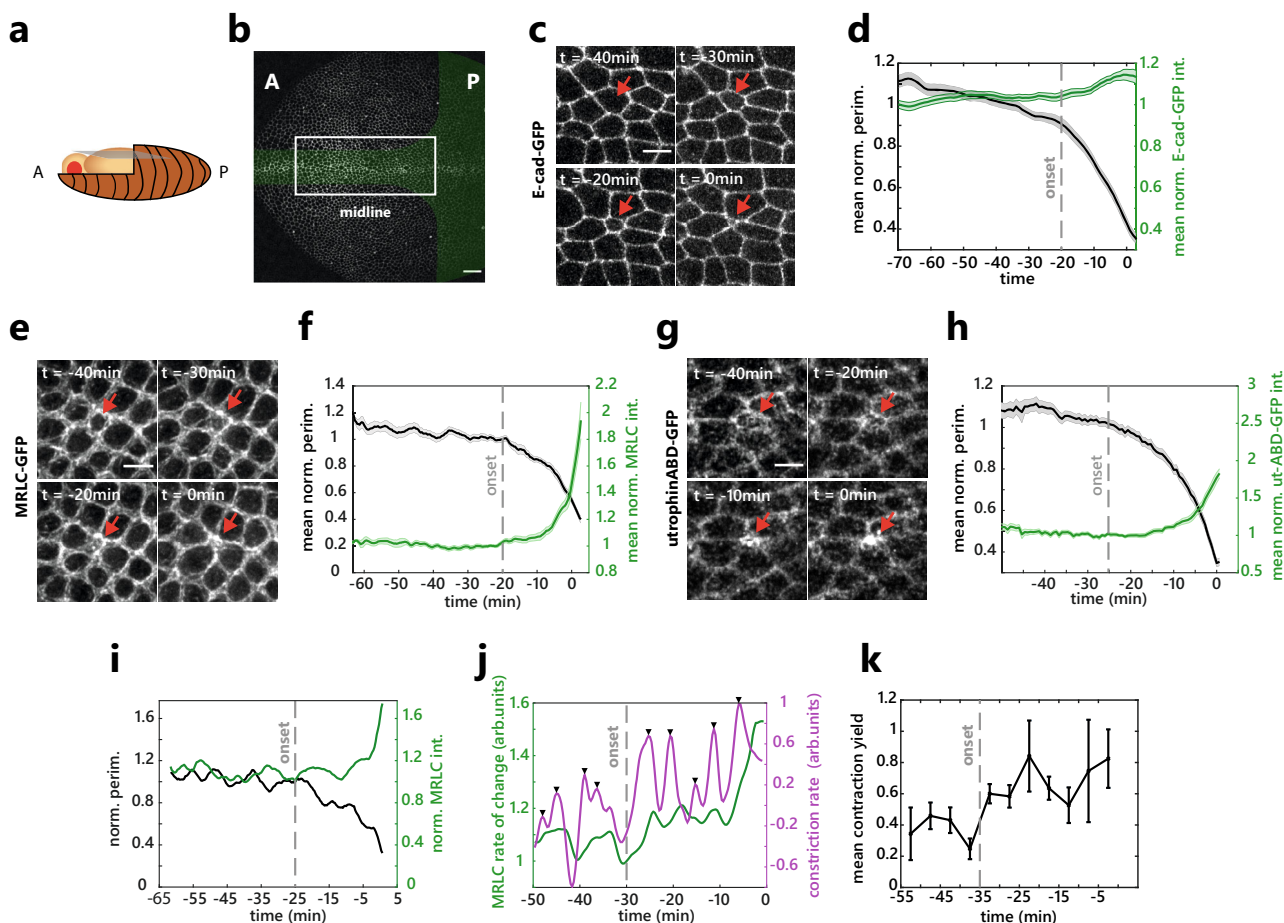


**Fig. 1 Actomyosin modulation is not responsible for the initiation of cell extrusion.** **a** Schematic of a *Drosophila* pupae. A: anterior, P: posterior. **b** Notum at 16 h after pupal formation (APF). Green zone: domains with a high rate of cell elimination, white rectangle: midline region. A: Anterior, P: Posterior. Scale bar, 25  $\mu$ m. **c** Snapshots of E-cad-GFP during cell extrusion. The red arrow shows an extruding cell.  $t_0$ , time of extrusion termination (apical area = 0). Scale bar, 5  $\mu$ m. **d** Averaged and normalised E-cad-GFP junctional signal during cell extrusion (green) and cell perimeter (black), light colour areas are SEM. The curves were aligned temporally by using the extrusion termination time point (see “Methods”). The grey dotted line represents the onset of extrusion marked by the inflection of the perimeter curve (see “Methods”).  $N = 2$  pupae,  $n = 27$  cells. **e** Snapshots of sqh-GFP (MRLC) during cell extrusion. The red arrow shows an extruding cell.  $t_0$ , time of extrusion termination. Scale bar, 5  $\mu$ m. **f** Averaged normalised sqh-GFP (MRLC) total signal (medial+junctional) during cell extrusion (green) and cell perimeter (black). The grey dotted line is the onset of extrusion, light colour areas are SEM.  $N = 2$  pupae,  $n = 15$  cells. **g** Snapshots of actin during cell extrusion (utrophin Actin-Binding domain fused to GFP, utABD-GFP). Red arrow points at an extruding cell.  $t_0$ , time of extrusion termination. Scale bar, 5  $\mu$ m. **h** Averaged normalised utABD-GFP total signal (medial + junctional) during cell extrusion (green) and cell perimeter (black). Grey dotted line represents the onset of extrusion, light colour areas are SEM.  $N = 2$  pupae,  $n = 37$  cells. **i** Single-cell representative curve of sqh-GFP (MRLC) total signal (green) and perimeter (black) showing MRLC pulsatility and perimeter fluctuations before and during cell extrusion. Grey dotted line represents the onset of extrusion. **j** Single-cell representative curve of sqh-GFP (MRLC) intensity rate of change (i.e., derivative, green) and the perimeter constriction rate (derivative of the perimeter, magenta). Black arrows show contraction pulses. Grey dotted line represents the onset of extrusion. **k** Averaged contraction yield (ratio of the constriction rate over MRLC junctional intensity) calculated in 5 min time windows (see “Methods”). The dotted line, extrusion onset, and error bars are SEM.  $N = 2$  pupae,  $n = 15$  cells. Source data are provided in the source data file.

parameters regulating the initiation of cell extrusion in the midline, we used a 2D vertex model. The apical area of cells in the model can be modulated by two main parameters: the line tension, a by-product of junctional actomyosin and cell–cell adhesion which tends to minimise the perimeter of the cell, and the area elasticity, which constrains the variation in the apical area of the cells and is thought to emerge from the incompressibility of cell volume and the properties of the medio-apical cortex<sup>28,29</sup>. The formation of a supracellular actomyosin cable, as observed in other instances of extrusion<sup>1,6</sup>, should lead to an increase of line tension/contractility. Note that the line tension parameter in the vertex model do not distinguish the contribution of the dying cell and its neighbours. We simulated such extrusion by implementing a progressive increase of the contractility parameter in a single cell (see “Methods”). This led to a progressive decrease in

cell apical area concomitant with cell rounding (Fig. 2a, c, e, g and Supplementary Movie 5, progressive increase of cell circularity), in good agreement with the profile of extrusion observed in the larval epidermal cells of the abdomen which are driven by an actomyosin purse string<sup>6</sup> (Fig. 2i and Supplementary Fig. 2a). This, however, did not fit the pattern we observed in the midline of the pupal notum, where the initial phase of cell constriction is not associated with cell rounding (Fig. 2j). Cell constriction could also be initiated by a reduction of the cell resting area, which corresponds to the targeted apical area of cells in the absence of external constrains. Accordingly, the reduction of the resting area of a single cell in the vertex model led to cell constriction concomitant with a progressive reduction of cell roundness (Fig. 2a, d, f, h and Supplementary Movie 5), in good agreement with the dynamics we observed during the first 20 min of extrusion in the



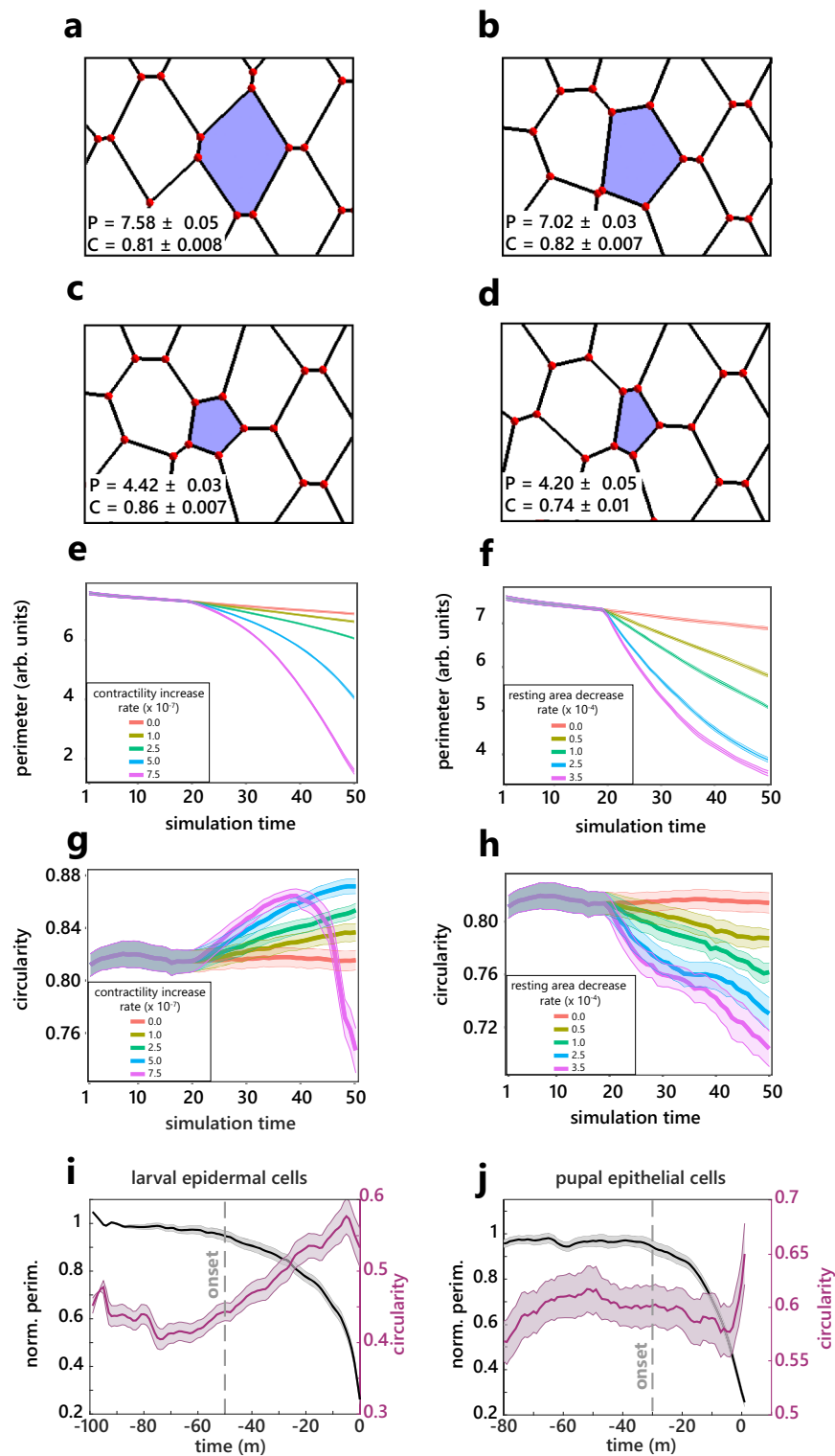


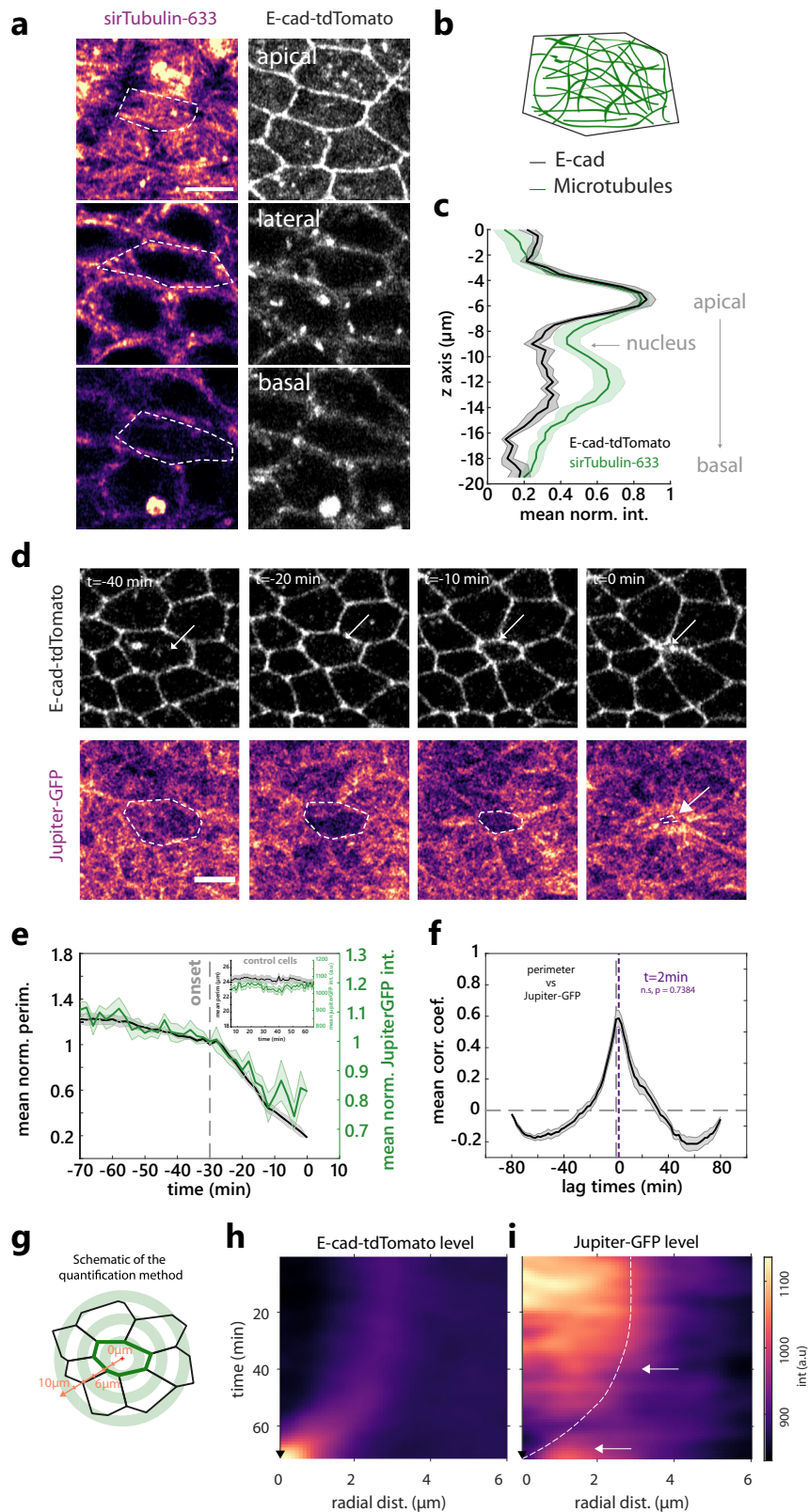
**Fig. 2** Cell extrusion in the midline is different from purse-string driven extrusion. **a–d** Examples of a tracked cell (blue) from a vertex model during the early extrusion phase at different simulation time steps (sts) and under different conditions.  $P$  is the average perimeter  $\pm$  SEM, and  $C$  denotes average circularity  $\pm$  SEM for the ten tracked cells of the simulations. **a** Initial state at sts = 1. **b** Control simulation (no change of parameter in the blue cell) at sts = 40. **c** Extrusion driven by increased cell contractility  $\bar{\Gamma}_\alpha$  (contractility increase rate  $c = 7.5 \cdot 10^{-7}$ ), at sts = 40. **d** Extrusion through the decreased resting area  $A\alpha^{(0)}$  (resting area decrease rate  $r = 3.5 \cdot 10^{-4}$ ) at sts = 40. **e, f** Averaged cell perimeter  $\pm$  SEM for ten tracked cells as a function of contractility increase rate (**e**) and of resting area decrease rate (**f**). Variation of contractility and resting area was initiated at sts = 20. **g, h** Average cell circularity  $\pm$  SEM for ten tracked cells as a function of contractility increase rate (**g**) and of resting area decrease rate (**h**). Variation of contractility and resting area was initiated at sts = 20. **i, j** Averaged cell circularity (magenta) and averaged and normalised cell apical perimeter (black) during cell extrusion in larval epidermal cells,  $n = 37$  cells,  $N = 2$  pupae. **i** and in the pupal notum epithelial cells,  $n = 22$  cells,  $N = 2$  pupae (**j**). Light colour areas are SEM. Grey dotted lines show the onset of extrusion. Source data are provided in the source data file.

notum (Fig. 2j), compare to yellow to purple lines in Fig. 2h with different rate of reduction of resting area). Importantly, while depleting ROCK (the main activator of MyoII<sup>30</sup>) by RNAi had a stringent effect on the epithelial morphology and blocked cytokinesis, it had no significant impact on the speed of extrusion (Supplementary Fig. 2b, c). In this context, the deformations occurring during extrusion were associated with a strong decrease of circularity and the absence of cell rounding in the late phase (Supplementary Fig. 2c), confirming the link between the late rounding observed in WT extrusion and the increase of actomyosin (Fig. 2j). Thus, global modulation of MyoII activation has little impact on cell extrusion in the notum, in agreement with an extrusion regime poorly relying on changes in line tension. Altogether, this confirmed that the initiation of cell extrusion in the midline is unlikely to be driven by an increase in line tension/junction contractility, but rather by a process modulating cell resting area/compressibility.

**The disassembly of microtubules correlates with the onset extrusion.** We next sought to identify which alternative factors could initiate cell extrusion in the midline of the pupal notum. Caspase activity can lead to a reduction of cell volume<sup>31</sup>, which could be responsible for the reduction of cell apical area. However, we did not observe a significant change in cell volume during the process of cell extrusion (Supplementary Fig. 2d, e and Supplementary Movie 6). Alternatively, a downregulation of extracellular matrix (ECM) binding on the cuticle side could facilitate apical area constriction. Yet we did not observe a modulation of integrin adhesion components at the onset of extrusion (Supplementary Fig. 2f and Supplementary Movie 7). We, therefore, checked the distribution of microtubules (MTs), which can also regulate epithelial cell shape<sup>32,33</sup>. MT filaments accumulate in the medio-apical region of the midline cells as well as along the apicobasal axis (Fig. 3a–c). We tracked the orientation of MT growth in the medio-apical plane using the plus-end binding protein EB1, and found no obvious radial orientation of MTs (Supplementary Fig. 3a, b check also the non-extruding cells in Supplementary Movie 8), in agreement with a non-centrosomal pool of MTs<sup>32</sup>. Strikingly, we observed a significant and reproducible depletion of apical MTs at the onset of cell extrusion (visualised with the MT-associated protein Jupiter-GFP, Fig. 3d–f, Supplementary Movie 9). This depletion is concomitant with the onset of apical constriction (Fig. 3e, f, peak of cross-correlation between MTs intensity and cell perimeter with no significant lag time). The same downregulation was observed with EB1-GFP, a marker of MT plus ends (Supplementary Fig. 3c–g, Supplementary Movie 10, Supplementary Movie 8 at high temporal resolution), or upon expression of a tagged human  $\alpha$ -tubulin (Supplementary Fig. 3h and Supplementary Movie 11). While we observed some fluctuations of MTs intensity in the non-extruding cells, the amplitude of these variations were much milder and non-persistent compared to the depletion observed during extrusion (see Fig. 3e inset and Supplementary Fig. 3g). Interestingly, MT depletion in the extruding cell was followed later-on by an accumulation in the neighbouring cells of MTs close to the junctions shared with the dying cell (Fig. 3d, g–i, Supplementary Fig. 3c–e and Supplementary Movies 9–11). This accumulation matches the timing of the actomyosin ring formation (Fig. 1e–h) and is reminiscent of the MTs reorganisation previously described near MDCK extruding cells<sup>34</sup>. The loss of apico-medial MTs may be driven by the reorganisation of the non-centrosomal MTs regulators Patronin and Shot<sup>33,35–38</sup>. However, we could not observe a clear modulation of their localisation/levels at the onset of cell extrusion (Supplementary Fig. 3i, j). Alternatively, the apical disappearance of MTs may be

driven by a basal shift of centrosomes (as observed in the dorsal folds of the early *Drosophila* embryo<sup>33</sup>), but we did not observe any change in the apicobasal position of the centrosomes at the onset of extrusion (Supplementary Fig. 3k). Finally, MTs downregulation may be driven by a global disassembly of MT filaments. Accordingly, the disappearance of MT filaments is not restricted to the most apical domain and seems to occur throughout the cell, as visualised with atub-mCherry (Supplementary Fig. 4a–c), or in single cells expressing EB1-GFP (Supplementary Fig. 4d, e). We then checked whether this depletion was dominated by a change of polymerisation rate or depolymerisation rate of MTs by assessing putative lag time between the changes of EB1 comets (new growing MTs) and changes in the total pool of MTs (using sirTubulin). We could not detect any significant lag time between the reduction of EB1 and total pool of MTs during extrusion (Supplementary Fig. 3l–n), which could be compatible with a process affecting both the polymerisation and the depolymerisation rate (see below and “Discussion”). Altogether, we observed a global disassembly of the MT network which is perfectly concomitant with the onset of cell extrusion and apical area reduction.

**MT depletion is effector caspase-dependent.** We then checked what could be responsible for MT disappearance. MT buckling driven by cell deformation can trigger MT disassembly<sup>39–41</sup>. As such, MT depletion during extrusion may be a cause or a consequence of the initiation of cell apical area constriction. To check if area constriction is sufficient to trigger MTs disassembly, we released tissue prestress in the notum by laser cutting a large tissue square<sup>20,42</sup>. The transient constriction of the cell apical area in the square region correlated with a transient increase of apical MT concentration (Supplementary Fig. 5a–d and Supplementary Movie 12), which is then followed by cell apical area re-expansion and MT intensity diminution. This suggests that cell apical constriction is not sufficient to disassemble MTs and that an active process must drive MT disassembly at the onset of extrusion. The activation of effector caspases is necessary for extrusion and always precedes cell constriction in the pupal notum<sup>18,20,22</sup>. We, therefore, checked whether effector caspase activation was necessary and sufficient for MT depletion. In agreement with caspase activation systematically preceding extrusion and MT depletion being concomitant with the onset of extrusion (this study), effector caspase activation (using the live marker GC3A1<sup>43</sup>) was systemically observed in cells depleting MTs and extruding (Supplementary Fig. 5e and Supplementary Movie 13). We then checked whether caspase activation was sufficient to deplete MTs. Previously, we developed an optogenetic tool (optoDronc<sup>21</sup>) which can activate *Drosophila* Caspase9 triggering apoptosis and cell extrusion upon blue light exposure (Fig. 4a). We observed a rapid depletion of MTs (visualised with injected sirTubulin) upon activation of optoDronc in clones which was concomitant with cell apical constriction (Fig. 4b–d and Supplementary Movie 14, top, no significant lag time between sirTub diminution and perimeter constriction). Importantly, we confirmed in this condition that MTs depletion was occurring throughout the cell both on the apical and the basal side (Supplementary Fig. 4f, g). Activating optoDronc while inhibiting effector Caspases through p35 dramatically slowed down the rate of cell extrusion (ref. <sup>21</sup> and Fig. 4e–g and Supplementary Movie 14, bottom). While we could still see a late accumulation of MyoII in these slow constricting cells (Supplementary Fig. 5f, 3 h post optoDronc activation), we could no longer observe MT depletion but rather a progressive increase (albeit variable) in the apical concentration of MTs (Fig. 4e–g and Supplementary Movie 14, bottom). This is in agreement with the appearance of



cells with the low apical area and strong tubulin accumulation that we observed in *hid-RNAi*/caspase-inhibited clones (Fig. 4h–j), a combination that we did not observe in WT cells. Interestingly, contrary to normal extrusions in the notum (Fig. 2j), circularity progressively increases during perimeter constriction upon optoDronc activation in cells expressing p35 (Fig. 4g). This fits with a slow constriction driven by an increase

of contractility/line tension. Altogether, this suggests that MT depletion during extrusion is driven directly or indirectly by effector caspases activation.

**MT up/downregulation can increase/decrease cell apical area.**  
The correlation between MT depletion and extrusion initiation

**Fig. 3 Microtubules depletion correlates with the onset of cell extrusion in the notum.** **a** Microtubules (MTs) visualised with sirTubulin (left, pseudocolour) and E-cad-tdTomato (right, greyscale) along the apicobasal axis in a midline cell. White dotted lines, cell contour. Scale bar, 5  $\mu\text{m}$ . **b** Schematic of MTs orientation in the junctional plane. **c** sirTubulin (green) and E-cad-tdTomato (black) averaged and normalised intensity along the apicobasal axis. 0  $\mu\text{m}$  is the most apical plane.  $N = 10$  cells. The light area is SEM. **d** Snapshots of Jupiter-GFP (total tubulin, bottom, pseudocolour) and E-cad-tdTomato (top, greyscale) during cell extrusion, white arrows and white dotted lines show the extruding cell.  $t_0$  min, termination of extrusion. Scale bar, 5  $\mu\text{m}$ . **e** Averaged normalised Jupiter-GFP medial signal (green) and cell perimeter (black) during cell extrusion. Grey dotted line, extrusion onset, light colour areas, SEM.  $t_0$  is the onset of extrusion.  $N = 2$  pupae,  $n = 24$  cells. Inset represents averaged perimeter (black) and Jupiter-GFP (green) intensity variations for control non-extruding cells.  $N = 2$  pupae,  $N = 21$  cells. **f** Averaged normalised cross-correlation of the cell perimeter vs Jupiter-GFP. The purple dotted line is at the maximum correlation coefficient ( $t = 2$  min, not significantly different from  $t = 0$  min,  $P$  value = 0.7384, movie frame rate 1 min). Horizontal grey dotted line at correlation coefficient = 0. Vertical dotted line is at lag time = 0 min. Light area is SEM.  $n = 24$  cells. **g** Schematic of the method used to represent averaged MTs intensity profile in space and time during extrusion using radial line intensity (orange line). Red cross shows the centre of the extruding cell (junctions, green). See “Methods”. **h** Radial averaged kymograph (see panel **g**) of E-cad-tdTomato (left, pseudocolour), time is on the  $y$  axis going downward,  $x$  axis is radial distance from the cell centre. **i** Radial averaged kymograph of Jupiter-GFP signal. The white dotted line represents the average cell contour (maximum of E-cad average signal for each time point). Top white arrow points at the onset of Jupiter-GFP depletion. The bottom arrow shows Jupiter-GFP accumulation in the neighbouring cells at the end of the extrusion.  $n = 24$  cells. Source data are provided in the source data file.

(Fig. 3), and the stabilisation of MTs observed upon caspase inhibition which prevents cell extrusion (Fig. 4), suggest that MT disassembly may be permissive for apical area constriction and extrusion initiation. Accordingly, previous studies in the *Drosophila* pupal wing and embryo have shown a role of medio-apical MTs in cell apical area stabilisation<sup>32,33</sup>. We, therefore, tested whether MTs could also modulate cell apical area in the pupal notum. We injected colcemid (a MT depolymerising drug) in pupae and assessed the efficiency of MT depletion through the disappearance of EB1-GFP comets and the inhibition of mitosis progression (Fig. 5a). UV exposure can locally inactivate colcemid<sup>44</sup>. Accordingly, local exposure to UV light (405 nm diode) led to a rapid recovery of EB1 comets (Fig. 5a–c, f and Supplementary Movie 15, bottom), although the initial organisation of MTs was not totally recovered. Strikingly, MT recovery was associated with a significant increase in cell apical area after few minutes, which was not observed in the control regions, or upon UV exposure in mock-injected pupae (Fig. 5e–h and Supplementary Movie 15, 4 min after the onset of UV exposure). This suggested that local MTs polymerisation is sufficient to increase cell apical area on a timescale of minutes. Importantly, the injection of colcemid did not lead to significant changes of MyoII levels during the first hours following injection, suggesting that these modulations are not driven by downstream effects on MyoII activation (Supplementary Fig. 6a–e).

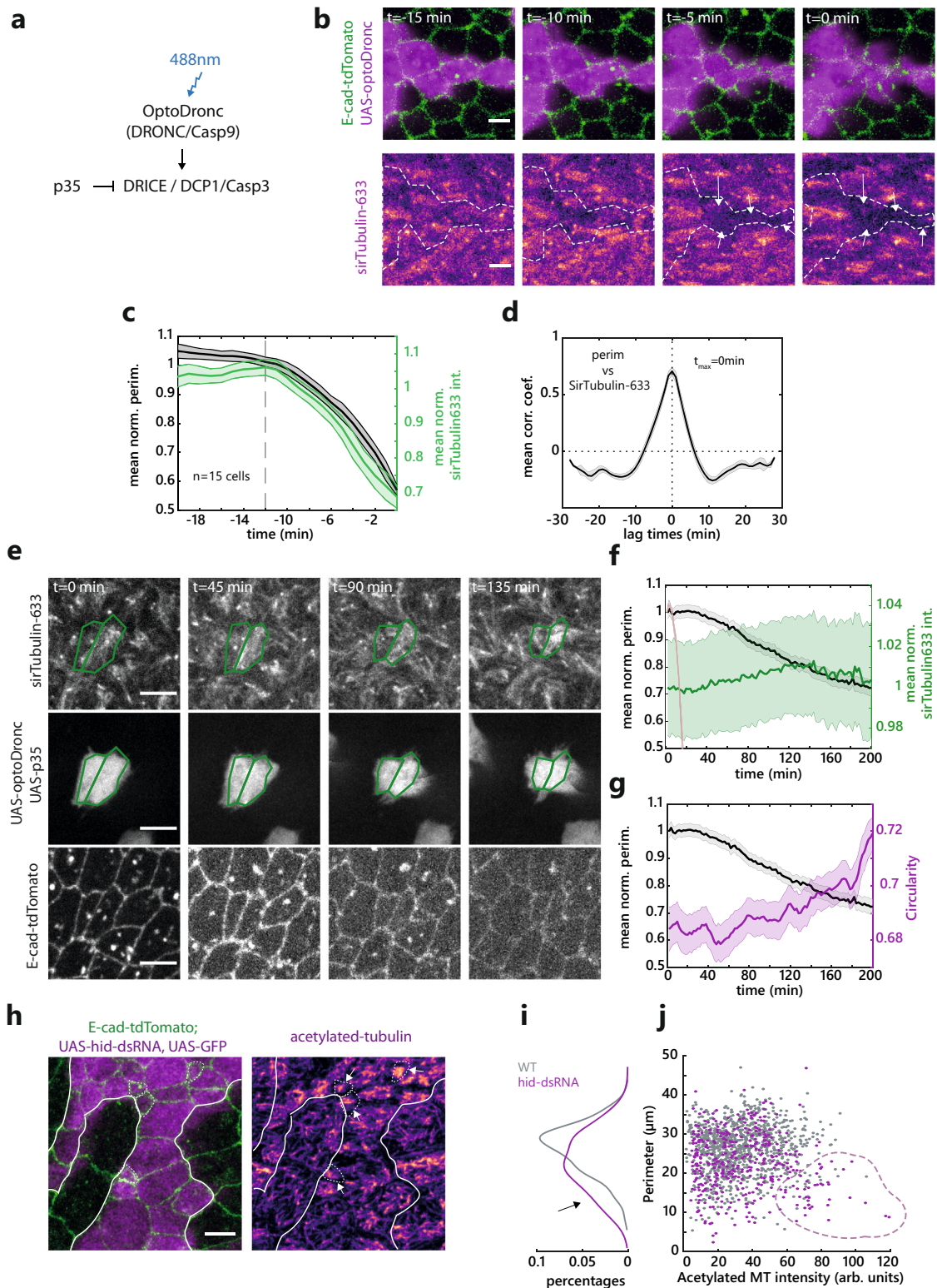
We then tried to perform the reverse experiment (fast local depletion of MTs). Optogenetics can be used to trigger fast clustering and sequestration of proteins of interest. We used the LARIAT system (Light-Activated Reversible Inhibition by Assembled Trap) to trigger the clustering of a GFP-tagged  $\alpha$ -tubulin upon blue light exposure<sup>45–47</sup>. Since the GFP-tagged  $\alpha$ -tubulin knock-in is not viable<sup>48</sup>, we instead used the over-expression of GFP- $\alpha$ -tubulin and LARIAT in clones to trigger a partial (endogenous tubulin is still present) depletion of  $\alpha$ -tubulin. Accordingly, blue light exposure led to rapid clustering of GFP- $\alpha$ -Tubulin, a mild reduction of sirTubulin signal (Supplementary Fig. 6f) and accordingly a mild but reproducible reduction of cell apical area without clear modulation of MyoII (Fig. 5i–k and Supplementary Movie 16). This apical area reduction was specific to tubulin sequestration since it was not observed upon clustering of a cytoplasmic GFP by LARIAT (Fig. 5k). Altogether, we concluded that a fast and local increase (or decrease) of MTs is sufficient to expand (or respectively constrict) cell apical area independently of noticeable MyoII modulation.

**The disassembly of MTs is an important rate-limiting step of extrusion.** We then checked whether MT depletion was sufficient

to trigger cell extrusion in the notum. Conditional induction of Spastin (a MT severing protein<sup>49</sup>) in clones was sufficient to deplete MTs (Supplementary Fig. 7a) and increase the rate of extrusion, including outside the midline in regions where no caspase activity is observed and where very few cells die in control conditions<sup>18,20,21</sup> (Fig. 6a–d and Supplementary Movie 17). To check whether MT depletion could indeed affect extrusion downstream of caspases, we assessed the impact of MT depletion on cells where caspase activation is inhibited. We used the inhibition of the proapoptotic gene *hid* which blocks caspase activation and cell extrusion in the notum<sup>20</sup>. While the depletion of *Hid* by RNAi drastically reduces the rate of extrusion<sup>20</sup>, colcemid injection restored the rate of extrusion in *hid*-RNAi clones almost back to that of WT cells (Fig. 6e–g and Supplementary Movie 18). Importantly, while caspase activation almost systematically precedes cell extrusion in control conditions<sup>18,20,21</sup>, a large proportion of cells underwent extrusion in the absence of caspase activation (visualised with GC3Ai<sup>21,43</sup>) in *hid* RNAi clones upon colcemid injection (Fig. 6h–j and Supplementary Movie 19). This suggested that MTs depletion can bypass the requirement of caspase activation for cell extrusion. Accordingly, while the inhibition of effector caspases (using UAS-p35) combined with Caspase9 activation (using optoDronc) drastically reduces the rate of extrusion and the cell constriction rate (Fig. 4f, g and Supplementary Movie 14, bottom), the rate of constriction was significantly enhanced upon MT depletion by colcemid injection (Fig. 6k, l and Supplementary Movie 20), albeit not back to WT speed. This confirmed that the accumulation of MTs we observed in optoDronc UAS-p35 clones (Fig. 4e, f) is one of the factors slowing down cell constriction and cell extrusion. To confirm that MTs depletion is indeed an important rate-limiting step of extrusion, we stabilised MTs using Taxol injection at a high concentration. While it did not totally block cell extrusion, it led to a global and drastic slowed-down of the speed of extrusion with variable durations (>threefolds increase of extrusion duration, Fig. 6m–o and Supplementary Movie 21). Moreover, the regime of deformation was now associated with a constant and significant increase of circularity (Fig. 6n), similar to the deformations observed upon increase of line tension (Fig. 2g), or upon optoDronc activation combined with p35 expression (Fig. 4g). Altogether, this demonstrates that the disassembly of MTs by effector caspases is an essential rate-limiting step of extrusion and one of the key initiators of cell constriction.

## Discussion

Our quantitative characterisation of cell extrusion in the pupal notum led to the surprising observation that actomyosin



dynamics are not sufficient to explain the early steps of cell extrusion. We found instead that the disassembly of an apical MTs network correlates with the initiation of cell apical constriction and cell extrusion, which is then followed by more typical actomyosin ring formation. This is, to our knowledge, one of the first descriptions of a permissive role of MTs depletion in the initiation of cell extrusion independently of MyoII. MTs have been previously shown to influence cell extrusion through their reorganisation in the neighbouring cells and the restriction of

Rho activity toward the basal side<sup>34</sup>. Accordingly, we also observed an accumulation of MTs filaments in the neighbouring cells during the late phase of extrusion, which strikingly matches the timing of formation of a supracellular actomyosin ring. On the contrary, the novel function of MTs in the initiation of apical constriction that we described here is likely to be independent of Rho regulation. First, the initiation of cell deformation does not correlate with a change of actomyosin concentration/localisation/dynamics, nor recruitment of Rho. Second, cells inhibited

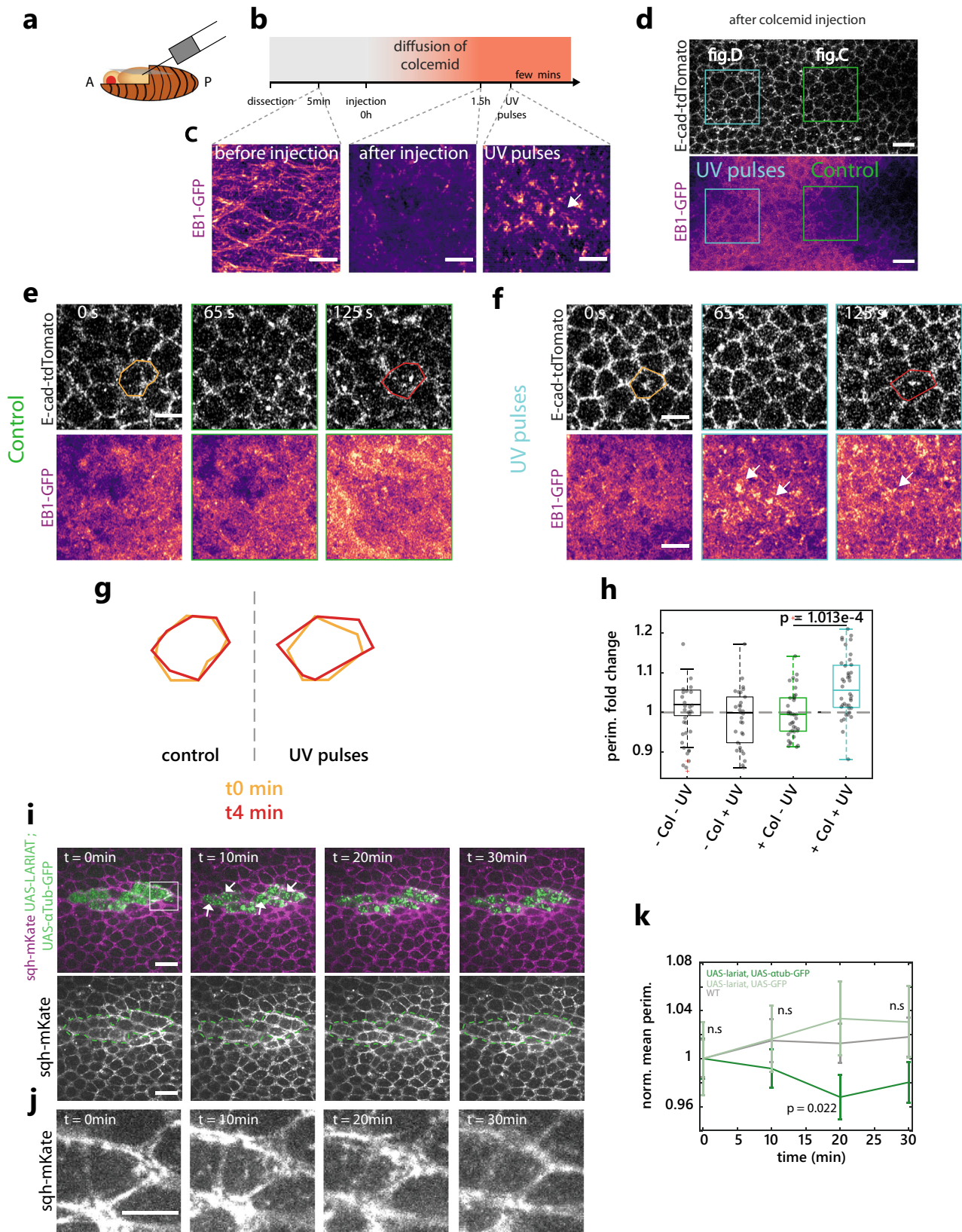
**Fig. 4 Microtubule depletion is effector caspase-dependent.** **a** Schematic of the caspase activation cascade, the effect optoDronc activation (caspase9) and p35 overexpression. **b** Snapshots of MTs depletion (SirTubulin, bottom, pseudocolour) upon activation of OptoDronc (Caspase9) by light. Top: E-cad-tdTomato (green) and a clone expressing OptoDronc-GFP (magenta). White dotted line, clone borders, white arrows, extruding cells. The scale bar is 5  $\mu\text{m}$ . **c** Averaged and normalised medial apical sirTub signal (green) and perimeter (black) during cell extrusion induced by optoDronc. Light colour areas, SEM. Grey dotted line, onset of extrusion.  $N = 1$  pupae,  $n = 15$  cells. **d** Averaged normalised cross-correlation of the cell perimeter vs sirTub. The maximum correlation coefficient is a  $t = 0$  min. The light area is SEM.  $n = 15$  cells. **e** Snapshots of UAS-optoDronc-GFP, UAS-p35 cells slowly contracting upon blue light exposure. Top row, sirTub, middle row, cells expressing UAS-OptoDronc-GFP and UAS-p35, bottom row, E-cad-tdTomato. Scale bars are 5  $\mu\text{m}$ . **f, g** Averaged and normalised medial apical sirTub signal (green), cell perimeter (black) (**f**) and averaged circularity (**g**, magenta) during the slow constriction of cell expressing UAS-OptoDronc-GFP and UAS-p35 upon blue light exposure. The pink curve shows the normal speed of extrusion upon optoDronc activation for comparison (see panel **c**).  $N = 2$  pupae,  $n > 99$  cells. Light colour areas are SEM. **h** z-projection of cells stained for acetylated tubulin (pseudocolour, right) and E-cad (green) inside and outside a clone depleted for the proapoptotic gene *hid* (UAS-*hid*-dsRNA, magenta). White lines: clone contour. White arrowheads, abnormal small cells in the clone accumulating acetylated tubulin (white dotted lines, cell contours). The scale bar is 5  $\mu\text{m}$ . Representative of four experiments. **i, j** Distribution of perimeter values for WT (grey) and UAS-*hid*-dsRNA cells (purple), percentage of the total cell population (**i**). Cloud plot of acetylated- $\alpha$ -tubulin levels (x axis) as a function of cell perimeter (y axis), one dot for one cell (**j**). Black arrow (**i**) and purple dotted area (**j**) highlight the population of small cells with high levels of acetylated- $\alpha$ -tubulin present only in the UAS-*hid*-dsRNA population.  $N = 5$  pupae,  $N = 1002$  WT cells and  $N = 405$  *hid*-dsRNA cells. Source data are provided in the source data file.

for caspases activation do not extrude, despite the significant accumulation of MyoII (upon depletion of *Hid*, Supplementary Fig. 1m, n or using optoDronc combined with p35, Fig. 4e–g, Supplementary Fig. 5f). Third, the evolution of apical cell shape during the early phase of extrusion does not match the evolution expected through an increase of line tension (unlike the extrusion of larval epidermal cells, Fig. 2). Fourth, the depletion of ROCK had a very minor effect on the speed of extrusion (Supplementary Fig. 2b, c), while MT stabilisation through Taxol injection led to a drastic slow-down of extrusion (Fig. 6m–o). Thus, the effect of MT stabilisation on extrusion cannot be explained by an indirect effect through the sequestration of Rho activators. Altogether, this strongly argues for an initiation of extrusion which is independent of the formation of an actomyosin purse string and a minor role of the modulation of line tension. As such, our study outlines a novel role of MTs in epithelial cell shape stabilisation which is independent of MyoII regulation. Recently, several works have described the central role of non-centrosomal MTs in epithelial morphogenesis, however, this was mostly through their impact on MyoII activity<sup>35–37</sup>. Our study reinforces the notion that MTs may also stabilise cell apical area independently of MyoII regulation, as previously shown during morphogenesis of the *Drosophila* embryo<sup>33</sup> or of the *Drosophila* pupal wing<sup>32</sup>. Interestingly, the accumulation of apical acetylated MTs promotes the capacity of cells to re-insert in an epithelial layer through radial intercalation in *Xenopus*<sup>50,51</sup>. This nicely mirrors the function of MTs disassembly that we found in cell extrusion.

Through which mechanisms could MTs stabilise cell apical area? MTs are well known for their stabilising function of cell membrane protrusions during cell migration<sup>52</sup> and can also modulate single-cell major-axis length<sup>53</sup>. Indeed, MTs embedded in the actomyosin network can bear significant compressive forces<sup>54,55</sup> and modulate cell compressibility<sup>56</sup>, or bear the compression driven by the constriction of cardiomyocytes<sup>57</sup>. Thus, apical MTs could directly resist the pre-existing cortical tension in the midline cells and their disassembly would be sufficient to trigger cell constriction. Alternatively, MTs may influence the contractile properties of the actomyosin cortex independently of Rho activity and MyoII phosphorylation, hence modulating cell deformation without apparent changes in actomyosin recruitment. Accordingly, MTs disassembly is sufficient to accelerate the kinetics of actomyosin constriction in vitro<sup>58</sup>. Finally, MTs may have a more indirect function either by modulating nuclei positioning<sup>59,60</sup>, hence releasing space to facilitate apical constriction, or by directly modulating cytoplasmic viscosity<sup>61</sup>.

We found that MTs disassembly is driven directly or indirectly by effector caspases. The disappearance of apical MTs is not driven by a shift of the centrosome position<sup>33</sup> (Supplementary Fig. 3k), nor reallocation of MTs or a change of MTs association with the centrosome<sup>35</sup>, or modulation of the localisation of the non-centrosomal MTs organisers Patronin and Shot<sup>33,36,37</sup> (Supplementary Fig. 3i, j). The disassembly occurs instead throughout the cell (Supplementary Fig. 4) and may be driven by a global modulation of core MTs components by caspases. The disassembly of MTs could either be driven by a reduction of the polymerisation rate, an increase of the depolymerisation rate or both. In principle, this could be sorted by comparing the number of EB1 positive comets relative to the total number of MTs over time. However, we found that EB1-GFP signal and total MT signal (using sirTubulin) decrease concomitantly during extrusion with no significant lag time (Supplementary Fig. 3l–n). While we cannot exclude that our limited temporal and spatial resolution may miss subtle time differences, this is compatible with a mechanism affecting both the polymerisation and the depolymerisation rate, as would happen upon sequestration and destruction of tubulin monomers. Accordingly,  $\alpha$ -tubulin and  $\beta$ -tubulin are both cleaved by caspases in S2 cells and these cleavages are conserved in humans<sup>62</sup>. This is in agreement with the depletion that we also observed with the tagged human  $\alpha$ -tubulin (Supplementary Fig. 3h). However, we could not address the functional relevance of these cleavages since the mutant form of  $\alpha$ -tubulin (mutation at the three cleavage sites) did not integrate properly in MT filaments either in S2 cells or in the notum (Supplementary Fig. 8). Since several core MT components are targets of caspases (including  $\alpha$ -tub and  $\beta$ -tub)<sup>62</sup>, we believe that the inhibition of the caspase-dependent disassembly of MTs will be hard to achieve. Moreover, we cannot exclude at this stage alternative mechanisms of MTs destabilisation based on the modulation of plus-end binding proteins or crosslinkers by caspases. Of note, the redundancy of multiple caspase targets triggering MT depletion and the high conservation of several cleavage sites may reflect the physiological importance of this regulatory process.

We showed previously that caspase activation is required for cell extrusion in the pupal notum, including during cell death events induced by tissue compaction<sup>18,20,21</sup>. This suggested that cell extrusion is unlikely to occur spontaneously upon cell deformation and that permissive regulatory steps are required to allow cell expulsion. Our work suggests that the disassembly of MTs by caspases may be one key rate-limiting step. Accordingly, MTs depletion is sufficient to bypass the requirement of caspase activity for cell extrusion (Fig. 6). Interestingly, several



mechanisms of MTs repair and stabilisation upon mechanical stress have been recently characterised<sup>39,40,63</sup>, including recent works characterising the mechanism of MT stabilisation upon compression<sup>64,65</sup>, which can reinforce the capacity of MTs to bear mechanical load<sup>57</sup>. Thus, stress generated by cell constriction and/or tissue compression is unlikely to be sufficient to trigger

MT disassembly. This is in good agreement with the transient accumulation of MTs that we observed upon tissue stress release (Supplementary Fig. 5a–c and Supplementary Movie 12), and outlines the requirement for an active disassembly mechanism by caspases to trigger MT depletion and extrusion. The stabilisation of MT upon cell constriction may help to buffer variations of the

**Fig. 5** MTs polymerisation/depolymerisation can increase/decrease cell apical area. **a** Schematic of the injection in the *Drosophila* pupae. **b, c** Timeline of the injection protocol and colcemid inactivation experiment (see “Methods”) and EB1-GFP signal (pseudocolour) before injection, 1.5 h after injection and after few minutes of colcemid inactivation by UV. Scale bars are 5  $\mu\text{m}$ . **d** Snapshot of the different experimental regions after colcemid injection, single plane. Top, E-cad-tdTomato, bottom, EB1-GFP (pseudocolour, note the disappearance of MT filament). Green, control region shown in **(e)**. Blue, UV-exposed region shown in **(f)**. Scale bar, 10  $\mu\text{m}$ . **e, f** Snapshots of a control region **(e)** and UV-exposed region **(f)** after colcemid injection. Top, E-cad-tdTomato. Bottom shows EB1-GFP (pseudocolour). Scale bars are 5  $\mu\text{m}$ . Orange and red contour, single representative cell at  $t_0$  and 4 min. **g** Examples of cell area evolution, orange  $t_0$ , red 4 min post UV exposition in the control region (left) or UV-exposed region (right). **h** Quantification of the cell perimeter fold changes. Col: colcemid. Green boxplot, colcemid without UV pulses, blue boxplot, colcemid and UV.  $N = 4$  colcemid injected pupae, 3 control pupae,  $n > 30$  cells per condition (one dot = one cell). Each boxplot shows the median value (middle line), and 25th and 75th percentiles. The whiskers show the most extreme data points not considered outliers. Outliers are plotted in red.  $P$  value, two-sided  $t$  test. **i** sqh-mKate (MRLC, purple, greyscale bottom) and a clone expressing UAS-LARIAT and UAS- $\alpha$ Tubulin-GFP (green dotted line, clone contours). Arrows show GFP clusters forming after 488-nm exposure.  $t_0$ , start of the movie. The white box highlights the cell shown in **(j)**. The scale bar is 10  $\mu\text{m}$ . **j** Snapshot of sqh-mKate in a cell upon LARIAT activation. Scale bar is 5  $\mu\text{m}$ . **k** Normalised averaged perimeter upon LARIAT clusterisation of  $\alpha$ Tubulin-GFP (dark green) compared to control cells (grey, outside the clone) or in control cells expressing UAS-LARIAT and UAS-GFP cytoplasmic (light green).  $N = 3$  pupae for each,  $n = 41$  WT and UAS-Lariat, UAS- $\alpha$ Tubulin-GFP cells  $n = 30$  UAS-lariat, UAS-GFP cells per time points. Error bars are SEM. n.s. not significant.  $P$  value, paired  $t$  test. Source data are provided in the source data file.

cell apical area despite the fluctuations of line tension<sup>26</sup> or external mechanical constrains. In absence of MTs, this negative feedback would be gone, hence allowing large fluctuations of cell area and the appearance of spontaneous extrusion driven by local mechanical instabilities<sup>66</sup>. Interestingly, depletion of MTs in other systems (e.g. the fly embryo<sup>35</sup>) does not seem to have the same impact on epithelial stability and cell extrusion, suggesting that the impact of MTs on epithelial cell stabilisation may be context-dependent. Finally, it should be noted that MT disassembly in caspase-inhibited cells does not completely rescue the speed and the rate of extrusion, thus other unidentified targets of caspases are likely to also participate in extrusion regulation.

Caspase activation in the pupal notum, and in other tissues, does not lead systematically to cell extrusion and cell death<sup>18,20,21,67</sup>. The mechanisms downstream of effector caspase activation governing cell survival or engagement in apoptosis remain poorly understood. Since the engagement of cells in extrusion in the WT notum systematically leads to cell death<sup>17,18</sup>, and since MT depletion is the earliest remodelling step associated with extrusion, the disassembly of MTs by caspases is likely to be one of the key decision steps, leading to engagement in apoptosis in the pupal notum. Future work connecting cell mechanical state, quantitative caspase dynamics and MT remodelling may lead to important insights about the decision of a cell to die or survive.

## Methods

### Experimental model and subject details

*Drosophila melanogaster* husbandry. All the experiments were performed with *Drosophila melanogaster* fly lines with regular husbandry techniques. The fly food used contains agar agar (7.6 g/l), saccharose (53 g/l) dry yeast (48 g/l), maize flour (38.4 g/l), propionic acid (3.8 ml/l), Nipagin 10% (23.9 ml/l) all mixed in one litre of distilled water. Flies were raised at 25 °C in plastic vials with a 12 h/12 h dark-light cycle at 60% of moisture unless specified in the legends and in the table below (alternatively raised at 18 °C or 29 °C). Females and males were used without distinction for all the experiments. We did not determine the health/immune status of pupae, adults, embryos and larvae, they were not involved in previous procedures, and they were all drug and test naive.

*Drosophila melanogaster* strains. The strains used in this study and their origin are listed in Table 1.

The exact genotype used for each experiment is listed in Table 2.

**Generation of  $\alpha$ -tub84B-mCherry WT and non-cleavable mutant.** The inserts mCherry- $\alpha$ Tub84B and mCherry- $\alpha$ TubD34A-D48A-D200A (mutation of the three caspase cleavage sites) were generated by PCR from pAc-mCh-Tub (Addgene 24288) with oligos containing mutations or not. The triple mutant at the three sites (mCherry- $\alpha$ TubD34A-D48A-D200A) was generated by using the following primers combination (see table below for primer sequence): F1 + R1, F2 + R2, F3 + R3. The WT form was generated using the F1 + R3 primers. The PCR products were then inserted in the pFRC4-3XUAS-IVS-mCD8::GFP

(Addgene 28243) linearised by NotI, XbaI digestion, using NEBuilder HiFi DNA Assembly Method. The construct was checked by sequencing and inserted at the attP site attP40A after injection by Bestgene. The primers used for the construct are listed below (inserted mutation sites are shown in red).

Primers	sequence
F1	taaccctaattcttatccttactcaggcggccgcaacatggtgagcaagggcgagga
F2	agatgacctctgacaagaccgtggcgaggatgatgCctcttcaacacctctcagc
F3	ccctggagcattccgCctgcccctcatggtcgaca
R1	ctccgccacggctctgacagggcctctggccaGcgggctggatccgtgctc
R2	accatgaagggcgagGcgggaatgctccaggggtggtg
R3	acagaagtaagttcctcacaagaatcctctagattagtagtactcctcagcgcct

**S2 cell culture.** S2R + (DGRC stock 150, RRID:CVCL\_Z831) cells were cultured in Schneider's *Drosophila* Medium with 10% foetal bovine serum, penicillin and streptomycin. S2R + cell were transfected with FUGENE HD (Promega, ref: E2311). Twenty-four hours after transfection, S2R + cells were plated on glass-bottom dishes coated with concanavalin A (con A). Cells were imaged in a spinning disk confocal 30–60 min after cell spreading on the dishes.

**Immunostaining.** Dissection and immunostainings of nota were performed as indicated in ref. <sup>68</sup> with standard formaldehyde fixation and permeabilisation/washes in PBT 0.4% Triton. The following antibody was used: mouse anti-acetylated-Tubulin (1/200, Sigma T7451, clone 611B1). A secondary antibody was produced in goat with Alexa 633 (1/100, Life technologies, A21052, lot 1712097). Dissected nota were mounted in Vectashield with DAPI (Vectorlab).

**Vertex modelling of cell extrusion.** To model the early steps of extrusion, we used a computational vertex model based on the existing computational framework for the study of developmental processes in the epithelial tissues of *Drosophila*<sup>29,69</sup>. The model was implemented in gfortran, using OpenGL to visualise the outputs.

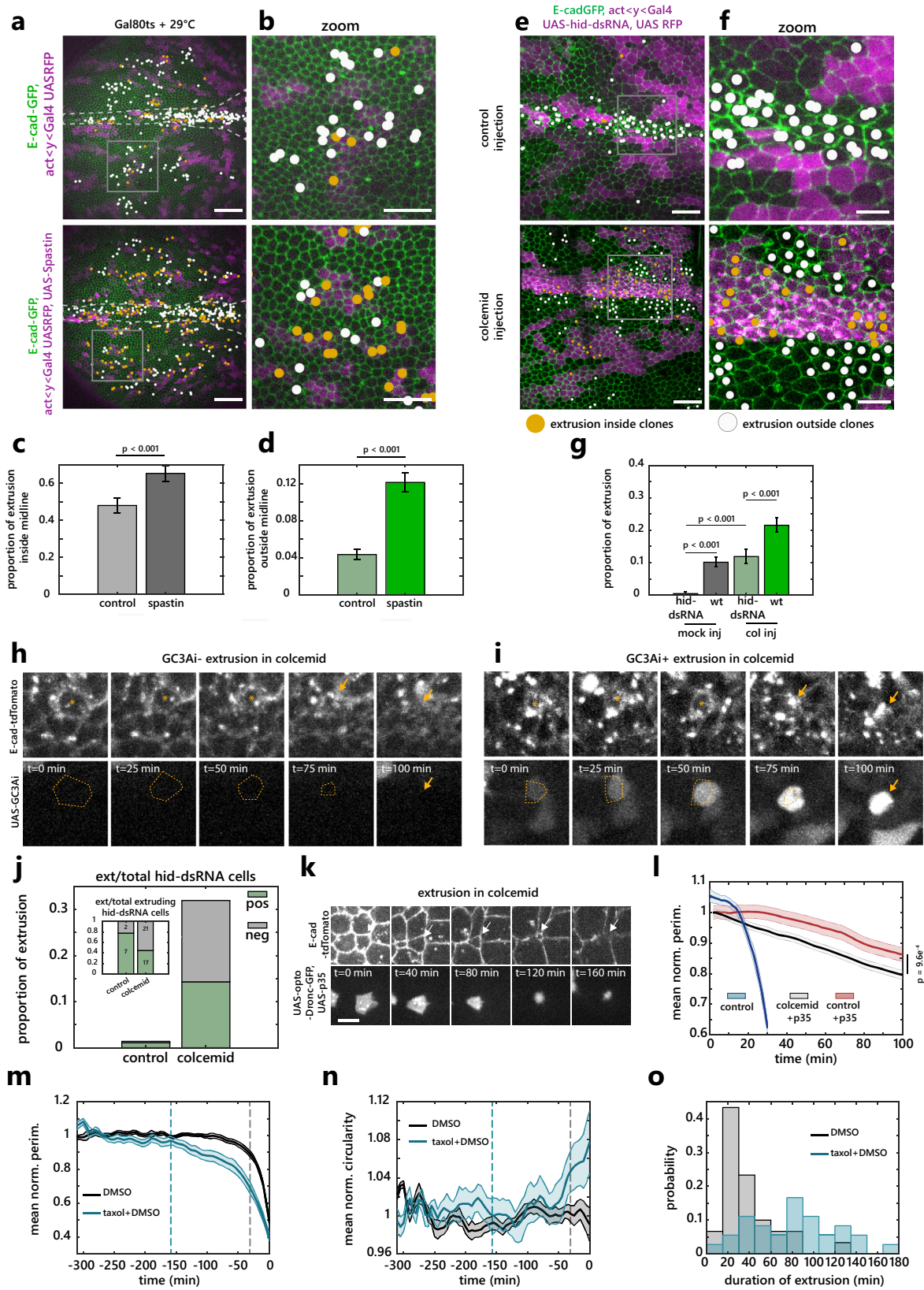
In the vertex model, only the apical sides of the cells are considered. Cells are represented as 2D polygons, made of vertices connected by edges. The vertices can move over time as a result of intra- and intercellular mechanical forces. The movement of the vertices is implemented by comparing the mechanical energy of a vertex in its current position  $(x, y)$  with the energy of a randomly chosen point nearby  $(x+\delta d, y+\delta d)$  with  $\delta d \in [0, 0.005]$ . When the energy in the new position is smaller, then the movement is accepted as the new vertex location. When the energy is bigger, the movement is accepted with probability  $P_{\text{accept}} (=0.05)$  in order to introduce stochastic fluctuations.

The energy  $E$  of a vertex  $i$  is given by

$$E(R_i) = \sum_{\alpha} \frac{K_{\alpha}}{2} (A_{\alpha} - A_{\alpha}^{(0)})^2 + \sum_{(i,j)} \Lambda_{ij} \cdot l_{ij} + \sum_{\alpha} \frac{\Gamma_{\alpha}}{2} \cdot L_{\alpha}^2 \quad (1)$$

where  $R_i = (x_i, y_i)$  is the position of the vertex  $i$ . The first and the third summations are over all the cells  $\alpha$  in which the vertex  $i$  is present, and the second summation is over all the cell edges  $[i, j]$  in which the vertex  $i$  is present.  $A_{\alpha}$  is the apical area of the cell  $\alpha$  and  $K$  is the area elasticity modulus, which is assumed to be equal for all the cells in our simulations.  $A_{\alpha}^{(0)}$  is the resting area of the cell  $\alpha$ . The distance and the line tension between the pairs of vertices  $[i, j]$  are denoted  $l_{ij}$  and  $\Lambda_{ij}$ , respectively. The third term includes the perimeter of the cell  $\alpha$  ( $L_{\alpha}$ ) and the perimeter contractility coefficient ( $\Gamma_{\alpha}$ ). By choosing  $\sqrt{A_{\alpha}^{(0)}}$  as a unit of length and  $(KA_{\alpha}^{(0)})^2$  as a unit of energy (as in ref. <sup>69</sup>), dividing both sides of Eq. (1) by





$(KA\alpha^{(0)})^2$  results in the following dimensionless equation:

$$\tilde{E}(R_t) = \sum_{\alpha} \frac{1}{2} \left( \frac{A_{\alpha}}{A\alpha^{(0)}} - 1 \right)^2 + \sum_{(i,j)} \tilde{\Lambda}_{ij} \cdot \frac{l_{ij}}{\sqrt{A\alpha^{(0)}}} + \sum_{\alpha} \frac{\tilde{\Gamma}_{\alpha}}{2} \cdot \frac{L_{\alpha}^2}{A\alpha^{(0)}} \quad (2)$$

Where  $(A_{\alpha}/A\alpha^{(0)})$ ,  $(l_{ij}/\sqrt{A\alpha^{(0)}})$  and  $(L_{\alpha}^2/A\alpha^{(0)})$  are, respectively, dimensionless area, bond length and perimeter. This model is characterised by dimensionless line

tension ( $\tilde{\Lambda}_{ij} = \Lambda_{ij}/K(A\alpha^{(0)})^{\frac{3}{2}}$ ) and dimensionless perimeter contractility ( $\tilde{\Gamma}_{\alpha} = \Gamma/K\alpha A\alpha^{(0)}$ ) that were set respectively to 0.06 and 0.02 as in ref. 70.

Rearrangements of the topology of the vertices (T1 transitions) were allowed when two vertices  $i, j$  were located less than a minimum distance  $d_{\min}$  ( $= 0.2$ ) apart, and a movement of one of the vertices was energetically favourable such that the distance between the vertices decreases.

**Fig. 6 The disassembly of MTs by caspases is an important rate-limiting step of extrusion.** **a, b** E-cad-GFP (green) in nota with control clones (magenta, top) or clones expressing conditionally Spastin (magenta, bottom). Coloured dots, extrusions inside (orange) or outside clones (white). White dotted lines, midline. White rectangles, regions are shown in **(b)**. Scale bars, 50 μm **(a)** and 25 μm **(b)**. **c, d** Proportion of cell elimination throughout the nota (see “Methods”) over 1000 min, inside **(c)** or outside **(d)** the midline. Error bars, 95% confidence interval, *P* values, Fisher exact test. Control, *N* = 2 pupae, 630 midline and 5105 outside-midline cells, Spastin, *N* = 3 pupae, 993 midline and 6997 outside-midline cells. **e, f** Nota expressing E-cad-GFP (green) and hid-dsRNA clones (magenta) injected with EtOH+H<sub>2</sub>O (top, control) or colcemid (bottom). Scale bars, 25 μm **(e)**, 10 μm **(f)**. White rectangles, regions are shown in **(f)**. **g** Proportion of cell elimination inside hid-dsRNA clones and outside (wt) in EtOH+H<sub>2</sub>O (left) or colcemid injected (right) pupae over 500 min throughout the notum. *P* values, Fisher exact test. Error bars, 95% confidence interval. *N* = 4 control pupae, 155 WT and 1150 hid-dsRNA cells, *N* = 3 colcemid pupae, 1388 WT and 926 hid-dsRNA cells. **h, i** hid-dsRNA cell extrusions after colcemid injection negative **(h)** or positive **(i)** for effector caspase activity (GC3Ai, bottom). Yellow dotted lines, extruding cell contour. Scale bars, 5 μm. **j** Proportion of hid-dsRNA cell extrusion positive or negative for GC3Ai in mock (*n* = 9 extrusions, 2 pupae) or colcemid injected pupae (*n* = 39 extrusions, 2 pupae). Inset, relative proportions and absolute numbers. **k** optoDronc, p35 extruding cell (white arrows) upon colcemid injection (E-cad-tdTomato, top, optoDronc-GFP bottom). Scale bar = 5 μm. **l** Normalised averaged perimeter of cells expressing optoDronc and p35 upon blue light exposure in controls (red, Fig. 4e–g) or upon colcemid injection (black). Blue curve, optoDronc only, from Fig. 4c. Light colour areas, SEM. *n* > 99 cells, *N* = 3 control and *N* = 2 colcemid pupae. **m, n** Normalised averaged perimeter **(m)** and circularity **(n)** of extruding cells upon taxol injection (blue, taxol in DMSO) or DMSO alone (black). Dotted lines, onset of extrusion. Light colour areas, SEM. **o** Distribution of extrusion duration in Taxol (blue) or DMSO alone injected pupae (black). *N* = 2 pupae, *n* = 30 control extruding cells, *n* = 36 taxol extruding cells. Source data are provided in the source data file.

**Table 1 *Drosophila melanogaster* strains used in this study.**

Fly line	Chromosome location	Origin (citation)	RRID
<i>E-cad-tdTomato</i> (KI)	II	76	BDSC_58789
<i>E-cad-GFP</i> (KI)	II	76	BDSC_60584
<i>hs-flp22; sqh-sqh-GFP; sqh-sqh-GFP</i>	II, III	Thomas Lecuit	Thomas Lecuit
<i>Sqh-utABD-GFP</i>	II	24	Thomas Lecuit
<i>ubi-aniRBD-GFP</i>	II	23	Thomas Lecuit
<i>Pnr-gal4</i>	III	Bloomington	BDSC_3039
<i>sqh-Sqh-3XmKate2</i>	II	77	Yohanns Bellaïche
<i>hs-flp22; sqh-Sqh-3XmKate2; act &lt; y &lt; gal4, UAS-BFP</i>	I, II, III	Yohanns Bellaïche	Yohanns Bellaïche
<i>Hs-flp22; act &lt; y &lt; gal4, UAS-mcd8RFP/Cyo</i>	I, II	Our group	Our group
<i>Hs-flp22;; act &lt; y &lt; gal4, UAS-nlsRFP/TM6b</i>	I, III	Bloomington	BDSC_30558
<i>Ubi-E-cad-GFP</i>	II	DGRC	DGRC_109007
<i>UAS-hid ds-RNA</i> (III)	III	VDRC GD 8269	VDRC
<i>UAS-p35</i>	III	Bloomington	BDSC_5073
<i>UAS-EB1-GFP</i>	III	Bloomington	BDSC_35512
<i>Jupiter-GFP</i>	Trap, III	Antoine Guichet	BDSC_6836
<i>Ubi-Talin-GFP</i>	X	Guy Tanentzapf <sup>78</sup>	Guy Tanentzapf
<i>UAS-Spastin</i>	III	Antoine Guichet	Antoine Guichet
<i>Ubi-Patronin-GFP</i>	II	Bloomington	BDSC_55128
<i>shot(L)-GFP (TRAP)</i>	II	DGRC	DGRC_109707
<i>Ubi-Sas4-GFP</i>	II	Renata Basto	FBal0240464 (flybase ID)
<i>UAS-human-αtub-mCherry</i>	II	Bloomington	BDSC_25774
<i>UAS-αtub-GFP</i>	III	Bloomington	BDSC_7253
<i>UAS-vhhGFP-CRY2-CIBN</i>	II	79	Xiaobo Wang
<i>UAS-optoDronc-GFP</i>	II (attp40)	21	Our group
<i>sqh-Sqh-3XmKate2</i>	II	77	Yohanns Bellaïche
<i>tub-Gal80ts</i>	II	Bloomington	BDSC_7019
<i>hs-flp22; Ubi-Ecad-GFP, UAS-RFP; act &lt; y &lt; gal4</i>	II	Loïc le Goff	Loïc le Goff
<i>UAS-GC3Ai</i>	III	43	Magalie Suzanne
<i>UAS-his3.3 mIFP-T2A-H01</i>	III	Bloomington	BDSC_64184
<i>Hs-flp22;; Act &lt; cd2 &lt; gal4,UAS-GFP</i>	I; III	20	20
<i>UAS-Cd4-mIFP-T2A-H01</i>	III	Bloomington	BDSC_64182
<i>UAS-α-tubulin-mCherry</i>	II	This study	This study
<i>UAS-α-tubulinmutABC-mCherry</i>	II	This study	This study
<i>endocadGFP, tub-Gal80ts/Cyo; Act &lt; y &lt; Gal4 UAS-nls-RFP/TM6B</i>	II, III	Our group	Our group
<i>UAS-Rok- dsRNA</i>	II	VDRC	VDRC 3793GD
<i>Sqh &gt; sqhGFP, FRT40A/Cyo GFP</i>	II	80	Yohanns Bellaïche
<i>FRT40A, sqhRFP[247]/Cyo</i>	II	80	Yohanns Bellaïche
<i>E-cad::3xmKate (KI)/Cyo GFP</i>	II	77	Yohanns Bellaïche

To avoid buckling at the boundary of the tissue, we assumed a greater stiffness of the cells edges located at the external boundary of the tissue, and set that the line tension for the external edges was higher ( $= 1.6 \cdot \bar{A}_{ij}$ ) than that of the internal edges.

Simulations started from a tissue of 1141 cells, among which 10 cells scattered in the tissue (far from the edge to avoid boundary effects) were tracked for circularity ( $C = 4 \cdot \pi \cdot (\text{area}/\text{perimeter}^2)$ ) and perimeter (*P*) changes during the

simulation run. In the initial topology, tracked cells have an average *P* of  $7.58 \pm 0.05$  (SEM) and an average *C* of  $0.81 \pm 0.088$  (Fig. 2a). Simulations were run for 6.5 million iterations, one iteration consisting in moving a randomly chosen vertex, updating its energy, and deciding to accept the movement or not. For clarity, the simulation run was divided in 50 simulation time steps (sts), with 1 sts = 130.000 vertex iterations.

**Table 2 Precise genotype used for each figure panel.**

Figure	Genotype	Clone induction	Dev. time
1b	E-cad-GFP(KI); pnr-Gal4	-	16 h APF
1c, d	hs-flp22; ubi-E-cad-GFP UAS-RFP/+; act<y < Gal4/UAS-hid-dsRNA (quantification outside clones)	-	16 h APF
1e, f, i-k; S1 a, c-g	hs-flp22; sqh-Sqh-GFP; sqh-Sqh-GFP	-	20 h APF
S1b	hsFLP; sqh-Sqh-GFP, FRT40A/ FRT40A, sqh-Sqh-RFP	48 h ACI, 12 min hs	16 h APF
1g, h, S1h, i	hs-flp; act<y < gal4, UAS-mcd8RFP/Cyo; sqh-GFP-utABD/TM6b	-	16 h APF
S1j-l	w; E-cad-tdTomato (KI)/+; +/-ubi-mE-AnilRBDGFP	-	16 h APF
S1m, n	hs-flp22; sqh-sqh::GFP/Cyo; act<cd2 < gal4, UAS-nlsRFP/UAS-hid-dsRNA	48 h ACI, 12 min hs	20 h APF
2i	w; E-cad-GFP(KI)	-	-
2j	w; E-cad-tdTomato(KI)/+; pnr-Gal4/UAS-EB1-GFP	-	-
S2a top	hs-flp22; sqh-Sqh::GFP; sqh-Sqh::GFP	-	20 h APF
S2a bottom	w; E-cad-GFP(KI)	-	20 h APF
S2b, c	w; E-cad::3xmKate(KI); pnr-Gal4/UAS-ROK-dsRNA	-	16 h APF
S2d, e	w; UAS-optoDroncCRY2-GFP/ E-cad-tdTomato; MKRS/act<y < Gal4 UAS-GFP	48 h ACI, 12 min hs	16 h APF
S2f	ubi-Talin::GFP/FM7	-	16 h APF
3a, c	w; E-cad-tdTomato(KI)	-	16 h APF
3d-i	w; E-cad-tdTomato(KI)/cyo; Jupiter-GFP/TM6B	-	16 h APF
S3a-g & l-n	w; E-cad-tdTomato(KI)/+; pnr-Gal4/UAS-EB1-GFP	-	16 h APF
S3h	w; E-cad-GFP(KI)/+; pnr-Gal4/UAS-alpha-Tub-mCherry-human	-	16 h APF
S3i	w; E-cad::3xmKate (KI)/shot(I)-GFP (TRAP)	-	16 h APF
S3j	w; ubi-p63-Patronin.A.GFP/Cyo	-	16 h APF
S3k	w; E-cad-tdTomato(KI)/ubi-Sas4-GFP	-	16 h APF
S4a-c	w; E-cad-GFP(KI)/UAS- $\alpha$ -tubulin-mCherry; pnr-Gal4/+	-	16 h APF
S4d-e	hs-flp22; sqh-sqhmKateX3/+; act<y < Gal4, UAS-BFP/UAS-EB1-GFP	48 h ACI, 12 min hs	16 h APF
S4f, g	w; UAS-optoDroncCRY2-GFP/ E-cad-tdTomato(KI); MKRS/act<y < Gal4 UAS-GFP	48 h ACI, 12 min hs	16 h APF
4a-d	w; UAS-optoDroncCRY2-GFP/ E-cad-tdTomato(KI); MKRS/act<y < Gal4 UAS-GFP	48 h ACI, 12 min hs	16 h APF
4e-g	w; UAS-optoDroncCRY2-GFP/ E-cad-tdTomato(KI); UAS-p35/act<y < Gal4 UAS-GFP	48 h ACI, 12 min hs	16 h APF
4h-j	hs-flp22; E-cad-tdTomato(KI)/Cyo; act<y < Gal4, UAS-GFP/UAS-hid-dsRNA	48 h ACI, 12 min hs	20 h APF
S5a-d	w; E-cad-GFP(KI)/UAS- $\alpha$ -tubulin-mCherry; pnr-Gal4/+	-	30 h APF
S5e	w; UAS- $\alpha$ -tubulin-mCherry/UAS-GC3A1; pnr-Gal4/+	-	-
S5f	w; sqh-sqh-mKateX3/ UAS-optoDroncCRY2-GFP; act<y < Gal4, UAS-BFP/UAS-p35	48 h ACI, 12 min hs	30 h APF
5a-h	w; E-cad-tdTomato(KI)/+; pnr-Gal4/UAS-EB1-GFP	-	16 h APF
5i-k	hs-flp22; sqh-sqh-mKateX3/UAS-vhhGFP-CRY2-CIBN; act<y < Gal4, UAS-BFP/UAS- $\alpha$ Tubulin-GFP	48 h ACI, 12 min hs	16 h APF
5k	hs-flp22; E-cad-mKateX3(KI)/UAS-vhhGFP-CRY2-CIBN; act<y < Gal4, UAS-GFP/+	48 h ACI, 12 min hs	16 h APF
S6 a-e	w; sqh-sqh-mKateX3/Cyo; pnr-gal4/TM6b	-	16 h APF
S6f	hs-flp22; sqh-sqh-mKateX3/UAS-vhhGFP-CRY2-CIBN; act<y < Gal4, UAS-BFP/UAS- $\alpha$ Tubulin-GFP	48 h ACI, 12 min hs	16 h APF
6a-d	hs-flp22; tub-Gal80ts/ ubi-E-cad-GFP, UAS-RFP; UAS-Spustin/act<y < Gal4	96 h ACI 18 °C, 12 min hs	16 h APF
6a-d	hs-flp22; tub-Gal80ts/ ubi-E-cad-GFP, UAS-RFP; MKRS/act<y < Gal4	96 h ACI 18 °C, 12 min hs	16 h APF
6e-g	hs-flp22; ubi-E-cad-GFP, UAS-RFP/+; act<y < Gal4/UAS-hid-dsRNA	48 h ACI, 12 min hs	16 h APF
6h-j	hs-flp22; E-cad-tdTomato(KI)/UAS-GC3A1; act<y < Gal4, UAS-His3-mIFP/UAS-hid-dsRNA	48 h ACI, 12 min hs	16 h APF
6k, l	hs-flp22; E-cad-tdTomato(KI)/ UAS-optoDroncCRY2-GFP; act<y < Gal4, UAS-GFP/UAS-p35	48 h ACI, 12 min hs	16 h APF
6m-o	w; E-cad::3xmKate(KI)/+; pnr-Gal4/UAS-EB1-GFP	-	16 h APF
S7a	hs-flp22; endocadGFP, tub-Gal80ts/+; Act<y < Gal4 UAS-nls-RFP/UAS-Spustin	96 h ACI 18 °C, 12 min hs	16 h APF
S8c, d	w; E-cad-GFP(KI)/UAS- $\alpha$ -tubulin-mCherry-ABC; pnr-Gal4/+	-	16 h APF
S8c, d	w; E-cad-GFP(KI)/UAS- $\alpha$ -tubulin-mCherry; pnr-Gal4/+	-	16 h APF

ACI time after clone induction, APF after pupal formation, hs heat shock at 37 °C.

At  $t = 20$  sts, three different conditions were examined to test for the effect of the mode of extrusion on cells circularity during the early stages of extrusion. In the first condition, the ten tracked cells had parameter values identical to all the other cells of the tissue (control). In the second condition, the ten tracked cells were forced to initiate extrusion by increasing at each iteration their contractility parameter ( $\bar{\Gamma}$ ) with a fixed rate  $c$  ( $\bar{\Gamma}_{t+1} = \bar{\Gamma}_t + c \cdot \bar{\Gamma}_t$ ) thus simulating a purse-string driven extrusion. Five different values were examined for  $c$ , with  $c = [0.0; 1.0; 2.5; 5.0; 7.5] \times 10^{-7}$ . In the third condition, the ten tracked cells were forced to initiate extrusion by decreasing after each iteration their resting area ( $A\alpha^{(0)}$ ) with a fixed rate  $r$  ( $A\alpha^{(0)}_{t+1} = A\alpha^{(0)}_t - r \cdot A\alpha^{(0)}_t$ ). Simulations were run for five  $r$  values ( $r = [0.0; 0.5; 1.0; 2.5; 3.5] \times 10^{-4}$ ).

#### Optogenetic control

**Induction of cell death using optoDronc.** For induction of optoDronc in clones in the pupal notum, *hs-flp; E-cad-tdTomato(KI); act < cd2 < G4, UAS-GFP* females

were crossed with homozygous *UAS-optoDronc* or *UAS-optoDronc; UAS-p35*. Clones were induced through a 12 min heat shock in a 37 °C water bath. Tubes were then maintained in the dark at 25 °C. White pupae were collected 48–72 h after clone induction and aged for 16 h at 25 °C in the dark. Collection of pupae and dissection were performed on a binocular with LED covered with a homemade red filter (Lee colour filter set, primary red) after checking that blue light was effectively cut (using a spectrometer). Pupae were then imaged on a spinning disc confocal (Gatca system). The full tissue was exposed to blue light using the diode 488 of the spinning disc system (12% AOTF, 200 ms exposure per plane, 1 stack/min). Extrusion profiles were obtained by segmenting extruding cells in the optoDronc clones with E-cad-tdTomato signal in the notum using the Fiji plugin Tissue analyzer<sup>71</sup> ([https://github.com/baigouy/tissue\\_analyzer](https://github.com/baigouy/tissue_analyzer)). Curves were aligned on the termination of extrusion (no more apical area visible) and normalised with the averaged area on the first five points. The same procedure was used upon control injection or injection of colcemid (see below) in optoDronc UAS-p35 background, except that curves were aligned to  $t_0$ , the onset of blue light

exposure. Note that in this condition, all cells of the clones were segmented irrespective of the size of the clone, which can affect by itself the speed of extrusion<sup>21</sup>.

**LARIAT mediated depletion of  $\alpha$ Tubulin-GFP.** UAS-vhhGFP-CRY2-CIBN (hereafter LARIAT) was expressed in Gal4-expressing clones. CRY2 dimerises with CIBN in a light-dependent manner. The association with the anti-GFP nanobody (vhhGFP) allows to trap the tubulin-GFP in these large clusters. Clones were induced through a 12 min heat shock in a 37 °C water bath. Tubes were then maintained in the dark at 25 °C. White pupae were collected 48–72 h after clone induction and aged for 16 h at 25 °C in the dark. Pupae were then dissected and imaged using the same method than described for the optoDronc condition. Quantification were made by segmenting manually cells from clones and in control population at four time points ( $t = 0, 10, 15, 20$  min). The same protocol was applied in the LARIAT control expressing cytoplasmic GFP.

**Live imaging and movie preparation.** Notum live imaging was performed as followed: the pupae were collected at the white stage (0 h after pupal formation), aged at 25° or 29°, glued on double-sided tape on a slide and surrounded by two home-made steel spacers (thickness: 0.64 mm, width 20 × 20 mm). The pupal case was opened up to the abdomen using forceps and mounted with a 20 × 40 mm #1.5 coverslip where we buttered halocarbon oil 10 S. The coverslip was then attached to spacers and the slide with two pieces of tape. Pupae were collected 48 or 72 h after clone induction and dissected usually at 16 to 18 h APF (after pupal formation). The time of imaging for each experiment is provided in the table above. Pupae were dissected and imaged on a confocal spinning disc microscope (Gatca systems, Metamorph software) with a ×40 oil objective (Nikon plan fluor, N.A. 1.30) or ×100 oil objective (Nikon plan fluor N.A. 1.30) or a LSM880 (Zen black software) equipped with a fast Airyscan using an oil ×40 objective (N.A. 1.3) or ×63 objective (N.A. 1.4), Z-stacks (0.5 or 1 μm/slice), every 5 min or 1 min using autofocus at 25 °C. The autofocus was performed using E-cad signal as a plane of reference (using a Zen Macro developed by Jan Ellenberg laboratory, MyPic) or a custom-made Metamorph journal on the spinning disc. Movies were performed in the nota close to the scutellum region containing the midline and the aDC and pDC macrochaetae. Movies shown are adaptive local Z projections. Briefly, E-cad plane was used as a reference to locate the plane of interest on sub-windows (using the maximum in Z of average intensity or the maximum of the standard deviation) through the Fiji plugin LocalZprojector or corresponding MATLAB routine<sup>72</sup>.

**Laser ablation.** Photo-ablation experiments were performed using a pulsed UV-laser (355 nm, Teem photonics, 20 kHz, peak power 0.7 kW) coupled to a Ilas-pulse module (Gatca systems) attached to our spinning disk microscope. The module was first calibrated and then set between 30 and 40% laser power to avoid cavitation. Images were taken every 1 min and ablation started after one time point. In all experiments, 400 × 400 μm rectangle were converted to line of 10 thickness in metamorph. Repetitions were set between 5 and 10 for proper cut to be achieved. Cell perimeter was obtained through cell segmentation and the tubulin signal quantified in the total area of each cell (contour +3px).

**Image processing and inflection point detection.** All images were processed using Matlab R2020a and Fiji (<http://fiji.sc/wiki/index.php/Fiji>). Movies for analysis were obtained after local Z projections of z-stacks using the Fiji LocalZprojector plugin<sup>72</sup>. As we were interested in apical signals, we set  $\Delta Z = 1$  so 3 planes of 0.5 μm or 1 μm were projected using maximum intensity projections. Then extruding cells were manually detected. When needed the signal was corrected for slight bleaching using CorrBleach macro from EMBL ([https://www.embl.de/camnet/html/bleach\\_correction.html](https://www.embl.de/camnet/html/bleach_correction.html)). In order to measure signal intensities, single cells were segmented using E-cad signal when it was possible (otherwise sqh or utABD signal). Depending on the data this was done directly using Tissue analyzer Fiji plugin after local z projections or after using EPySeg (<https://github.com/baigouy/EPySeg>)<sup>73</sup>. Once segmented, ROI of the cell contour was extracted to Fiji and custom macro was used to measure the mean px intensities of medio-apical signal (−3px from the junction), total signal (+3px from the contour) or junctional signal (transformation to an area of 6px wide encompassing the junctions). The perimeter was measured using the real cell contour. In addition, the noise was removed for spinning disc movies when needed by subtracting the signal measured in a 20 × 20-px ROI outside the tissue. Results were then analysed in MATLAB.

For analysis, single curves were aligned either by the end (i.e., the moment of the end of extrusion) or by the inflection point of the perimeter. Inflection points were automatically detected using a homemade MATLAB function. Briefly, it uses two moving linear fits after smoothing the perimeter using MATLAB moving average (taking into account five data point windows). The point with minimal error between the two fits and real data corresponds to the point where the perimeter starts to constrict i.e., the inflection point. Average, standard deviation and SEM were calculated after the alignment.

Radial averaged kymograph were obtained by tracking the centroid of every extruding cell and measuring the intensity along concentric circles of 3px at different distances from the cell centre. The values were averaged for every tracked extruding cell. E-cad signal was used to detect cell contour and define MTs signal from the extruding cell and from the neighbours.

**Quantifications along the apicobasal axis.** The cell average intensity per plane was quantified in extruding cells −45, −30 and −15 min before the end of extrusion using a 20 × 20-px square over the whole cell with a resolution of  $z = 0.5$  μm. Z axis profiles were aligned by the maximum value of E-cad-GFP to correct for small variation in z in the z-stack and align to the apical plane. For each cell, intensities were normalised by a min-max normalisation to make comparison possible after the removal of background noise. P values are obtained by pairwise and single-tailed t tests.

For the single-cell example, the apical area was measured by segmenting the cell. The intensity of apical MT was measured in two consecutive apical planes. The basal intensity was measured in the two consecutive planes below the nucleus. The represented side views are selected where we observe the largest cross-section of the nucleus in this cell.

**Myosin peak detection and yield computation and cross-correlation.** First, the signal was smoothed using a rolling average of 0.07 (using the LOESS option in the smooth method in MATLAB) in order to filter for noise. We then computed the contraction rate as following  $-\frac{d \text{ perimeter}}{dt}$  and the myosin rate of change as  $\frac{d \text{ myosin}}{dt}$ . In order to assess how closely changes in myosin relate to constriction, we computed the cross-correlation between myosin level or myosin rate of change and the constriction rate. The cross-correlation was calculated on Matlab with the *xcorr* function with the “coef” option (normalised cross-correlation after subtracting the mean). All the curves (one per cell) were then aggregated and averaged.

Contraction peak and myosin peak were detected using the findpeaks function in Matlab by setting “MinPeakProminence” to 7 in order to filter for noise. The yield was calculated for each contraction peak of each single curve as follow

$\frac{\text{contraction}_{T_{\text{peak}}}}{\text{myosin}_{\text{int}_{T_{\text{peak}}}}}$ . Perimeter and intensity curves were temporally aligned and normalised by their inflection point and yield data were sorted relative to the onset in 5-min time windows. Then single curves were aggregated and averaged. In order to compute myosin pulse duration, amplitude and frequency we detected myosin pulses. We then returned the peak parameters:  $T_{\text{peak}}$  (Time at peak maximum),  $W_{\text{peak}}$  (width at half peak maximum) and  $A_{\text{peak}}$  (peak amplitude). Myosin pulse frequency was computed as followed:  $\frac{N_{\text{peak}}}{\text{Total Time}_{\text{before onset}}}$  or  $\frac{N_{\text{peak}}}{\text{Total Time}_{\text{after onset}}}$ . Finally, all curves were aligned based on lag times (lag time = 0 min) for the averaging.

**Injection in pupal notum.** In all, 16 h APF pupae were glued on double-sided tape and the notum was dissected with a red filter. Pupae were then injected using homemade needles (borosilicate glass capillary, outer diameter 1 mm, internal diameter 0.5 mm, 10 cm long, Sutter instruments) pulled with a Sutter instrument P1000 pipette pulling apparatus. Injections were performed in the thorax of the pupae using a Narishige IM400 injector using a constant pressure differential (continuous leakage). Colcemid (Sigma Demeccolcine D7385 5 mg) was diluted in ethanol to a stock concentration of 20 mM and was then injected at 2.5 mM in the thorax of the pupae. Note that some cells seem to enlarge (see for instance Fig. 6k in the neighbouring cells) due to entry in mitosis and failure to complete mitosis. Taxol (Sigma Taxol/Paclitaxel T7402, 5 mg) was diluted in DMSO to a stock concentration of 60 mM (50 mg/mL) and was then injected at this concentration in the thorax of the pupae. SirTubulin was diluted in DMSO to a stock solution of 1 mM and then diluted to a concentration of 100 μM and injected in the thorax.

**Colcemid inactivation by UV and effect of MT re-polymerisation on cell area.** Pupae were dissected and mounted as described above. We first imaged EB1-GFP to assess its dynamics prior to colcemid injection. Then pupae were unmounted and we injected colcemid as described in this protocol. We then waited for 1 hour and 30 min for colcemid to diffuse in the notum. Next, we re-imaged EB1-GFP and assessed colcemid effect through the loss of EB1-GFP comets and diffusion of the GFP pool as well as cell division arrest (cell division arrest was later used to assess colcemid effect whenever we could not image EB1-GFP signal).

We then image a single z-plane every second for 240 s. We inactivated colcemid locally by pulsing 405 nm diode (0.44% AOTF) in a restricted region of the imaging field and compared this to a control region. We assessed MT re-polymerisation by looking at the formation of EB1-GFP foci and comets. In order to measure the effect of re-polymerisation on cell size, we segmented the cell in the UV or control regions at  $t_0$  and  $t_{240s}$ . As we are interested in the relative changes of cell perimeter between these two time points we computed a perimeter fold change for each cell as the following ratio  $\frac{\text{perim}_{t_{240s}}}{\text{perim}_{t_0}}$  and compared the condition with colcemid to a control condition injected with H<sub>2</sub>O + ethanol.

#### Proportion of cell elimination in clones

**Spastin clones.** Since we could not recover clone upon Spastin overexpression, we generated clones allowing conditional induction of Spastin with act<y < Gal4 UAS-RFP, UAS-Spastin with tub-Gal80<sup>ts</sup>. Gal80<sup>ts</sup> binds Gal4 and represses Gal4-driven expression. Upon switching to 29 °C Gal80<sup>ts</sup> becomes inactive allowing Gal4-driven expression.

Due to the maturation time of RFP following the temperature shift to 29 °C, it is difficult to track the position of the clones initially following the temperature shift. For that reason, we decided to measure the proportion of cell extrusion by looking at the global rate of cell extrusion at 29 °C in the condition with control UAS-RFP

of UAS-Spantin, UAS-RFP clones. Thus, we tend to underestimate the real increase in extrusion rate. Because of the high rates of cell extrusion in the midline we separated the quantification between the inside of the midline and outside. We did that by tracing manually the midline using the position of the most central Sensory Organ Precursors which define the midline. We then manually detected all the extrusions over 1000 min and defined automatically if they belong to the midline or not. We then segmented the tissue at  $t_0$  to count the number of cells inside the midline or outside and then used these values to compute the proportion of extrusion as following:  $\frac{N_{extrusion\ midline}}{N_{cell\ midline}}$  or  $\frac{N_{extrusion\ outside}}{N_{cell\ outside}}$ .

**Rescue of extrusion in *hid-dsRNA* following colcemid injection.** For these experiments, colcemid was injected as described above and this condition was compared with control injections ( $H_2O + ethanol$ ). We then manually detected all the extrusions at each time points and for each condition during the 500 first minutes. Clones were segmented at each time point using the UAS-RFP signal and we used this segmentation to automatically define if extrusions belong to UAS-*hid-dsRNA* clones or not. We then segmented the tissue at  $t_0$  min to count the number of cells in the clones or outside the clones and used these values to compute the proportion of extrusion inside or outside the clone as following  $\frac{N_{extrusion\ clones}}{N_{cell\ clones}}$  or  $\frac{N_{extrusion\ wt}}{N_{cell\ wt}}$ .

**Detection of Caspase signal in *hid-dsRNA* clones.** Colcemid was injected as described previously in this protocol and this condition was compared with control injections ( $H_2O + ethanol$ ). We then manually detected all the extrusions at each time point and for each condition and manually defined if they are positive or negative for caspase activation using the UAS-GC3AI-GFP signal. We then either computed the proportion of each “type” of extrusion relative to the total number of cell in the clones or to the total number of extrusions in the clones.

**Microtubule stabilisation and delay of extrusion.** Taxol was injected as explained previously (see methods injection) and results were compared to pupae injected with DMSO only. To make the comparison possible, all cells were aligned by the end and normalised by the average perimeter value before the onset of extrusion (or similarly by the average circularity value before the onset).

The duration of extrusion was measured as the difference between the time at the end of extrusion and the time at the inflexion point. The represented distribution is normalised by the total number of observed extrusions in each condition.

**Statistics.** Data were not analysed blindly. No specific method was used to pre-determine the number of samples. The definition of  $n$  and the number of samples is given in each figure legend and in the table of the Experimental model section. Error bars are standard error of the mean (SEM).  $P$  values are calculated through  $t$  test if the data passed the normality test (Shapiro–Wilk test), or Mann–Whitney test/rank-sum test if the distribution was not normal, or the Fisher exact test for comparison of proportion (see legends). Statistical tests were performed on Matlab.

**Reporting summary.** Further information on research design is available in the Nature Research Reporting Summary linked to this article.

## Data availability

All the data generated in this study (images, local projections of movies) have been deposited on Zenodo with the following link <https://doi.org/10.5281/zenodo.6546831><sup>74</sup>. The quantified data used for every graph are provided in a single excel source data file (one sheet per figure panel). Further information and requests for resources and reagents should be directed to and will be fulfilled by the corresponding author, Romain Levayer (romain.levayer@pasteur.fr). All the reagents generated in this study will be shared upon request to the corresponding author without any restrictions. Source data are provided with this paper.

## Code availability

All codes generated in this study have been deposited on Github and can be accessible with the following link <https://doi.org/10.5281/zenodo.6545302><sup>75</sup>. Further explanations and help can be provided upon request to the lead contact.

Received: 22 October 2021; Accepted: 10 June 2022;

Published online: 25 June 2022

## References

- Rosenblatt, J., Raff, M. C. & Cramer, L. P. An epithelial cell destined for apoptosis signals its neighbors to extrude it by an actin- and myosin-dependent mechanism. *Curr. Biol.* **11**, 1847–1857 (2001).
- Ohsawa, S., Vaughen, J. & Igaki, T. Cell extrusion: a stress-responsive force for good or evil in epithelial homeostasis. *Dev. Cell* **44**, 532 (2018).
- Gudipaty, S. A. & Rosenblatt, J. Epithelial cell extrusion: pathways and pathologies. *Semin. Cell Dev. Biol.* **67**, 132–140 (2017).
- Kuipers, D. et al. Epithelial repair is a two-stage process driven first by dying cells and then by their neighbours. *J. Cell Sci.* **127**, 1229–1241 (2014).
- Duszyc, K. et al. Mechanotransduction activates RhoA in the neighbors of apoptotic epithelial cells to engage apical extrusion. *Curr. Biol.* **31**, 1326–1336.e1325 (2021).
- Teng, X., Qin, L., Le Borgne, R. & Toyama, Y. Remodeling of adhesion and modulation of mechanical tensile forces during apoptosis in *Drosophila* epithelium. *Development* **144**, 95–105 (2017).
- Michael, M. et al. Coronin 1B reorganizes the architecture of F-actin networks for contractility at steady-state and apoptotic adherens junctions. *Dev. Cell* **37**, 58–71 (2016).
- Grieve, A. G. & Rabouille, C. Extracellular cleavage of E-cadherin promotes epithelial cell extrusion. *J. Cell Sci.* **127**, 3331–3346 (2014).
- Kocgozlu, L. et al. Epithelial cell packing induces distinct modes of cell extrusions. *Curr. Biol.* **26**, 2942–2950 (2016).
- Le, A. P. et al. Adhesion-mediated heterogeneous actin organization governs apoptotic cell extrusion. *Nat. Commun.* **12**, 397 (2021).
- An, Y. et al. Apical constriction is driven by a pulsatile apical myosin network in delaminating *Drosophila* neuroblasts. *Development* **144**, 2153–2164 (2017).
- Atieh, Y., Wyatt, T., Zaske, A. M. & Eisenhoffer, G. T. Pulsatile contractions promote apoptotic cell extrusion in epithelial tissues. *Curr. Biol.* **31**, 1129–1140.e1124 (2021).
- Thomas, M., Ladoux, B. & Toyama, Y. Desmosomal junctions govern tissue integrity and actomyosin contractility in apoptotic cell extrusion. *Curr. Biol.* **30**, 682–690.e685 (2020).
- Ambrosini, A. et al. Apoptotic forces in tissue morphogenesis. *Mech. Dev.* **144**, 33–42 (2017).
- Crawford, E. D. & Wells, J. A. Caspase substrates and cellular remodeling. *Annu. Rev. Biochem.* **80**, 1055–1087 (2011).
- Gagliardi, P. A. et al. MRCKalpha is activated by caspase cleavage to assemble an apical actin ring for epithelial cell extrusion. *J. Cell Biol.* **217**, 231–249 (2017).
- Marinari, E. et al. Live-cell delamination counterbalances epithelial growth to limit tissue overcrowding. *Nature* **484**, 542–545 (2012).
- Levayer, R., Dupont, C. & Moreno, E. Tissue crowding induces caspase-dependent competition for space. *Curr. Biol.* **26**, 670–677 (2016).
- Guirao, B. et al. Unified quantitative characterization of epithelial tissue development. *eLife* **4**, e08519 (2015).
- Moreno, E., Valon, L., Levillayer, F. & Levayer, R. Competition for space induces cell elimination through compaction-driven ERK downregulation. *Curr. Biol.* **29**, 23–34.e28 (2019).
- Valon, L. et al. Robustness of epithelial sealing is an emerging property of local ERK feedback driven by cell elimination. *Dev. Cell* **56**, 1–12 (2021).
- Fujisawa, Y., Shinoda, N., Chihara, T. & Miura, M. ROS regulate caspase-dependent cell delamination without apoptosis in the *Drosophila* pupal notum. *iScience* **23**, 101413 (2020).
- Munjal, A., Philippe, J. M., Munro, E. & Lecuit, T. A self-organized biomechanical network drives shape changes during tissue morphogenesis. *Nature* **524**, 351–355 (2015).
- Rauzi, M., Lenne, P. F. & Lecuit, T. Planar polarized actomyosin contractile flows control epithelial junction remodelling. *Nature* **468**, 1110–1114 (2010).
- Martin, A. C., Kaschube, M. & Wieschaus, E. F. Pulsed contractions of an actin-myosin network drive apical constriction. *Nature* **457**, 495–499 (2009).
- Curran, S. et al. Myosin II controls junction fluctuations to guide epithelial tissue ordering. *Dev. Cell* **43**, 480–492.e486 (2017).
- Clement, R., Dehapiot, B., Collinet, C., Lecuit, T. & Lenne, P. F. Viscoelastic dissipation stabilizes cell shape changes during tissue morphogenesis. *Curr. Biol.* **27**, 3132–3142.e3134 (2017).
- Alt, S., Ganguly, P. & Salbreux, G. Vertex models: from cell mechanics to tissue morphogenesis. *Philos. Trans. R. Soc. Lond. B Biol. Sci.* **372**, 20150520 (2017).
- Fletcher, A. G., Osterfield, M., Baker, R. E. & Shvartsman, S. Y. Vertex models of epithelial morphogenesis. *Biophys. J.* **106**, 2291–2304 (2014).
- Levayer, R. & Lecuit, T. Biomechanical regulation of contractility: spatial control and dynamics. *Trends Cell Biol.* **22**, 61–81 (2012).
- Saias, L. et al. Decrease in cell volume generates contractile forces driving dorsal closure. *Dev. Cell* **33**, 611–621 (2015).
- Singh, A. et al. Polarized microtubule dynamics directs cell mechanics and coordinates forces during epithelial morphogenesis. *Nat. Cell Biol.* **20**, 1126–1133 (2018).
- Takeda, M., Sami, M. M. & Wang, Y. C. A homeostatic apical microtubule network shortens cells for epithelial folding via a basal polarity shift. *Nat. Cell Biol.* **20**, 36–45 (2018).
- Slattum, G., McGee, K. M. & Rosenblatt, J. P115 RhoGEF and microtubules decide the direction apoptotic cells extrude from an epithelium. *J. Cell Biol.* **186**, 693–702 (2009).

35. Booth, A. J. R., Blanchard, G. B., Adams, R. J. & Roper, K. A dynamic microtubule cytoskeleton directs medial actomyosin function during tube formation. *Dev. Cell* **29**, 562–576 (2014).
36. Gillard, G., Girdler, G. & Roper, K. A release-and-capture mechanism generates an essential non-centrosomal microtubule array during tube budding. *Nat. Commun.* **12**, 4096 (2021).
37. Ko, C. S., Tserunyan, V. & Martin, A. C. Microtubules promote intercellular contractile force transmission during tissue folding. *J. Cell Biol.* **218**, 2726–2742 (2019).
38. Nashchekin, D., Fernandes, A. R. & St Johnston, D. Patronin/shot cortical foci assemble the noncentrosomal microtubule array that specifies the *Drosophila* anterior-posterior axis. *Dev. Cell* **38**, 61–72 (2016).
39. Xu, Z. et al. Microtubules acquire resistance from mechanical breakage through intraluminal acetylation. *Science* **356**, 328–332 (2017).
40. Schaedel, L. et al. Microtubules self-repair in response to mechanical stress. *Nat. Mater.* **14**, 1156–1163 (2015).
41. Janson, M. E., de Dood, M. E. & Dogterom, M. Dynamic instability of microtubules is regulated by force. *J. Cell Biol.* **161**, 1029–1034 (2003).
42. Bonnet, I. et al. Mechanical state, material properties and continuous description of an epithelial tissue. *J. R. Soc. Interface* **9**, 2614–2623 (2012).
43. Schott, S. et al. A fluorescent toolkit for spatiotemporal tracking of apoptotic cells in living *Drosophila* tissues. *Development* **144**, 3840–3846 (2017).
44. Jankovics, F. & Brunner, D. Transiently reorganized microtubules are essential for zippering during dorsal closure in *Drosophila melanogaster*. *Dev. Cell* **11**, 375–385 (2006).
45. Lee, S. et al. Reversible protein inactivation by optogenetic trapping in cells. *Nat. Methods* **11**, 633–636 (2014).
46. Osswald, M., Santos, A. F. & Morais-de-Sa, E. Light-induced protein clustering for optogenetic interference and protein interaction analysis in *drosophila* S2 cells. *Biomolecules* **9**, 61 (2019).
47. Qin, X. et al. Cell-matrix adhesion and cell-cell adhesion differentially control basal myosin oscillation and *Drosophila* egg chamber elongation. *Nat. Commun.* **8**, 14708 (2017).
48. Jenkins, B. V., Saunders, H. A. J., Record, H. L., Johnson-Schlitz, D. M. & Wildonger, J. Effects of mutating alpha-tubulin lysine 40 on sensory dendrite development. *J. Cell Sci.* **130**, 4120–4131 (2017).
49. Roll-Mecak, A. & Vale, R. D. The *Drosophila* homologue of the hereditary spastic paraplegia protein, spastin, severs and disassembles microtubules. *Curr. Biol.* **15**, 650–655 (2005).
50. Collins, C., Majekodunmi, A. & Mitchell, B. Centriole number and the accumulation of microtubules modulate the timing of apical insertion during radial intercalation. *Curr. Biol.* **30**, 1958–1964.e1953 (2020).
51. Collins, C. et al. Tubulin acetylation promotes penetrative capacity of cells undergoing radial intercalation. *Cell Rep.* **36**, 109556 (2021).
52. Garcin, C. & Straube, A. Microtubules in cell migration. *Essays Biochem.* **63**, 509–520 (2019).
53. Picone, R. et al. A polarised population of dynamic microtubules mediates homeostatic length control in animal cells. *PLoS Biol.* **8**, e1000542 (2010).
54. Ingber, D. E. Tensegrity I. Cell structure and hierarchical systems biology. *J. Cell Sci.* **116**, 1157–1173 (2003).
55. Brangwynne, C. P. et al. Microtubules can bear enhanced compressive loads in living cells because of lateral reinforcement. *J. Cell Biol.* **173**, 733–741 (2006).
56. Wu, Y., Stewart, A. G. & Lee, P. V. S. High-throughput microfluidic compressibility cytometry using multi-tilted-angle surface acoustic wave. *Lab Chip* **21**, 2812–2824 (2021).
57. Robison, P. et al. Detyrosinated microtubules buckle and bear load in contracting cardiomyocytes. *Science* **352**, aaf0659 (2016).
58. Lee, G. et al. Myosin-driven actin-microtubule networks exhibit self-organized contractile dynamics. *Sci. Adv.* **7**, eabe4334 (2021).
59. Tissot, N. et al. Distinct molecular cues ensure a robust microtubule-dependent nuclear positioning in the *Drosophila* oocyte. *Nat. Commun.* **8**, 15168 (2017).
60. Lee, H. O. & Norden, C. Mechanisms controlling arrangements and movements of nuclei in pseudostratified epithelia. *Trends Cell Biol.* **23**, 141–150 (2013).
61. Hurst, S., Vos, B. E. & Betz, T. Intracellular softening and fluidification reveals a mechanical switch of cytoskeletal material contributions during division. Preprint at <https://www.biorxiv.org/content/10.1101/2021.01.07.425761v1> (2021).
62. Crawford, E. D. et al. Conservation of caspase substrates across metazoans suggests hierarchical importance of signaling pathways over specific targets and cleavage site motifs in apoptosis. *Cell Death Differ.* **19**, 2040–2048 (2012).
63. Triclin, S. et al. Self-repair protects microtubules from destruction by molecular motors. *Nat. Mater.* **20**, 883–891 (2021).
64. Li, Y. et al. Compressive forces stabilise microtubules in living cells. Preprint at *bioRxiv* <https://doi.org/10.1101/2022.02.07.479347> (2022).
65. Ju, R. J. et al. A microtubule mechanostat enables cells to navigate confined environments. Preprint at *bioRxiv* <https://doi.org/10.1101/2022.02.08.479516> (2022).
66. Okuda, S. & Fujimoto, K. A mechanical instability in planar epithelial monolayers leads to cell extrusion. *Biophys. J.* **118**, 2549–2560 (2020).
67. Ding, A. X. et al. CasExpress reveals widespread and diverse patterns of cell survival of caspase-3 activation during development in vivo. *eLife* **5**, e10936 (2016).
68. Jauffred, B. & Bellaïche, Y. Analyzing frizzled signaling using fixed and live imaging of the asymmetric cell division of the *Drosophila* sensory organ precursor cell. *Methods Mol. Biol.* **839**, 19–25 (2012).
69. Farhadifar, R., Roper, J. C., Aigouy, B., Eaton, S. & Julicher, F. The influence of cell mechanics, cell-cell interactions, and proliferation on epithelial packing. *Curr. Biol.* **17**, 2095–2104 (2007).
70. Tsuboi, A. et al. Competition for space is controlled by apoptosis-induced change of local epithelial topology. *Curr. Biol.* **28**, 2115–2128.e2115 (2018).
71. Etournay, R. et al. TissueMiner: a multiscale analysis toolkit to quantify how cellular processes create tissue dynamics. *eLife* **5**, e14334 (2016).
72. Herbert, S. et al. LocalZProjector and DeProj: a toolbox for local 2D projection and accurate morphometrics of large 3D microscopy images. *BMC Biol.* **19**, 136 (2021).
73. Aigouy, B., Cortes, C., Liu, S. & Prud'Homme, B. EPySeg: a coding-free solution for automated segmentation of epithelia using deep learning. *Development* **147**, dev194589 (2020).
74. Villars, A., Matamoros-Vidal, A., Levillayer, F. & Levayer, R. Microtubule disassembly by caspases is an important rate-limiting step of cell extrusion, raw data. *Zenodo* [https://zenodo.org/record/6546831#\\_YrMiUnZBxdg](https://zenodo.org/record/6546831#_YrMiUnZBxdg) (2022).
75. Villars, A., Matamoros-Vidal, A., Levillayer, F. & Levayer, R. Microtubule disassembly by caspases is an important rate-limiting step of cell extrusion. *GitHub*. [https://zenodo.org/record/6545302#\\_YrMh-HZBxdg](https://zenodo.org/record/6545302#_YrMh-HZBxdg) (2022).
76. Huang, J., Zhou, W., Dong, W., Watson, A. M. & Hong, Y. From the cover: directed, efficient, and versatile modifications of the *Drosophila* genome by genomic engineering. *Proc. Natl Acad. Sci. USA* **106**, 8284–8289 (2009).
77. Pinheiro, D. et al. Transmission of cytokinesis forces via E-cadherin dilution and actomyosin flows. *Nature* **545**, 103–107 (2017).
78. Yuan, L., Fairchild, M. J., Perkins, A. D. & Tanentzapf, G. Analysis of integrin turnover in fly myotendinous junctions. *J. Cell Sci.* **123**, 939–946 (2010).
79. Qin, X. et al. A biochemical network controlling basal myosin oscillation. *Nat. Commun.* **9**, 1210 (2018).
80. Herszterg, S., Leibfried, A., Bosveld, F., Martin, C. & Bellaïche, Y. Interplay between the dividing cell and its neighbors regulates adherens junction formation during cytokinesis in epithelial tissue. *Dev. Cell* **24**, 256–270 (2013).

## Acknowledgements

We thank members of RL lab for critical reading of the manuscript. We would like to thank Jakub Voznica for his observations on the abdomen during his internship. We are also grateful to Antoine Guichet, Thomas Lecuit, Magalie Suzanne, Yohanns Bellaïche, Xiaobo Wang, Renata Basto, the Bloomington *Drosophila* Stock Centre, the *Drosophila* Genetic Resource Centre and the Vienna *Drosophila* Resource Centre, Flybase for sharing essential information, stocks and reagents. We also thank Benoît Aigouy for the Tissue Analyser software and Jan Ellenberg group for MyPic autofocus macro. A.V. is supported by a PhD grant from the doctoral school “Complexité du Vivant” Sorbonne Université and from an extension grant of La Ligue contre le Cancer, work in RL lab is supported by the Institut Pasteur (G5 starting package), the ERC starting grant CoSpADD (Competition for Space in Development and Disease, grant number 758457), the Cercle FSR and the CNRS (UMR 3738).

## Author contributions

R.L. and A.V. discussed and designed the project and wrote the manuscript. A.M.V. performed the vertex simulations. F.L. designed the tubulin mutant construct. A.V. performed all the other experiments and analyses. Every author has commented and edited the manuscript.

## Competing interests

The authors declare no competing interests.

## Additional information

**Supplementary information** The online version contains supplementary material available at <https://doi.org/10.1038/s41467-022-31266-8>.

**Correspondence** and requests for materials should be addressed to Romain Levayer.

**Peer review information** *Nature Communications* thanks the anonymous, reviewer(s) for their contribution to the peer review of this work. Peer reviewer reports are available.

**Reprints and permission information** is available at <http://www.nature.com/reprints>

**Publisher's note** Springer Nature remains neutral with regard to jurisdictional claims in published maps and institutional affiliations.



**Open Access** This article is licensed under a Creative Commons Attribution 4.0 International License, which permits use, sharing, adaptation, distribution and reproduction in any medium or format, as long as you give appropriate credit to the original author(s) and the source, provide a link to the Creative Commons license, and indicate if changes were made. The images or other third party material in this article are included in the article's Creative Commons license, unless indicated otherwise in a credit line to the material. If material is not included in the article's Creative Commons license and your intended use is not permitted by statutory regulation or exceeds the permitted use, you will need to obtain permission directly from the copyright holder. To view a copy of this license, visit <http://creativecommons.org/licenses/by/4.0/>.

© The Author(s) 2022





CHAPTER  
**DECISION-MAKING** 3

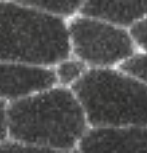




## **Table of contents**

<b>1. Decision making &amp; apoptosis: non-apoptotic functions of caspases .....</b>	<b>132</b>
<b>1.1. Survival to caspase activation during development: non-apoptotic function in physiological contexts .....</b>	<b>134</b>
1.1.1. Regulation of proliferation by caspases .....	134
1.1.2. Regulation of survival .....	135
1.1.3. Cellular remodelling by caspases.....	135
1.1.4. Cell differentiation.....	138
<b>1.2. Role in cancer.....</b>	<b>142</b>
<b>1.3. Mechanism of caspase regulation for non-apoptotic functions .....</b>	<b>143</b>
1.3.1. Balancing levels through induction of caspase inhibitors .....	143
1.3.2. Dynamic regulation of caspase and their proteolytic activity .....	145
1.3.3. Spatial regulation of caspases and substrate availability .....	146
1.3.4. Recovery from early apoptosis: a caspase threshold? .....	149
<b>2. Results: Decision-making in cell extrusion .....</b>	<b>152</b>
<b>2.1. Introduction.....</b>	<b>152</b>
<b>2.2. Results.....</b>	<b>153</b>
<b>2.3. Discussion.....</b>	<b>160</b>



# 1. Decision making & apoptosis: non-apoptotic functions of caspases

In the previous chapter, I illustrated how caspases initiate and regulate cell extrusion. When introducing the apoptotic pathway, I highlighted several positive feedbacks that lead to a cascade of caspase activation. Such feedbacks supposedly ensure that a cell, activating caspase, fully commits to apoptosis and is eliminated. Consequently, caspase activation was seen as a point of no return always leading to apoptosis. However, recent advances in the field have highlighted numerous non-apoptotic functions of caspases (reviewed in <sup>320-322</sup>). These functions are broad and are involved in the control of cell fate, differentiation, pluripotency, reprogramming, proliferation, and migration both in *Drosophila* and mammals (**Figure 31**). Yet, what sets the balance between these non-lethal levels and the irreversible engagement in apoptosis remains unclear. It has been proposed that this balance is set by a threshold of caspase <sup>323-326</sup>. Below this threshold of caspase activation, cells would survive and above it, they would irreversibly commit to apoptosis. However, this has never been characterized experimentally and quantitatively. Therefore, whether such a threshold exists and how it is set remains unclear. In other words, how does a cell take the decision to enter extrusion & apoptosis? How is the cell sensitivity to caspases set? What are the parameters monitored by the cell which modulate its sensitivity? Can we predict cell sensitivity based on these parameters?

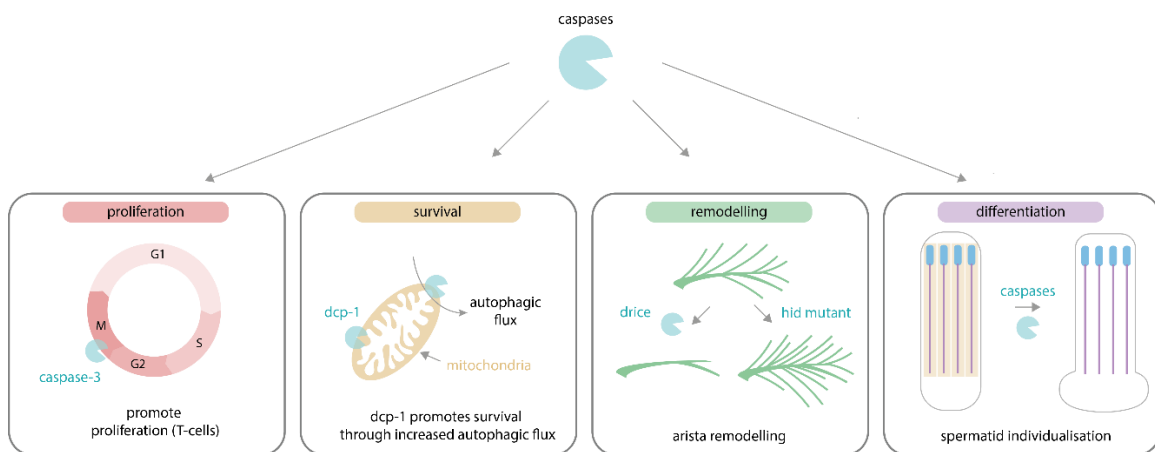


**Figure 31** - Summary of non-apoptotic caspases functions. Caspase function in regulating T-cells proliferation (left, red). Caspase function in regulating survival through autophagy (middle left, orange). Caspase function in cellular remodeling of the *Drosophila* arista (middle right, green). Caspase function in differentiation of spermatid (right, purple).

In this chapter, I will first review a few of the non-apoptotic functions of caspases (**Figure 3I**). Because the number of caspases involved in non-apoptotic function is large, I will mainly focus on the role of Caspase-9 (Dronc in *Drosophila*) or activator caspases (Caspase-3/Drice, Caspase-7). Indeed, these caspases are the main mediators of the apoptotic pathway. I will not cover non-cell-autonomous functions of caspase as in the case of Apoptosis Induced Proliferation. This will allow me to present some mechanisms which ensure that caspase activation remains non-lethal. Then I will show how these properties can be hijacked by cancerous cells. Finally, I will focus on data showing cell survival to caspase activation during development. This review will allow me to introduce how the idea of a caspase threshold has emerged. Moving forward, I will present the results I obtained during my PhD on the decision-making step leading to extrusion.

## 1.1. Survival to caspase activation during development: non-apoptotic function in physiological contexts

### 1.1.1. Regulation of proliferation by caspases

Non-apoptotic functions of caspases have been characterised in several different physiological contexts<sup>320-322</sup>. Interestingly, non-apoptotic caspase activity is necessary for cell proliferation in what may appear as a counter-intuitive process given the ability of caspases to trigger cell death (**Figure 32**). For instance, Caspase-3 (Cas3) is specifically activated in proliferative cells from sebaceous glands in the epidermis<sup>327</sup>. Cas3 cleaves  $\alpha$ -catenin which leads to YAP translocation and subsequent activation. Surprisingly, the levels of the Cas3 inhibitor XIAP are increased by Cas3 activation in a YAP-dependent manner, and it acts as negative feedback to prevent overgrowth (**Figure 32a**). A similar effect of Cas3 levels was observed in the regulation of Mouse T-cells proliferation. Cas3 levels correlate with the entry in proliferation of T-cells. Interestingly, these levels are maintained to an intermediate level higher than non-activated T-cells and lower than T-cells in which death is induced by Fas-L<sup>328</sup>. Yet, the exact mechanism remains unknown.

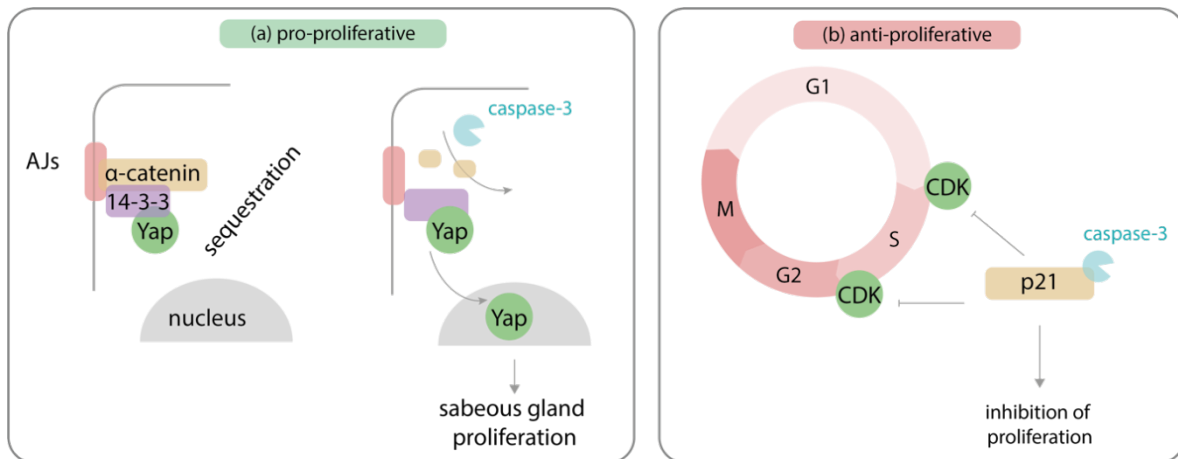


**Figure 32** - Caspase-dependent regulation of cell proliferation. (a) Caspase-3 regulates pro-proliferative functions through the cleavage of  $\alpha$ -catenin. This releases YAP sequestration and leads to its relocalisation to the nucleus. Ultimately this promotes proliferation of sebaceous gland cells. (b) Caspase-3 inhibits proliferation through the cleavage of p21 in splenic B cells.

Finally, human mammary cells retained their proliferative ability upon EGF stimulation even when they exhibit non-apoptotic Cas3 activation<sup>329</sup>. Here again, the mechanism that maintains Cas3 to a non-apoptotic range is undetermined. Conversely to what I just described, sub-lethal activation of Cas3 may negatively regulate proliferation (**Figure 32b**). Cas3 activation inhibits the proliferation of splenic B cells through the cleavage of p21 (an inhibitor of CDK). Cas3 mutant mice displayed normal

apoptosis but a higher number of Splenic B cells because of higher proliferation<sup>330</sup>. This shows that Cas3 negatively regulates cell proliferation independently of its ability to regulate apoptosis. Taken together, this demonstrates how Cas3 activation at sublethal levels regulates proliferation. However, that regulation is either pro or antiproliferative (**Figure 32**). Therefore, Cas3 action might be context-dependent and might depend on caspase levels or localisation. Finally, in wing disc, Dcp-1 and Decay (Caspase-3 homologues in *Drosophila*) promote tissue growth. Interestingly, this is both independent of Dronc activation or Drice function<sup>331</sup>.

### 1.1.2. Regulation of survival

Another, counter-intuitive function of sub-lethal caspase activation, is the promotion of survival. One of the classical examples is the regulation of autophagy by caspases. Indeed, autophagy and apoptosis present high levels of crosstalk which results in a dynamic balance between survival and death<sup>332</sup>. For instance, in the *Drosophila* ovary, Dcp-1 localises to the mitochondria and promotes starvation-induced autophagy. This happens through the inhibition of SesB (a stress-sensitive protein) which results in increased survival. Accordingly, loss of Dcp-1 (Cas3 homologue in *Drosophila*) induces a reduction in autophagic flux<sup>333</sup>. Similarly, non-apoptotic cleavage promotes mice survival upon various stresses. This is mediated by a partial cleavage of RasGAP (a regulator of Ras and Rho-GTPases). Cells expressing a non-cleavable form of RasGAP fail to activate Akt (an anti-apoptotic protein) and to survive. Accordingly, survival is reduced in Cas3 KO mice<sup>334</sup>. Overall, this shows that sub-lethal levels of Cas3 can activate apoptotic inhibitors and promote survival.

### 1.1.3. Cellular remodelling by caspases

Caspases also have major functions in cellular remodelling and cell shape changes which ultimately may be important for cell extrusion (**Figure 33**). As I have mentioned in part **2.3.2**, ROCK1 is activated by Cas3. Cas3 constitutively activates ROCK by the cleavage of its C-Ter. This in turn phosphorylates MyoII and leads to higher contractility and membrane blebbing. This is part of the apoptotic process. Yet, Cas3 activation may also modulate the actin network in a non-apoptotic manner. Cas3 activation regulates the differentiation and maturation of macrophages<sup>335,336</sup>. Additionally, Cas3-dependent cleavage of ROCK1 also regulates macrophage polarity assembly and maintenance of Focal Adhesion.



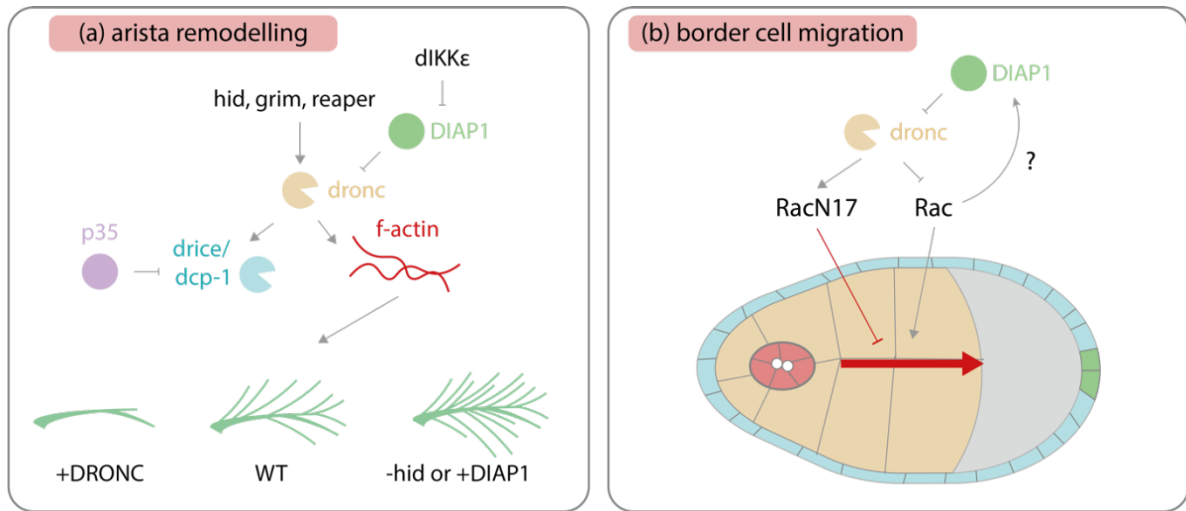


**Figure 33** - Caspase-dependent cellular remodelling. (a) Dronc (yellow) mediates the morphogenesis of the arista (green branches) through the modulation of F-actin (red). Inhibition of Dronc through *hid* mutation or Diap1 overexpression increases the number of branches (bottom right). This is independent of Caspase-3 homologues Drice and Dcp-1 (blue) because their inhibition through p35 (purple) doesn't affect arista branching. The kinase IKK negatively regulates Diap1. (b) Border cell migration is negatively regulated by caspases. RacN17 (dominant-negative, red arrow on the left side) inhibits border cell migration. This is rescued by Dronc inhibition (left side of the figure). Thus Dronc, under the control of Diap1 (green) negatively regulates Rac and border cell migration (right side of the figure).

The relative simplicity of the caspase pathway in *Drosophila* has made it a good model to study non-apoptotic functions of caspases. This has been specifically useful in the understanding of cell remodelling events such as the formation of the arista or the migration of border cells (**Figure 33a**). The arista is a terminal segment of the *Drosophila* antenna made of a core and extensions<sup>337</sup>. Stimulating or inhibiting caspase activation leads reciprocally to the lack of branch formation or ectopic branching. Accordingly, overexpression of the caspase inhibitor Diap1 is sufficient to induce an abnormal arista morphology associated with an increased number of branches<sup>338</sup>. Moreover, a mutation in the pro-apoptotic gene *hid* led to the formation of extra branches. Thus, caspases negatively regulate the process of branching, but how can caspase affect cell cytoskeleton? Diap1 degradation seems to negatively regulate F-actin (**Figure 33a**)<sup>339</sup>. It is known that Diap1 regulates Dronc activity. Additionally, p35 overexpression that blocks effector caspases did not affect arista branching. Conversely, Dronc mutants that survive have extra arista branches<sup>340</sup>. This suggests that the process is independent of effector caspase activation. Yet, how Dronc or Diap1 might control F-actin is not known. Together, these experiments show how caspase activation negatively regulates arista branching in *Drosophila* under Diap1-mediated control and highlight another non-apoptotic function

of caspase in cellular remodelling. This happens independently of Drice activation as it is suggested by the p35 experiment.

Yet, in some cases, non-apoptotic functions of caspases in *Drosophila*, are mediated by Drice activity. This is the case of the elongation of the *Drosophila* tracheal system: a set epithelial tubes important for gas exchanges. Drice acts downstream of Yorkie (Yki) to regulate trachea length<sup>341</sup>. Accordingly, trachea failed to elongate in *Drice* null mutant but were too long upon mutant in *thread*: the gene coding for the caspase inhibitor Diap1 which is a target of Ykie. These cells are competent to enter apoptosis, yet they rarely do in WT highlighting the non-apoptotic function of Drice. This function is mediated by the ability of Drice to regulated endocytic trafficking of several polarity and junctional proteins<sup>341</sup>.

Caspases also regulate cell cytoskeleton during key steps of development such as the maturation of the oocyte in *Drosophila* ovaries. This tissue is made of 16 cells linked together through ring canals which allow them to share cytoplasmic content. Once the oocyte is specified, all nurse cells dump their content into the oocyte and degenerate. While these cells die at a later stage after dumping, Dcp-1 (Caspase-3 homologue) is necessary at early stages of the process for the formation of ring canals and cytoplasmic actin bundles formation. Both of these structures are necessary for the contraction process leading to the dumping. This points to a non-apoptotic function of Dcp-1. Moreover, nurse cells still function over a long period and contribute functional proteins and mitochondria to the oocyte suggesting that they may resist apoptosis early on. Finally, Dcp-1 can also be transmitted to the oocyte which further suggests that a mechanism protecting the oocyte from cell death may take place<sup>342</sup>.

The oocyte and nurse cells are surrounded by an epithelium that forms the ovarian follicle. A group of 6 to 10 anterior cells get out of the follicle epithelium and migrate as a cluster toward the posterior end of the follicle where the oocyte is located (**Figure 33b**)<sup>343</sup>. Cell migration can be inhibited by the overexpression of a RacN17 dominant-negative<sup>343</sup>. Curiously, Diap1 overexpression suppresses migration defects in that context<sup>323</sup>. Interestingly, homozygous mutant clones for the gene coding for Diap1 stinkingly lack apoptosis<sup>323</sup>. This may suggest that these cells are very resistant to apoptosis or that the regulation of apoptosis in these cells is independent of Diap1. Still, the inhibition of Dronc also rescues RacN17 migration defects (**Figure 33b**). This indicates that Dronc negatively regulates border cell migration. This is coherent with the

observation that Caspase-3 cleaves and inhibits its GTPase function in lymphocytes. Therefore, Rac could be another substrate of caspase<sup>344</sup>. This is supported by the fact that Diap1 and Rac both physically associated. Interestingly, overexpression of Rac in border cells increased Diap1 levels and suggests potential feedbacks (**Figure 33b**). Finally, non-apoptotic caspase activation may also trigger cell remodelling by influencing the Microtubule network. During development, C4da neurons undergo a step of dendrites pruning. This is regulated by caspase-dependent remodelling of the cortical F-actin network<sup>345,346</sup>, and MTs<sup>346</sup>. Indeed, The IKK kinase ik2 regulates katanin and severing of Microtubules<sup>346</sup>. Ik2 similarly to IKK $\epsilon$  functions upstream of Diap1 and induce its degradation. Accordingly, inhibition of caspase inhibits pruning. All these results demonstrate how caspase can regulate cell shape changes and cytoskeleton independently of their apoptotic functions.

#### 1.1.4. Cell differentiation

Another important role for caspase sublethal activation is the regulation of cell differentiation. For instance, in the *Drosophila* notum and scutellum, sensory organ precursors (SOP) divide asymmetrically which gives rise to a set of large bristles called macrochaetae (see **Figure 36b**). Overexpression of p35 or mutant for DARK or its downstream target Dronc leads to extra macrochaetae formation<sup>223,347-349</sup>. This suggests that caspase activity limits the number of macrochaetae. However, caspase activation in this context isn't correlated to apoptosis, here again enforcing a non-apoptotic role for caspase activation<sup>350</sup>. Spermatid terminal differentiation happens through a step of spermatid individualization (**Figure 34a**). Activation of the pro-apoptotic gene *hid* leads to Dronc activation<sup>351,352</sup>. This is mediated by the Cytochrome-C-D release from the mitochondrial membrane and activation of Dark (homologue of APAF1) and leads to the activation of the apoptotic caspases in these cells<sup>353</sup>. Indeed, this leads to Drice activation which mediates cytoplasm removal and results in the elimination of cytoplasmic bridges and individualization of single spermatids<sup>353</sup>. Additionally, dFADD (FADD homologue) is equally activated and leads to the cleavage of Dredd and is necessary for the process. Accordingly, double mutant for Dark and Dronc or dFADD and Dredd lead to sterile males<sup>351</sup>. This process seems to be morphologically similar in mammals and active Caspase-3 was also observed suggesting partial conservation (**Figure 34a**)<sup>353</sup>.

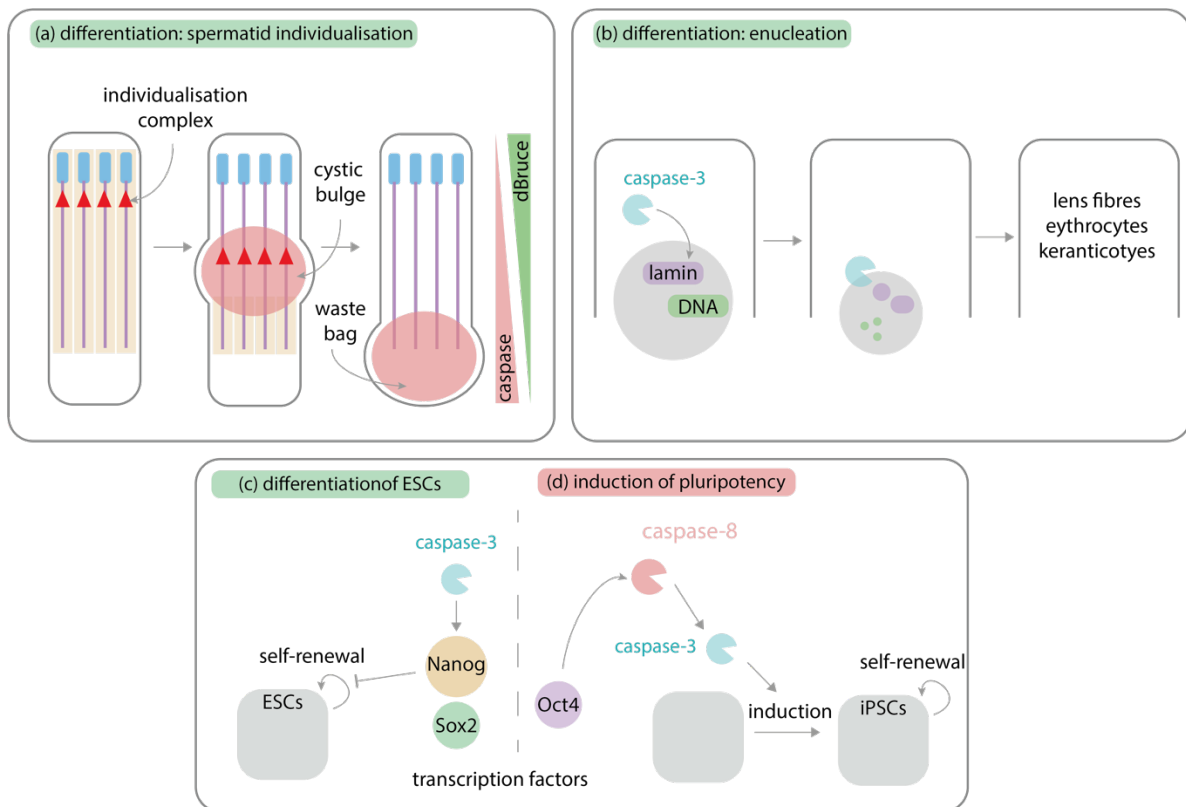


**Figure 34** - Caspase-dependent regulation of cell differentiation. (a) Caspase regulates spermatid individualisation in *Drosophila* and mammals. Here is the process for *Drosophila*. Cytoplasmic bridges (light yellow) hold together the forming spermatids (blue head, purple tail). The individualisation complex (red triangle) will shift basally when the cystic bulge (containing caspase, red circle) shifts basally. This is regulated by opposite gradient of caspases and inhibitors. (b) Regulation of differentiation of different cell types through enucleation. Caspase-3 leads to nucleus condensation and disappearance through cleavage of Lamin or DNA depending on the context. (c-d) Regulation of pluripotency by the interaction between transcription factors and caspases. (c) Caspase-3 cleaves Nanog (yellow) and inhibits ESCs renewal, therefore promoting differentiation. (d) Oct4 transcription factor (purple) induces Caspase-8 activation (red). This in turn induces Caspase-3 activation which promotes induction of iPSCs from differentiated cells.

Caspase-dependent differentiation in mammals has been observed in multiple instances. Some of these events are dependent on the removal of nuclei (**Figure 34b**). For instance, cell nuclei are removed from epithelial cells during lens fibre differentiation in rodents<sup>354</sup>. This process is dependent on Cas3-like activity as the inhibition by the pan-caspase inhibitor zVAD-fmk leads to the suppression of this process. Similarly, the formation of pro-platelet cells relies on Cas3-dependent formation of thin cytoplasmic extension from megakaryocytes<sup>355</sup>. The terminal differentiation of erythrocytes also requires nuclear condensation and enucleation. This happens through a succession of nuclear opening and closing which release histones and lead to nuclear condensation<sup>356</sup>. The expression of a form of Lamin-B non-cleavable by Cas3 in mouse foetal liver culture leads to the inhibition of nuclear opening (**Figure 34b**). Therefore, this process is also mediated by caspase and is tightly connected to the cell cycle suggesting a potential regulation by cell

cycle cdk<sup>356</sup>. Finally, DNA condensation and nuclear loss is also mediated by Caspase-3 in keratinocytes<sup>357</sup>. On the contrary, Cas3 is necessary for the terminal differentiation of monocytes in macrophages without enucleation or removal of organelles<sup>335,336</sup>.

Mouse embryonic stem cells (ESCs) self-renew and differentiate. This differentiation is dependent on several transcription factors Sox2, Oct4 and Nanog. Interestingly, overexpression of a non-cleavable form of Nanog in ESCs promotes self-renewal (**Figure 34c**). This shows that Cas3 cleaves Nanog during the differentiation of ESCs<sup>358</sup>. Alternatively, Oct-4 leads to Cas8 activation which activates Cas3 during the induction of pluripotent stem cells (iPSC, **Figure 34c**). This occurs soon after the transduction of iPSC and is necessary for their reprogramming. Indeed, the inhibition of either of these caspases completely prevents the induction of iPSC<sup>359</sup>.

Taken together, these experiments highlight how caspase activation is essential during the differentiation of numerous cell types both in *Drosophila* and mammals. In many instances, these differentiations involve DNA condensation and removal from the cell type or complete cytoplasmic removal. This highly resembles the apoptotic process which ultimately leads to DNA condensation and nuclear fragmentation. However, in these cases, cells survive and continue to mediate their functions. More surprisingly, these non-apoptotic caspase events happen in key cells for development such as spermatids which ultimately fecundate oocytes. All of these call for a tight spatial regulation in order to remove either the nucleus or only the cytoplasm and a tight temporal regulation to prevent passing high caspase levels to the cell progeny.

*Conclusion: Take-home messages.*

In this part, I have illustrated how caspases, which are classically involved in apoptosis can mediate cellular functions independently of their role in cell death. I have outlined some of their role in processes such as cell proliferation, cell survival, cell remodelling and differentiation to illustrate the sub-lethal ability of caspases. Caspase activity is proteolytic and therefore their functions rely on their ability to cleave proteins. However, this may rapidly lead to apoptosis and therefore requires tight regulation of caspase non-apoptotic functions. What may appear from the example above is the association of caspase activation with a high level of their inhibitors. More generally, caspase regulation may happen through the modulation of caspase levels, catalytic activity, substrate accessibility or caspase localisation or dynamics, all of which are not mutually exclusive. In the following part, I will cover some of the existing examples highlighting these mechanisms.

## 1.2. Role in cancer

Nearly all non-apoptotic functions can potentially be co-opted by transformed cells to promote cancer formation. This is coherent with the role of caspases tumour suppressors. Accordingly, cancer formation is associated with both increased cell proliferation and an escape from cell death. Some cancers such as breast cancers have mutations abolishing caspase activation<sup>360</sup>. Conversely, Caspase-3, 7, 8 and 9 are constitutively activated in some human tumours together with high levels of inhibitors<sup>361</sup>. Work in HeLa cells (uteric cancer) showed that inhibition of Cas3 and Cas7 by injection of specific inhibitors or through overexpression of XIAP domains specific to Cas3 and Cas7 led to reduced proliferation. This arrest was specific to the G2/M phase<sup>362</sup>. Overall, this suggests that non-apoptotic caspase activation in some tumours might favour overproliferation through the loss of cell cycle checkpoints. Caspase activation may typically be considered an anti-tumoral process given that it mainly leads to apoptosis.

However, recent evidence showed that Cas3 activation may promote carcinogenesis upon ionizing radiation. The dysregulation of non-apoptotic caspase functions in the regulation of proliferation of survival may be co-opted by transformed cells. Accordingly, Caspase-3 knockout mice delay AML-induced myeloid leukemogenesis demonstrating that Cas3 tend to promote leukemogenesis. In this context, the caspase substrate ULK1 is cleaved and upregulated by caspase which promotes survival through enhanced autophagy<sup>363</sup>. Similarly, cells survive Cas3 activation which promotes genomic instabilities ultimately promoting tumour formation. Accordingly, Cas3<sup>-/-</sup> mutant mice exhibit delayed apparition of carcinomas as well as smaller and less frequent tumours upon TPA treatment<sup>364</sup>. Alternatively, caspase-induced genomic defects such as double-strand breaks may lead to increased tumour aggressiveness and motility via the activation of NF- $\kappa$ b and Stat3, both of which are known drivers of tumour growth<sup>365</sup>. In *Drosophila*, basal localisation of Dronc by Myo1D in undead cells promotes its non-apoptotic functions<sup>217</sup>. These functions include secreting ROS to attract haemocytes and promote the proliferation of neighbouring cells. Ras<sup>V12</sup>, Scrib<sup>-/-</sup> clones promote tumour formation and undead cell behaviour. Equally in that context, Dronc is basally localised by myo1D. Consequently, Myo1D knockdown in Ras<sup>V12</sup>, Scrib<sup>-/-</sup> clones reduces clone growth and invasiveness. Therefore, Myo1D-dependent localisation of Dronc in Ras<sup>V12</sup>, Scrib<sup>-/-</sup> promotes tumorigenesis and invasiveness. Finally, Akt1 and dCIZ1 promote cell survival to caspase activation in Ras<sup>V12</sup> transformed cells. Accordingly, dCIZ1 knockdown

by RNAi increases the number of transformed cells undergoing apoptosis and prevents the overgrowth of these cells<sup>366</sup>. Altogether, these data show how non-apoptotic or sub-lethal caspase activation can be hijacked by transformed cells to promote their proliferation and/or invasiveness.

### 1.3. Mechanism of caspase regulation for non-apoptotic functions

I described above some of the non-apoptotic functions of caspases in various processes. In some of these cases, caspases are maintained to an intermediate level to perform functions in various processes such as cell proliferation, cell survival, cell remodelling or cell differentiation (**Figure 31**). However, information on how caspase catalytic activity is maintained at non-apoptotic levels remains scarce. I will now first highlight how caspases' proteolytic activity or level can be modulated. Then, I will present how regulating caspase dynamics modulate their function. Moving forward, I will introduce mechanisms to regulate the non-apoptotic functions of caspases through changes in caspase subcellular localisation.

#### 1.3.1. *Balancing levels through induction of caspase inhibitors*

In many instances of non-apoptotic caspase functions, caspases also activate their inhibitor. For instance, the regulation of proliferation by Cas3 through the cleavage of alpha-cat leads to the translocation of YAP to the nucleus. This subsequently leads to XIAP activation that negatively regulates caspase levels (**Figure 35a left**)<sup>327</sup>. In mice, Cas3 is necessary to promote survival upon stresses. This happens through the cleavage of RasGAP which increases the level of Akt: an inhibitor of apoptosis (**Figure 35a right**)<sup>333,334</sup>. Non-lethal Cas3 activation is required during the terminal differentiation of lens fibres in mice or in chicks and is associated with elevated levels of Bcl-2 another caspase inhibitor<sup>367,368</sup>. Bcl-2 levels in these conditions may be required to prevent catastrophic levels of Cas-3 that would lead to death. However, whether Bcl-2 is activated by Cas3 itself is not known. Finally, in the branching of the *Drosophila* arista, Diap1, a caspase inhibitor is key to maintaining caspases at a level sufficient to form a correct number of branches<sup>337,339</sup>. Similarly, Diap1 levels appear to be key in the regulation of border cell migration<sup>323</sup>. Taken together, this demonstrates how caspase activation, associated with the activation of their own inhibitors, restricts caspase activity to non-apoptotic functions. More generally, it has been suggested that the balance between pro-apoptotic and anti-apoptotic members of the BCL-2 family is key to regulating the balance between cell death and non-apoptotic functions of caspases<sup>369</sup>. This highlight one



mode of regulation of caspase that depends on the regulation of caspase levels (**Figure 35c**).

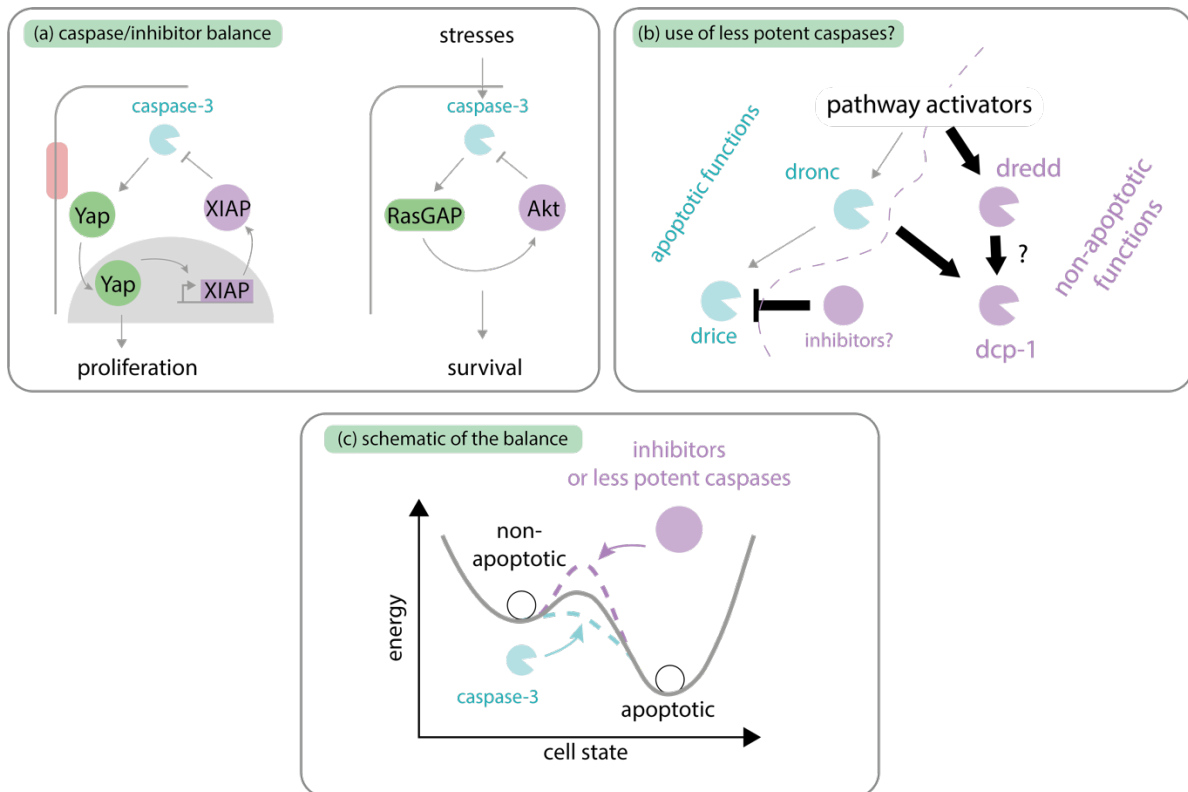


**Figure 35** - non-apoptotic caspase functions by limiting caspase levels. (a) Maintenance of low caspase levels through the induction of inhibitors. Left is the process regulating sebaceous gland proliferation. Caspase-3 induces YAP translation to the nucleus which drives the expression of XIAP. XIAP (purple) inhibits Caspase-3 in a negative feedback loop while keeping low caspase levels. Right: Similar process during the survival of mice cells upon stresses. RasGAP is cleaved by caspase and induces the caspase inhibitor Akt (purple) to maintain low caspase levels. (b) a putative mechanism to maintain low caspase levels by using less potent caspase such as Dredd or Dcp-1 (purple) instead of Dronc and Drice. Dcp-1 is less potent than Drice. However, it is unknown whether such a mechanism is actually accurate. (c) Visualisation of the energy cost to enter apoptosis. Caspase-3 activation would lower the energy cost needed to enter apoptosis (blue). Conversely, caspase inhibitors or less potent caspases would increase the energy cost to enter extrusion (purple). (c) is adapted from<sup>370</sup>.

It is noteworthy to mention another layer of regulation that seems to appear between the lines. Indeed, in many examples, non-apoptotic functions of caspases seem to be mediated by apical/activator caspases such as Caspase-8, Dronc or DREDD<sup>351</sup>. The substrate range of these caspases may be restricted compared to effector caspases such as Caspase-3 which are the ones mainly mediating apoptotic remodelling. Therefore, provided Caspase-3 is inhibited this may be a mechanism by which to mediate non-apoptotic functions using less potent caspases (**Figure 35b**). Differences in caspases' ability to induce apoptosis may equally be diverted during non-apoptotic process. For instance, Dcp-1 and Drice are unequally efficient at inducing apoptosis in the *Drosophila* wing disc. Dcp-1 is less potent than Drice and therefore could be preferentially used to

mediate non-apoptotic functions (**Figure 35b**)<sup>326</sup>. In conclusion, the equilibrium between caspase levels and their inhibitor levels ensures that caspase activation is maintained below a cellular execution threshold. Caspase activity could also be maintained below this threshold by using less potent caspases (**Figure 35c**). Both mechanisms may regulate the cell sensitivity to apoptosis. However, why in some circumstances similar caspase activation leads to cell death or to non-apoptotic functions still remains unknown.

### 1.3.2. Dynamic regulation of caspase and their proteolytic activity

Another layer of caspase regulation is through post-translational modification of caspases or their inhibitors. For instance, Cas3 phosphorylation by p38-MAPK reduces its apoptotic activity because of lower enzymatic activity in primary human neutrophils (**Figure 36a**).<sup>371</sup> Conversely, dephosphorylation at the same site increases apoptosis of neutrophils<sup>372</sup>. In *Drosophila*, the IKK-related kinase (DmIKK $\epsilon$ ) phosphorylates Diap1 which leads to its degradation<sup>373</sup>. In the case of arista branching, the expression of a dominant-negative form of the kinase DmIKK $\epsilon$  negatively regulates the amount of Diap1 and its nonapoptotic activity. This leads to excessive branching and is enhanced by Dronc or DARK knockdown<sup>339</sup>. Likewise, the overexpression of DmIKK $\epsilon$  inhibits border cell migration by the activation of Dronc<sup>339,373</sup>. This is conserved in mammals as IKK can phosphorylate XIAP<sup>374</sup>. More generally, caspase functions can be regulated by diverse Post Translation Modifications. We have already cover phosphorylation and ubiquitylation, but they can also be regulated by SUMOylations. All these drastically affects their catalytic activity and promote their non-apoptotic functions (reviewed here<sup>375</sup>).

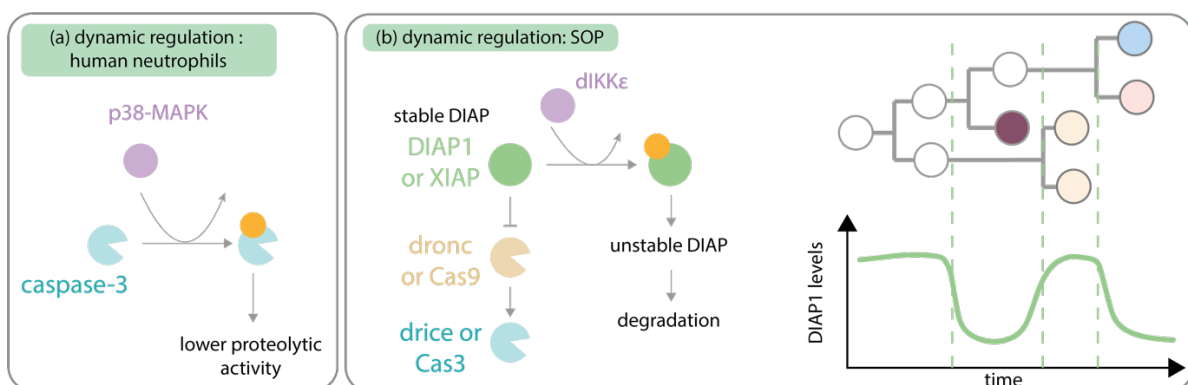


**Figure 36** - Dynamic regulations of caspases & their proteolytic activity. (a) regulation of caspase phosphorylation (orange circle) by p38-MAPK lowers its proteolytic activity. (b) Dynamic regulation of IAP. Left: Regulation of DIAP or XIAP stability by phosphorylation (orange circle). DIKK $\epsilon$  lowers IAP stability which leads to its degradation. Right: In SOP, this regulation of IAP levels is dynamic and depends on the cell type in the lineage. Top right: SOP lineage. PI divides in pIIa and pIIb. pIIb divides in pIIIb and a glial cell dies (dark red).

pIIIb then divides in the neuron (blue) and sheath (pink). On the other side pIIa divides in the socket and the shaft (yellow). This is adapted from<sup>376</sup>.

Additionally, the control of non-apoptotic caspase function by phosphorylation may also be regulated dynamically in time (**Figure 36b**). For instance, the precise regulation of SOP numbers seems to be dependent on transient caspase activity. Indeed, transiently blocking caspases leads to increased SOP numbers<sup>376</sup>. All these functions seem to be modulated by the stability of Diap1 which determines its turnover. Indeed, Diap1 stability and degradation are tightly regulated<sup>244</sup>. Accordingly, the inhibition of DmIKK $\epsilon$  by RNAi leads to the loss of Diap1 phosphorylation and increases Diap1 stability (**Figure 36b left**). More stable Diap1 then suppresses caspase activity which leads to extra macrochaetae<sup>373,376</sup>. These results were further confirmed using a live reporter of Diap1: PRAP<sup>376</sup>. The SOP forms through a sequence of divisions leading to different cell types forming a neuron, a shaft, and a socket. PRAP was detected up to the 2-cell stage of SOP formation, then disappeared and was only detected again in the final shaft and socket cells and at different levels (**Figure 36b, right**)<sup>376</sup>. This shows that Diap1 dynamics are transient and that Diap1 levels are cell type dependent. Accordingly, knock-down of DmIKK $\epsilon$  in the shaft resulted in delayed Diap1 degradation and abnormal bristle phenotype<sup>373</sup>. This temporal regulation of Diap1 turnover is important to direct caspase activation toward apoptotic or non-apoptotic functions.

### 1.3.3. Spatial regulation of caspases and substrate availability

In part 1.1.4 of the present chapter, I illustrated the resemblance between caspase-mediated differentiation mechanisms and apoptosis (**Figure 34**). Indeed, caspases induce either cytoplasm removal such as in spermatid differentiation or enucleation such as in rodent lens fibre. In both instances, the rest of the cellular structures are preserved which highly suggests spatial regulation of caspase activation inside the cell. Alternatively, this may suggest a regulation of substrate availability in different regions of the cells. Spermatid terminal differentiation in male *Drosophila* provides a nice example of spatial caspase regulation<sup>353</sup>. First, caspases are restricted in cystic bulges. Second, the giant ubiquitin-conjugating (E2) enzyme dBruce is required to protect the nucleus against condensation. Interestingly, dBruce is regulated by Soti from the cullin complex. Soti forms a gradient from the basal to the apical of differentiating spermatids. This results in a gradient of dBruce with the same orientation<sup>377</sup>. Consequently, caspases are high at the head of the spermatid and form an inverse gradient toward the tail side. The removal of spermatid structures also happens progressively from head to tail. Therefore, this

gradient ensures that the last region of the spermatid to individualise experiences the lowest caspase activation.

In *Drosophila* salivary glands, Dronc mediates either non-apoptotic or pro-apoptotic functions. The shift between these two functions depends on the localisation of Dronc activation (**Figure 37b**). The cytoplasmic function of Dronc is regulated by dark and leads to apoptosis while Dronc localisation to the cortex by Tango-7 mediates non-apoptotic functions (**Figure 37b, purple**). Indeed, localisation of Dronc to the cortex dismantles F-actin<sup>378</sup>. This controls tissue elasticity and is necessary to regulate glue secretion by these glands. The overexpression of Diap1 or p35 inhibits F-actin breakdown suggesting that this cleavage may be mediated by Cas3 in this context. Of note, this process is also temporally regulated as it only happens at specific larval stages and under transient, sublethal pulses of IAP antagonists such as *reaper*<sup>378</sup>. Interestingly, dendrite pruning, another non-apoptotic caspase process seems to also be regulated by Tango-7 (**Figure 37b**). C4da neurons are pruned through the caspase-dependent remodelling of the cortical F-actin network<sup>345,346,378</sup>. This process is regulated by the local activation of Caspase-3<sup>345,379,380</sup>. Indeed, local mitochondrial destruction by photo-stimulation led to local dendritic spine retraction and elimination in a Caspase-3-dependent manner<sup>381</sup>. Interestingly, the knockdown of Tango-7 impairs pruning while loss of dark had no effect suggesting that the local regulation of dendritic pruning is equally under the control of Tango-7<sup>378</sup>. Finally, Tango-7 is an important regulator of the apoptosome (**Figure 37a**)<sup>382</sup>. Interestingly, during spermatid individualization, Tango-7 activates the apoptosome specifically in the investment cones of migrating individualizing complex: specialized cytoskeletal structures where the non-apoptotic functions are mediated (**Figure 34a**)<sup>382</sup>. Therefore, it appears that Tango-7 might be a common spatial regulator specific of non-apoptotic functions of caspases.

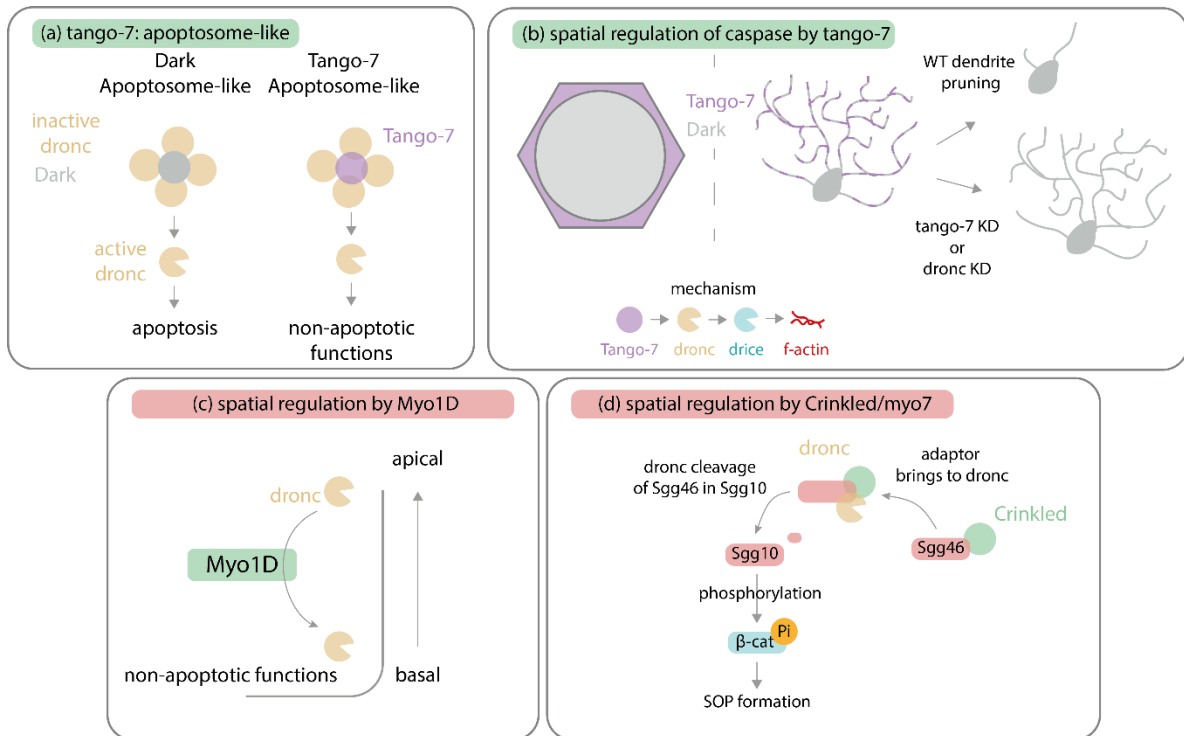


**Figure 37** - Spatial caspase regulation. Green titles show *tango-7* dependent spatial regulation of caspases functions, red titles show spatial regulation of caspases by non-conventional Myosins. (a) *Tango-7* is an apoptosome like adaptor which mediates non-apoptotic functions. It binds inactive *Dronc* similarly to *dark* (*Drosophila* *Apaf1* related Kinase). (b) Spatial regulation of non-apoptotic caspase function by *Tango-7*. Left: *Tango* is located at the cortex of salivary gland cells and mediates F-actin cleavage. On the contrary, *Dark* is located at the medioapical region and mediates apoptotic functions. Right: *Tango-7* is in dendrites to mediate dendrite pruning. Loss of *tango-7* or *Dronc* knockdown leads to an inhibition of normal pruning. *Tango-7* mediates *Dronc* activation of *Drice* which mediates F-actin cleavage in both mechanisms. (c) The unconventional myosin *Myo1D* relocates *Dronc* to the basal plasma membrane where it conducts non-apoptotic functions. (d) Another unconventional myosin *Crinkled* (*CRK*) regulates non-apoptotic functions of caspase spatially. *Crinkled* binds *Sgg46* and binds *Dronc*. Thus, it acts as an adaptor to bring *sgg46* to *Dronc*. *Dronc* then cleaves *Sgg46* into *Sgg1a* which then phosphorylates *B-cat*. This regulates SOP formation.

Local targeting to different membrane, or cytoskeleton compartments for non-apoptotic functions of caspases can also be regulated by unconventional myosin (**Figure 37c**). *Myo1D* localises *Dronc* to the basal side of wing disc cells both in undead wing disc cells and salivary gland cells<sup>217</sup>. Similar regulation of caspases activity is also co-opted in mammals. For instance, during platelets differentiation from megakaryocytes, active Caspase-3 is only detected in a punctuate cytoplasmic distribution. Conversely, a diffuse Caspase-3 detection led to senescence and apoptosis of megakaryocytes<sup>355</sup>. Similarly, the differentiation of monocytes was associated with a removal of pro-caspases from their cytoplasmic localisation<sup>335,383</sup>. However, in many instances such as lens fibre or erythrocytes terminal differentiation which include enucleation, no clear mechanism explains why the nucleus is specifically targeted and removed<sup>354,356</sup>.

Finally, spatial regulation of caspases may also be achieved through local substrate availability (**Figure 37d**). For instance, during SOP specification, the unconventional myosin Crinkled binds to Dronc<sup>384</sup>. It functions as a substrate adaptor which brings the kinase Sgg46 to Dronc. Dronc in turn cleaves Sgg46 into its functional form Sgg10 which in turn triggers the degradation of  $\beta$ -catenin and contributes to SOP specification (**Figure 37d**)<sup>350,385</sup>. Some evidence suggest that this mechanism seems to be conserved in mammals. Indeed, Crinkled the ortholog of Myo7A binds to Caspase-8. More generally, substrate availability may be key to mediating the balance between apoptotic or non-apoptotic responses to caspase activation. This may even be reflected between different cell types. For instance, p21 is a caspase target in the regulation of splenic B cells cycle but not in T cells where no caspase-dependent regulation of the cycle has been observed<sup>330</sup>.

#### *1.3.4. Recovery from early apoptosis: a caspase threshold?*

While these studies focused on the balance between apoptosis and survival, it is still unclear whether the engagement in apoptosis is irreversible or not. This is well demonstrated by anastasis: a process by which cells are rescued from apoptosis (**Figure 38**). This process was first noticed when cultures of liver cells or fibroblast NIH 3T3 cells were exposed to ethanol. This exposure triggers apoptotic remodelling events such as membrane blebbing, cell shrinkage, nuclear condensation and annexin-V flipping (**Figure 38a1**)<sup>325</sup>. This together with increased cleaved-Caspase-3 levels, shows signs of commitment to apoptosis. However, after washing, these cells no longer reported caspase activation and returned to normal shapes, although still exhibiting Annexin-V to the outer membrane (**Figure 38a1** the purple cells, or **Figure 38a2** dynamics of caspases). These cells experienced DNA damage during the process as well as the apparition of genetic alteration after reversal. While no clear mechanism was assessed, the reversal is associated with increased levels of BCL-2 and XIAP as well as elevated HSP levels (**Figure 38a2**)<sup>325</sup>. Thus, it suggests that the withdrawal of acute stresses induces the activation of caspase inhibitors to survive. This work was later followed in the same group using CasExpress or CasTracker reporters (**Figure 38b1**)<sup>386,387</sup>. Both reporters consist of a Gal4 tethered to the membrane by a CD8 domain fused to a DQVD sequence. This DQVD domain is the consensus sequence recognised and cleaved by caspases.

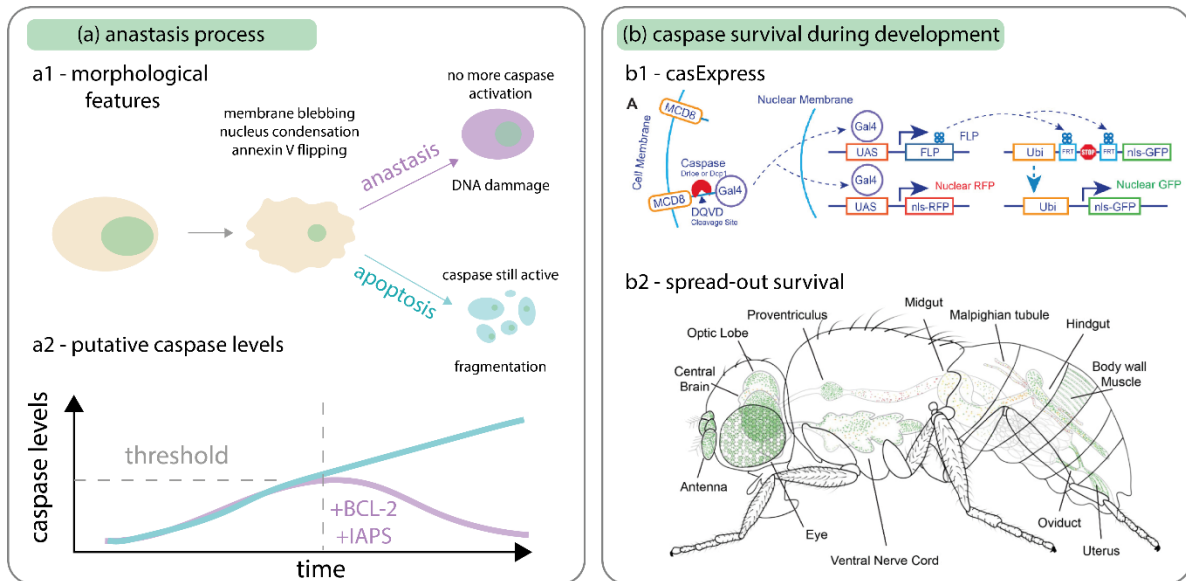


**Figure 38 - Anastasis: caspase threshold.** (a) the process of anastasis. (a1) The cell exhibit morphological changes typical of apoptosis upon exposure to ethanol. Upon the removal of ethanol, the cell activates inhibitors of caspases and survives in a process called anastasis (purple). However, it still demonstrate DNA damages. If ethanol is sustained the cell commits fully to apoptosis (blue). (a2) Putative representation of caspase levels during anastasis. In both cases upon exposure to ethanol the cell activate caspase up to a threshold. If the ethanol is washed the cell activates BCL-2 and IAPs inhibiting caspase to maintain it below the commitment threshold and allowing survival (purple). Otherwise, the caspase levels keep increasing and the cell enter apoptosis (blue). (b) Widespread survival to caspase activation during development. (b1) Tool casExpress to follow the lineage of cells surviving caspase activation. (b2) All the tissue labelled in green have cell which experienced caspase activation and still survived (all green dots).

Upon caspase cleavage, the Gal4 is released from the membrane and translocated to the nucleus where it activates the G-trace system. It will drive the expression of a cytoplasmic RFP and drives the expression of a flipase. This flipase will in turn lead to a recombination event and drive the stable and ubiquitous expression of a nuclear GFP. These tools transiently labels in red the cells currently activating caspase and stably labels in green the progeny of cells that have activated caspases in the past. This revealed that cell survival to caspase activation is widespread during *Drosophila* development (**Figure 38b2**). However, that tool may only report events of transient and sublethal levels of caspases activation and not necessarily anastasis. Finally, The combination of that tool with classical RNAi *Drosophila* screening identified akt1 and dCIZ1 as two additional factors preventing death from caspase activation<sup>366</sup>.

**Conclusion: Take-home messages.**

In the current part, I showed that the balance between cell survival and apoptosis may be dependent on a caspase threshold. This threshold may be set by 3 primary modes of regulation:

- the balance between caspase activation and their inhibitor
- the dynamic regulation of caspase activation by phosphorylation of caspases or their inhibitor
- the spatial regulation of caspases, inhibitors, or substrates.

These studies suggest that the decision-making toward the engagement in apoptosis is more complex than it was originally anticipated. Accordingly, many cells survive caspase activation during development. Interestingly, cells are able to survive fairly advance apoptotic events when stresses are withdrawn. This would suggest that the decision to irreversibly commit to apoptosis and die is set very late and that early events of remodelling are not necessarily signatures of apoptosis conversely to what was though previously.



## 2. Results: Decision-making in cell extrusion

### 2.1. Introduction

In the **part0** of the current chapter, I have described the different biological processes in which the non-apoptotic functions of caspases are involved. These processes involve the regulation of the cell cycle, the regulation of survival, cell remodelling and cell differentiation. Moreover, there are numerous cells that survive caspase activation and are widespread during development<sup>386</sup>. All these processes are functional because caspase inhibition clearly affects tissue size, cell shape or cell state. Furthermore, they can be dysregulated and lead to tumorigenesis for instance by favouring proliferation<sup>217</sup>. They imply that caspase activation doesn't necessarily lead to cell death and therefore demonstrate the existence of a balance between apoptosis and survival in the presence of caspase activation. Thus, the decision-making step leading to the irreversible engagement in apoptosis is more complex than previously anticipated. Caspase activation is definitely not a point of no return toward apoptosis<sup>388</sup>. Several studies have tried to understand how these cells can survive caspase activation. Some mechanisms have been proposed to modulate caspase levels, dynamics, activity, or localisation in order to mediate these non-apoptotic functions. Furthermore, cells seem to manage to survive very advance apoptotic remodelling. Taken together, they suggest that there might be an execution threshold below which cells keep surviving even in the presence of caspases<sup>326</sup>.

However, whether such a threshold exists was never formally quantitatively assessed, certainly due to the lack of a tool to follow live caspase activation. It seems straightforward to consider that this threshold may be different depending on the cell types because cells express different caspase substrates. However, it is unclear whether all cells within the same population, for instance in the *Drosophila* pupal notum, experience the same caspase threshold. This is supported by the observation that the pattern of cells that survive caspase activation in each tissue is not reproducible from one individual to another<sup>386</sup>. Therefore, predicting which cell will die or not within the tissue has remained difficult. In other words, it is not clear whether all cells have the same sensitivity to caspase activation. In the notum caspase activation precedes and is necessary for cell extrusion which is systematically followed by fragmentation and apoptosis. What are the putative factors that may influence the probability to enter in apoptosis downstream of caspase activation? The idea that mechanics may influence caspase activity has recently been suggested (reviewed in<sup>370</sup>). Therefore, we will first focus

on morphological features, mechanics and regional parameters to try to predict the cell sensitivity to caspase activation.

## 2.2. Results

The *Drosophila* pupal notum is a single-layer epithelium which displays a high rate of cell extrusion (**Figure 39a**). Previous observations by the lab suggested that extruding cells activate caspases with various lag times prior to the extrusion in the notum. Because caspase accumulates over time in these cells, this suggests that cells extrude with different levels of caspase. To test this hypothesis, we used E-cad to visualize apical cell-cell junctions (**Figure 39a**). This allowed the systematic segmentation and tracking of all the cells in the notum. To measure caspase activation dynamics in the notum, we expressed the live caspase reporter GC3AI (Green Caspase Activity Indicator) under the control of a specific driver throughout the notum (pnr-Gal4, **Figure 39b**). Upon Caspase-3 cleavage, GC3Ai becomes rapidly fluorescent and allows the monitoring of caspase activation. However, GC3AI's half-life is about 40h<sup>201</sup>. Thus, GC3AI acts as a cumulative read-out of caspase activation, and fluorescent levels only build up over time (**Figure 39c**). In order to access real-time caspase activity, we monitored GC3AI's rate of change by looking at the derivative of this signal ( $\partial_{GC3AI}$ , **Figure 39c**). Interestingly, we could observe various caspase dynamics (**Figure 39d**). The majority of cells accumulated caspase exponentially before the onset of extrusion (**Figure 39d, top**). However, many cells displayed transient pulses of caspase activity (**Figure 39d, bottom**). Additionally, numerous cells seemed to activate caspase but were not extruding during the duration of the movie (8h, not shown). Conversely, some cells entered extrusion very rapidly after caspase activation. Taken together, this suggests that cells enter extrusion at different caspase levels.

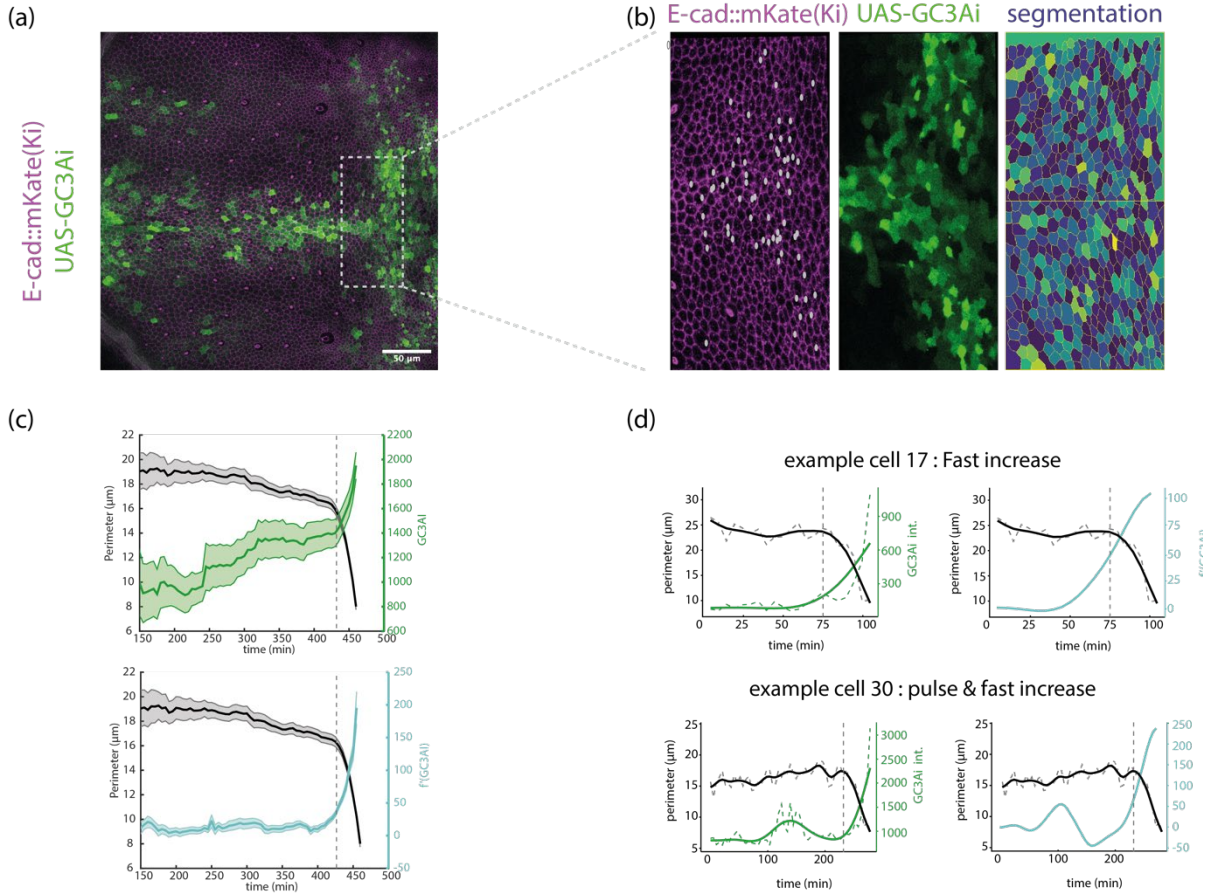


**Figure 39** - Quantification of caspase activity. (a) representative movie of a pupal notum epithelium expressing E-cad::3xmKate and UAS-GC3Ai. (b) movie representative of the region shown in (a), (dotted rectangle). E-cad allows the segmentation of cell contours to measure intracellular GC3Ai levels and shape descriptor (i.e. perimeter here). (c) The top shows GC3Ai levels for  $n=87$  extruding cells. The bottom shows  $\partial_{GC3Ai}$  levels for the same extruding cells. (d) Example of two different types of caspase dynamics. The top shows an exponential increase of GC3Ai and  $\partial_{GC3Ai}$  representative of most of the cells. The bottom shows transient activation followed by reversion and then a final exponential increase.

Previous results in *Drosophila* suggest that cells can survive up to a certain threshold of activity. To quantitatively test this hypothesis, we first tried to identify a decision point at which cells irreversibly commit to extrusion. Because all cells that started to constrict were always extruded, we defined the inflexion point of the apical perimeter as the decision point (**Figure 40a**). Therefore, we defined this point at the onset because it's the last point at which we cannot make any difference between extruding cells and control cells. This point was automatically detected in all single cells using a double-fit method (see method paper1). We could then extract the caspase value  $\partial_{GC3Ai}$  at that time point for each cell. Interestingly, we observe a broad distribution of  $\partial_{GC3Ai}$  at the onset. This further shows that cells enter in extrusion at different values of  $\partial_{GC3Ai}$  which might reflect different sensibility and therefore different thresholds. We, therefore, tried to predict the probability of a cell entering in extrusion depending on  $\partial_{GC3Ai}$  value.

We used the inflexion point as a cutting point to define the probability of each cell being in extrusion (**Figure 40a,b**). As we considered it the decision point, we set the probability of being in extrusion to 0 before that point and 1 after (**Figure 40b**). To further test the idea of a threshold across the cell population we pooled the data from extruding cells with data from cells activating caspase but not extruding. These cells never extrude and therefore have a 0 probability of being in extrusion. This results in a bimodal distribution of the fate of cell depending on  $\partial_{GC3AI}$ . Interestingly, this response curve is best fitted by a sigmoid (logistic regression) rather than by a step function (**Figure 40c**). This implies that there is no single threshold value across the population. Rather, the probability of a cell to be extruding scales quasi-linearly with the value of  $\partial_{GC3AI}$ . Additionally, there was a non-null probability of being in extrusion even at a very low value of  $\partial_{GC3AI}$ . Taken together, this shows that there is no single threshold of  $\partial_{GC3AI}$  in the notum above which cells would enter in extrusion and apoptosis. It seems that the threshold of  $\partial_{GC3AI}$  is set for each cell. What then modulates the  $\partial_{GC3AI}$  threshold value for each cell?

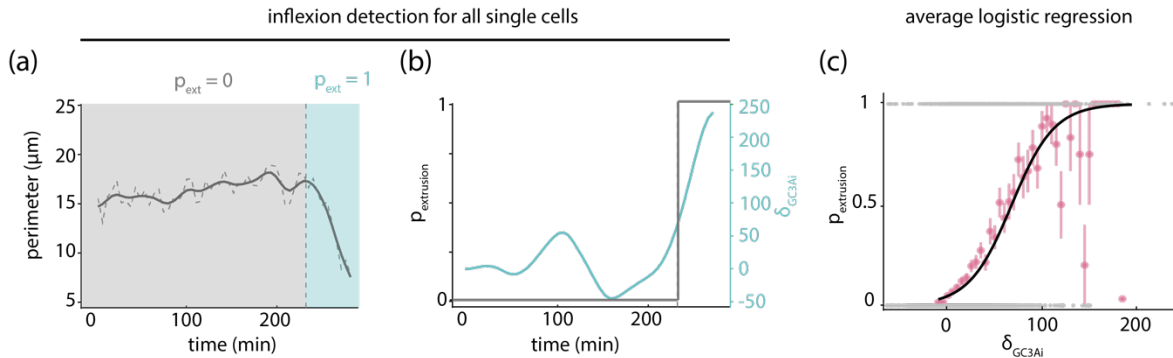


**Figure 40** - Threshold detection & probability to be in extrusion. (a-b) Inflexion detection and probability settings. The inflexion point is detected and set as the decision step. Therefore, the probability of being in extrusion prior to that decision point is  $p=0$  (gray area) and is  $p=1$  after the onset (decision point, blue area). (b) This results in a step function and the value of  $\partial_{GC3AI}$  can be extracted for each probability. (c) The probability of extrusion as a function of  $\partial_{GC3AI}$ . Grey dots represent the probability of extrusion of each measured cell (either 0 or 1). The pink dots are the average probability of being in extrusion and the associated error is the standard error of the mean. Black curve is the model drawn from the logistic regression.

We then tried to grasp a better understanding of the parameters that might influence a single cell's  $\partial_{GC3AI}$  threshold. For the sake of clarity, I will now use  $C3_{onset}$  to refer to the  $\partial_{GC3AI}$  threshold. We, therefore, tried to model the  $C3_{onset}$  value depending on some parameters (**Figure 41a-d**). This was performed specifically for the extruding cells as we never see a decision point in non-extruding cells that activate caspases. Cell constriction during extrusion is an event that depends on cell mechanics. Thus, we reasoned that geometrical, and mechanical parameter might be predictive of the cell's sensitivity to

caspase. For the geometrical parameters, we extracted the area and perimeter but also morphological descriptors such as the circularity, aspect ratio, roundness, and solidity (**Figure 41c**). For the mechanical parameters, we extracted the tension and pressure both in the extruding cells and the neighbours. Because we have no way of directly measuring these parameters in our systems, these parameters were extracted from mechanical inference on the segmented movies. This is done through a force inference approach. This technique is very powerful. It allows us to infer forces in an epithelium from a snapshot of the tissue, assuming that forces are balanced at each vertex in an epithelium. For this I adapted the technique from Kong et al<sup>389</sup>. Additionally, we included past cumulative caspase activity in the parameters (GC3Ai). For the sake of simplicity, we only included linear models (**Figure 41d**). We thus sought to determine how these parameters are predictive of  $C3_{onset}$ .

For that, we extracted all these parameters by windows of 10min prior to the decision and linearly correlated them with the  $C3_{onset}$  (**Figure 41b**). To control our correlative approach, we included the correlation between  $C3_{onset}$  and  $\partial_{GC3AI}$ . As expected, close to the decision point (from -30min to 0min) these correlations yielded very high ( $r=0.98$ , **Figure 41e**, blue square) positive correlations with significant associated p-values ( $p<0.005$ , **Figure 41e'**). Thus, our method correctly correlates the different parameters. Most of the selected parameters were not correlated significantly with  $C3_{onset}$ . However, the area and perimeter from -30 to 0min before the onset were negatively correlated with  $C3_{onset}$  (**Figure 41e**). In other words, cells with a high area or perimeter enter in extrusion at lower thresholds. Interestingly, we could observe that past GC3Ai levels (past cumulative caspase activity) from -180min to -100min displayed a significant negative correlation with  $C3_{onset}$  (**Figure 41e**, red square in the black box). This shows that past caspase activity is associated with a lower caspase threshold (cells are more sensitive to caspases). None of the mechanical parameters was significantly associated with the  $\partial_{GC3AI}$  except for the tension in the neighbours and the pressure in the extruding cells -120min before the onset (**Figure 41e**). This correlation happens in a very sharp window of time which might indicate an artefact. Indeed, we wouldn't expect any correlation to change as abruptly as this. Overall, this correlation analysis shows that geometrical parameters (area and perimeter), as well as past caspase activity, are good candidates to predict the caspase threshold of a cell.

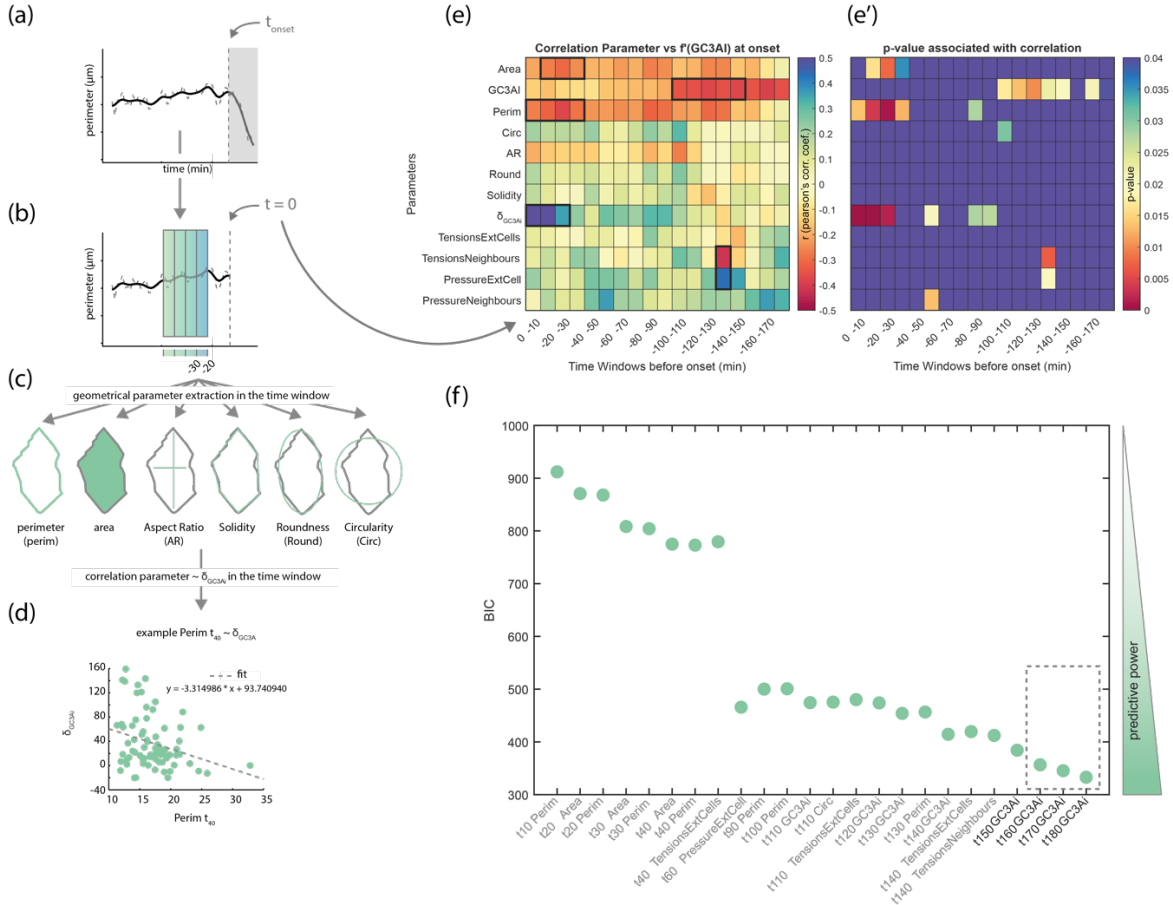


**Figure 41** - Prediction of the threshold value. (a) The inflexion point is extracted through the double-fit method (see method paper1). We only focus on what happens before that decision point. (b) The onset is set to  $T = 0$  and all-time before that are negative. Parameters are extracted in windows of 10min before the onset. (c) Schematic representation of the morphological/geometrical parameters. The extracted geometrical parameters are the perimeter, the area, the aspect ratio, the solidity, the roundness, and the circularity. (d) For all cells, these parameters are extracted in different time windows before the onset. Then for each time window, a correlation between the parameter values for all cells and their  $C3_{onset}$  is computed. (e) The matrix summarizes the correlation coefficient values for each parameter in each time window vs  $C3_{onset}$ . (e') Associated p-values. Only the significant p-values are displayed. The non-significant p-values are displayed in dark blue. (f) The Bayesian Inference Criterion for all significant correlations. The dotted rectangle highlights the lowest BIC value which corresponds to the most predictive models.

We then sought to find which of these properties is the most predictive of cell sensitivity to caspase. To do so we conducted a model selection analysis using Bayesian approaches. We restricted this analysis only to the time parameters with a significant correlation to the  $C3_{onset}$  (p-value < 0.05). This method allows the comparison between all statistical models. For each model, a Bayesian Information Criterion (BIC) is computed. It weights the model by the number of parameters and by comparing it to the most plausible model. The model with the lowest BIC is the most parsimonious and plausible model. This showed that the 3 most predictive features are the GC3Ai values from -160min to -180min (**Figure 41f**, grey dotted rectangle). The more caspase is

activated in the past, the less you need to activate at the moment of the decision. Taken together, these data show that this method allows to fish parameters potentially modulating the cell sensitivity to caspase. However, the data so far were obtained in a very restricted region (both spatially and temporally) at the posterior of the notum. This might not reflect the whole spatial and temporal decision-making that happens in the notum.

Recently, machine-learning enhanced segmentation models were pre-trained on *Drosophila* epithelia. This together with the use of better E-cad reporters (E-cad::3xmKate, Yohanns Bellaiche lab) drastically facilitated the segmentation process in the notum. Therefore, we have tried to generalise our observations to the whole tissue. We used a similar approach to the one described before, except the segmentation was first made by epyseg which decreased further manual correction (**Figure 42a**)<sup>390</sup>. First, we could confirm a similar response curve showing that no single caspase threshold is detected across the movie (not shown). We could detect 1017 extruding cells. For each cell, the inflexion point was detected and then cells were sorted in temporal bins of 150min according to when their inflexion point happened (i.e., a cell which starts to constrict at 180min will be displayed in the 150-300min window). Then each cell was plotted according to its position at the onset. The parameter maps in (**Figure 42b**) were then obtained by binning the results in xy windows of 80 pixels (px size = 0.21  $\mu\text{m}$ ). Like what has been reported before<sup>281</sup>, cells first extrude in the midline (1<sup>st</sup> row, 1<sup>st</sup> column, cells extrude mainly in the horizontal region). They then progressively started to extrude from the posterior band (**Figure 42b** 1<sup>st</sup> row, 2<sup>nd</sup> and 3<sup>rd</sup> column). The perimeter value at the onset seemed roughly homogeneous over space and time (**Figure 42b** last row, all columns, the color is homogeneous). Conversely, GC3Ai levels and the threshold at the onset ( $C3_{onset}$ ) are heterogeneous and displayed a salt and pepper values in space (**Figure 42b** 2<sup>nd</sup> and 3<sup>rd</sup> row). Indeed, cells in neighbouring spatial bins with similar density of extrusion displayed drastically different average threshold values. This confirms that cells enter in extrusion (onset) with different GC3AI and  $C3_{onset}$  values all along the movie.

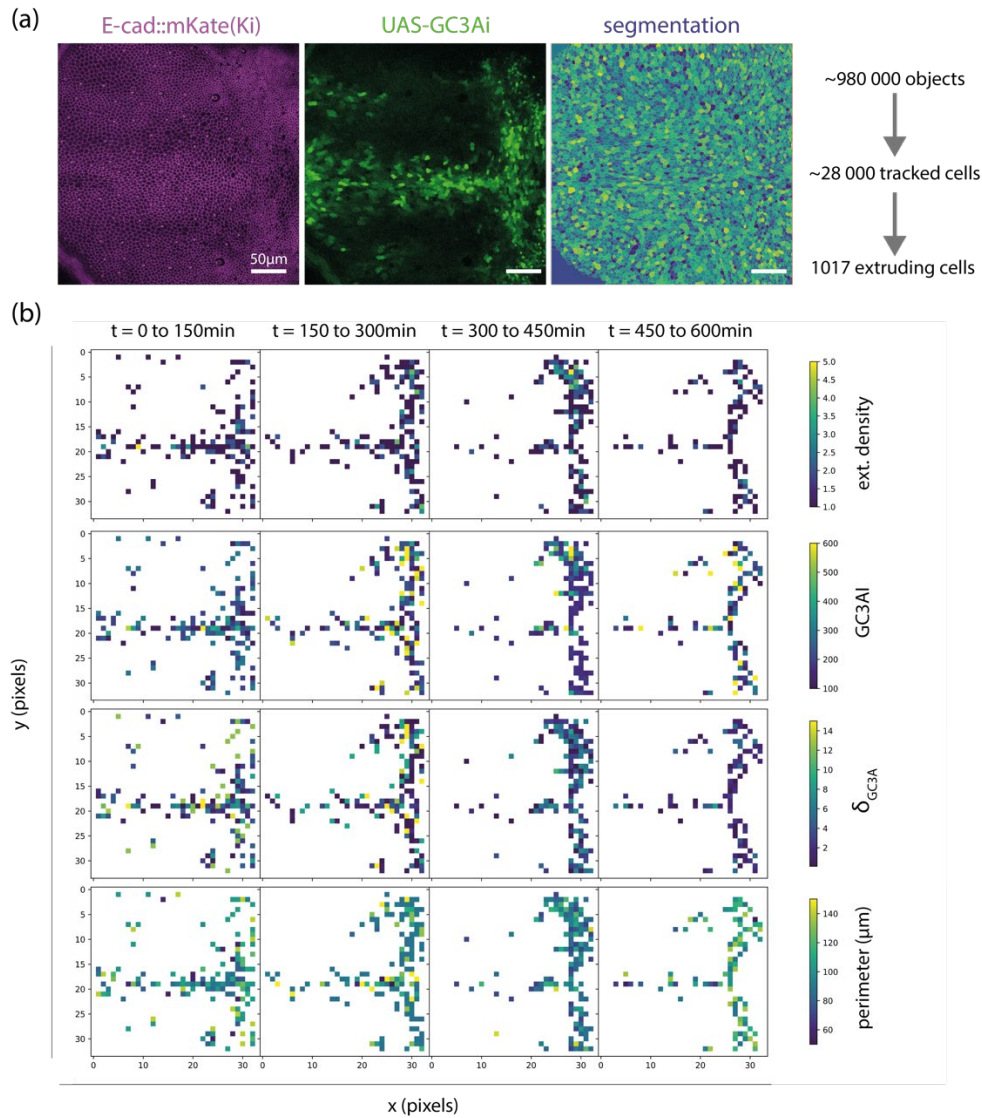


**Figure 42** - Spatio-temporal statistics of cell sensitivity to caspase. (a) Movie of the whole notum expressing E-cad::3xmKate(KI) and pnr-Gal4 > UAS-GC3Ai. E-cad::3xmKate allows the segmentation the cell contours. Close to 1millions individual cells are segmented which represents close to 28000 different tracked cells across 16h (192 time points of 5min intervals). 1017 cells were detected. (b) Spatial cell sensitivity across windows of 150min. After 600min only few extrusions were detected which led to low statistical power. The columns are the different time windows. Lines are different spatial parameters (row1: extrusion density, row2: GC3Ai levels, row3:  $\delta_{GC3Ai}$ , row4: perimeter). For each map, vertical axis is the position along the y axis of the movie, horizontal axis is the position along the x axis of the movie. Color values indicate the value of the perimeter displayed in the row (blue is low and yellow is high values)

Additionally, the average threshold ( $C3_{onset}$ ) value seemed to decrease after 300min (Figure 42b 3<sup>rd</sup> row, 3<sup>rd</sup> column compared to 3<sup>rd</sup> row, 2<sup>nd</sup> column). This indicates that the average caspase threshold decreases overtime. However, cells in neighbouring spatial bins still experienced different levels of  $C3_{onset}$ . Overall, this further confirm that there is no common threshold of caspase activation above which cells would extrude and die in the notum. Rather, cells are differently sensitive to caspase levels. Interestingly, this sensitivity increases over time and cell enter in extrusion at lower caspase levels.



### 2.3. Discussion

Using a combination of systematic cell segmentation, tracking and live caspase reporter we could show that caspase activation in the notum isn't a point of no return irreversibly leading to cell extrusion and cell death. We could show that some cells activate caspase but don't undergo cell extrusion. In fact, cells can survive a high level of caspase activation before entering extrusion. Through an automatic method, we could stereotypically identify a decision point after which cells irreversibly constrict and always extrude. We defined that decision point at the inflexion of the perimeter curve. By this method, we observed that different cells take the decision to undergo extrusion at different levels of caspase. Moving forward we could see that there is no single threshold of caspase activation in the notum. Rather, caspase levels seemed to modulate the probability to extrude like a "rheostat". Therefore, different cells experience different sensitivity to the same caspase level. We wondered what parameter could be responsible for the modulation of such threshold. We could systematically extract parameters in time windows and correlate them to the threshold in a single cell manner. This allowed us to demonstrate that past caspase activity from 2h30 to 3h before extrusion was the best parameter to predict the level of caspase at the point of decision. Finally, we showed that cell sensitivity to caspase is not homogenous in space in time. To my knowledge, this study is the first one to cover quantitatively the decision-making step leading to the irreversible commitment in extrusion and apoptosis. However few ideas need to be explored.

What modulates the decrease of the caspase threshold over time remains unknown. If caspase activation in the notum is constant over time, then the decrease observed after 300min of the movie would be coherent with the idea that past caspase activity may modulate the caspase threshold. Similarly, we don't know through what mechanism past caspase activity may be able to modulate cells' sensitivity to caspases. I will cover some proposed mechanisms in the discussion chapter of this manuscript and put them in perspective to the results observed in the first story of this manuscript (see discussion chapter part Error! Reference source not found.). Additionally, this approach bears some limitations. First, we are so far limited to the identification of parameters set by the user. Therefore, we may miss important modulators of the caspase threshold. Second, this analysis requires to segment all the cells which typically involves a lot of manual correction even using deep-learning enhanced segmentation methods. Therefore, the

statistical power of this analysis comes from the large number of extrusion events observed in one notum. However, it would require the analysis of a few other replicates to generalize the findings. Now we have generated new labelled data by correcting the segmentation of 16h of notum images. Thus, we can retrain the network with these data and replicate the data on new experiments faster. Third, this approach is so far only correlative. To test the linear association between  $\partial_{GC3AI}$  and the probability to extrude we could use the optoDronc system to optogenetically induce caspase activation. We could therefore make a gradient of activation of optoDronc and check if this scales with the probability to extrude. Furthermore, we could use the same tool to activate caspase at sub-lethal levels in different windows of time and check if this increases the probability to die 3h after the pulse. Finally, we focused here on parameters that are mostly cell autonomous. We could additionally extract parameters from neighbouring cells. Ultimately this would allow us to find predictive parameters setting the sensitivity of cell to caspase activation. On the long term it may allow the understanding of the balance between non-apoptotic and apoptotic caspase functions.

CHAPTER  
**DETECTION OF EXTRUSION** 4

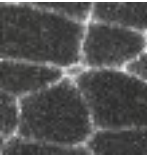




## **Table of contents**

<b>1. Introduction .....</b>	<b>166</b>
<b>2. Machine Learning.....</b>	<b>167</b>
2.1. The case of linear regression.....	168
2.2. Logistic regression: classification problem.....	170
2.3. Neural networks.....	173
2.4. Sequential models.....	176
<b>3. Results: Dextrusion: Machine-Learning enhanced tool for epithelial event detection</b>	<b>177</b>
<b>3.1. Introduction.....</b>	<b>177</b>
<b>3.2. The dataset .....</b>	<b>177</b>
<b>3.3. The architecture .....</b>	<b>180</b>
3.3.1. Model architecture.....	180
3.3.2. Hyperparameters .....	180
<b>3.4. Reducing overfitting .....</b>	<b>180</b>
3.4.1. Normalization & regularization .....	181
3.4.2. Data Augmentation .....	181
<b>3.5. Results .....</b>	<b>181</b>
3.5.1. Learning curve .....	181
3.5.2. Results on test set .....	182
3.5.3. Generalisation to full movie .....	183
3.5.4. Results of the prediction on full movie .....	184
<b>3.6. Discussion .....</b>	<b>186</b>
3.6.1. Division .....	186
3.6.2. Generalisation to other epithelia .....	186
3.6.3. Graphical user interface .....	186



## 1. Introduction

The detection of cell extrusion is critical to characterise its property quantitatively. For instance, the analysis of the evolution of morphometric parameters during the extrusion process requires the identification and segmentation of extruding cells. In addition, precise mapping of cell extrusion is necessary to identify regions of different sensitivity to cell death or detect specific feedback events. This also requires the detection of cell extrusion. However, extrusion in epithelial tissue is often sporadic. In the *Drosophila* pupal notum epithelium, while extrusions mostly happen in a specific patterned region, their distribution is stochastic over space and time. Moreover, numerous cells extrude in these regions. Similar observations were made in other epithelial tissue in *Drosophila*<sup>37</sup>. For instance, Larval Epithelial Cells also extrude randomly in a defined region and are spread over time. Finally, the same applies to the detection of division. Therefore, detecting cell extrusions or more general sequential events happening in epithelia poses specific challenges for quantitative analysis.

In most of the cases, these analyses were performed using manual and laborious detection of these events. This takes time which limits the number of events that can be tracked and the number of replicates that can be observed. Hence, it limits the statistical power which is instrumental to these analyses. Thus, there is a need for a tool that would allow the detection of extrusions or of sequential events in epithelia. This problem can be solved through image segmentation algorithms which allow the detection of extruding cells in epithelia as T2 transitions (when a cell's ID disappear). Yet, this method typically entails extensive manual correction. This is true even when using machine learning enhanced segmentation methods and it can be painstaking when large fields of view with many cells are acquired as in the case of the notum<sup>390</sup>. Similarly, it should be in theory possible to identify such events through classical signal processing methods. However, initial tests in our system showed very unconvincing results. Finally, this tool should be able to perform across a different range of image noise, magnification, and rate of acquisition. Ideally, this tool should be able to generalise to many different images of epithelia and should be easily sharable and adaptable to everyone's needs.

To answer these challenges, I developed a supervised machine learning model. Classical Neural Networks (a class of machine learning model) typically take only one image as input and showed very unconvincing accuracy to detect extrusion. This motivated the use of a specific sequential neural network model called GRU. The final development of

that tool was made in collaboration with Gaëlle Letort. The validation of the tool was made on data acquired by Tom Cumming.

What exactly are neural networks and why are they useful for biological-image processing? In this chapter, I will briefly explain the logic behind machine learning algorithms to finally describe neural networks and the specific case of GRU. Moving forward, I will present Dextrusion (DEtect eXTRUSION) and the results we obtained on the pupal notum epithelia.

## **2. Machine Learning**

What exactly is machine learning? How is it different from artificial intelligence or deep learning? Artificial intelligence refers to any computational techniques able to mimic part of human intelligence. It encompasses the field of machine learning. Machine learning algorithms are computational techniques which allows a software to learn to perform a specific task without that task being specifically programmed. Moreover, it improves at that task with experience over time. Different types of machine learning exist. However, I will only refer here to supervised machine learning which can be seen as performing pairing between examples and their labels. Finally, Deep Learning is a specific field of machine learning. It usually performs more complicated tasks such as image recognition and relies on the use of neural networks: a network of units connected to each other in a series of layers. These units are called neurons, and each can be seen as performing a specific subtask. These types of models are very useful in biology because they allow to learn and extract information on convoluted data. I will start by describing the case of linear regression which represents a basic form of machine learning. This will introduce few key concepts necessary to understand the tool I developed. I will then briefly describe the case of neural networks and the specific model we use before presenting the Dextrusion tool. This introduction doesn't require advanced linear algebra. Equations are mostly based on sums and simple derivative. What is most important is the intuition behind each concept and how they are reused all over the field of machine learning.



## 2.1. The case of linear regression

The case of linear regression is the simplest form of a machine learning algorithm. It is a linear approach to model the evolution of a variable  $y$  by an input variable  $x$ . For instance, to predict the size of the cell based on its content in a given protein. It is a form of supervised learning because each of the training data comes in the form of a pair  $(x, y)$ . To follow on the analogy, in that case  $x$  is the protein and  $y$  is the size of the cell. Based on a set of initial training dataset, a model is trained and will predict the output ( $y$ ) based on new, unseen data ( $x$ ). It is often opposed to the classification problem because it predicts continuous-valued output and not discrete-output. This simple technique allows the introduction of key concept for more advanced deep learning techniques.

If a dataset contains  $m$  observations ( $m$  cells), the hypothesis, or model  $h_{\theta}$  thus ‘maps’ the values from  $x^i$  to  $y^i$  for all  $i$  elements in  $m$  and takes the following form (see also **Figure 43**).

$$h_{\theta}(x) = \theta_0 + \theta_1 x \quad (1)$$

In this simple equation,  $\theta$  are weights and  $x$  the input variable (**Figure 43a**). At the beginning weights are initialised randomly and a random model is drawn (**Figure 43a, green**). Then the model needs to be compared to the training set to measure how well it predicts the data in its current form. For that an error is computed between the prediction and each  $y^i$  as the following (**Figure 43a, pink dotted line**).

$$h_{\theta}(x^i) - y^i \quad (2)$$

Such error is computed for all the  $m$  training observations and summed. Therefore, it results in a loss function  $J(\theta_0, \theta_1)$  for the initial set of randomly initialised weights  $(\theta_0, \theta_1)$ . The simplest form of loss function is the squared error function as (**Figure 43b, gray line**).

$$J(\theta_0, \theta_1) = \frac{1}{2m} \sum_{i=1}^m (h_{\theta}(x^i) - y^i)^2 \quad (3)$$

For the model to converge and to have the best prediction (**Figure 43c, green line**), the weights must be updated so that the loss with the real training data is minimized. A local gradient is computed which gives the slope toward where the new weights must be

updated (**Figure 43b**, orange dot is the error, purple line the gradient). This update happens with a step size  $\alpha$  (**Figure 43b**, blue arrows) and is computed as:

$$\theta_j = \theta_j - \alpha \frac{\partial}{\partial \theta_j} J(\theta_0, \theta_1) \quad (4)$$

This process is then repeated until a local minimum is reached. Once this minimum is reached, the training stops and a model with given weights (here the slope  $\theta_0$  and intercept  $\theta_1$ ) is generated.

The same principle applies during multivariate regression except in that case more than one explanatory variable are used. For  $n$  variables, instead of  $x$  being a single variable associated with weight  $\theta$ , we now have a vector of variables and vector of weights:

$$X = \begin{bmatrix} x_0 \\ x_1 \\ \dots \\ x_n \end{bmatrix}, \quad \theta = \begin{bmatrix} \theta_0 \\ \theta_1 \\ \dots \\ \theta_n \end{bmatrix} \quad (5)$$

We now have a pairing between the observation values for all the variable and the output  $y$  such as  $(x_0, x_1, \dots, x_n; y)$  it can also be written as  $(X; y)$ . To follow on the previous example, the size of the cell  $y$  is now model depending on the content in  $n$  different proteins  $(x_1, \dots, x_n)$ . The model thus becomes the following.

$$h_{\theta}(x) = \theta_0 x_0 + \theta_1 x_1 + \theta_2 x_2 + \dots + \theta_n x_n \quad (6)$$

The error of that model is then similarly minimized which the same reasoning. Therefore, I have introduced here the 3 key concepts of supervised machine learning which are:

- The hypothesis  $h_{\theta}(x)$  (the model) needs to be as close as possible to the training data to have the best prediction possible upon new inputs.
- The loss function  $J(\theta)$  computes the error between the model and the data.
- The optimisation algorithm, most often in the form the gradient descent, reduces the measured loss at each step.

However, the detection of extrusion is rather a classification problem because we want to know whether the sequence of image represents an extruding cell or not. Therefore, I will now briefly introduce the case of logistic regression for classification problems and show that the same logic applies.

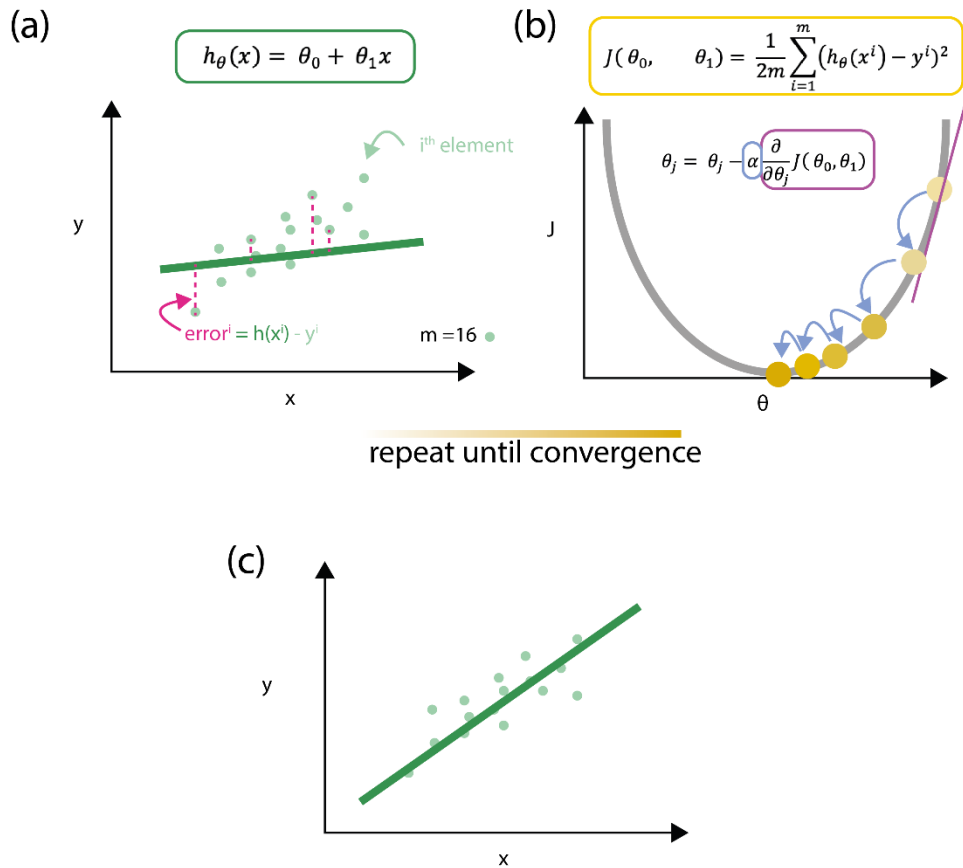


**Figure 43** - Schematic of the linear regression process. (a) an initial model is drawn with random weights. The error between the model and each  $i^{\text{th}}$  element is computed. (b) The error is then plot on an error function (yellow dot). A local gradient is computed (purple line) which gives the direction toward which to update the weight in order to reduce the loss with the real data. The weights are then updated with a step  $\alpha$ . This operation is repeated until a local minimum is reached (increasingly darker yellow points). (c) A model as converge which minimizes the error with the training data.

## 2.2. Logistic regression: classification problem

In the case of classification problems linear regression cannot be used. Indeed, in its simplest form a classification problem involves making a binary decision between two classes. For instance, in our case, whether a cell is extruding or not depending on some input variable. That variable could be the cell size. In that case, the output to predict is  $y$  with  $y \in \{0, 1\}$  with 0 the negative class (not-extruding) and 1 the positive class (extruding). Therefore, the model  $h_{\theta}(x)$  cannot yield negative values or values over 1 as it would in the case of linear regression (**Figure 44a**). Instead, we want the model to be  $0 \leq h_{\theta}(x) \leq 1$ . For that instead of using linear models as I have described in linear regression, we use activation functions. The simplest of activation functions is the sigmoid function, with  $\theta^T$  a vector of parameters such as:

$$h_{\theta}(x) = g(\theta^T x) = \frac{1}{1 + e^{-\theta^T x}} \quad (7)$$

To decide whether we predict 0 or 1 given the observation  $x$ , we need to set a decision boundary over which one outcome will be predicted and below which the other one will be predicted. Thus, suppose we set a decision boundary as a threshold at  $h_{\theta}(x) = 0.5$  then we predict (**Figure 44b**):

$$y = \begin{cases} 1, & h_{\theta}(x) \geq 0.5 \\ 0, & h_{\theta}(x) < 0.5 \end{cases} \quad (8)$$

Then for instance, if  $h_{\theta}(\text{cell size}) \geq 0.5$ , we consider the cell as extruding.

Now, it is possible to consider a more complex problem where a decision boundary must be drawn between two populations with more than one explanatory variable. Like the case of multivariate regression, we have 2 or more variables and corresponding weights. Such as in (5). For instance, these variables could be the cell area and cell perimeter or cell roundness etc... We can multiply the matrix  $X$  and  $\theta$  and the model is therefore the following (see **Figure 44c** for an example with a pair of variables  $(x_1, x_2, ; y)$ ):

$$h_{\theta}(x) = g(\theta_0 x_0 + \theta_1 x_1 + \theta_2 x_2) \quad (9)$$

The same reasoning applies when more than two variables. In this case the model takes the form in (10) and a decision boundary is drawn to separate as best as possible the two populations (**Figure 44c**).

$$h_{\theta}(x) = g(\theta_0 x_0 + \theta_1 x_1 + \theta_2 x_2 + \dots + \theta_n x_n) \quad (10)$$

Different cost functions and gradient descent functions are used in this case. However, overall, the same logic applies. First, the model is initialised with random weights. We then compute the difference between the model and the real data and update the weights of the model to reduce the error and maximise the boundary. This process repeats iteratively until it converges to minimize the error with the real data and separates best the training data. This ensures that the model is close to the reality and will predict or classify well unseen data.

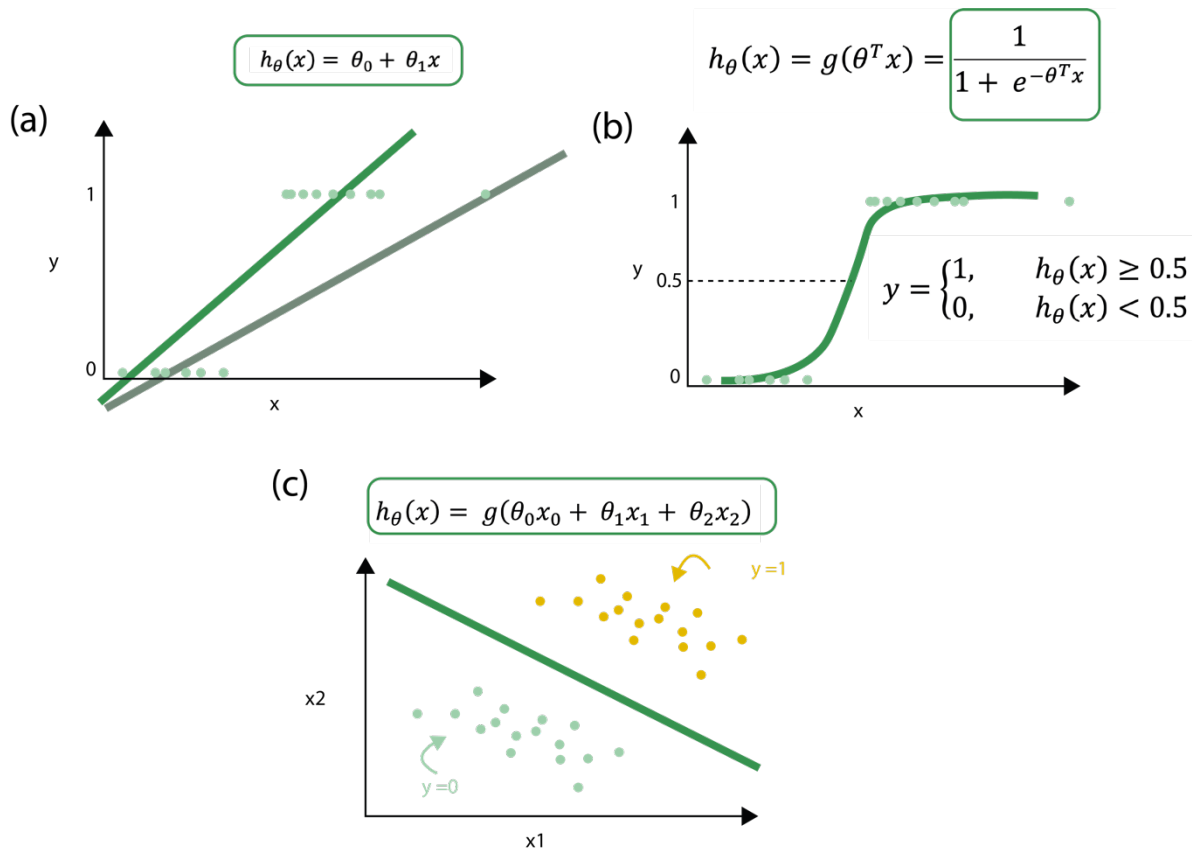


**Figure 44** - Classification. (a) Linear regression cannot be used in classification problems. Indeed, in a binary decision problem output are either 0 or 1 and a linear regression will yield output below 0 and over 1 (green). Moreover, linear regression doesn't allow to draw simple decision boundary (gray). (b) Instead, activation function such as the sigmoid function are used (green). They are limited between 0 and 1 and allow to have simple decision boundary through simple threshold (gray dotted line at  $y=0.5$ ). (c) More than one variable can be used as an input. The activation function allows to draw a decision boundary in 2D or in more complex space between the two (or more) population (light green and yellow). Similarly, to the linear regression problem, weights are updated to converge to a decision boundary.

**Conclusion: Take-home messages.**

Both linear regression and classification uses the same set of basic logic to converge to a model. The model is compared to the training data, the resulting error needs to be minimized to have the best predicting model. For that the weights are iteratively updated. Interestingly, the same principles are then reused during the use of neural networks.

### 2.3. Neural networks

Artificial neural networks (ANN) or neural networks for short (NN) were developed to mathematically model information processing by brains. The first model was called the perceptron and its architecture resembles that of a neuron which gave its name to this type of network (**Figure 45**,<sup>391</sup>). In this model, an input layer is connected to a node (neuron) which processes the input information and transforms it in some output. These three layers: the input layer (**Figure 45**, green), the hidden layer (**Figure 45**, yellow), the output layer (**Figure 45**,  $h_{\theta}(x)$ ) are at the basis of the architecture of a neural network. In this simple form the network is very limited in its prediction and is the same as a multivariate classifier (10) above. However, the power of NN comes from the possibility to increase the number of node or hidden layers and the connexion between them so that they are able to model complex, convoluted and non-linear relationships.

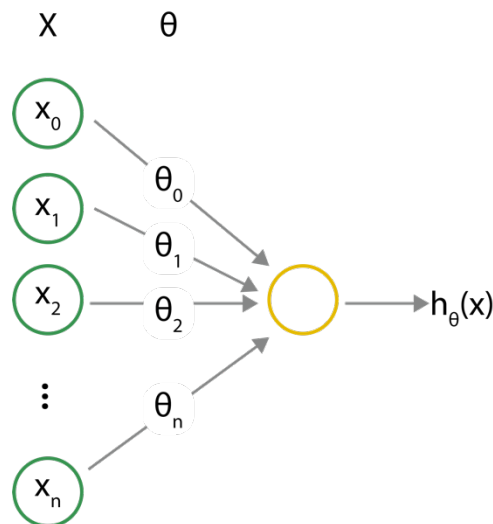


**Figure 45** - The Perceptron. The variables in the input (green) are linked to the hidden layer node (yellow). The multiplication of the values of these variables by the weights (value on the link) of their link to the next layer is passed in an activation function which results in the output  $h_{\theta}(x)$ .

Each input unit (neuron) of the input layer corresponds to an input variable  $x_n$  (**Figure 45**). Each of these unit is connected to the unit in the hidden layer by a weight  $\theta_n$ . Both correspond to the vector  $X$  and  $\theta$  described in (5). The unique unit in the ‘hidden’ layer (**Figure 45**, yellow) then applies an activation function to the linear combination of  $X$  and  $\theta$  such as:

$$h_{\theta}(x) = g(\theta_0 x_0 + \theta_1 x_1 + \theta_2 x_2 + \dots + \theta_n x_n); \quad g(\theta^T x) = \frac{1}{1 + e^{-\theta^T x}} \quad (11)$$

Finally, this unit transmit the result to the output unit. In that situation, the activation function is a sigmoid function as in the classification problem I described in the previous part, but it can be swept for any other activation function.

In the context of the classification of extrusion, the problem becomes a classification problem and input is an image. In that case, the vector  $X$  represents all pixels in the image (Figure 46a). Indeed, one image is a matrix of pixels with  $n_{pixels} = width * height$  of the image (Figure 46b). For instance, the image in the Figure 46a. has  $n_{pixels} = 44 * 44 = 1936$ . Each pixel can then be considered as a different variable which is helpful to tell the difference between two images and is represented by the vector  $X$  (Figure 46c).

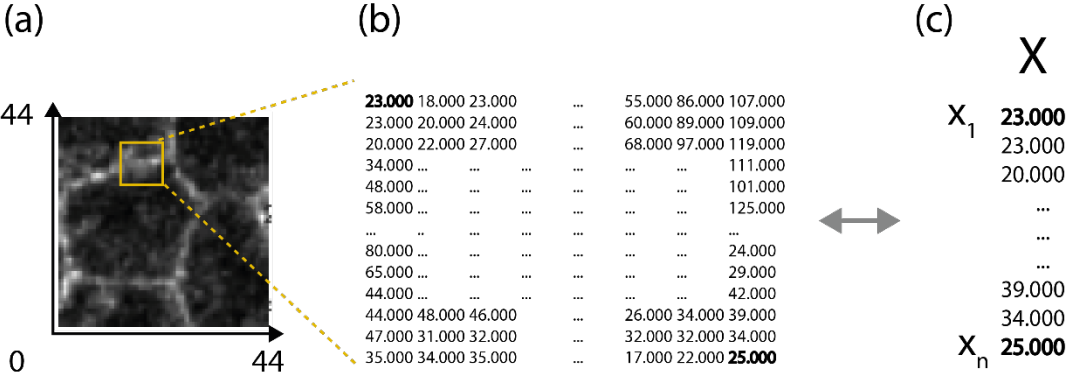


Figure 46 - image as a matrix. (a) the image of an notum epithelial cell. (b) The pixel values in the yellow square. (c) The linear vector  $X$  of all pixel values in the image.

More complex models can then be used to classify these images (Figure 47). In the first layer, the value of each pixel is multiplied by the weight associated to the connexion with the second layer. This gives the activation  $a^2$ . All of these activation nodes can somehow be seen as each performing logistic regression with a sigmoid exactly like in the simple classification, as the example I gave in part 2.2.. This is then repeated for all the layers  $l$  until the output layer. The output is then a vector with 2 possible outcomes classifying the image  $[0,1]$  is not an extruding cell,  $[1,0]$  is an extruding cell. This process is called forward propagation.

As for the previous examples of classification, the weights need to be updated to reduce the error between the prediction and the real data. For that, the prediction is compared to the real training data. In other word, did the model correctly classified the image? Did it correctly predict an extruding cell or not? This error is computed as previously explained for simple classification problems. In the case of an example network in Figure 47, with  $n = 4$  layers and the training example  $y^i$ , it is computed as follows.

$$d^n = a^n - y^i \tag{12}$$

Then, that error is propagated in the  $n - 1$  previous layers that are not connected to the output directly.

$$d^{n-1} = \theta^n d^n \cdot g'(z^{n-1}) \tag{13}$$

Following the same principle, the error is propagated to all the previous layers which allows the update of the weights associated to each node in each layer. This process is called back propagation and it reduces the loss compared to the training data. Similarly, to the previous example of classification, both forward propagation and back propagation are iteratively repeated until the model reaches a minimal error.

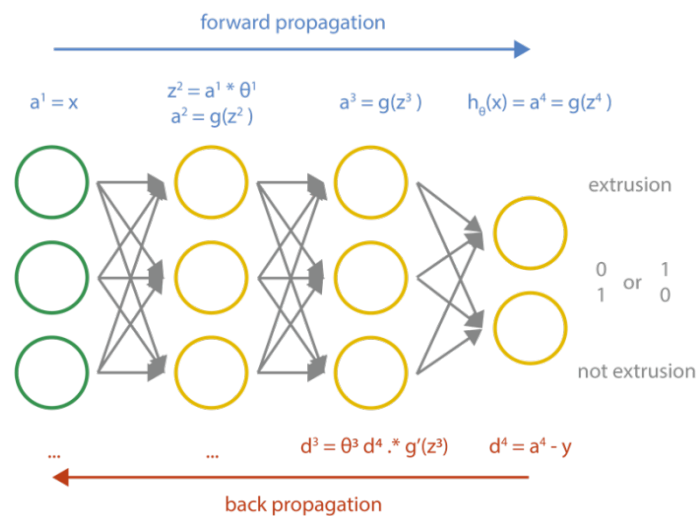


**Figure 47** - propagations. The model has 4 layers. The input (green) is fed in the model. Each node is an activation function (yellow) that takes as an input the result of each previous node it is connected to multiplied by the weight of the link. This is repeated until the output layer and is called forward propagation. The resulting prediction is compared to the training data and an error is computed. That error is then propagated in time to update the weight of link. The process then repeats until a local minimum is reached.

So far, I have presented the logic behind Neural Networks and how they are trained. The training process is linear such as the connexion between the nodes. Each node is only connected to the one in the next layer. In simpler term, there is no memory built into this type of network. However, dynamic events are per definition encoded in time. This is the case for cell extrusion. Indeed, stopping the video of an extruding cell at any frame will just show a cell, although of different size. We know the cell is extruding when looking at the movie because we have memory of the size of that cell in previous frames. Thus, we see that it constricts overtime and is therefore different compared to any other cell. However, a neural network like the one I have presented so far will consider any



frame as a new frame and will yield very unpredictable outputs. I will now describe models able to solve these problems.

## 2.4. Sequential models.

Some NN have recurrence built into them and allow to solve problems with sequential properties. These are called Recurrent Neural Networks or sequential models. I will now briefly mention the logic behind them before describing how we have harvested such model to detect cell extrusion in epithelia. Such models are often used to recognize patterns in sequence of data in biology like time series in microscopy or text sequences like genomes. Their built-in recurrency allows them to use prediction or activation from precedent instances in the sequence during the prediction of new instances (**Figure 48**). The loop in the network therefore allows for information to persist from  $t - 1$  to  $t$ .

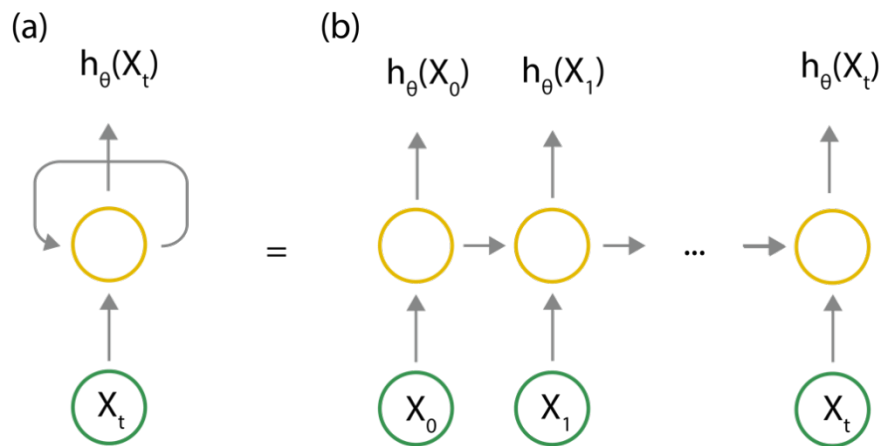


**Figure 48** - Recurrence in Neural Networks. (a) Condensed visualisation of a simple Recurrent Neural Network. (b) The recurrence loop can be visualised as a chain where the activation of the node of the precedent sequence event is fed to the next node together with the next input in the sequence.

For a simpler representation, that recurrence can be unrolled in a succession of units which are connected to the output and the next time unit. So far, we haven't considered the weight of each link. In the previous type of neural networks, weights were specific to each unit. Here the weight needs to be share across the recurrence. This way, parameters are shared across the chain which allows unit to depend on each other. Then, very similar forward and backpropagation can be used except the input in any hidden unit comes both from the previous timestep and the input layer.

Finally, if the input is too long, the time information vanishes across time layers. To solve this problem, specific models such as Long Short-Term Memory (LSTM) or Gated Recurrent Unit (GRU) were developed. These are the models we used. They allow to

handle long-term dependencies across sequences of data. In other term, they possess gates which allow to focus on, or forget specific part of the sequence depending on the input.

### **3. Results: Dextrusion: Machine-Learning enhanced tool for epithelial event detection**

#### **3.1. Introduction**

Epithelia are far from static tissue. They turnover very quickly through cell division and cell extrusion. Quantitative analysis of these dynamic events is key to understand how these processes are coordinated and how they contribute to the homeostasis or development of organs. For instance, analysing the pattern of cell extrusion/death and cell division is instrumental to understand tissue growth. This typically requires that a high number of events are correctly positioned in space and time to ensure precision and sufficient statistical coverage. This is typically performed manually by users and can be laborious.

Recently, deep learning and convolutional neural networks have help in the field of computer vision. Specifically, new techniques have been moving forward the field of image segmentation. However, they still require manual corrections or visual checking to ensure that the positioning of cell division or cell extrusion is correct. This is even more true upon high frame rate acquisition and when Signal-to-Noise Ratio is low. By the development of python libraries, Deep Learning techniques have been made accessible to a broader range of communities but still requires coding skills. Moreover, typically the detection of extrusion or division events shouldn't require the segmentation of thousands of cells which takes time and limits the number of replicates one can measure.

To address these limitations, I present here a proof of principle detection system for cell extrusion called: Dextrusion. This tool based on a type of Recurrent Neural Network (RNN) predicts the position of extrusion in epithelial tissues. It allows for fast and precise detection on cell death without the requirement for high-end computers. Ultimately, this method will be transferred for the detection of cell division.

#### **3.2. The dataset**

The dataset for this project was made of 24 epithelium movies obtained in the lab on a Zeiss LSM880 or a Gattaca spinning disc. The movies were selected because of their

different magnification, pixel size, signal-to-noise ratio (SNR) and frame rate. This was done to have the broader representation possible of the type of data represented in the lab. These movies were obtained using different junctional markers. These markers included ubi-Ecad::GFP, Ecad-KI::GFP, Ecad-KI-tdTomato, Ecad-KI-mKate2 (**Figure 49d**). XYZT movies were converted to XYT movies through localZprojection (**Figure 49a-b**). Briefly, this tool developed by our lab detects the surface of a curved object like the epithelium of the *Drosophila* pupal notum and projects it in 2D. We used this method without correcting for local curvature.

For each movie, the position of extruding cells and Sensory Organ Precursor cells (SOP, a type of differentiated cells in the tissue) were positioned. The position was obtained by clicking the termination point of the extruding cell using FIJI (when no more apical area is observed). SOPs cells undergo asymmetric cell division followed by a contraction event. As a result, only a very little apical area remains. For that reason, upon initial tests, these cells were often mistaken as extruding cells. Therefore, their initial positions were clicked to be eliminated from the prediction later. In total, 4362 extruding cells & 2860 SOPs were positioned over these movies. In parallel, control points were selected automatically and randomly in each movie so that they don't overlap with the extruding cells and SOPs. These controls are event were no extrusion or SOP division takes place. To make sure that all types of classes are represented during batch training, we ensured that extruding cells plus SOP were balanced with control positions. Then the data were split in 80% for the training set and 20% for the control set. This resulted in a total training size of 15960 events and a validation set of 3960 events after data augmentation (see reducing overfitting for details on data augmentation). This dataset was then split in a total number of 399 batches given a batch size of 40 events for the training.

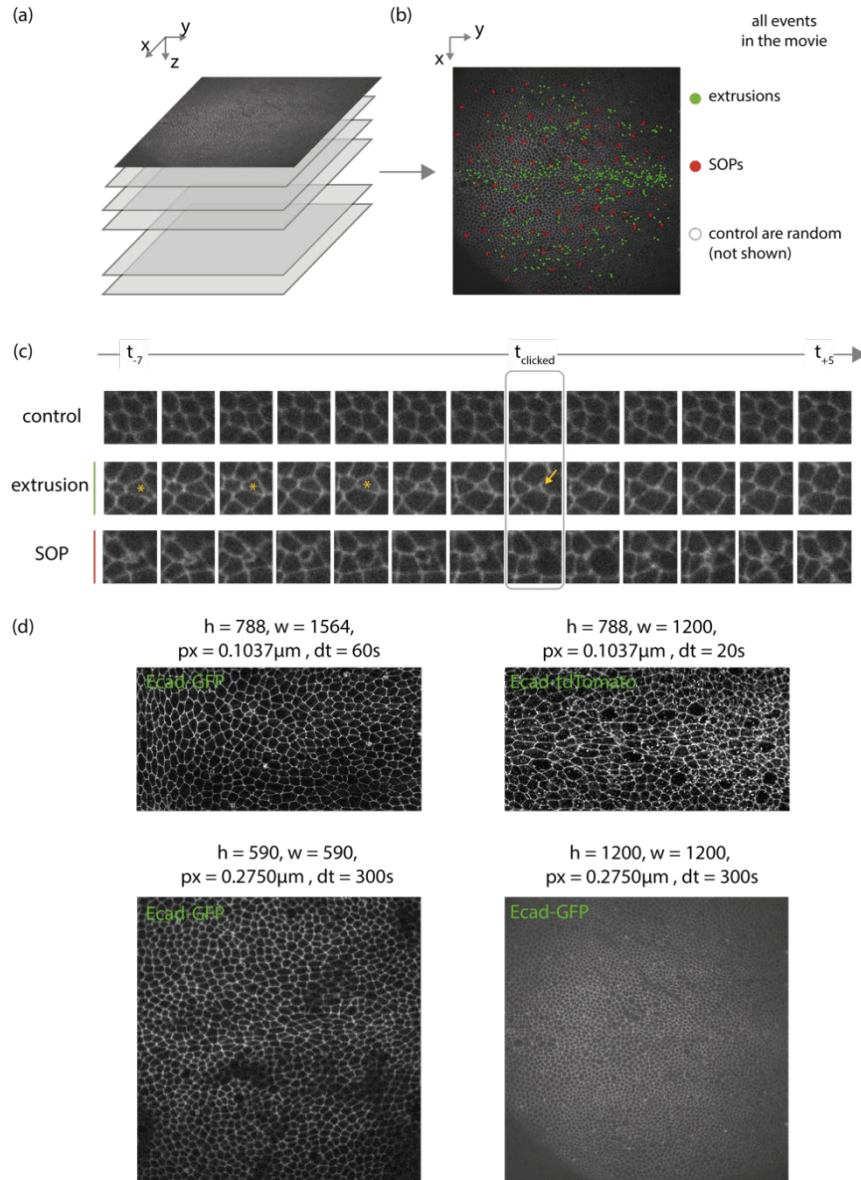


**Figure 49** - Description of the dataset. (a) The 3D+T volume acquired is projected in 2D in (b). (b) All the position of extrusion events and SOPs for that example movie. Controls are not shown because they are position randomly. (c) data input for the model. 7 time points are selected before the time at which the extrusion is clicked and 5 time points after. This image sequence is the input of the model. Same logic applies for the 2 other classes. (d) Example of different data types in the datasets. They have different pixel size, frame rate of acquisition, and signal to noise ratio (not specified here).

To detect extrusion over time, these initial clicked positions were transformed in time series by taking 7 frames before and 5 frames after the frame the time frate at which the cell was positioned (**Figure 49c**). After initial tests, the windows width and height were each empirically set to a half size of 22 pixels centred around the extrusion position (**Figure 49c**). This ensured better performance upon training while keeping enough information and variation in the data to ensure correct learning. Therefore, each input is an image sequence of size  $w_{halfsize} = 22, h_{halfsize} = 22, t = 12$ . Finally, because of

their initial different pixel size and frame rate, all movies were normalised to a fixed pixel size of  $0.2750 \mu\text{m}$ . This pixel size was selected because upon initial testing of the model, only movies with that pixel size were available. Similarly, the default frame rate was set to 300s and all movies were rescaled accordingly.

### 3.3. The architecture

#### 3.3.1. Model architecture

The model was built using tensorflow 2.8.0 and keras models 2.8.0. The first module of the network consists of a time distributed layer (**Figure 50a**). Each frame of the input sequence goes through 4 layers of convolution, normalization, and max pooling. This ‘encodes’ the sequence of image by reducing the number of variables through sequential convolutions. The input shape is (12,45,45) and is transform in an output of shape (12,64) that is then distributed to the Gated Recurrent Unit (GRU, **Figure 50a**). This allows as stated in the introduction to learn feature that are time dependent and act as a time convolution layer. Therefore, the output of that layer is a single vector of size (64). This is then passed to the decision network which a chain of dense layer (a layer with a lot of connexions) and dropout. The final output is then a vector of size (3) which gives the prediction (control, SOP, extrusion).

#### 3.3.2. Hyperparameters

The model was trained during 50 epochs. An epoch corresponds to the time it takes to do a complete passage on all the training dataset until local convergence. The training was done on either a NVIDIA RTX A5000 or a NVIDIA Quadro M2000. We used SGD (standard gradient descent) as an optimizer with a learning rate  $\alpha = 0.1$  and a momentum of 0.95. No measures were taken to reduce the learning rate upon convergence of the model. The loss was computed through classical categorical crossentropy, and the model was measured using accuracy.

### 3.4. Reducing overfitting

One of the caveats of highly connected network is that training may result in overfitting. Overfitting is the property of a network to be highly specific to the training data. This results in a poor capacity of the network to generalize to new incoming unseen data which makes it unusable. The strategy to avoid this is twofold. First, we can increase the variance in the data. Secondly, we can add normalization and regularization step.

### *3.4.1. Normalization & regularization*

The first step of normalization was applied on the input sequences. Each frame was normalized to the min and max pixel values (between 0 and 255). This ensures that training is not biased by high pixel values in the data. Additionally, it ensures that data with different bit depth can be used for the training and the prediction.

The regularization was provided by the dropout layers (**Figure 50a**). These layers randomly set input nodes to 0 with a given frequency rate which helps preventing overfitting. In other term, it temporarily suppresses some neurons from the dense (highly connected) layers at each epoch during training. This perturbs the features learnt by the model and ensures that the model is not too specific of the training data.

### *3.4.2. Data Augmentation*

In order to increase the variability in the data and to provide sufficient variance for the model to generalize, input data were first balanced to each other in order to match the category with the most observation. This ensures that there is an equal property of observing any of the category in any batch during training. Additional images were provided by shuffling the data randomly around the clicked positions. No further augmentation was used.

## **3.5. Results**

### *3.5.1. Learning curve*

The model converged under 50 epochs and performance stopped increasing on the validation set (**Figure 50b**). An epoch corresponds to the time it takes to do a complete pass through the full dataset. The model results are summarized in the figure. The model reaches 0.9881 accuracy on the training set and 0.9682 on the validation set (**Figure 50c**).

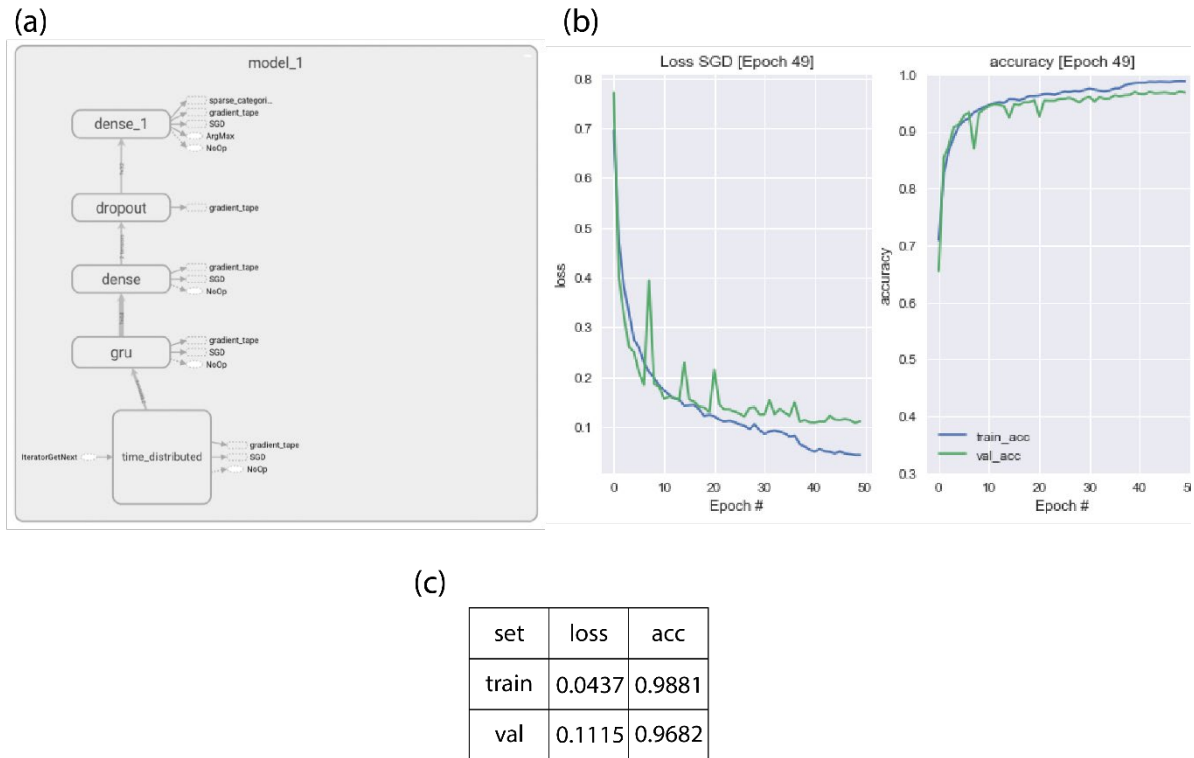


**Figure 50** - Model architecture and training. (a) Detail of the model. The time data goes through a `time_distributed` layer which encode the data by convolution. This is then passed into the Recurrent Model (GRU). Then different layers separated by dropouts leads to the final decision. (b) Training of the model on 50 epochs. The loss is reduced, and the model converge (left). This increases the accuracy of the model (right). (c) Summary of the training values.

### 3.5.2. Results on test set

To test the model generalisation, we first tested the accuracy of the model in predicting data formatted similarly to the training input. For this we used the test set previously described. Similarly, to the training set this dataset contains image sequences of size  $w_{halfsize} = 22$ ,  $h_{halfsize} = 22$ ,  $t = 12$ . It contains 2120 total events from 4 different movies. The accuracy on this dataset was high (0.9353) as expected. Therefore, the model generalises well to unseen data inputs when they are provided in same format as the training data. We obtained a false-negative rate of 0.0723 and a similar false-positive rate of 0.0721. However, these predictions are made on ground truth examples which don't reflect real data.

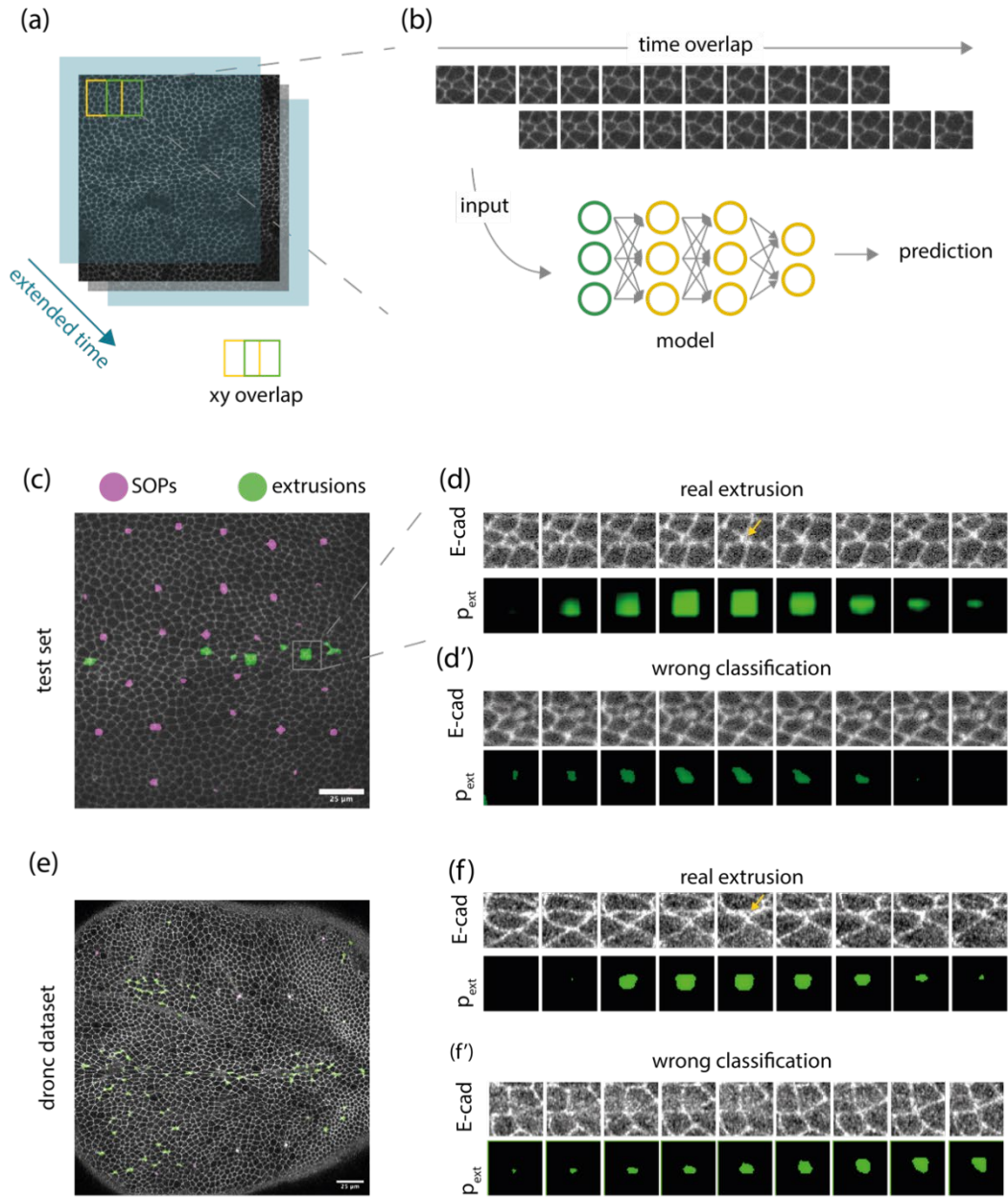


**Figure 51** - model prediction on full movies. (a) Movies are extended in time to ensure prediction of early and late time point without missing data. Then movies are split in boxes with an overlap of 10 pixels (yellow and green boxes represent that overlap in the schematic). (b) These boxes also overlap in time. Batches of these data are then input in the model which predict for each if there is an extrusion in the sequence or not. This results in a probability map for each category and each movie (not shown). (c) These probability maps are thresholded to keep only probability over 200/255 both for SOPs (purple) or extrusions (green). (d) Real movie and associated probability maps. The model correctly predicts extrusion position in the majority of the time (top). Some errors still exist (bottom, a SOP is classified as extruding). (e) Generalization of the model on other datasets. (f) example of a real extrusion correctly predicted. (f) Wrong classification in noisy area.

### 3.5.3. Generalisation to full movie

Ultimately, the model needs to predict extrusion on a full movie as a direct input (Figure 51). However, these movies are of different size and shape. Because the model



has been trained on a specific data format, new input data needs to be transformed to fit this requirement. To do so, first the new input movie is rescaled to a pixel size of  $0.2750\ \mu\text{m}$  and a frame rate of 300s as for the training. Then, each movie is cropped in image sequence of size  $w_{halfsize} = 22$ ,  $h_{halfsize} = 22$ ,  $t = 13$ . This was performed using a sliding window with a size of  $d_{xy} = 10$  and  $d_t = 2$  this ensures sufficient overlap in x, y and overtime (**Figure 51a-b**). This overlap is supposed to decrease false-negative rate because each position will be covered several times with slight shifts in x, y and t. Therefore, the model shouldn't miss many extrusions. These parameters can be changed to increase processing speed as it will reduce the total number of events to test. However, this will be done at the expense of accuracy and coverage. Additionally, the time dimension of the total movie was increase by adding frames before and after (**Figure 51a**). This was made to handle time boundary of the total movie to avoid missing early and late extrusion.

Several outputs were produced. First, we generated probability maps (**movie sup 1**). These maps were rescaled between 0 and 255 and show for each screened position the predicted probability that either an SOP or an extrusion happens at that position. To refine the output, these probability maps were thresholded to keep only prediction with high probability ( $p > 200/255$ , **Figure 51c-f**). This act as a first filter to exclude weak predictions. This first output is very useful for the user as it allows to screen all potential extrusions quickly and visually.

Finally, this map can be transformed into precise positions in the form of ROIs which can be opened in the ROI manager of Fiji (not shown). This allows the precise identification of the positions of extrusions and SOPs and thus to have a spatial representation for the mapping of these events. To obtain these positions, we extracted local maxima or centres of mass in x, y and t. This was done by applying a maximum filter of size  $x = 11$ ,  $y = 11$  and  $t = 7$  to the probability map.

#### *3.5.4. Results of the prediction on full movie*

To assess the prediction quality on full movie we generated predictions on movies from the test set. For instance, for a movie of Initial shape: (t=196, x=590, y=590), the extended shape is: (t=208, x=590, y=590) and results in 296450 image sequences of events to screen. To increase processing speed the prediction was performed on batch of 50000 events and parallelized using multithreading. Using a NVIDIA RTX A500 GPU the prediction was done in 272.568s. We then compared the ROIs output from the

prediction to the ROIs positions that were clicked for the training. Because of the overlap windows and the result from the maximum filter we tolerated a spatial distance of 10 pixels and temporal distance of 5 frames to the ground truth ROIs. The results are summarized in the **Box 2**.

	test set1	dronc1	dronc2	dronc3	dronc4	dronc5	average
TP	142	122	217	149	168	91	
FP	1346	179	194	186	225	86	
FN	57	73	106	72	68	28	
precision	0.0954	0.4	0.5279	0.4447	0.42	0.51	0.46052
recall	0.714	0.635	0.67182	0.642	0.71186	0.7647	0.685076
duration	272.568	463,127	490,55	497,902	463,76	493,171	481,702
T init	196	36	37	37	36	37	36.6
X init	590	1278	1278	1278	1278	1278	1278
Y init	590	1278	1278	1278	1278	1278	1278
T rescaled	208	48	49	49	48	49	48.6
X rescaled	590	1278	1278	1278	1278	1278	1278
Y rescaled	590	1278	1278	1278	1278	1278	1278
N events	296450	276768	292144	292144	276768	292144	285993.6

**Box 2** - Results of the model on test set and optoDronc dataset. The test\_set1 column corresponds to test performed on data with the same input shape. Dronc1 to Dronc5 correspond to full movies unseen in the training and with slightly different extrusion characteristics. The average summarize the performance of the trained model on all the Dronc dataset.

However, upon visual assessment of the results using the probability map, it seems the model performs better than what is measured using the ROI output (**movie sup 2**). To further challenge the model, we tested the prediction on a different type of dataset (**Box 2**). In this dataset, cell death is triggered using an optogenetic tool to activate caspases called optoDronc. Upon light exposure, this tool activates caspase which triggers cell death and cell extrusion. Upon uniform light exposure of the tissue, high rates of extrusion can happen locally. This triggers hole formation in the tissue. We reasoned that the termination of extrusion in this background would be different to the one in the training dataset which could potentially impairs the detection of extrusion. The prediction on that dataset was made using a NVIDIA Quadro M2000 GPU and took 481.7s per movie on average. Although slower, that prediction could be ran on a Mac M1 chip showing that the model can perform prediction on simpler machines. Surprisingly, the model performed similarly to the prediction on the test set. It even showed higher precision compared to the test set. Similarly, visual assessment yielded higher quality results when looking at the probability map.

## 3.6. Discussion

Taken together these results demonstrate how this model achieves precise and fast detection of cell extrusion in *Drosophila* epithelia. I showed that this tool generalises well on completely unseen data. Moreover, Dextrusion yield an excess of false positive results. Therefore, one could increase the precision of the tool by adding a fast and manual screening on the false positive results to keep only true extrusion.

### 3.6.1. Division

Dextrusion yields very accurate detection of cell extrusion in the notum. Ideally, this tool would be more complete if it could detect cell divisions. So far, it seems suitable for the detection of divisions. Indeed, it was able to detect sequential events such as SOP formation with far less training data compared to extrusion. Additionally, previous results in the lab using simple neural network showed very accurate results for the detection of cell division. This is certainly because their spatial signature is more easily recognizable by classical Neural Networks compared to cell extrusion. Thus, it provides encouraging results for this tool to apply equally well on the detection of division provided adequate training datasets.

### 3.6.2. Generalisation to other epithelia

So far Dextrusion is a proof of concept specifically focused on cell extrusion in the *Drosophila* pupal notum. Ultimately, in order to share this tool to other, we will harvest extrusion datasets in other epithelial tissues such as in quail epithelium or delamination of neurons in zebrafish telencephalon. Adding these datasets to our training dataset will help to make this tool generalisable. Finally, a more long-term goal would be to make this tool amenable to transfer learning. As a result, the community could provide their datasets and further train their model specifically on their data to increase accuracy if it doesn't perform well on their data out of the box.

### 3.6.3. Graphical user interface

Finally, in order to share this tool with the community we must make it accessible to as many users as possible. In its current form, it is in the format of a Jupyter notebook that can be easily shared as is the case with other machine learning tools. However, it remains slightly difficult to access for people without coding skills. To overcome this lack, we plan to develop a user interface. Recently, napari is emerging as a replacement for Fiji under python. It's convenient interface makes it easy to juggle between different

images and to interoperate between code and user interface. In addition, a recent effort has transferred a lot of Fiji plugins to napari. This is possible because napari presents a set of tools that facilitate plugin development. This way we can develop a plugin that facilitates the use of Dextrusion for both detection and training. Additionally, this plugging could be coupled to the development of localZprojector under napari. This would therefore provide a complete toolbox for the analysis of epithelia development and homeostasis under python which is free, open access and the most represented programming language.

CHAPTER  
**DISCUSSION & PERSPECTIVES**

5

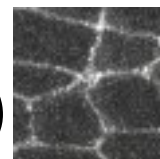




## **Table of contents**

<b>1. Remodelling during extrusion .....</b>	<b>192</b>
<b>1.1. Putative mechanisms for MT depletion by caspases .....</b>	<b>192</b>
1.1.1. Direct cleavage .....	192
1.1.2. Cleavage of a modulator .....	193
<b>1.2. Tensegrity .....</b>	<b>195</b>
<b>1.3. Cell shape stabilisation .....</b>	<b>197</b>
1.3.1. MT in apical stabilisation .....	197
1.3.2. Hypothesis1: MT resistance to compressive load .....	197
1.3.3. Hypothesis2: Steric hindrance and crosslink modulate flexural rigidity .....	199
<b>1.4. Sensitivity to compression .....</b>	<b>200</b>
1.4.1. Role of MT in differential sensitivity to compression in competition .....	200
1.4.2. Context-dependent roles of microtubules .....	202
<b>1.5. Cell insertion .....</b>	<b>204</b>
<b>2. Decision making .....</b>	<b>206</b>
<b>2.1. Parameters influencing the caspase threshold.....</b>	<b>207</b>
2.1.1. Single-cell caspase threshold.....	207
2.1.2. Past caspase activity as a sensitizer? .....	208
2.1.3. Other predictive parameters and exploration.....	209
<b>2.2. Microtubule depletion: a decision step?.....</b>	<b>210</b>
<b>3. Prediction of cell death .....</b>	<b>211</b>
<b>3.1. Can we harvest the model to find predictive features of extrusion?.....</b>	<b>211</b>
<b>3.2. How to use the model for something else?.....</b>	<b>213</b>





## 1. Remodelling during extrusion

In the second chapter of this manuscript, I have shown that the initiation of cell extrusion happens without any changes in localisation or dynamics of the classical cell shape regulators such as E-cad, myosin, actin, or Rho. Surprisingly, we observed that microtubules are depleted in the cell downstream of caspase activation. I could show that this depletion is concomitant with the onset of extrusion and is driven by caspase activation. Additionally, I demonstrated that inducing microtubule repolymerisation is sufficient to trigger apical area increase. Conversely, fast depletion of microtubules led to a reproducible constriction of cells. This indicates that microtubules are able to modulate the apical area of epithelial cells. Moving forward I showed that microtubule depletion is sufficient to induce extrusion and bypass the requirement of caspase for cell extrusion. Conversely, microtubule stabilisation strongly impairs and slows down cell extrusion. Taken together, this study shows how microtubule disassembly by caspase is an important rate-limiting step of extrusion. More generally, it shows how microtubules can modulate the apical area of epithelial cells and stabilise their shape. I will now discuss some of these findings. I will provide putative explanations or mechanisms regarding how effector caspases might lead to microtubule depletion and through what mechanisms they may stabilise cell shape. Then I will put in perspective our data with data from the literature.

### 1.1. Putative mechanisms for MT depletion by caspases

#### 1.1.1. *Direct cleavage*

The most parsimonious hypothesis to explain the disassembly of microtubules upon caspase activation is to consider that microtubules are directly cleaved by caspases. This idea is supported by different studies showing  $\alpha$ -tubulin cleavage for instance through two-dimensional electrophoresis in Jurkat Cells<sup>258</sup>. More recently, using Mass Spectrometry,  $\alpha$ -tubulin or  $\beta$ -tubulin were shown to be cleaved in *Drosophila* S2 cells further supporting this hypothesis<sup>219,253</sup>. However, we have failed to produce a functional  $\alpha$ -tubulin mutant inhibiting its caspase cleavage to test its requirement during the initiation of extrusion. Because  $\alpha$ -tubulin is a very small and conserved protein, the mutations in its caspase cleavage sites impaired  $\alpha$ -tubulin<sup>ABC</sup> incorporation in functional microtubules. Indeed, the change of the consensus sequence from DEVD to DEVA certainly leads to failure to correctly fold. This made the mutant unable to be used to

test the effect of putative microtubule cleavage on regulating the initiation in extrusion because it couldn't integrate properly in the network.

Moreover,  $\alpha$ -tubulin cleavage during apoptosis remains unclear to this day. Indeed, it was first shown to be cleaved in neurons during the early stages of apoptosis which could correspond to the initiation phase of extrusion<sup>392</sup>. However, this doesn't seem to be conserved in A431 epithelial cells (epidermal carcinoma). While  $\alpha$ -tubulin appears transiently reduced in these cells during the mid-stage of apoptosis, its depletion doesn't play a role in blebbing<sup>269</sup>. This suggests it may not significantly contribute to the contractility in their system. Moreover, microtubule levels seem to increase at late apoptosis stages<sup>269</sup>. Indeed, microtubules rather seem to be stabilised and promote the late-stage formation of apoptotic blebs in these cells<sup>393</sup>. Therefore, it is unclear whether microtubule disassembly at the initiation of cell extrusion is due to direct  $\alpha$ -tubulin cleavage or not. An alternative hypothesis for a direct microtubule cleavage would be through the cleavage of  $\beta$ -tubulin as it was recently shown to be a caspase target<sup>253</sup>. However, fewer studies have focused on  $\beta$ -tubulin cleavage which ultimately motivated our choice to target  $\alpha$ -tubulin. Moving forward, a careful analysis of the 3D structure may allow to mutate  $\alpha$ -tubulin by changing the D at the p1 position for an amino acid more conservative of the protein structure. If this mutant correctly folds, then  $\alpha$ -tubulin<sup>MUT</sup> might integrate properly in microtubules and can act as a dominant-negative. This will allow us to test the implication of the direct cleavage to the resistance to constriction.

### 1.1.2. *Cleavage of a modulator*

Through their mass spectrometry analysis, Crawford et al<sup>253</sup>, identified 118 caspases substrate in *Drosophila* S2 cells after treatment with doxorubicin, cycloheximide or actinomycin D. Thus, caspases have multiple substrates even in *Drosophila*. Given the ability of caspases to cleave numerous substrates and because there are numerous microtubule interactors, it would be expected that microtubule disassembly is due to a pleiotropic effect. Accordingly, several microtubule interactors have been identified as caspase substrates in this study. Among them, MAP205 is a Microtubule Associated Protein that stabilises MT. A cleavage by caspase would then destabilise microtubules which could promote their depolymerisation. A similar function could be proposed in the case of *ncd*, another caspase substrate. Non-claret dysjunctional (*ncd*) is a member of the kinesin-14 family: a minus-end directed microtubule motor<sup>141</sup>. Kinesins-14 have been

proposed to have microtubule-destabilising properties<sup>394</sup>. One possible mechanism could be a potential cleavage of *ncd* by caspase which would enhance the MT-destabilising property of *ncd*. This would enhance microtubule disassembly upon caspase activation. Finally, CG1943 is another interesting substrate interacting with MTs. This coding gene encodes a protein homologous to the human JPT1 (Jupiter Microtubule Associated Homolog 1). In *Drosophila*, Jupiter is a MAP that has been shown to associate with both tubulin monomers and MTs and positively regulate MT polymerisation<sup>395</sup>. Interestingly, Jupiter-GFP levels are equally reduced during the initiation phase of extrusion (our data). Therefore, a caspase-inhibitory cleavage of CG1943 could eventually lead to a reduced polymerisation and to MT disassembly. Alternatively, MAPs can mediate MT lateral reinforcement. It has been shown that lateral reinforcement enhanced the compressive loads MT can bear<sup>181</sup>. Here we have shown that MT modulate the resting area of the cell (see **1.3.1** and **1.3.2** of the discussion). We could assume that MT do so through their ability to resist compression. Thus, the depletion of MAPs by caspase would lower their ability to resist compression by losing lateral reinforcement.

The mass spectrometry analysis conducted by Crawford et al is remarkably powerful. It has revealed a multitude of protein cleavages that are conserved between vertebrates and *Drosophila*. However, this approach is not fully recapitulating all known cleaved substrate in epithelial cells. Indeed, some substrates such as  $\beta$ -catenin are not present in the substrates identified by this study even though several articles demonstrate its cleavage in the *Drosophila* embryo<sup>264,265</sup>. This can be explained by the fact that this study was conducted in S2 cells which are different from epithelial cells. Nevertheless, some substrates are conserved between cell types such as Dlg. Interestingly, Dlg is known to bind to APC (a known regulator of MT dynamics) which enhances MT polymerisation. Therefore, it could be another putative caspase target influencing the disassembly of MT at the onset of extrusion.

To test their putative requirement to the initiation of constriction, we could express reporter lines combined with RNAi-based knockdown of these proteins. We could mutate their cleavage site and assess the probability of extrusion or the speed of extrusion in the mutant context. This will indicate whether these proteins are indeed regulating cell extrusion. We could equally test if their effect goes through microtubule depletion or not by monitoring microtubule levels in extruding cells expressing RNAi against these targets. However, it is not guaranteed that such an approach would produce any results given

the high number of MT interactors. Because they are numerous, MT interactors may have partially redundant functions making this approach difficult.

## 1.2. Tensegrity

### 1.2.1. *The tensegrity model and MT: description & limitations*

Our observations fit with the predictions from the tensegrity model. To my knowledge, it has been difficult to provide a coherent model integrating all the different cytoskeletal component and their interaction together. One attempt to do so is through the tensegrity model<sup>57,58</sup>. It recapitulates cell mechanical behaviour by considering that a cell stabilises its shape through structural struts which bear compression of a tensed network. Thus, local compression and global tension balance each other and result in a stable shape. The cell tension is provided by actin and myosin filaments which generate cell prestress. These are balanced by microtubules through their higher persistence length or ECM and together bear compression forces. In cells, MTs often appear curved while actin filaments are mostly straight which enforces the idea that MTs are under compression and actin filaments are tensed<sup>181</sup>. This model needs three main properties to be satisfied:

- The cell needs to behave as a discrete mechanical network not a continuous one.
- Cytoskeletal prestress needs to be a dominant determinant of cell deformation.
- MTs and ECM needs to resist compression together

There have been several attempts to measure these *in vitro*. Good evidence in cell cultures supports the fact that local deformation on cell through micropipette manipulations or force application through beads lead to directed deformations. These deformations happens both at the surface and deep in the cells, supporting the first argument (reviewed in <sup>57</sup>). There are multitude of data showing how cell pre-stress is a major determinant of cell stability. For instance, laser ablation in different systems lead to the retraction of cell edges (for instance in the notum<sup>210</sup>). Some early experiment *in vitro* on single MT suggested that MT can bear far too little compressive forces compared to what is needed to resist (reviewed in <sup>396</sup>). However, in cells, MTs are crosslinked with another filament. These lateral reinforcements increase drastically the ability of MTs to resist these loads<sup>181</sup>. Accordingly, I have highlighted throughout this manuscript the different roles of MTs in bearing compressive. For instance, they are highly necessary for the stability of neuronal prolongation such as dendrites. Their localised depletion through non-apoptotic and caspase-dependent mechanisms leads to the retraction of dendrites<sup>345</sup>.

Therefore, the tensegrity model provides a good framework in addition to the existing one to better understand cell shape stability & mechanics.

### 1.2.2. *Could we check the tensegrity model in our system?*

The tensegrity model hasn't been globally accepted as a mechanical model for cell shape stability *in vivo*. One of the reasons is that this model is discrete, static and at equilibrium while the cells' cytoskeleton is dynamic, away from equilibrium and turnovers. One of the other limitations is the fact that cells must behave as a mechanically discrete network and not as a continuum like viscoelastic models. First, viscoelastic models have been shown to recapitulate well mechanical cell behaviours. Second, many different materials do transmit forces at a distance within the structure even in non-tensegrity structure. Another caveat is the lack of tools to measure *in vivo* the ability of microtubules or other intracellular structures such as intermediate filaments to bear compressive forces. For instance, it is not clear how microtubules behave in an *in vivo* epithelium upon compressive stresses. Yet, this model may be useful to some extent and there has been some attempt to reconcile both views. Accordingly, in rat cardiomyocyte cultures, detyrosinated microtubule buckle and resist contraction through their crosslinking to sarcomere structures<sup>180</sup>.

Here, we provide data showing that MT somehow modulate the resting area of the cell or the cell elasticity. One way of explaining this behaviour is to consider that MTs resist contractile forces (see 1.3.2. of the discussion). Additionally, we know cells are pre-stressed in the notum. One prediction of the tensegrity model is that if the resistance to compression is lowered by removing MTs, it will be transferred to ECM adhesion. As a consequence, ECM adhesion should increase to bear more compressive loads. We could test such an assumption by looking more in detail at ECM adhesion partners during cell extrusion. First observations regarding Talin (another ECM adhesion partner) levels during extrusion didn't show any significant increase during the initiation of the process. Rather we observed a late accumulation when the actomyosin ring forms (data not shown). In parallel to data shown in this manuscript, I have performed a screen to identify putative targets of caspase which modulate cell extrusion downstream of caspase activation (not shown). Interestingly, one of the most significant targets to modulate cell extrusion was Paxillin. One could thoroughly measure Paxillin levels during cell extrusion. The observation of a Paxillin increase during the onset of extrusion where MTs are disassembled would further support the tensegrity model in our system.

## 1.3. Cell shape stabilisation

### 1.3.1. *MT in apical stabilisation*

In chapter 2, part 4, we have demonstrated how microtubules stabilise epithelial apical areas. This conclusion was motivated by several observations. First, the onset of extrusion is not associated with major changes in cell circularity. This fits the prediction from the vertex model. Indeed, the model predicts that a constriction triggered by changes in the resting area/ area elasticity of the cell would be shape-conservative. Second, MT polymerisation and depolymerisation respectively increase and decrease cell apical area. Finally, the stabilisation of MTs is sufficient to slow down the extrusion speed. All this is in good agreement to argue for a role of MTs in modulating the resting area/ compressibility of epithelial cells in the notum. However, it is still unclear how exactly MTs can modulate cell compressibility and thus mediate apical area stabilisation. This question overlaps with another point left unanswered in our study: how do MT disassembly increase the contraction yield? I showed in chapter 1, parts **3.3.2** and **3.3.3** the role of MTs in regulating apical area mechanics through direct pushing forces, through the resistance to compressive loads or through their interaction with the actomyosin cortex. Here I will propose some putative mechanisms relying on these properties by which MTs stabilise the apical cell area and by which MT disassembly can increase the actomyosin yield. These mechanisms are not mutually exclusive.

### 1.3.2. *Hypothesis1: MT resistance to compressive load*

Our first hypothesis is that MTs mediate apical stability by resisting compressive forces or contraction through their long persistence length. Therefore, MT disassembly could increase the actomyosin yield by removing this resistance to the contraction induced by actomyosin. Several observations support this role of MTs. Cells on micropatterns submitted to cycles of compression experience MT bending<sup>175,178</sup>. This triggers a CLASP2-dependent mechanosensitive response which stabilises MTs. This increased stabilisation allows them to better resist and even to counteract compressive forces. Additionally, MTs provide structural rigidity for cells undergoing apical insertion in *Xenopus*<sup>397,398</sup>. Several studies converge to show how MTs can regulate cell morphogenesis through active pushing forces. For instance, during dorsal fold formation in the *Drosophila* embryo, Patronin organises an apicobasal pool of MTs. This pool exerts forces on the apical area through Dynein motors. Thus, the basal shift of Patronin displaces the MT network which weakens the apical area and drives apical constriction<sup>399</sup>. Comparably,

MT reorientation during *Drosophila* amnioserosa changes the direction of pushing forces which drives cell flattening<sup>172</sup>. Additionally, MT pushing forces maintain mechanical stability in *Drosophila* wing<sup>171</sup> (see Chapter1 part **3.3** for more details). Alternatively, MT pushing forces were shown to regulate aster centring in various cells (see later part **1.4.2**). Therefore, there are good pieces of evidence to argue that MT could resist actomyosin-based contraction either passively by their persistence length or through active pushing forces.

Accordingly, the MT disassembly at the onset of extrusion would lead to a reduction of these forces and an increase in the constriction yield without increasing actomyosin levels. To directly test this hypothesis, we could locally ablate MTs oriented toward the cell boundary. This will allow to assess whether MT-based pushing forces are exerted on the cortex (similarly to the approach in <sup>171</sup>). If MTs push against the cortex, then their ablation should lead to a substantial local inward bend of the membrane. We tried to perform such experiment in the notum. However, the lack of subcellular resolution impaired our ability to precisely perform ablation of single MTs or MT bundles. Consequently, our ablation may have equally affected the actomyosin cortex. Thus, we were not able to observe any reproducible inward movement of the membrane upon ablation of MT in the notum (data not shown). While this observation suggests that MTs don't push enough on the membrane, the technical limitations impair our ability to formally conclude on this point. We would need to replicate this experiment with higher resolution imaging coupled with more precise 3D targeting of the ablation laser. Finally, we lack absolute measurements of both MT pushing forces and actomyosin contractile forces. In absence of such numbers and of better resolution, we cannot definitively access the role of MT pushing forces.

To measure MT response to compression, the Théry team plated RPE1 cells on adhesive micropatterned silicon sheets. These were then submitted to cycles of compression: 10 cycles of 10% Stretch and Compression Cycles for 2 minutes. Unfortunately, it is not possible for us to use such techniques to measure MT resistance to compression *in vivo*. An alternative could be to use optogenetic modulation of cell contractility. Two approaches are possible. First, we could express optoRhoGEF2 in clones together with a reporter of MT<sup>400</sup>. This tool allows for fast activation of Rho1 upon light activation by bringing RhoGEF2-CRY2 to the membrane through light-induced dimerization of the couple CIBN-CRY2. We could then do sequences of light pulses and

relaxation with high resolution and look at MT bending and dynamics in this context. Second, we could inject sirTubulin to label all microtubules across the notum. Then, we could express optoRhoGAP in large clones. This unpublished tool is currently in development in the lab and allows for fast inhibition of Rho1. By the same sequence of light exposure, we could release tension in large optoRhoGAP clones which would compact the neighbouring WT patch of cells. Then we will look at MTs bending in these cells. Albeit not perfect, these complementary approaches should indicate this would be a readout of whether they are under compression and bend or not. This coupled to the use of higher resolution imaging will allow to assess MT resistance to compression.

### *1.3.3. Hypothesis2: Steric hindrance and crosslink modulate flexural rigidity*

Finally, our last hypothesis is that MTs contribute to apical area stabilisation through their interactions with the actomyosin cortex. This could be purely by steric hindrance or through active crosslinking with the actomyosin network. This idea is supported by the observation that MT resist the contraction of muscles when they are attached to sarcomeres<sup>180</sup>. Additionally, in vitro reconstituted networks of actin, myosin and microtubules are more contractile in the absence of MTs. MTs crosslink with actin, which increases the flexural rigidity. Therefore, the network has fewer degrees of freedom to constrict in the presence of MTs than without it<sup>166</sup>. Similarly, the removal of MTs from an already established actomyosin network increases actomyosin purse-string contraction during *Xenopus* subcellular wound healing<sup>164</sup>. Following this idea, the removal of MTs at the onset of extrusion would allow the same actomyosin network to constrict more efficiently by removing restrictions on the network. Several Spektraplakins such as Shot mediate crosslinking between actin and MT. To test this hypothesis and the putative requirement of these proteins, one could express optoRhoGEF2 in clones together with RNAi targeting different actin-MT crosslinkers. One could then assess the constriction of these clones in a given region of the notum and at a well controlled developmental time. For instance, if Shot is necessary to mediate actin-MT crosslinking and to restrain the constriction, then shot-RNAi/optoRhoGEF2 clones should contract more upon light exposure than clones expressing control RNAi. This will allow to check if the interaction between the actomyosin network and the MT network restrains constriction which would explain why the yield increases upon MT removal.



## 1.4. Sensitivity to compression

### 1.4.1. *Role of MT in differential sensitivity to compression in competition*

Given that microtubules can resist compression, they might be co-opted in the context of cell competition. This process is a context-dependent elimination of cells from one cell population which drives the expansion of another population. It is context-dependent because each of these two populations develops normally on its own and is eliminated only in contact with a competitor. Several examples of cell competition induced by polarity mutant have been shown to rely on mechanical cell competition and differential resistance to compression. Polarity mutant clones such as *scribble*<sup>-/-</sup> are compressed by the neighbouring cells<sup>401</sup>. Additionally, they display lower homeostatic density which leads to their preferential elimination<sup>402,403</sup>. This concept reflects the ability of one cell type to reach a steady state at which cell death balances cell division in that population. When crowding is increased, cell death will increase and bring back the population to its preferred homeostatic density. If a population with a lower homeostatic density (or homeostatic pressure) is put in contact with a population which has a higher homeostatic density, then cell death will be preferentially induced in the first population.

Two parameters have been proposed to be important modulators of mechanical cell competition. The first is the cell stiffness/compressibility which reflects the deformability of a cell. The second, is the ability of a cell to survive compression. Both a higher compressibility and a lower survival to compression might explain why *scribble* mutant cells are eliminated when in contact with WT neighbours<sup>404</sup>. So far, we do not know if the microtubule network is different in that context or whether such clones are indeed eliminated as a result of compression *in vivo* in *Drosophila* epithelia. However, several pieces of evidence suggest that microtubule organisation or dynamics may be different in polarity mutant-induced cell competition (Lgl, Dlg, *scribble*). For instance, Scribble has been shown to physically interact with Pins to anchor the microtubule spindle at the apical cortex in neuroblast<sup>405</sup>. Loss of *scribble* could then shift the position of the spindle basally and therefore apical area might be more amenable to compression. This could lead to *scribble* having a higher sensitivity to compression. Disc Large (Dlg) mutant clones are also eliminated through cell competition<sup>406</sup>. However, to my knowledge, the relative stiffness of polarity mutant clones compared to WT or their relative survival to compression hasn't been thoroughly tested *in vivo*. Nevertheless, Dlg/Scrib/Lgl form an important complex together regulating apico-basal polarity. Therefore, similar

mechanisms may lead to their elimination. Moreover, Dlg also interacts with microtubules. Dlg interacts with Dynein, an MT motor, via its interaction with GKAP which modulates MT organization<sup>407</sup>. Additionally, Scrib and Dlg both modulate APC, an important MT partner that interacts with EB1 at MT plus tip and promotes their polymerisation<sup>408</sup>. Dlg binding to APC leads to MT polarization<sup>409</sup>. This is regulated by scribble to promote cell orientation<sup>410</sup>. Therefore, loss of Dlg or Scrib may result in reduced polymerisation and misorientation of the MT network. This could lead to a reduced stiffness or a reduced ability to survive compression. The last actor of that complex, Lgl, controls shot and Patronin. These proteins are minus-binding proteins forming non-centrosomal Microtubule Organizing Centres (MTOC) in epithelial cells like the one in our study<sup>159</sup>. Lower levels of Lgl could then impair non-centrosomal MTOC which would lead to cell apical collapse upon compression.

Finally, Scribble also physically interacts with *thickvein* (*tkv*) a receptor of Dpp signalling<sup>411</sup>. Interestingly, *tkv*<sup>-/-</sup> clones form cysts that are basally eliminated from the wing disc through the depletion of an apical MT network<sup>412,413</sup>. Conversely, the network is maintained in neighbouring WT cells. Additionally, *tkv*<sup>-/-</sup> *bsk*<sup>-/-</sup> clones are equally eliminated. This shows that the extrusion of *tkv*<sup>-/-</sup> clone is independent of JNK-induced apoptosis. Additional results show that their extrusion doesn't correlate with cleaved-Caspase-3 staining<sup>412</sup>. This is coherent with our results showing that depleting MTs is sufficient to induce extrusion independently of caspase activation. Given that *scrib* regulates *tkv*, this could be a potential mechanism explaining the preferential elimination of *scrib*<sup>-/-</sup> clones through a lower resistance to compression.

To test this hypothesis, we could first induce *scrib*<sup>-/-</sup> or *scrib*<sup>KD</sup> clones in the notum and in the wing disc (a classical epithelium model for competition scenario). Then we would need to check the relative pressure in these clones compared to surrounding cells. We could do that first by applying mechanical inference to segmentation data similar to what is shown in the third chapter of this PhD manuscript. Additionally, we could measure relative area reduction in these cells. To formally test if these clones are eliminated by compression, we could directly change density by contracting neighbouring cells. For instance, by releasing tension through laser cuts. Additionally, we could try to prevent *scrib*<sup>-/-</sup> compression by stretching the neighbouring cells for instance by the activation of optoRhoGEF2 in the neighbours. To check for the requirement of microtubules in that context, we could inject sirTubulin or express a live reporter of microtubule organization.

This will allow the measurement of the relative positioning of the apical MT network in *scrib*<sup>-/-</sup> or *scrib*<sup>KD</sup> clones compared to the neighbours. If our assumptions are valid, then we would expect the MT levels to be reduced or the MT network to be shifted basally in *scrib*<sup>-/-</sup> clones. Additionally, we could measure MT polymerisation by looking at EB1-GFP comets or MT dynamics by doing FRAP in clones compared to neighbours. If we see any effect on MTs, we could check if the mislocalisation is indeed due to tkv position shift in *scrib*<sup>-/-</sup> by doing immunolabelling against tkv in both the notum and wing discs.

If all of this is confirmed, we will then check the requirement for MT in compression-driven competition. On one hand, we could check whether the tkv<sup>-/-</sup> clones are indeed eliminated by compression. Indeed, in that context, the mislocalisation of MT would be independent of scrib mispositioning. For this we could perform live imaging of these clones in the notum and apply mechanical inference. Additionally, we could trigger the contraction of the WT neighbouring cells by activating optoRhoGEF to prevent the potential compression of the clones. Then we can check if this prevents the elimination of the clone cells. On the other hand, we could stabilise microtubules in *scrib*<sup>KD</sup> clones and check if we rescue the probability of these cells being eliminated. For that, we could overexpress in *scrib*<sup>KD</sup> clones, aTAT1 (a MT acetylase which stabilises MT) or stabilising isoforms of Tau. Conversely, we could reduce MT stability by overexpression of HDAC (MT de-acetylase).

Finally, we could mimic cell compression by triggering local tissue relaxation and check this if this is sufficient to drive the elimination of clones lacking MT or with impaired MT organisation. For instance, we could do a large laser cut in the notum. Because the tissue is under tension, these will release tension and trigger local cell compaction. One could apply this approach to clones expressing lower levels of MTs or conversely stabilised MT and test their relative compression and elimination. Alternatively, we could use optoRhoGAP to release tension in WT cells which would similarly lead to the compaction of clonal cells. Taken together, these experiments will first confirm that polarity mutants are also eliminated because of differential resistance to compression in vivo. Second, it will enforce the role of MT in the stabilisation of apical areas and will provide an molecular mechanism for mechanical cell competition of polarity mutants.

#### 1.4.2. *Context-dependent roles of microtubules*

It is striking to see how microtubules can play very different roles and at different magnitudes depending on the context. The elimination of Larval Epidermal Cells during

the expansion of histoblasts is dependent on caspase activation similarly to what we have observed in the notum. However, in this case, the mechanism seems to rely mostly on the formation of an actomyosin ring and the increase of junctional tension rather than a change in MT. Why do some cells rely more or less on microtubule disassembly for cell extrusion? This discrepancy with our observation may be due to the differences in cell size. Indeed, large cells MT reach sizes more amenable for them to buckle. These considerations are well exemplified by studies on spindle/aster centring. Indeed, spindle centring is the result of a balance between pushing and pulling forces<sup>414</sup>. In small cells<sup>415</sup>, or in a microfabricated chamber, pushing forces are dominant and sufficient to explain aster centring<sup>416</sup>. When polymerising MT reach the cell boundaries, they produce a pushing force that positions the aster at the centre of the cell. This mechanism is not possible in larger cells<sup>417</sup>. Indeed, MT pushing forces inversely scale with their length<sup>418</sup>. This is because the compressive forces that they can bear are limited by their buckling<sup>419</sup>. Conversely, in large cells, aster or nuclear positioning is rather dependent on MT pulling forces mediated by Dynein motors associated with cargos<sup>420</sup>, or to the cortex<sup>418</sup>. Overall, these data support the idea that MT resistance to compression as a lower contribution to apical shape stabilisation of larger cells. As a result, larger cells like LECs would rely less on MT depletion and rather on MyoII contraction to induce apical constriction during extrusion. However, this remains to be tested.

Moreover, this may not be the only discrepancy between cell types. Many other parameters regulate MT resistance to compression. For instance, MT pushing forces scales with MT numbers and stiffness<sup>418</sup>. These could also mediate the differences between cell types. To assess this we could inject siTubulin in LECs and check the architecture and dynamics of their MT network using high resolution imaging.

Finally, depending on the cell type, MT can also be necessary to regulate cell constriction. In invaginating cells of the *Drosophila* salivary gland, MTs stabilise and maintain a pulsatile and medial actomyosin pool necessary for apical cell constriction and invagination<sup>162</sup>. Thus, the depletion of MTs through the overexpression of the severing protein Spastin lengthens MyoII pulses which impairs cell invagination. This is thought to be mediated by the relocalisation of the MTs minus-end organising factor Shot from the junctions to the medio-apical area. This is in contradiction with our observation that Spastin overexpression in clones in the notum is sufficient to drive cell constriction and cell extrusion. The difference between these two contexts is mainly the

orientation of MTs. Indeed, due to Shot relocalisation, MTs rotate between early and late embryonic stage 11 in the salivary gland. MTs undergo a 90° transition from an in-plane network at the junctional levels to an apicobasal array. Apicobasal MTs are organised by minus-end binding proteins that interact with myosin in different contexts<sup>147,148,158,159,421</sup>. This could explain the discrepancies with our results. Because this microtubule network is apicobasally oriented it is possible that it has a structural function preferentially along the apicobasal axis of the cell. At the same time, it would have a lower structural maintenance role in the apical junctional plane compared to the network we observed in the notum. As a result, MT role on MyoII activation would dominate in the salivary gland cells.

Ultimately, the overall contribution of MTs disassembly to apical constriction may be dependent on cortical stiffness/tension and cortex architecture. First, both factors regulate MT gliding and therefore the amount of compressive forces they can bear<sup>85,418,422</sup>. Second, MT disassembly may provide a way to constrict the cell without increasing actomyosin levels. Indeed, in an epithelium under very high tension such as the notum, it may be difficult to further increase tension to constrict a cell. Thus, lowering MT levels would constrict a cell through a local decrease in area elasticity, without increasing actomyosin levels. This may further explain the discrepancy between extrusion in the notum where tension is high and in LEC where tension is lower (personal data not shown).

## **1.5. Cell insertion**

Apical emergence is a process by which a cell radially intercalates in an already existing epithelium. Interesting parallels can be drawn between apical emergence and cell extrusion. Indeed, both processes involve a change in the local number of cells in the epithelial layer. This requires a drastic change in cell shape and the need to remodel adhesion to constantly maintain tissue sealing. Both processes, therefore, share similar features. For instance, both are cooperative. Accordingly, studies on the insertion of multiciliated cells (MCCs) in the *Xenopus* mucociliary epithelium have shown that apical emergence is a two-step process<sup>423</sup>. The first step of initial emergence is mostly regulated by cell-autonomous mechanisms and the later step involves pulling from neighbouring cells. Accordingly, increasing neighbouring cell rigidity by the expression of a constitutively active form of RhoA slowed down apical emergence and led to smaller emerging cells. Conversely, a dominant-negative RhoA triggered the opposite results<sup>423</sup>. This shows how tension and rigidification in the neighbours modulate cell insertion.

Similarly, the extrusion process depends on a cell-autonomous step followed by the formation of a supracellular actomyosin ring in the neighbours<sup>270</sup>. Likewise, this is modulated by tension in the neighbours. Hypertensile stress in the neighbours induced through caveolin1 knockdown inhibits cell extrusion of RasV12 cell in MDCK layers<sup>290</sup>. For the cell to extrude, the tension in orthogonal junctions is first immediately relaxed. This induces Src Kinase activation which further drives active mechanical relaxation to permit extrusion<sup>289</sup>.

Similarly, the apical area expansion of MCC shares similarities with cell extrusion and particularly with our results. Indeed, pulling forces from the neighbours only seem to dominate at the end of the process. Conversely, the initial emergence is driven by increasing 2D pressure inside the MCC. During that process, the cell remained round and most of the apical area changes were independent of changes in cell circularity. This is most certainly due to a homogenous pressure pushing on a rigid cortex. We observed similar behaviour during the onset of extrusion. The reduction of the area elasticity at the onset of extrusion induced a reduction of the apical area independent of changes in cell circularity. This supports the idea that pressure-induced area changes are shape-conservative during the initiation of both processes. The onset of extrusion in the notum is regulated by the disassembly of MT. Conversely, the increase of 2D pressure during MCC apical emergence has been shown to rely on formin-mediated actin pushing forces<sup>423</sup>. This would tend to point toward different mechanisms regulating the stability of the apical area in these two contexts.

However, it seems that microtubules are equally involved during the apical emergence of both MCC and ionocytes (ICs). First, Par3 is apically localised in inserting cells leading to the apical localisation of centrioles<sup>398,424</sup>. Interestingly, the number of centrioles correlates with the speed and timing of insertion. Indeed, ICs with fewer centrioles are inserted later than MCCs that are multiciliated (many centrioles). This is due to the centriole-mediated recruitment of MT. Accordingly, increasing the number of centrioles increased the number of microtubules and led to faster and precocious insertion. Second, apical localisation of the PAR complex apically recruits CLAMP<sup>424</sup>. CLAMP is a MAP that promotes MT stabilisation which is required for the apical emergence of both MCCs and ICs. Indeed, CLAMP morpholinos, specifically in the MCCs led to a majority of failed insertions similarly to decreased number of MT<sup>424</sup>. More precisely decreasing MT acetylation by the overexpression of HDAC led to delays in insertion. Conversely,

promoting MT acetylation by ATAT1 led to faster insertion<sup>397</sup>. This shows how MT stabilisation promotes cell insertion. It is still unclear how MTs promote cell insertion. MTs are preferentially oriented with their (+) end toward the apical side of both MCC and IC. However, inverting the polarity by the overexpression of CAMSAP (a minus-end binding) led to similar or even faster insertion speed<sup>398</sup>. Therefore, it argues against a role for MT-based pushing forces or directed trafficking. It rather suggests that regardless of their orientation MTs provide increased structural rigidity to the apical surface necessary for apical emergence. To further develop the parallel with extrusion in the notum, the stabilisation of MTs by taxol led to slower extrusion. Similarly, MT polymerisation leads to increased cell area in the notum. It shows how similar regulations can be differentially used in both the emergence and extrusion: promoting MT assembly or stability favours area extension during emergence and resists cell extrusion. Conversely, MT disassembly promotes cell extrusion and delays apical emergence. Taken together, this shows how microtubules can regulate cell pressure or at least the stability of the apical area.

## **2. Decision making**

In the third chapter of this PhD manuscript, I have shown that there is no unique caspase threshold above which cells enter extrusion in the notum. Rather, caspase activity modulates the probability to enter extrusion quasi-linearly like a ‘rheostat’. Therefore, cells’ sensitivity to caspase is set in a cell-dependent manner and varies across the tissue. Through a Bayesian statistical approach, we have demonstrated that past caspase activity 2 to 3 hours prior to cell extrusion increases the cell sensitivity to further caspase activation. Additionally, we have shown that cell area negatively correlates with the sensitivity to enter extrusion. Finally, the cell sensitivity seems to depend on both the development timing and the spatial position of the cell in the tissue. This argues for the existence of developmental regulation of caspase sensitivity through unidentified factors. These preliminary results are the first quantitatively investigating the decision-making leading to the irreversible commitment to cell extrusion. Here I will discuss putative mechanisms by which the past caspase activity may lower the sensitivity threshold of a cell to caspase. I will put these results in perspective with the main results of my PhD which showed that microtubule depletion is a limiting step for extrusion.

## 2.1. Parameters influencing the caspase threshold

### 2.1.1. *Single-cell caspase threshold*

The approach described in the chapter 3 mainly relies on correlative approaches. Therefore, we would first need to check whether the cell probability to enter extrusion scales linearly with the levels of caspases. For this, we could use optoDronc. This system allows to photo-activate Dronc (the initiator Caspase-9 homologue). We could drive UAS-OptoDronc expression under pnr-Gal4 to express the tool across the whole notum. We have recently identified regions in the notum with very low sensitivity to caspases on the lateral region on each part of the midline (results in collaboration with Tom Cumming, data not shown). Therefore, we could drive the activation of the tool in these regions to assess how the levels of caspase activation correlate with the probability to extrude. We will combine sublethal activation levels together with a graded activation in space in order to replicate the sigmoidal response we observed in the notum.

So far, our approach is only focused on parameters extracted from the segmentation of notum expressing UAS-GC3Ai. Therefore, we can only have access to morphology-related parameters or parameters related to caspase dynamics. Additionally, would need to look at reporters of the caspase cascade and their relationship with the caspase threshold. For instance, one could look at Diap1 or hid expression levels across the notum and correlate their levels to single-cell caspase thresholds. This would inform us on putative balance between the levels of inhibitors such as Diap1 and caspase levels. Indeed, this may also help to set the caspase threshold. So far, Hid-GFP levels seemed relatively homogenous in regions activating caspase. This would tend to suggest that local differences in pro-apoptotic genes expression cannot explain local differences in caspase threshold. Finally, several pieces of evidence show that the regulation of subcellular caspase dynamics or location (or their inhibitor) helps to set the balance between apoptotic and non-apoptotic caspase functions. Thus, it would be interesting to measure Diap1 dynamics across the notum. For this, we are currently building a Diap1-mScarlett Knock-In line in the lab. By coupling it with GC3Ai we will measure in real time the balance between caspases and their inhibitor. We are mainly using GC3Ai which reports for global caspases activation within the cell. It would be interesting to look at organelle-bound version of this tool. For instance, we could express a CAAX-GC3Ai reporter to specifically report for caspase levels at the membrane. On the long term, we will test whether caspase



activation at different location within the cell influences the probability of a cell to commit to extrusion and apoptosis.

### *2.1.2. Past caspase activity as a sensitizer?*

It seems that caspase activity from 2 to 3 hours prior to the inflexion sensitises the cell. Yet, this is only correlative. We will equally test the correlation between past caspase activity and the lower caspase threshold. The approach will be twofold. First, we will drive sublethal caspase activation in the lateral region using optoDronc. Then we will measure the probability of extrusion following a second sublethal pulse in that region 2h, 2.5h and 3h after the first induction. Because these lateral regions are symmetric on each side of the midline, we can then compare the probability of extrusion internally between the light-exposed side and the control side. This will tell us about the potential causal relationship between past-caspase activation and the probability to enter into extrusion. Finally, Florence Levillayer in the lab, has developed a non-tagged version of optoDronc. We have now coupled that tool with UAS-GC3Ai. Therefore, we will now be able to follow, the level of caspase activation upon optoDronc induction. We will repeat the previous experiments and see if we manage to reduce the caspase threshold 3h after sublethal induction of optoDronc.

We could observe that the threshold of caspase associated with the irreversible entry in extrusion reduces during the development of the notum. This would be coherent with the idea that past caspase activation sensitizes the cell for extrusion only if we assume that the average caspase level across the notum increases as well. To test this idea, one would need to measure for each time point the levels of caspases in all cells across the notum. First, this would be informative about the temporal regulation of caspase activation in the notum. Second, it will allow us to check if the correlation we observe is a tissue-wise property or is local.

We don't have yet a mechanism explaining how past caspase activity can increase cell sensitivity to caspase and lower the caspase threshold needed to enter in extrusion. Because of the proteolytic activity of caspase, it is expected that this effect is mediated by the cleavage of a caspase substrate. For instance, for past caspase activity to have a perduring effect, it could deplete a substrate that resists cell extrusion. Thus, this would be lowering the amount of caspase needed in the future to cleave the remaining substrate left. Caspase cleavage could initiate a slow positive feedback loop which could progressively lower the threshold. One hypothesis could be that Drice (Caspase-3

homologue) cleaves Diap1. Indeed, Diap1 can be cleaved by Drice and Dcp-1. This is thought to lower the caspase threshold necessary to enter in extrusion<sup>226,244</sup>. Indeed, the cleavage of Diap1 by Drice leads to its degradation by the N-rule pathway. This subsequently leads to progressively less inhibition of the caspase cascade and therefore a commitment to apoptosis at lower caspase levels. Yet, it is hard to foresee what would be the result of Diap1 cleavage in the notum. Indeed, Diap1 cleavage by Drice can also leads to its activation and triggers a negative feedback loop<sup>245</sup>. The turnover of Diap1 is close to 30min in the notum. Thus, any modulation of Diap1 turnover upon caspase activation would influence the caspase threshold by affecting the levels of inhibitors. We could test this hypothesis by expressing PRAP, a live reporter of Diap1 dynamics or Diap1-Venus<sup>376</sup>. Alternatively, we could use the Diap1-mScarlett Knock-In line currently under construction in the lab to quantitatively relate the turnover of DIAP to the caspase threshold.

### *2.1.3. Other predictive parameters and exploration*

I voluntarily didn't focus on the correlation between the cell area or perimeter with the caspase threshold. Indeed, such correlations may arise from the detection of the inflexion point. Because we detect the inflexion point when the cell starts to shrink, if there are imprecisions in the detection, we may artificially detect cells that are already smaller hence leading to a negative correlation. Therefore, these parameters would not be totally independent. Additionally, we would have to check nested correlation. We know from mapping cell sensitivity to caspase (work from Tom Cumming in the lab) that cells in the midline are more sensitive to caspase activation. Moreover, cells in this area are usually bigger. This could explain why we observe a negative correlation between the perimeter and the caspase threshold associated with the entry in extrusion (bigger cells tend to have lower caspase threshold).

Finally, to extend our approach, we could add non-linear correlations to the already existing ones. Indeed, caspase activity is exponentially increasing during the extrusion process. Thus, we could perform similar correlations between our parameters and the  $\log(\partial GC3AI)$  instead of  $\partial GC3AI$ . This will most likely increase some correlation values that we may have missed because of the non-linear increase of both GC3AI and  $\partial GC3AI$ . As I mentioned in part 2.1.1 of this chapter, we now have a spatial map of cell sensitivity to caspase activation. This tends to indicate that different regions have different sensitivity to caspase. To account for this regional effect, we could input non-autonomous

parameters into the model over time. For instance, we could measure the average tension in the direct neighbours or in small regions around an extruding cell. We could also focus on specific junctions. Indeed, it was shown before that tension in orthogonal junctions negatively regulates the ability of a cell to extrude<sup>290</sup>. This will allow us to evaluate how the neighbouring environment may affect the caspase threshold of an extruding cell. We would need to compare these data with tissue-wide properties. For instance, we know that the average tension in the notum is increasing over development<sup>280</sup>. Moreover, it seems that the caspase threshold associated with the entry in extrusion reduces over notum development. This would suggest a negative correlation between tension and the caspase threshold: higher tension would be associated with a lower threshold. This further highlights the need to apply inference methods across the notum to check this correlation. Finally, we could use a less biased approach by using neural networks. We could then screen the trained network to learn features that may not be intuitive at first (see part 3 of this chapter).

## **2.2. Microtubule depletion: a decision step?**

In this study, we have extensively used the inflexion of the perimeter as a readout of the decision-making leading to cell extrusion. Indeed, that point is the last point after which the cell irreversibly shrinks its apical area and never comes back. Interestingly, this point also corresponds to the moment where microtubules are disassembled from the medio-apical region. We have shown that this depletion of microtubules is a rate-limiting step for extrusion. Therefore, MT depletion may be one of the decision steps leading to the irreversible commitment to extrusion. We could imagine a mechanism by which the amount of caspases required to enter in extrusion corresponds to the quantity necessary to cleave enough MT to induce cell constriction. Cells with more microtubules will require higher caspase levels compared to cells with weaker MT pools.

After that, a positive feedback loop could ensure that the cell irreversibly commits to cell extrusion. Accordingly, microtubules are necessary to sequester Bim a pro-apoptotic member of the BCL-2 family. Bim binds to the light chain of the Dynein complex (a MT motor). Upon apoptotic signalling, Bim is released and binds to BCL-2 to inhibit its anti-apoptotic function in mouse kidney cell lines<sup>425</sup>. In this context, Bim is released prior to caspase activation. Thus, it suggests it acts as an initiating event of apoptosis. Yet, other results show that caspase activity also leads to the cleavage of Dynein<sup>426,427</sup>. This could be a putative mechanism by which microtubules act as a key decision step. The initiation

of MTs cleavage or the cleavage of interactors such as Dyneins would then lead to a positive feedback loop ensuring that the cell irreversibly commits to extrusion. In *Drosophila* Bim function is supported by its homologue BH3-only Debel which inhibits the BCL-2 homologue Buffy<sup>428,429</sup>. Whether the proposed mechanism could also take place in *Drosophila* is purely speculative. Indeed, there is currently no proof of Debel interaction with MTs. It rather seems that Debel and Buffy are both localised to the mitochondrial membrane<sup>430</sup>.

Alternatively, MT disassembly could affect the probability to enter extrusion in a more direct way. For instance, because the depletion of MT increases the constriction yield, their depletion could precipitate the cell toward cell extrusion. Accordingly, a cell with a less dense MT network would require less caspase activation to disassemble that network. Therefore, the extrusion of that cell would happen at a lower caspase threshold. MTs depletion is the only rate-limiting step prior to extrusion commitment that we could observe so far. Therefore, it is likely to somewhat play a role in the decision-making step prior to extrusion commitment. At the moment, we do not have any information about the MT network or the actomyosin levels in our predictive pipeline. If we observe any parameters that may be related to these factors, it would be interesting to couple our pipeline with the expression of reporters for these factors.

### **3. Prediction of cell death**

In the last part of my PhD manuscript, I have developed together with Gaëlle Letort a method to automatically detect cell extrusion in epithelial tissue. This tool would be very useful to increase the speed of analysis and therefore increase the statistical power for the analysis of temporal events in epithelia. I have shown a proof of concept for this tool using the detection of cell extrusion: Dextrusion. However, this tool can be equally useful to detect events such as cell division, provided the good training data. Accordingly, one could imagine generalising this tool to the analysis of any temporal events taking place in epithelial tissue if one has the initial training data. Hereafter, I will discuss different ways to use this tool which could be the subject of further development.

#### **3.1. Can we harvest the model to find predictive features of extrusion?**

So far, we have tested the network to predict cell extrusion by focusing on the accuracy of detection. We did that in two ways. First, to specifically detect extrusion, we set a threshold to select only predictions associated with high probability. Second, prior to

this, we provided the network with time series centred around the termination of extrusion (7 frames before the closure and 5 steps after). Thus, the predictive output of the network is expected to be maximum at closure. We could train the network with data only prior to the extrusion. Then we could try to screen the network to find features that are predictive for extrusion. The rationale to build a homemade model was to make it complex enough to learn to recognize extrusion but simple enough so that we can try to reverse-engineer the network. Indeed, highly efficient models exist to perform segmentation such as LinkNet, or classification problems and image-captioning problems such as ImageNet (AlexNet) or GoogleNet<sup>431,432</sup>. However, they have high number of convolution layers and densely connected layers. This makes it impossible to understand the decision-making happening in these networks and leading to the classification. That's why deep learning is considered a 'black box'. Yet, deconstructing and interpreting neural networks has recently been proven to be very useful. For instance, a generative neural network was used to classify patient-derived melanoma cells depending on their metastatic abilities<sup>433</sup>. The neural network first generated a latent representation of the input images and made a classification out of that. This step is called the encoder. Then a decoder was used to reconstruct the image based on the latent representation. The low number of features allows to find the most predictive feature of the classification. One can then explore/tune these most predictive features and check how they relate to biological meaning. Through the exaggeration of the most significant feature, the images showed pseudopodia-like extensions and increased light scattering. These were then confirmed by live imaging. Therefore, it allowed the identification of cellular properties predictive of metastatic susceptibility that are hard for the user to identify just by looking at the image<sup>433</sup>. A similar approach could be used with our model.

We could train the network with image sequences prior to the extrusion or even prior to the decision point. We could then screen the network to find the most predictive node and check if we manage to relate that to cellular features. Through this means we could learn new features predictive of the decision to enter in extrusion. However, this network is not amenable to predicting the cell sensitivity to caspase. Indeed, one would need to pair data between images of extruding cells and corresponding caspase threshold levels. Nevertheless, an approach similar to the one just described could be used to find features less biased compared to the one set by the user.

### **3.2. How to use the model for something else?**

Finally, if we manage to detect and predict cell extrusion or division enough in advance, we could predict the event live during imaging at the microscope. This would allow adapting the imaging to explore questions that we cannot answer at the moment. For instance, we still are unaware of potential changes in microtubule dynamics prior to the onset compared to after. If we could detect in advance the cell that extrude, we could zoom on that cell and perform for instance FRAP on  $\alpha$ -tubulin-GFP before and after the onset to check potential changes in network's turnover. As a results we could quantitatively measure dynamic behaviour which we can't currently access.

# Table of Illustrations

<b>Figure 1</b> - Epithelial organization.	21
<b>Figure 2</b> - Mechanical parameters.	25
<b>Figure 3</b> - In-plane tissue deformation through cell death and cell shape changes.	26
<b>Figure 4</b> - Out-of-plane tissue deformations through cell death and cell shape changes.	28
<b>Figure 5</b> - Globular actin, filamentous actin, polymerization.	32
<b>Figure 6</b> - Diversity in the regulation of the actin network.	34
<b>Figure 7</b> - Regulation of polymerisation.	35
<b>Figure 8</b> - depolymerization mechanisms:	37
<b>Figure 9</b> - crosslinking.	39
<b>Figure 10</b> - Rho-GTPases cycle.	40
<b>Figure 11</b> - Myosin motors.	42
<b>Figure 12</b> - Mechanisms of pulse generation.	43
<b>Figure 13</b> - Actomyosin pulses during endoderm invagination.	45
<b>Figure 14</b> - actomyosin ring.	46
<b>Figure 15</b> - Ecad structure and adhesion.	49
<b>Figure 16</b> - E-cad influence on morphogenesis.	52
<b>Figure 17</b> - Microtubule structure and dynamics.	55
<b>Figure 18</b> - Microtubule interactors.	56
<b>Figure 19</b> - MT affects cell morphogenesis through interactions with the actomyosin cortex.	58
<b>Figure 20</b> - Roles of MT in morphogenesis.	62
<b>Figure 21</b> - death diversity.	71
<b>Figure 22</b> - Role of apoptosis during development.	74
<b>Figure 23</b> - Caspases family.	77
<b>Figure 24</b> - conservation of the apoptosis pathway between	79
<b>Figure 25</b> - BCL2 superfamily.	82
<b>Figure 26</b> - Caspase substrate specificity and conservation.	85
<b>Figure 27</b> - Some drivers of extrusion.	91
<b>Figure 28</b> - contraction during cell extrusion.	95
<b>Figure 29</b> - Apical or basal & the role of S1P signalling.	98
<b>Figure 30</b> - Caspases and extrusion.	101

<b>Figure 31</b> - Summary of non-apoptotic caspases functions.	132
<b>Figure 32</b> - Caspase-dependent regulation of cell proliferation.	134
<b>Figure 33</b> - Caspase-dependent cellular remodelling.	136
<b>Figure 34</b> - Caspase-dependent regulation of cell differentiation.	139
<b>Figure 35</b> - non-apoptotic caspase functions by limiting caspase levels.	144
<b>Figure 36</b> - Dynamic regulations of caspases & their proteolytic activity.	145
<b>Figure 37</b> - Spatial caspase regulation..	148
<b>Figure 38</b> - Anastasis: caspase threshold.	150
<b>Figure 39</b> - Quantification of caspase activity.	154
<b>Figure 40</b> - Threshold detection & probability to be in extrusion.	155
<b>Figure 41</b> - Prediction of the threshold value.	157
<b>Figure 42</b> - Spatio-temporal statistics of cell sensitivity to caspase.	159
<b>Figure 43</b> - Schematic of the linear regression process.	170
<b>Figure 44</b> - Classification.	172
<b>Figure 45</b> - The Perceptron.	173
<b>Figure 46</b> - image as a matrix.	174
<b>Figure 47</b> - propagations.	175
<b>Figure 48</b> - Recurrence in Neural Networks.	176
<b>Figure 49</b> - Description of the dataset..	179
<b>Figure 50</b> - Model architecture and training.	182
<b>Figure 51</b> - model prediction on full movies.	183



## References

1. Leys, S. P. & Riesgo, A. Epithelia, an evolutionary novelty of metazoans. *Journal of Experimental Zoology Part B: Molecular and Developmental Evolution* **318**, 438–447 (2012).
2. Dudin, O. *et al.* A Unicellular Relative of Animals Generates an Epithelium-Like Cell Layer by Actomyosin-dependent Cellularization. *SSRN Electronic Journal* **8**, (2019).
3. and, U. T., Tanentzapf, G., and, R. W. & Fehon, R. Epithelial Cell Polarity and Cell Junctions in *Drosophila*. <http://dx.doi.org/10.1146/annurev.genet.35.102401.091415> **35**, 747–784 (2003).
4. Watson, A. J. M., Duckworth, C. A., Guan, Y. & Montrose, M. H. Mechanisms of epithelial cell shedding in the mammalian intestine and maintenance of barrier function. *Ann N Y Acad Sci* **1165**, 135–142 (2009).
5. Schweisguth, F., Lepesant, J. A. & Vincent, A. The serendipity alpha gene encodes a membrane-associated protein required for the cellularization of the *Drosophila* embryo. *Genes & Development* **4**, 922–931 (1990).
6. Tanentzapf, G. & Tepass, U. Interactions between the crumbs, lethal giant larvae and bazooka pathways in epithelial polarization. *Nature Cell Biology* *2002 5:1* **5**, 46–52 (2002).
7. Bilder, D., Schober, M. & Perrimon, N. Integrated activity of PDZ protein complexes regulates epithelial polarity. *Nature Cell Biology* *2002 5:1* **5**, 53–58 (2002).
8. Harris, T. J. C. & Peifer, M. Adherens junction-dependent and -independent steps in the establishment of epithelial cell polarity in *Drosophila*. *Journal of Cell Biology* **167**, 135–147 (2004).
9. Salbreux, G., Charras, G. & Paluch, E. Actin cortex mechanics and cellular morphogenesis. *Trends in Cell Biology* **22**, 536–545 (2012).
10. Brückner, B. R. & Janshoff, A. Elastic properties of epithelial cells probed by atomic force microscopy. *Biochimica et Biophysica Acta (BBA) - Molecular Cell Research* **1853**, 3075–3082 (2015).
11. Takeichi, M. Historical review of the discovery of cadherin, in memory of Tokindo Okada. *Development, Growth & Differentiation* **60**, 3–13 (2018).
12. Furuse, M. *et al.* Claudin-based tight junctions are crucial for the mammalian epidermal barrier: A lesson from claudin-1-deficient mice. *Journal of Cell Biology* **156**, 1099–1111 (2002).
13. Markov, A. G., Aschenbach, J. R. & Amasheh, S. Claudin clusters as determinants of epithelial barrier function. *IUBMB Life* **67**, 29–35 (2015).

14. Burridge, K. Focal adhesions: a personal perspective on a half century of progress. *FEBS Journal* **284**, 3355–3361 (2017).
15. Collinet, C. & Lecuit, T. Programmed and self-organized flow of information during morphogenesis. *Nature Reviews Molecular Cell Biology* (2021) doi:10.1038/s41580-020-00318-6.
16. Lecuit, T. & Lenne, P. F. Cell surface mechanics and the control of cell shape, tissue patterns and morphogenesis. *Nature Reviews Molecular Cell Biology* 2007 8:8 **8**, 633–644 (2007).
17. Salbreux, G., Charras, G. & Paluch, E. Actin cortex mechanics and cellular morphogenesis. *Trends in Cell Biology* **22**, 536–545 (2012).
18. Kelkar, M., Bohec, P. & Charras, G. Mechanics of the cellular actin cortex: From signalling to shape change. *Current Opinion in Cell Biology* **66**, 69–78 (2020).
19. Chugh, P. *et al.* Actin cortex architecture regulates cell surface tension. *Nature Cell Biology* 2017 19:6 **19**, 689–697 (2017).
20. Gilmour, D., Rembold, M. & Leptin, M. From morphogen to morphogenesis and back. *Nature* 2017 541:7637 **541**, 311–320 (2017).
21. Lecuit, T. & le Goff, L. Orchestrating size and shape during morphogenesis. *Nature* 2007 450:7167 **450**, 189–192 (2007).
22. Munjal, A., Hannezo, E., Tsai, T. Y. C., Mitchison, T. J. & Megason, S. G. Extracellular hyaluronate pressure shaped by cellular tethers drives tissue morphogenesis. *Cell* **184**, 6313–6325.e18 (2021).
23. Nishimura, T. & Takeichi, M. Shroom3-mediated recruitment of Rho kinases to the apical cell junctions regulates epithelial and neuroepithelial planar remodeling. *Development* **135**, 1493–1502 (2008).
24. Yen, W. W. *et al.* PTK7 is essential for polarized cell motility and convergent extension during mouse gastrulation. *Development* **136**, 2039–2048 (2009).
25. Williams, M., Yen, W., Lu, X. & Sutherland, A. Distinct apical and basolateral mechanisms drive planar cell polarity-dependent convergent extension of the mouse neural plate. *Developmental Cell* **29**, 34–46 (2014).
26. Wallingford, J. B. & Harland, R. M. Neural tube closure requires Dishevelled-dependent convergent extension of the midline. *Development* **129**, 5815–5825 (2002).
27. Rozbicki, E. *et al.* Myosin-II-mediated cell shape changes and cell intercalation contribute to primitive streak formation. *Nature Cell Biology* 2014 17:4 **17**, 397–408 (2015).
28. Irvine, K. D. & Wieschaus, E. Cell intercalation during Drosophila germband extension and its regulation by pair-rule segmentation genes. *Development* **120**, 827–841 (1994).
29. Bertet, C., Sulak, L. & Lecuit, T. Myosin-dependent junction remodelling controls planar cell intercalation and axis elongation. *Nature* 2004 429:6992 **429**, 667–671 (2004).

30. Blankenship, J. T., Backovic, S. T., Sanny, J. S. S. P., Weitz, O. & Zallen, J. A. Multicellular Rosette Formation Links Planar Cell Polarity to Tissue Morphogenesis. *Developmental Cell* **11**, 459–470 (2006).
31. Elul, T. & Keller, R. Monopolar Protrusive Activity: A New Morphogenic Cell Behavior in the Neural Plate Dependent on Vertical Interactions with the Mesoderm in *Xenopus*. *Developmental Biology* **224**, 3–19 (2000).
32. Davidson, L. A. & Keller, R. E. Neural tube closure in *Xenopus laevis* involves medial migration, directed protrusive activity, cell intercalation and convergent extension. *Development* **126**, 4547–4556 (1999).
33. Weng, S., Huebner, R. J. & Wallingford, J. B. Convergent extension requires adhesion-dependent biomechanical integration of cell crawling and junction contraction. *Cell Reports* **39**, 110666 (2022).
34. Mangione, F. & Martín-Blanco, E. The Dachshous/Fat/Four-Jointed Pathway Directs the Uniform Axial Orientation of Epithelial Cells in the *Drosophila* Abdomen. *Cell Reports* **25**, 2836-2850.e4 (2018).
35. Diaz-de-la-Loza, M. del C. *et al.* Apical and Basal Matrix Remodeling Control Epithelial Morphogenesis. *Developmental Cell* **46**, 23-39.e5 (2018).
36. Widmann, T. J. & Dahmann, C. Dpp signaling promotes the cuboidal-to-columnar shape transition of *Drosophila* wing disc epithelia by regulating Rho1. *Journal of Cell Science* **122**, 1362–1373 (2009).
37. Teng, X., Qin, L., le Borgne, R. & Toyama, Y. Remodeling of adhesion and modulation of mechanical tensile forces during apoptosis in *Drosophila* epithelium. *Development (Cambridge)* **144**, 95–105 (2017).
38. Muliylil, S., Krishnakumar, P. & Narasimha, M. Spatial, temporal and molecular hierarchies in the link between death, delamination and dorsal closure. *Development* **138**, 3043–3054 (2011).
39. Leptin, M. & Grunewald, B. Cell shape changes during gastrulation in *Drosophila*. *Development* **110**, 73–84 (1990).
40. Baker, P. C. & Schroeder, T. E. Cytoplasmic filaments and morphogenetic movement in the amphibian neural tube. *Developmental Biology* **15**, 432–450 (1967).
41. Kakfunkel, P. The Activity of Microtubules and Microfilaments in Neurulation in the Chick.
42. Martin, A. C., Kaschube, M. & Wieschaus, E. F. Pulsed contractions of an actin-myosin network drive apical constriction. *Nature* **457**, 495–499 (2009).
43. Chung, M. I., Nascone-Yoder, N. M., Grover, S. A., Drysdale, T. A. & Wallingford, J. B. Direct activation of Shroom3 transcription by Pitx proteins drives epithelial morphogenesis in the developing gut. *Development* **137**, 1339–1349 (2010).

44. Burnside, B. Microtubules and microfilaments in newt neurulation. *Developmental Biology* **26**, 416–441 (1971).
45. Krueger, D., Tardivo, P., Nguyen, C. & Renzis, S. de. Downregulation of basal myosin-II is required for cell shape changes and tissue invagination. *The EMBO Journal* **37**, e100170 (2018).
46. Hildebrand, J. D. & Soriano, P. Shroom, a PDZ Domain-Containing Actin-Binding Protein, Is Required for Neural Tube Morphogenesis in Mice. *Cell* **99**, 485–497 (1999).
47. Roellig, D. *et al.* Force-generating apoptotic cells orchestrate avian neural tube bending. *Dev Cell* **57**, 707-718.e6 (2022).
48. Martin, A. C. & Goldstein, B. Apical constriction: themes and variations on a cellular mechanism driving morphogenesis. *Development* **141**, 1987–1998 (2014).
49. Martin, A. C., Gelbart, M., Fernandez-Gonzalez, R., Kaschube, M. & Wieschaus, E. F. Integration of contractile forces during tissue invagination. *Journal of Cell Biology* **188**, 735–749 (2010).
50. Vasquez, C. G. & Martin, A. C. Force transmission in epithelial tissues. *Developmental Dynamics* **245**, 361–371 (2016).
51. Ko, C. S., Tserunyan, V. & Martin, A. C. Microtubules promote intercellular contractile force transmission during tissue folding. *The Journal of Cell Biology* **218**, 2726–2742 (2019).
52. Wang, Y. C., Khan, Z., Kaschube, M. & Wieschaus, E. F. Differential positioning of adherens junctions is associated with initiation of epithelial folding. *Nature* **2012** 484:7394 **484**, 390–393 (2012).
53. Lohmann, I., McGinnis, N., Bodmer, M. & McGinnis, W. The Drosophila Hox Gene Deformed Sculpts Head Morphology via Direct Regulation of the Apoptosis Activator reaper. *Cell* **110**, 457–466 (2002).
54. Monier, B. *et al.* Apico-basal forces exerted by apoptotic cells drive epithelium folding. *Nature* **518**, 245–248 (2015).
55. Röper, K. Microtubules enter centre stage for morphogenesis. *Philosophical Transactions of the Royal Society B* **375**, 20190557 (2020).
56. Dogterom, M. & Koenderink, G. H. Actin–microtubule crosstalk in cell biology. *Nature Reviews Molecular Cell Biology* **2018** 20:1 **20**, 38–54 (2018).
57. Ingber, D. E. Tensegrity I. Cell structure and hierarchical systems biology. *Journal of Cell Science* **116**, 1157–1173 (2003).
58. Ingber, D. E. Tensegrity II. How structural networks influence cellular information processing networks. *Journal of Cell Science* **116**, 1397–1408 (2003).
59. Pollard, T. D. & Cooper, J. A. Actin, a central player in cell shape and movement. *Science* (1979) **326**, 1208–1212 (2009).

60. Prost, J., Jülicher, F. & Joanny, J. F. Active gel physics. *Nature Physics* 2014 11:2 **11**, 111–117 (2015).
61. Pollard, T. D. & Borisy, G. G. Cellular Motility Driven by Assembly and Disassembly of Actin Filaments. *Cell* **112**, 453–465 (2003).
62. Lee, S. H. & Dominguez, R. Regulation of actin cytoskeleton dynamics in cells. *Molecules and Cells* 2010 29:4 **29**, 311–325 (2010).
63. Welch, M. D. & Mullins, R. D. Cellular Control of Actin Nucleation. <http://dx.doi.org/10.1146/annurev.cellbio.18.040202.112133> **18**, 247–288 (2003).
64. Zallen, J. A. *et al.* SCAR is a primary regulator of Arp2/3-dependent morphological events in Drosophila. *Journal of Cell Biology* **156**, 689–701 (2002).
65. Martin, E. *et al.* Arp2/3-dependent mechanical control of morphogenetic robustness in an inherently challenging environment. *Developmental Cell* **56**, 687-701.e7 (2021).
66. Chen, Q. & Pollard, T. D. Actin filament severing by cofilin is more important for assembly than constriction of the cytokinetic contractile ring. *Journal of Cell Biology* **195**, 485–498 (2011).
67. Chan, C., Beltzner, C. C. & Pollard, T. D. Cofilin Dissociates Arp2/3 Complex and Branches from Actin Filaments. *Current Biology* **19**, 537–545 (2009).
68. Homem, C. C. F. & Peifer, M. Diaphanous regulates myosin and adherens junctions to control cell contractility and protrusive behavior during morphogenesis. *Development* **135**, 1005–1018 (2008).
69. Higgs, H. N. Formin proteins: a domain-based approach. *Trends in Biochemical Sciences* **30**, 342–353 (2005).
70. Courtemanche, N. Mechanisms of formin-mediated actin assembly and dynamics. *Biophysical Reviews* **10**, 1553 (2018).
71. Pantaloni, D., le Clainche, C. & Carlier, M. F. Mechanism of actin-based motility. *Science (1979)* **292**, 1502–1506 (2001).
72. Blanchoin, L., Boujemaa-Paterski, R., Sykes, C. & Plastino, J. Actin dynamics, architecture, and mechanics in cell motility. *Physiological Reviews* **94**, 235–263 (2014).
73. Berro, J., Michelot, A., Blanchoin, L., Kovar, D. R. & Martiel, J. L. Attachment Conditions Control Actin Filament Buckling and the Production of Forces. *Biophysical Journal* **92**, 2546–2558 (2007).
74. Vogel, S. K., Petrasek, Z., Heinemann, F. & Schwille, P. Myosin motors fragment and compact membrane-bound actin filaments. *Elife* **2013**, (2013).
75. Levayer, R. & Lecuit, T. Biomechanical regulation of contractility: spatial control and dynamics. *Trends in Cell Biology* **22**, 61–81 (2012).
76. Koenderink, G. H. & Paluch, E. K. Architecture shapes contractility in actomyosin networks. *Current Opinion in Cell Biology* **50**, 79–85 (2018).

77. Klein, M. G. *et al.* Structure of the Actin Crosslinking Core of Fimbrin. *Structure* **12**, 999–1013 (2004).
78. Stossel, T. P. *et al.* Filamins as integrators of cell mechanics and signalling. *Nature Reviews Molecular Cell Biology* *2001 2:2* **2**, 138–145 (2001).
79. Jodoin, J. N. *et al.* Stable Force Balance between Epithelial Cells Arises from F-Actin Turnover. *Developmental Cell* **35**, 685–697 (2015).
80. Fox, D. T. & Peifer, M. Abelson kinase (Abl) and RhoGEF2 regulate actin organization during cell constriction in *Drosophila*. *Development* **134**, 567–578 (2007).
81. Laporte, D., Ojčić, N., Vavylonis, D. & Wu, J. Q.  $\alpha$ -actinin and fimbrin cooperate with myosin II to organize actomyosin bundles during contractile-ring assembly. *Molecular Biology of the Cell* **23**, 3094–3110 (2012).
82. Reymann, A. C. *et al.* Actin network architecture can determine myosin motor activity. *Science (1979)* **336**, 1310–1314 (2012).
83. Koenderink, G. H. & Paluch, E. K. Architecture shapes contractility in actomyosin networks. *Current Opinion in Cell Biology* **50**, 79–85 (2018).
84. Yu, Q., Li, J., Murrell, M. P. & Kim, T. Balance between Force Generation and Relaxation Leads to Pulsed Contraction of Actomyosin Networks. *Biophysical Journal* **115**, 2003–2013 (2018).
85. Ennomani, H. *et al.* Architecture and Connectivity Govern Actin Network Contractility. *Current Biology* **26**, 616–626 (2016).
86. Bretscher, A., Edwards, K. & Fehon, R. G. ERM proteins and merlin: integrators at the cell cortex. *Nature Reviews Molecular Cell Biology* *2002 3:8* **3**, 586–599 (2002).
87. Etienne-Manneville, S. & Hall, A. Rho GTPases in cell biology. *Nature* *2002 420:6916* **420**, 629–635 (2002).
88. Matsumura, F. Regulation of myosin II during cytokinesis in higher eukaryotes. *Trends in Cell Biology* **15**, 371–377 (2005).
89. Humphrey, D., Duggan, C., Saha, D., Smith, D. & Käs, J. Active fluidization of polymer networks through molecular motors. *Nature* *2002 416:6879* **416**, 413–416 (2002).
90. Sellers, J. R. Myosins: a diverse superfamily. *Biochimica et Biophysica Acta (BBA) - Molecular Cell Research* **1496**, 3–22 (2000).
91. Holden, H. M. *et al.* Structure of the actin-myosin complex and its implications for muscle contraction. *Science (1979)* **261**, 58–65 (1993).
92. Vicente-Manzanares, M., Ma, X., Adelstein, R. S. & Horwitz, A. R. Non-muscle myosin II takes centre stage in cell adhesion and migration. *Nat Rev Mol Cell Biol* **10**, 778 (2009).
93. Finer, J. T., Simmons, R. M. & Spudis, J. A. Single myosin molecule mechanics: piconewton forces and nanometre steps. *Nature* *1994 368:6467* **368**, 113–119 (1994).

94. Köhler, S., Schaller, V. & Bausch, A. R. Structure formation in active networks. *Nature Materials* 2011 10:6 **10**, 462–468 (2011).
95. Sedzinski, J. *et al.* Polar actomyosin contractility destabilizes the position of the cytokinetic furrow. *Nature* 2011 476:7361 **476**, 462–466 (2011).
96. Roh-Johnson, M. *et al.* Triggering a cell shape change by exploiting preexisting actomyosin contractions. *Science (1979)* **335**, 1232–1235 (2012).
97. Munro, E., Nance, J. & Priess, J. R. Cortical flows powered by asymmetrical contraction transport PAR proteins to establish and maintain anterior-posterior polarity in the early *C. elegans* embryo. *Developmental Cell* **7**, 413–424 (2004).
98. Haviv, L., Gillo, D., Backouche, F. & Bernheim-Groswasser, A. A Cytoskeletal Demolition Worker: Myosin II Acts as an Actin Depolymerization Agent. *Journal of Molecular Biology* **375**, 325–330 (2008).
99. Lenz, M., Thoresen, T., Gardel, M. L. & Dinner, A. R. Contractile units in disordered actomyosin bundles arise from f-actin buckling. *Physical Review Letters* **108**, 238107 (2012).
100. Coravos, J. S. & Martin, A. C. Apical Sarcomere-like Actomyosin Contracts Nonmuscle *Drosophila* Epithelial Cells. *Developmental Cell* **39**, 346–358 (2016).
101. He, L., Wang, X., Tang, H. L. & Montell, D. J. Tissue elongation requires oscillating contractions of a basal actomyosin network. *Nature Cell Biology* 2010 12:12 **12**, 1133–1142 (2010).
102. Pérez-Verdugo, F., Reig, G., Cerda, M., Concha, M. L. & Soto, R. Geometrical characterization of active contraction pulses in epithelial cells using the two-dimensional vertex model. *Journal of the Royal Society Interface* **19**, (2022).
103. Solon, J., Kaya-Çopur, A., Colombelli, J. & Brunner, D. Pulsed Forces Timed by a Ratchet-like Mechanism Drive Directed Tissue Movement during Dorsal Closure. *Cell* **137**, 1331–1342 (2009).
104. Martin, A. C. Pulsation and stabilization: Contractile forces that underlie morphogenesis. *Developmental Biology* **341**, 114–125 (2010).
105. Vasquez, C. G., Tworoger, M. & Martin, A. C. Dynamic myosin phosphorylation regulates contractile pulses and tissue integrity during epithelial morphogenesis. *Journal of Cell Biology* **206**, 435–450 (2014).
106. Michaux, J. B., Robin, F. B., McFadden, W. M. & Munro, E. M. Excitable RhoA dynamics drive pulsed contractions in the early *C. Elegans* embryo. *Journal of Cell Biology* **217**, 4230–4252 (2018).
107. Jülicher, F. & Prost, J. Cooperative molecular motors. *Physical Review Letters* **75**, 2618–2621 (1995).

108. Julicher, F. & Prost, J. Spontaneous Oscillations of Collective Molecular Motors. *Physical Review Letters* **78**, 4510–4513 (1996).
109. Plaças, P. Y., Balland, M., Guérin, T., Joanny, J. F. & Martin, P. Spontaneous oscillations of a minimal actomyosin system under elastic loading. *Physical Review Letters* **103**, (2009).
110. Franke, J. D., Montague, R. A. & Kiehart, D. P. Nonmuscle Myosin II Generates Forces that Transmit Tension and Drive Contraction in Multiple Tissues during Dorsal Closure. *Current Biology* **15**, 2208–2221 (2005).
111. Atieh, Y., Wyatt, T., Zaske, A. M. & Eisenhoffer, G. T. Pulsatile contractions promote apoptotic cell extrusion in epithelial tissues. *Current Biology* (2021) doi:10.1016/j.cub.2020.12.005.
112. An, Y. *et al.* Apical constriction is driven by a pulsatile apical myosin network in delaminating *Drosophila* neuroblasts. *Development (Cambridge)* **144**, 2153–2164 (2017).
113. Xue, Z. & Sokac, A. M. Back-to-back mechanisms drive actomyosin ring closure during *drosophila* embryo cleavage. *Journal of Cell Biology* **215**, 335–344 (2016).
114. Herszterg, S., Pinheiro, D. & Bellaïche, Y. A multicellular view of cytokinesis in epithelial tissue. *Trends in Cell Biology* vol. 24 285–293 Preprint at <https://doi.org/10.1016/j.tcb.2013.11.009> (2014).
115. Harrison, O. J. *et al.* The Extracellular Architecture of Adherens Junctions Revealed by Crystal Structures of Type I Cadherins. *Structure* **19**, 244–256 (2011).
116. Brasch, J., Harrison, O. J., Honig, B. & Shapiro, L. Thinking outside the cell: how cadherins drive adhesion. *Trends in Cell Biology* **22**, 299–310 (2012).
117. Takeichi, M. Dynamic contacts: rearranging adherens junctions to drive epithelial remodelling. *Nature Reviews Molecular Cell Biology* 2014 15:6 **15**, 397–410 (2014).
118. Rakshit, S., Zhang, Y., Manibog, K., Shafraz, O. & Sivasankar, S. Ideal, catch, and slip bonds in cadherin adhesion. *Proc Natl Acad Sci U S A* **109**, 18815–18820 (2012).
119. Hansen, S. D. *et al.*  $\alpha$ -catenin actin-binding domain alters actin filament conformation and regulates binding of nucleation and disassembly factors. *Molecular Biology of the Cell* **24**, 3710–3720 (2013).
120. Seddiki, R. *et al.* Force-dependent binding of vinculin to  $\alpha$ -catenin regulates cell–cell contact stability and collective cell behavior. *Molecular Biology of the Cell* **29**, 380–388 (2018).
121. Buckley, C. D. *et al.* The minimal cadherin-catenin complex binds to actin filaments under force. *Science (1979)* **346**, (2014).
122. Shewan, A. M. *et al.* Myosin 2 Is a Key Rho Kinase Target Necessary for the Local Concentration of E-Cadherin at Cell-Cell Contacts □ D. *Molecular Biology of the Cell* **16**, 4531–4542 (2005).



123. Ratheesh, A. *et al.* Centralspindlin and  $\alpha$ -catenin regulate Rho signalling at the epithelial zonula adherens. *Nature Cell Biology* 2012 14:8 **14**, 818–828 (2012).
124. Yonemura, S., Hirao-Minakuchi, K. & Nishimura, Y. Rho localization in cells and tissues. *Experimental Cell Research* **295**, 300–314 (2004).
125. Smith, A. L., Dohn, M. R., Brown, M. v. & Reynolds, A. B. Association of Rho-associated protein kinase 1 with E-cadherin complexes is mediated by p120-catenin. *Molecular Biology of the Cell* **23**, 99–110 (2012).
126. Levayer, R. & Lecuit, T. Oscillation and Polarity of E-Cadherin Asymmetries Control Actomyosin Flow Patterns during Morphogenesis. *Developmental Cell* **26**, 162–175 (2013).
127. Lecuit, T. & Yap, A. S. E-cadherin junctions as active mechanical integrators in tissue dynamics. *Nature Publishing Group* (2015) doi:10.1038/ncb3136.
128. Kale, G. R. *et al.* Distinct contributions of tensile and shear stress on E-cadherin levels during morphogenesis. *Nature Communications* **9**, (2018).
129. Cavanaugh, K. E. *et al.* Force-dependent intercellular adhesion strengthening underlies asymmetric adherens junction contraction. *Current Biology* **32**, 1986–2000.e5 (2022).
130. Duszyc, K. *et al.* Mechanotransduction activates RhoA in the neighbors of apoptotic epithelial cells to engage apical extrusion. *Current Biology* (2021) doi:10.1016/j.cub.2021.01.003.
131. Leerberg, J. M. *et al.* Tension-sensitive actin assembly supports contractility at the epithelial zonula adherens. *Current Biology* **24**, 1689–1699 (2014).
132. Michael, M. *et al.* Coronin 1B Reorganizes the Architecture of F-Actin Networks for Contractility at Steady-State and Apoptotic Adherens Junctions. *Developmental Cell* **37**, 58–71 (2016).
133. Acharya, B. R. *et al.* A Mechanosensitive RhoA Pathway that Protects Epithelia against Acute Tensile Stress. *Developmental Cell* **47**, 439–452.e6 (2018).
134. Mandelkow, E. M., Schultheiss, R., Rapp, R. & Müller, M. On the surface lattice of microtubules: helix starts, protofilament number, seam, and handedness. *Journal of Cell Biology* **102**, 1067–1073 (1986).
135. Akhmanova, A. & Steinmetz, M. O. Control of microtubule organization and dynamics: two ends in the limelight. *Nature Reviews Molecular Cell Biology* 2015 16:12 **16**, 711–726 (2015).
136. Akhmanova, A. & Steinmetz, M. O. Tracking the ends: a dynamic protein network controls the fate of microtubule tips. *Nature Reviews Molecular Cell Biology* 2008 9:4 **9**, 309–322 (2008).
137. Waterman-Storer, C. M. & Salmon, E. D. Actomyosin-based Retrograde Flow of Microtubules in the Lamella of Migrating Epithelial Cells Influences Microtubule Dynamic

- Instability and Turnover and Is Associated with Microtubule Breakage and Treadmilling. *Journal of Cell Biology* **139**, 417–434 (1997).
138. Wu, J. & Akhmanova, A. Microtubule-Organizing Centers. <https://doi.org/10.1146/annurev-cellbio-100616-060615> **33**, 51–75 (2017).
  139. Brouhard, G. J. *et al.* XMAP215 Is a Processive Microtubule Polymerase. *Cell* **132**, 79–88 (2008).
  140. Komarova, Y. *et al.* Mammalian end binding proteins control persistent microtubule growth. *Journal of Cell Biology* **184**, 691–706 (2009).
  141. McDonald, H. B., Stewart, R. J. & Goldstein, L. S. B. The kinesin-like *ncd* protein of *Drosophila* is a minus end-directed microtubule motor. *Cell* **63**, 1159–1165 (1990).
  142. Desai, A., Verma, S., Mitchison, T. J. & Walczak, C. E. Kin I Kinesins Are Microtubule-Destabilizing Enzymes. *Cell* **96**, 69–78 (1999).
  143. Jiang, K. *et al.* Microtubule Minus-End Stabilization by Polymerization-Driven CAMSAP Deposition. *Developmental Cell* **28**, 295–309 (2014).
  144. Kollman, J. M., Merdes, A., Mourey, L. & Agard, D. A. Microtubule nucleation by  $\gamma$ -tubulin complexes. (2011) doi:10.1038/nrm3209.
  145. Petry, S., Groen, A. C., Ishihara, K., Mitchison, T. J. & Vale, R. D. Branching Microtubule Nucleation in *Xenopus* Egg Extracts Mediated by Augmin and TPX2. *Cell* **152**, 768–777 (2013).
  146. Tanaka, N., Meng, W., Nagae, S. & Takeichi, M. Nezha/CAMSAP3 and CAMSAP2 cooperate in epithelial-specific organization of noncentrosomal microtubules. *Proc Natl Acad Sci U S A* **109**, 20029–20034 (2012).
  147. Hendershott, M. C. & Vale, R. D. Regulation of microtubule minus-end dynamics by CAMSAPs and Patronin. *Proc Natl Acad Sci U S A* **111**, 5860–5865 (2014).
  148. Goodwin, S. S. & Vale, R. D. Patronin Regulates the Microtubule Network by Protecting Microtubule Minus Ends. *Cell* **143**, 263–274 (2010).
  149. Delgehyr, N., Sillibourne, J. & Bornens, M. Microtubule nucleation and anchoring at the centrosome are independent processes linked by ninein function. *Journal of Cell Science* **118**, 1565–1575 (2005).
  150. Meng, W., Mushika, Y., Ichii, T. & Takeichi, M. Anchorage of Microtubule Minus Ends to Adherens Junctions Regulates Epithelial Cell-Cell Contacts. *Cell* **135**, 948–959 (2008).
  151. Dogterom, M. & Koenderink, G. H. Actin–microtubule crosstalk in cell biology. *Nature Reviews Molecular Cell Biology* **20**, 38–54 (2018).
  152. Janson, M. E., de Dood, M. E. & Dogterom, M. Dynamic instability of microtubules is regulated by force. *J Cell Biol* **161**, 1029–1034 (2003).

153. Suozzi, K. C., Wu, X. & Fuchs, E. Spectraplakins: Master orchestrators of cytoskeletal dynamics. *Journal of Cell Biology* vol. 197 465–475 Preprint at <https://doi.org/10.1083/jcb.201112034> (2012).
154. Bartolini, F. *et al.* The formin mDia2 stabilizes microtubules independently of its actin nucleation activity. *Journal of Cell Biology* **181**, 523–536 (2008).
155. McNally, F. J. Mechanisms of spindle positioning. *J Cell Biol* **200**, 131–140 (2013).
156. Sanchez, A. D. & Feldman, J. L. Microtubule-organizing centers: from the centrosome to non-centrosomal sites. *Current Opinion in Cell Biology* **44**, 93–101 (2017).
157. Ning, W., Yu, Y., Xu, H., Wang, J. & Wang, Y. The CAMSAP3-ACF7 Complex Couples Noncentrosomal Microtubules with Actin Filaments to Coordinate Their Dynamics. *Developmental Cell* **39**, 61–74 (2016).
158. Nashchekin, D., Fernandes, A. R. & St Johnston, D. Patronin/Shot Cortical Foci Assemble the Noncentrosomal Microtubule Array that Specifies the Drosophila Anterior-Posterior Axis. *Developmental Cell* **38**, 61–72 (2016).
159. Khanal, I., Elbediwy, A., de la Loza, M. del C. D., Fletcher, G. C. & Thompson, B. J. Shot and Patronin polarise microtubules to direct membrane traffic and biogenesis of microvilli in epithelia. *Journal of Cell Science* **129**, 2651–2659 (2016).
160. Applewhite, D. A., Grode, K. D., Duncan, M. C. & Rogers, S. L. The actin-microtubule cross-linking activity of Drosophila Short stop is regulated by intramolecular inhibition. *Molecular Biology of the Cell* **24**, 2885–2893 (2013).
161. Applewhite, D. A. *et al.* The spectraplakin short stop is an actin-microtubule cross-linker that contributes to organization of the microtubule network. *Molecular Biology of the Cell* **21**, 1714–1724 (2010).
162. Booth, A. J. R., Blanchard, G. B., Adams, R. J. & Röper, K. A Dynamic Microtubule Cytoskeleton Directs Medial Actomyosin Function during Tube Formation. *Developmental Cell* **29**, 562 (2014).
163. Lee, J. Y. & Harland, R. M. Actomyosin contractility and microtubules drive apical constriction in *Xenopus* bottle cells. *Developmental Biology* **311**, 40–52 (2007).
164. Mandato, C. A. & Bement, W. M. Actomyosin Transports Microtubules and Microtubules Control Actomyosin Recruitment during *Xenopus* Oocyte Wound Healing. *Current Biology* **13**, 1096–1105 (2003).
165. Bement, W. M., Mandato, C. A. & Kirsch, M. N. Wound-induced assembly and closure of an actomyosin purse string in *Xenopus* oocytes. *Current Biology* **9**, 579–587 (1999).
166. Lee, G. *et al.* *Myosin-driven actin-microtubule networks exhibit self-organized contractile dynamics.* *Sci. Adv* vol. 7 <http://advances.sciencemag.org/> (2021).

167. Garcia De Las Bayonas, A., Philippe, J. M., Lellouch, A. C. & Lecuit, T. Distinct RhoGEFs Activate Apical and Junctional Contractility under Control of G Proteins during Epithelial Morphogenesis. *Current Biology* **29**, 3370-3385.e7 (2019).
168. Slattum, G., McGee, K. M. & Rosenblatt, J. P115 RhoGEF and microtubules decide the direction apoptotic cells extrude from an epithelium. *Journal of Cell Biology* **186**, 693–702 (2009).
169. Gomez, J. M., Chumakova, L., Bulgakova, N. A. & Brown, N. H. Microtubule organization is determined by the shape of epithelial cells. *Nature Communications* **7**, 1–13 (2016).
170. Picone, R. *et al.* A Polarised Population of Dynamic Microtubules Mediates Homeostatic Length Control in Animal Cells. *PLOS Biology* **8**, e1000542 (2010).
171. Singh, A. *et al.* Polarized microtubule dynamics directs cell mechanics and coordinates forces during epithelial morphogenesis. *Nature Cell Biology* **20**, 1126–1133 (2018).
172. Pope, K. L. & Harris, T. J. C. Control of cell flattening and junctional remodeling during squamous epithelial morphogenesis in *Drosophila*. *Development* **135**, 2227–2238 (2008).
173. Fraire-Zamora, J. J., Jaeger, J. & Solon, J. Two consecutive microtubule-based epithelial seaming events mediate dorsal closure in the scuttle fly *Megaselia abdita*. *Elife* **7**, 1–20 (2018).
174. Takeda, M., Sami, M. M. & Wang, Y. C. A homeostatic apical microtubule network shortens cells for epithelial folding via a basal polarity shift. *Nature Cell Biology* **20**, 36–45 (2018).
175. Théry, M. & Blanchoin, L. Microtubule self-repair. *Current Opinion in Cell Biology* **68**, 144–154 (2021).
176. Schaedel, L. *et al.* Microtubules self-repair in response to mechanical stress. *Nature Materials 2015 14:11* **14**, 1156–1163 (2015).
177. Schaedel, L. *et al.* Lattice defects induce microtubule self-renewal. *Nature Physics 2019 15:8* **15**, 830–838 (2019).
178. Li, Y. *et al.* Compressive forces stabilise microtubules in living cells. *bioRxiv* 2022.02.07.479347 (2022) doi:10.1101/2022.02.07.479347.
179. Ju, R. J. *et al.* A Microtubule Mechanostat Enables Cells to Navigate Confined Environments. *bioRxiv* 2022.02.08.479516 (2022) doi:10.1101/2022.02.08.479516.
180. Robison, P. *et al.* Detyrosinated microtubules buckle and bear load in contracting cardiomyocytes. *Science (1979)* **352**, (2016).
181. Brangwynne, C. P. *et al.* Microtubules can bear enhanced compressive loads in living cells because of lateral reinforcement. *Journal of Cell Biology* **173**, 733–741 (2006).
182. Hurst, S., Vos, B. E. & Betz, T. Intracellular softening and fluidification reveals a mechanical switch of cytoskeletal material contributions during division. *bioRxiv* 2021.01.07.425761 (2021) doi:10.1101/2021.01.07.425761.

183. D'Angelo, A., Dierkes, K., Carolis, C., Salbreux, G. & Solon, J. In Vivo Force Application Reveals a Fast Tissue Softening and External Friction Increase during Early Embryogenesis. *Current Biology* **29**, 1564-1571.e6 (2019).
184. Fuchs, Y. & Steller, H. Live to die another way: Modes of programmed cell death and the signals emanating from dying cells. *Nature Reviews Molecular Cell Biology* **16**, 329–344 (2015).
185. Clarke, P. G. H. & Clarke, S. Nineteenth century research on naturally occurring cell death and related phenomena. *Anatomy and Embryology 1996 193:2* **193**, 81–99 (1996).
186. Kerr, J. F. R., Wyllie, A. H. & Currie, A. R. Apoptosis: A Basic Biological Phenomenon with Wideranging Implications in Tissue Kinetics. *British Journal of Cancer 1972 26:4* **26**, 239–257 (1972).
187. Denning, D. P., Hatch, V. & Robert Horvitz, H. Programmed elimination of cells by caspase-independent cell extrusion in *C. elegans*. *Nature* **488**, 226–230 (2012).
188. Ellis, H. M. & Horvitz, H. R. Genetic control of programmed cell death in the nematode *C. elegans*. *Cell* **44**, 817–829 (1986).
189. Yuan, J. & Horvitz, H. R. The *Caenorhabditis elegans* genes *ced-3* and *ced-4* act cell autonomously to cause programmed cell death. *Developmental Biology* **138**, 33–41 (1990).
190. Yuan, J., Shaham, S., Ledoux, S., Ellis, H. M. & Horvitz, H. R. The *C. elegans* cell death gene *ced-3* encodes a protein similar to mammalian interleukin-1 $\beta$ -converting enzyme. *Cell* **75**, 641–652 (1993).
191. Jacobson, M. D., Weil, M. & Raff, M. C. Programmed Cell Death in Animal Development. *Cell* **88**, 347–354 (1997).
192. Cornillon, S. *et al.* Programmed cell death in *Dictyostelium*. *Journal of Cell Science* **107**, 2691–2704 (1994).
193. Büttner, S. *et al.* Why yeast cells can undergo apoptosis: death in times of peace, love, and war. *Journal of Cell Biology* **175**, 521–525 (2006).
194. Galluzzi, L. *et al.* Molecular mechanisms of cell death: recommendations of the Nomenclature Committee on Cell Death 2018. *Cell Death & Differentiation 2018 25:3* **25**, 486–541 (2018).
195. Schweisguth, F. Asymmetric cell division in the *Drosophila* bristle lineage: from the polarization of sensory organ precursor cells to Notch-mediated binary fate decision. *Wiley Interdisciplinary Reviews: Developmental Biology* **4**, 299–309 (2015).
196. Gho, M., Bellaïche, Y. & Schweisguth, F. Revisiting the *Drosophila* microchaete lineage: a novel intrinsically asymmetric cell division generates a glial cell. *Development* **126**, 3573–3584 (1999).
197. Fichelson, P. & Gho, M. The glial cell undergoes apoptosis in the microchaete lineage of *Drosophila*. *Development* **130**, 123–133 (2003).

198. Lindsten, T. *et al.* The Combined Functions of Proapoptotic Bcl-2 Family Members Bak and Bax Are Essential for Normal Development of Multiple Tissues. *Molecular Cell* **6**, 1389–1399 (2000).
199. Toyama, Y., Peralta, X. G., Wells, A. R., Kiehart, D. P. & Edwards, G. S. Apoptotic force and tissue dynamics during *Drosophila* embryogenesis. *Science (1979)* **321**, 1683–1686 (2008).
200. Manjón, C., Sánchez-Herrero, E. & Suzanne, M. Sharp boundaries of Dpp signalling trigger local cell death required for *Drosophila* leg morphogenesis. *Nature Cell Biology* *2006 9:1* **9**, 57–63 (2006).
201. Schott, S. *et al.* A fluorescent toolkit for spatiotemporal tracking of apoptotic cells in living *Drosophila* tissues. *Development* **144**, 3840–3846 (2017).
202. Ranft, J. *et al.* Fluidization of tissues by cell division and apoptosis. *Proc Natl Acad Sci U S A* **107**, 20863–20868 (2010).
203. Suzanne, M. *et al.* Coupling of Apoptosis and L/R Patterning Controls Stepwise Organ Looping. *Current Biology* **20**, 1773–1778 (2010).
204. Kuranaga, E. *et al.* Apoptosis controls the speed of looping morphogenesis in *Drosophila* male terminalia. *Development* **138**, 1493–1499 (2011).
205. Clavería, C. & Torres, M. Cell Competition: Mechanisms and Physiological Roles. *Annual Review of Cell and Developmental Biology* **32**, 411–439 (2016).
206. Morata, G. & Ripoll, P. Minutes: Mutants of *Drosophila* autonomously affecting cell division rate. *Developmental Biology* **42**, 211–221 (1975).
207. Simpson, P. & Morata, G. Differential mitotic rates and patterns of growth in compartments in the *Drosophila* wing. *Developmental Biology* **85**, 299–308 (1981).
208. Moreno, E., Basler, K. & Morata, G. Cells compete for decapentaplegic survival factor to prevent apoptosis in *Drosophila* wing development. *Nature* **416**, 755–759 (2002).
209. Yamamoto, M., Ohsawa, S., Kunimasa, K. & Igaki, T. The ligand Sas and its receptor PTP10D drive tumour-suppressive cell competition. *Nature* **542**, 246–250 (2017).
210. Moreno, E., Valon, L., Levillayer, F. & Levayer, R. Competition for Space Induces Cell Elimination through Compaction-Driven ERK Downregulation. *Curr Biol* **29**, 23–34.e8 (2019).
211. Wagstaff, L. *et al.* Mechanical cell competition kills cells via induction of lethal p53 levels. *Nature Communications* **7**, (2016).
212. Brumby, A. M. & Richardson, H. E. scribble mutants cooperate with oncogenic Ras or Notch to cause neoplastic overgrowth in *Drosophila*. *EMBO Journal* **22**, 5769–5779 (2003).
213. Levayer, R., Hauert, B. & Moreno, E. Cell mixing induced by myc is required for competitive tissue invasion and destruction. *Nature* **524**, 476–480 (2015).

214. Clavería, C., Giovinazzo, G., Sierra, R. & Torres, M. Myc-driven endogenous cell competition in the early mammalian embryo. *Nature* **500**, 39–44 (2013).
215. Farhadifar, R., Röper, J. C., Aigouy, B., Eaton, S. & Jülicher, F. The Influence of Cell Mechanics, Cell-Cell Interactions, and Proliferation on Epithelial Packing. *Current Biology* **17**, 2095–2104 (2007).
216. Matamoro-Vidal, A., Cumming, T., Davidović, A. & Levayer, R. Patterned apoptosis has an instructive role for local growth and tissue shape regulation in a fast-growing epithelium. *bioRxiv* 2022.03.11.484029 (2022) doi:10.1101/2022.03.11.484029.
217. Amcheslavsky, A. *et al.* Plasma Membrane Localization of Apoptotic Caspases for Non-apoptotic Functions. *Developmental Cell* **45**, 450-464.e3 (2018).
218. Haynie, J. L. & Bryant, P. J. The effects of X-rays on the proliferation dynamics of cells in the imaginal wing disc of *Drosophila melanogaster*. *Wilhelm Roux's archives of developmental biology* 1977 183:2 **183**, 85–100 (1977).
219. Crawford, E. D. & Wells, J. A. Caspase Substrates and Cellular Remodeling. *Annual Review of Biochemistry* **80**, 1055–1087 (2011).
220. Taylor, R. C., Cullen, S. P. & Martin, S. J. Apoptosis: controlled demolition at the cellular level. *Nature Reviews Molecular Cell Biology* 2008 9:3 **9**, 231–241 (2008).
221. Nagasaka, A., Kawane, K., Yoshida, H. & Nagata, S. Apaf-1-independent programmed cell death in mouse development. *Cell Death & Differentiation* 2010 17:6 **17**, 931–941 (2009).
222. Srivastava, M. *et al.* ARK, the Apaf-1 related killer in *Drosophila*, requires diverse domains for its apoptotic activity. *Cell Death & Differentiation* 2007 14:1 **14**, 92–102 (2006).
223. Rodriguez, A. *et al.* Dark is a *Drosophila* homologue of Apaf-1/CED-4 and functions in an evolutionarily conserved death pathway. *Nature Cell Biology* 1999 1:5 **1**, 272–279 (1999).
224. Cain, K., Brown, D. G., Langlais, C. & Cohen, G. M. Caspase activation involves the formation of the aposome, a large (~700 kDa) caspase-activating complex. *Journal of Biological Chemistry* **274**, 22686–22692 (1999).
225. Adams, J. M. & Cory, S. Apoptosomes: engines for caspase activation. *Current Opinion in Cell Biology* **14**, 715–720 (2002).
226. Muro, I., Means, J. C. & Clem, R. J. Cleavage of the Apoptosis Inhibitor DIAP1 by the Apical Caspase DRONC in Both Normal and Apoptotic *Drosophila* Cells. *Journal of Biological Chemistry* **280**, 18683–18688 (2005).
227. Xu, D., Li, Y., Arcaro, M., Lackey, M. & Bergmann, A. The CARD-carrying caspase Dronc is essential for most, but not all, developmental cell death in *Drosophila*. *Development* **132**, 2125–2134 (2005).

228. Cooper, D. M., David, A. E., Ae, J. G. & Lowenberger, C. The insect caspases. doi:10.1007/s10495-009-0322-1.
229. Harvey, N. L. *et al.* Characterization of the Drosophila Caspase, DAMM. *Journal of Biological Chemistry* **276**, 25342–25350 (2001).
230. Lakhani, S. A. *et al.* Caspases 3 and 7: Key mediators of mitochondrial events of apoptosis. *Science (1979)* **311**, 847–851 (2006).
231. Miura, M. *et al.* A crucial role of caspase-3 in osteogenic differentiation of bone marrow stromal stem cells. *Journal of Clinical Investigation* **114**, 1704–1713 (2004).
232. Vaux, D. L. & Silke, J. IAPs, RINGs and ubiquitylation. *Nature Reviews Molecular Cell Biology* **2005** *6:4* **6**, 287–297 (2005).
233. Crook, N. E., Clem, R. J. & Miller, L. K. An apoptosis-inhibiting baculovirus gene with a zinc finger-like motif. *Journal of Virology* **67**, 2168–2174 (1993).
234. Bergmann, A., Yang, A. Y. P. & Srivastava, M. Regulators of IAP function: coming to grips with the grim reaper. *Current Opinion in Cell Biology* **15**, 717–724 (2003).
235. Wang, S. L., Hawkins, C. J., Yoo, S. J., Müller, H. A. J. & Hay, B. A. The Drosophila Caspase Inhibitor DIAP1 Is Essential for Cell Survival and Is Negatively Regulated by HID. *Cell* **98**, 453–463 (1999).
236. Harlin, H., Reffey, S. B., Duckett, C. S., Lindsten, T. & Thompson, C. B. Characterization of XIAP-Deficient Mice. *Molecular and Cellular Biology* **21**, 3604–3608 (2001).
237. White, K. *et al.* Genetic Control of Programmed Cell Death in Drosophila. *Science (1979)* **264**, 677–683 (1994).
238. Shi, Y. A conserved tetrapeptide motif: potentiating apoptosis through IAP-binding. *Cell Death & Differentiation* **9**, 93–95 (2002).
239. Sandu, C., Ryoo, H. D. & Steller, H. Drosophila IAP antagonists form multimeric complexes to promote cell death. *J Cell Biol* **190**, 1039–52 (2010).
240. Fuchs, Y. *et al.* Sept4/ARTS regulates stem cell apoptosis and skin regeneration. *Science (1979)* **341**, 286–289 (2013).
241. Gottfried, Y., Rotem, A., Lotan, R., Steller, H. & Larisch, S. The mitochondrial ARTS protein promotes apoptosis through targeting XIAP. *The EMBO Journal* **23**, 1627–1635 (2004).
242. Goyal, L., McCall, K., Agapite, J., Hartwig, E. & Steller, H. Induction of apoptosis by Drosophila reaper, hid and grim through inhibition of IAP function. *The EMBO Journal* **19**, 589–597 (2000).
243. Lisi, S., Mazzon, I. & White, K. Diverse Domains of THREAD/DIAP1 Are Required to Inhibit Apoptosis Induced by REAPER and HID in Drosophila. *Genetics* **154**, 669–678 (2000).



244. Ditzel, M. *et al.* Degradation of DIAP1 by the N-end rule pathway is essential for regulating apoptosis. *Nature Cell Biology* 2003 5:5 **5**, 467–473 (2003).
245. Ditzel, M. *et al.* Inactivation of Effector Caspases through Nondegradative Polyubiquitylation. *Mol Cell* **32**, 540 (2008).
246. Dwivedi, V. K. *et al.* Replication stress promotes cell elimination by extrusion. *Nature* 2021 593:7860 **593**, 591–596 (2021).
247. Browne, K. A., Johnstone, R. W., Jans, D. A. & Trapani, J. A. Filamin (280-kDa Actin-binding Protein) Is a Caspase Substrate and Is Also Cleaved Directly by the Cytotoxic T Lymphocyte Protease Granzyme B during Apoptosis. *Journal of Biological Chemistry* **275**, 39262–39266 (2000).
248. Kaufmann, T., Strasser, A. & Jost, P. J. Fas death receptor signalling: roles of Bid and XIAP. *Cell Death and Differentiation* **19**, 42 (2012).
249. Kale, J., Osterlund, E. J. & Andrews, D. W. BCL-2 family proteins: changing partners in the dance towards death. *Cell Death & Differentiation* 2018 25:1 **25**, 65–80 (2017).
250. Ding, J. *et al.* After Embedding in Membranes Antiapoptotic Bcl-XL Protein Binds Both Bcl-2 Homology Region 3 and Helix 1 of Proapoptotic Bax Protein to Inhibit Apoptotic Mitochondrial Permeabilization. *Journal of Biological Chemistry* **289**, 11873–11896 (2014).
251. O’neill, K. L., Huang, K., Zhang, J., Chen, Y. & Luo, X. Inactivation of prosurvival Bcl-2 proteins activates Bax/Bak through the outer mitochondrial membrane. *Genes & Development* **30**, 973–988 (2016).
252. Lüthi, A. U. & Martin, S. J. The CASBAH: a searchable database of caspase substrates. *Cell Death & Differentiation* 2007 14:4 **14**, 641–650 (2007).
253. Crawford, E. D. *et al.* Conservation of caspase substrates across metazoans suggests hierarchical importance of signaling pathways over specific targets and cleavage site motifs in apoptosis. *Cell Death and Differentiation* **19**, 2040–2048 (2012).
254. Enari, M. *et al.* A caspase-activated DNase that degrades DNA during apoptosis, and its inhibitor ICAD. *Nature* 1998 391:6662 **391**, 43–50 (1998).
255. Communal, C. *et al.* Functional consequences of caspase activation in cardiac myocytes. *Proc Natl Acad Sci U S A* **99**, 6252–6256 (2002).
256. Browne, K. A., Johnstone, R. W., Jans, D. A. & Trapani, J. A. Filamin (280-kDa Actin-binding Protein) Is a Caspase Substrate and Is Also Cleaved Directly by the Cytotoxic T Lymphocyte Protease Granzyme B during Apoptosis \*. *Journal of Biological Chemistry* **275**, 39262–39266 (2000).
257. Martin, S. J. *et al.* Proteolysis of Fodrin (Non-erythroid Spectrin) during Apoptosis. *Journal of Biological Chemistry* **270**, 6425–6428 (1995).
258. Gerner, C. *et al.* The Fas-induced Apoptosis Analyzed by High Throughput Proteome Analysis. *Journal of Biological Chemistry* **275**, 39018–39026 (2000).

259. Kothakota, S. *et al.* Caspase-3-Generated Fragment of Gelsolin: Effector of Morphological Change in Apoptosis. *Science (1979)* **278**, 294–298 (1997).
260. Coleman, M. L. *et al.* Membrane blebbing during apoptosis results from caspase-mediated activation of ROCK I. *Nature Cell Biology 2001 3:4* **3**, 339–345 (2001).
261. Sebbagh, M. *et al.* Caspase-3-mediated cleavage of ROCK I induces MLC phosphorylation and apoptotic membrane blebbing. *Nature Cell Biology 2001 3:4* **3**, 346–352 (2001).
262. Steinhusen, U. *et al.* Cleavage and Shedding of E-cadherin after Induction of Apoptosis. *Journal of Biological Chemistry* **276**, 4972–4980 (2001).
263. Brancolini, C., Lazarevic, D., Rodriguez, J. & Schneider, C. Dismantling Cell–Cell Contacts during Apoptosis Is Coupled to a Caspase-dependent Proteolytic Cleavage of  $\beta$ -Catenin. *Journal of Cell Biology* **139**, 759–771 (1997).
264. Kessler, T. & Müller, H. A. J. Cleavage of armadillo/beta-catenin by the caspase DrICE in drosophila apoptotic epithelial cells. *BMC Developmental Biology* **9**, 1–13 (2009).
265. Chandraratna, D., Lawrence, N., Welchman, D. R. & Sanson, B. An in vivo model of apoptosis: Linking cell behaviours and caspase substrates in embryos lacking DIAP1. *Journal of Cell Science* **120**, 2594–2608 (2007).
266. Klaiman, G., Petzke, T. L., Hammond, J. & LeBlanc, A. C. Targets of caspase-6 activity in human neurons and Alzheimer disease. *Molecular and Cellular Proteomics* **7**, 1541–1555 (2008).
267. Seo, M. Y. & Rhee, K. Caspase-mediated cleavage of the centrosomal proteins during apoptosis. doi:10.1038/s41419-018-0632-8.
268. Oropesa-Avila, M. *et al.* Apoptotic microtubules delimit an active caspase free area in the cellular cortex during the execution phase of apoptosis. *Cell Death & Disease 2013 4:3* **4**, e527–e527 (2013).
269. Moss, D. K., Betin, V. M., Malesinski, S. D. & Lane, J. D. A novel role for microtubules in apoptotic chromatin dynamics and cellular fragmentation. *Journal of Cell Science* **119**, 2362–2374 (2006).
270. Rosenblatt, J., Raff, M. C. & Cramer, L. P. An epithelial cell destined for apoptosis signals its neighbors to extrude it by an actin- and myosin-dependent mechanism. *Current Biology* **11**, 1847–1857 (2001).
271. Degoeij, J. M. *et al.* Cell kinetics of the marine sponge *Halisarca caerulea* reveal rapid cell turnover and shedding. *Journal of Experimental Biology* **212**, 3892–3900 (2009).
272. Alexander, B. E. *et al.* Cell turnover and detritus production in marine sponges from tropical and temperate benthic ecosystems. *PLoS ONE* **9**, e109486 (2014).
273. Valon, L. *et al.* Robustness of epithelial sealing is an emerging property of local ERK feedback driven by cell elimination. *Developmental Cell* **56**, 1700–1711.e8 (2021).

274. Eisenhoffer, G. T. *et al.* Crowding induces live cell extrusion to maintain homeostatic cell numbers in epithelia. *Nature* **484**, 546–549 (2012).
275. Campinho, P., Lamperti, P., Boselli, F., Vilfan, A. & Vermot, J. Blood Flow Limits Endothelial Cell Extrusion in the Zebrafish Dorsal Aorta. *Cell Reports* **31**, 107505 (2020).
276. Mleynek, T. M. *et al.* Endothelia extrude apoptotic cells to maintain a constant barrier. *bioRxiv* 268946 Preprint at <https://doi.org/10.1101/268946> (2018).
277. CREAMER, B., SHORTER, R. G. & BAMFORTH, J. The turnover and shedding of epithelial cells. *Gut* **2**, 110–116 (1961).
278. Bullen, T. F. *et al.* Characterization of epithelial cell shedding from human small intestine. *Laboratory Investigation* 2006 86:10 **86**, 1052–1063 (2006).
279. Williams, J. M. *et al.* Epithelial Cell Shedding and Barrier Function: A Matter of Life and Death at the Small Intestinal Villus Tip. *Veterinary Pathology* **52**, 445–455 (2015).
280. Marinari, E. *et al.* Live-cell delamination counterbalances epithelial growth to limit tissue overcrowding. *Nature* **484**, 542–545 (2012).
281. Levayer, R., Dupont, C. & Moreno, E. Tissue Crowding Induces Caspase-Dependent Competition for Space. *Current Biology* **26**, 670–677 (2016).
282. Saw, T. B. *et al.* Topological defects in epithelia govern cell death and extrusion. *Nature* **544**, 212–216 (2017).
283. Lolo, F. N., Casas-Tintó, S. & Moreno, E. Cell Competition Time Line: Winners Kill Losers, which Are Extruded and Engulfed by Hemocytes. *Cell Reports* **2**, 526–539 (2012).
284. Valon, L. & Levayer, R. Dying under pressure: cellular characterisation and in vivo functions of cell death induced by compaction. *Biology of the Cell* vol. 111 51–66 Preprint at <https://doi.org/10.1111/boc.201800075> (2019).
285. Kajita, M. & Fujita, Y. EDAC: Epithelial defence against cancer - Cell competition between normal and transformed epithelial cells in mammals. *Journal of Biochemistry* **158**, 15–23 (2015).
286. Vidal, M., Larson, D. E. & Cagan, R. L. Csk-Deficient Boundary Cells Are Eliminated from Normal Drosophila Epithelia by Exclusion, Migration, and Apoptosis. *Developmental Cell* **10**, 33–44 (2006).
287. Vidal, M. *et al.* A Role for the Epithelial Microenvironment at Tumor Boundaries: Evidence from Drosophila and Human Squamous Cell Carcinomas. *The American Journal of Pathology* **176**, 3007–3014 (2010).
288. Kajita, M. *et al.* Interaction with surrounding normal epithelial cells influences signalling pathways and behaviour of Src-transformed cells. *Journal of Cell Science* **123**, 171–180 (2010).
289. Teo, J. L. *et al.* Src kinases relax adherens junctions between the neighbors of apoptotic cells to permit apical extrusion. *Molecular Biology of the Cell* **31**, 2557–2569 (2020).

290. Teo, J. L. *et al.* Caveolae Control Contractile Tension for Epithelia to Eliminate Tumor Cells. *Developmental Cell* **54**, 75-91.e7 (2020).
291. Kajita, M. *et al.* Filamin acts as a key regulator in epithelial defence against transformed cells. *Nature Communications* *2014 5:1* **5**, 1–13 (2014).
292. Anton, K. A., Kajita, M., Narumi, R., Fujita, Y. & Tada, M. Src-transformed cells hijack mitosis to extrude from the epithelium. *Nature Communications* **9**, (2018).
293. Porazinski, S. *et al.* EphA2 Drives the Segregation of Ras-Transformed Epithelial Cells from Normal Neighbors. *Current Biology* **26**, 3220–3229 (2016).
294. Kon, S. *et al.* Cell competition with normal epithelial cells promotes apical extrusion of transformed cells through metabolic changes. *Nature Cell Biology* *2017 19:5* **19**, 530–541 (2017).
295. Vaughen, J. & Igaki, T. Slit-Robo Repulsive Signaling Extrudes Tumorigenic Cells from Epithelia. *Developmental Cell* **39**, 683–695 (2016).
296. Eisenhoffer, G. T. & Rosenblatt, J. Bringing balance by force: Live cell extrusion controls epithelial cell numbers. *Trends in Cell Biology* **23**, 185–192 (2013).
297. Bastounis, E. E. *et al.* Mechanical competition triggered by innate immune signaling drives the collective extrusion of bacterially infected epithelial cells. *Developmental Cell* **56**, 443–460.e11 (2021).
298. Slattum, G., Gu, Y., Sabbadini, R. & Rosenblatt, J. Autophagy in oncogenic K-Ras promotes basal extrusion of epithelial cells by degrading S1P. *Current Biology* **24**, 19–28 (2014).
299. Fadul, J. *et al.* KRas-transformed epithelia cells invade and partially dedifferentiate by basal cell extrusion. doi:10.1038/s41467-021-27513-z.
300. Gu, Y. *et al.* Defective apical extrusion signaling contributes to aggressive tumor hallmarks. *Elife* **4**, (2015).
301. Slattum, G. M. & Rosenblatt, J. Tumour cell invasion: An emerging role for basal epithelial cell extrusion. *Nature Reviews Cancer* **14**, 495–501 (2014).
302. Gu, Y. & Rosenblatt, J. New emerging roles for epithelial cell extrusion. *Current Opinion in Cell Biology* **24**, 865–870 (2012).
303. Gudipaty, S. A. & Rosenblatt, J. Epithelial cell extrusion: Pathways and pathologies. *Seminars in Cell and Developmental Biology* **67**, 132–140 (2017).
304. Buchon, N., Broderick, N. A., Kuraishi, T. & Lemaitre, B. Drosophila EGFR pathway coordinates stem cell proliferation and gut remodeling following infection. *BMC Biology* **8**, 1–19 (2010).
305. Knodler, L. A. *et al.* Dissemination of invasive Salmonella via bacterial-induced extrusion of mucosal epithelia. *Proc Natl Acad Sci U S A* **107**, 17733–17738 (2010).

306. Pentecost, M., Otto, G., Theriot, J. A. & Amieva, M. R. *Listeria monocytogenes* Invades the Epithelial Junctions at Sites of Cell Extrusion. *PLOS Pathogens* **2**, e3 (2006).
307. Marshall, T. W., Lloyd, I. E., Delalande, J. M., Näthke, I. & Rosenblatt, J. The tumor suppressor adenomatous polyposis coli controls the direction in which a cell extrudes from an epithelium. *Molecular Biology of the Cell* **22**, 3962–3970 (2011).
308. An, Y. *et al.* Apical constriction is driven by a pulsatile apical myosin network in delaminating *Drosophila* neuroblasts. *Development (Cambridge)* **144**, 2153–2164 (2017).
309. Michel, M. & Dahmann, C. Tissue mechanical properties modulate cell extrusion in the *Drosophila* abdominal epidermis. *Development (Cambridge)* **147**, (2020).
310. Lubkov, V. & Bar-Sagi, D. E-cadherin-mediated cell coupling is required for apoptotic cell extrusion. *Current Biology* **24**, 868–874 (2014).
311. Wu, S. K., Lagendijk, A. K., Hogan, B. M., Gomez, G. A. & Yap, A. S. Active contractility at E-cadherin junctions and its implications for cell extrusion in cancer. *Cell Cycle* **14**, 315–322 (2015).
312. Grieve, A. G. & Rabouille, C. Extracellular cleavage of E-cadherin promotes epithelial cell extrusion. *Journal of Cell Science* **127**, 3331–3346 (2014).
313. Thomas, M., Ladoux, B. & Toyama, Y. Desmosomal Junctions Govern Tissue Integrity and Actomyosin Contractility in Apoptotic Cell Extrusion. *Current Biology* **30**, 682-690.e5 (2020).
314. Dusek, R. L. *et al.* The Differentiation-dependent Desmosomal Cadherin Desmoglein 1 Is a Novel Caspase-3 Target That Regulates Apoptosis in Keratinocytes. *Journal of Biological Chemistry* **281**, 3614–3624 (2006).
315. Le, A. P. *et al.* Adhesion-mediated heterogeneous actin organization governs apoptotic cell extrusion. *Nature Communications* **12**, 1–18 (2021).
316. Kocgozlu, L. *et al.* Epithelial Cell Packing Induces Distinct Modes of Cell Extrusions. *Current Biology* **26**, 2942–2950 (2016).
317. Gu, Y., Forostyan, T., Sabbadini, R. & Rosenblatt, J. Epithelial cell extrusion requires the sphingosine-1-phosphate receptor 2 pathway. *Journal of Cell Biology* **193**, 667–676 (2011).
318. Andrade, D. & Rosenblatt, J. Apoptotic regulation of epithelial cellular extrusion. *Apoptosis* **16**, 491–501 (2011).
319. Ghazavi, F. *et al.* Executioner caspases 3 and 7 are dispensable for intestinal epithelium turnover and homeostasis at steady state. *Proc Natl Acad Sci U S A* **119**, (2022).
320. Nakajima, Y. I. & Kuranaga, E. Caspase-dependent non-apoptotic processes in development. *Cell Death and Differentiation* **24**, 1422–1430 (2017).
321. Eskandari, E. & Eaves, C. J. Paradoxical roles of caspase-3 in regulating cell survival, proliferation, and tumorigenesis. *J Cell Biol* **221**, (2022).

322. Launay, S. *et al.* Vital functions for lethal caspases. *Oncogene* 2005 24:33 **24**, 5137–5148 (2005).
323. Geisbrecht, E. R. & Montell, D. J. A role for Drosophila IAP1-mediated caspase inhibition in Rac-dependent cell migration. *Cell* **118**, 111–125 (2004).
324. Sun, G. *et al.* A molecular signature for anastasis, recovery from the brink of apoptotic cell death. *Journal of Cell Biology* **216**, 3355–3368 (2017).
325. Tang, H. L. *et al.* Cell survival, DNA damage, and oncogenic transformation after a transient and reversible apoptotic response. *Molecular Biology of the Cell* **23**, 2240–2252 (2012).
326. Florentin, A. & Arama, E. Caspase levels and execution efficiencies determine the apoptotic potential of the cell. *Journal of Cell Biology* **196**, 513–527 (2012).
327. Yosefzon, Y. *et al.* Caspase-3 Regulates YAP-Dependent Cell Proliferation and Organ Size. *Molecular Cell* **70**, 573-587.e4 (2018).
328. Misra, R. S. *et al.* Effector CD4+ T Cells Generate Intermediate Caspase Activity and Cleavage of Caspase-8 Substrates. *The Journal of Immunology* **174**, 3999–4009 (2005).
329. Knapp, D. J. H. F., Kannan, N., Pellacani, D. & Eaves, C. J. Mass Cytometric Analysis Reveals Viable Activated Caspase-3+ Luminal Progenitors in the Normal Adult Human Mammary Gland. *Cell Reports* **21**, 1116–1126 (2017).
330. Woo, M. *et al.* Caspase-3 regulates cell cycle in B cells: a consequence of substrate specificity. *Nature Immunology* 2003 4:10 **4**, 1016–1022 (2003).
331. Shinoda, N., Hanawa, N., Chihara, T., Koto, A. & Miura, M. Dronc-independent basal executioner caspase activity sustains Drosophila imaginal tissue growth. *Proc Natl Acad Sci U S A* **116**, 20539–20544 (2019).
332. Martin, D. N. & Baehrecke, E. H. Caspases function in autophagic programmed cell death in Drosophila. *Development* **131**, 275–284 (2004).
333. DeVorkin, L. *et al.* The Drosophila effector caspase Dcp-1 regulates mitochondrial dynamics and autophagic flux via SesB. *Journal of Cell Biology* **205**, 477–492 (2014).
334. Khalil, H. *et al.* Caspase-3 protects stressed organs against cell death. *Mol Cell Biol* **32**, 4523–33 (2012).
335. Sordet, O. *et al.* Specific involvement of caspases in the differentiation of monocytes into macrophages. *Blood* **100**, 4446–4453 (2002).
336. Sztiller-Sikorska, M., Jakubowska, J., Wozniak, M., Stasiak, M. & Czyz, M. A non-apoptotic function of caspase-3 in pharmacologically-induced differentiation of K562 cells. *British Journal of Pharmacology* **157**, 1451–1462 (2009).
337. He, B. & Adler, P. N. Cellular mechanisms in the development of the Drosophila arista. *Mechanisms of Development* **104**, 69–78 (2001).

338. Cullen, K. & McCall, K. Role of programmed cell death in patterning the *Drosophila* antennal arista. *Developmental Biology* **275**, 82–92 (2004).
339. Oshima, K. *et al.* IKK $\epsilon$  Regulates F Actin Assembly and Interacts with *Drosophila* IAP1 in Cellular Morphogenesis. *Current Biology* **16**, 1531–1537 (2006).
340. Baum, J. S., Arama, E., Steller, H. & McCall, K. The *Drosophila* caspases Strica and Dronc function redundantly in programmed cell death during oogenesis. *Cell Death & Differentiation* **2007 14:8 14**, 1508–1517 (2007).
341. McSharry, S. S. & Beitel, G. J. The Caspase-3 homolog DrICE regulates endocytic trafficking during *Drosophila* tracheal morphogenesis. *Nature Communications* **2019 10:1 10**, 1–10 (2019).
342. McCall, K. & Steller, H. Requirement for DCP-1 caspase during *Drosophila* oogenesis. *Science (1979)* **279**, 230–234 (1998).
343. Montell, D. J. Border-cell migration: the race is on. *Nature Reviews Molecular Cell Biology* **2003 4:1 4**, 13–24 (2003).
344. Zhang, B., Zhang, Y. & Shacter, E. Caspase 3-Mediated Inactivation of Rac GTPases Promotes Drug-Induced Apoptosis in Human Lymphoma Cells. *Molecular and Cellular Biology* **23**, 5716–5725 (2003).
345. Williams, D. W., Kondo, S., Krzyzanowska, A., Hiromi, Y. & Truman, J. W. Local caspase activity directs engulfment of dendrites during pruning. *Nature Neuroscience* **2006 9:10 9**, 1234–1236 (2006).
346. Lee, H. H., Jan, L. Y. & Jan, Y. N. *Drosophila* IKK-related kinase Ik2 and Katanin p60-like 1 regulate dendrite pruning of sensory neuron during metamorphosis. *Proc Natl Acad Sci U S A* **106**, 6363–6368 (2009).
347. Kanuka, H. *et al.* Control of the Cell Death Pathway by Dapaf-1, a *Drosophila* Apaf-1/CED-4-Related Caspase Activator. *Molecular Cell* **4**, 757–769 (1999).
348. Chew, S. K. *et al.* The Apical Caspase dronc Governs Programmed and Unprogrammed Cell Death in *Drosophila*. *Developmental Cell* **7**, 897–907 (2004).
349. Mendes, C. S. *et al.* Cytochrome c-d regulates developmental apoptosis in the *Drosophila* retina. *EMBO Rep* **7**, 933–939 (2006).
350. Kanuka, H. *et al.* *Drosophila* caspase transduces Shaggy/GSK-3 $\beta$  kinase activity in neural precursor development. *The EMBO Journal* **24**, 3793–3806 (2005).
351. Huh, J. R. *et al.* Multiple Apoptotic Caspase Cascades Are Required in Nonapoptotic Roles for *Drosophila* Spermatid Individualization. *PLOS Biology* **2**, e15 (2003).
352. Muro, I. *et al.* The *Drosophila* caspase Ice is important for many apoptotic cell deaths and for spermatid individualization, a nonapoptotic process. *Development* **133**, 3305–3315 (2006).

353. Arama, E., Agapite, J. & Steller, H. Caspase Activity and a Specific Cytochrome C Are Required for Sperm Differentiation in *Drosophila*. *Developmental Cell* **4**, 687–697 (2003).
354. Ishizaki, Y., Jacobson, M. D. & Raff, M. C. A role for caspases in lens fiber differentiation. *Journal of Cell Biology* **140**, 153–158 (1998).
355. de Botton, S. *et al.* Platelet formation is the consequence of caspase activation within megakaryocytes. *Blood* **100**, 1310–1317 (2002).
356. Zhao, B. *et al.* Nuclear Condensation during Mouse Erythropoiesis Requires Caspase-3-Mediated Nuclear Opening. *Developmental Cell* **36**, 498–510 (2016).
357. Weil, M., Raff, M. C. & Braga, V. M. M. Caspase activation in the terminal differentiation of human epidermal keratinocytes. *Current Biology* **9**, 361–365 (1999).
358. Fujita, J. *et al.* Caspase Activity Mediates the Differentiation of Embryonic Stem Cells. *Cell Stem Cell* **2**, 595–601 (2008).
359. Li, F. *et al.* Apoptotic caspases regulate induction of iPSCs from human fibroblasts. *Cell Stem Cell* **7**, 508–520 (2010).
360. Jänicke, R. U. MCF-7 breast carcinoma cells do not express caspase-3. *Breast Cancer Research and Treatment* *2008 117:1* **117**, 219–221 (2008).
361. Coexistence of High Levels of Apoptotic Signaling and Inhibitor of Apoptosis Proteins in Human Tumor Cells | Cancer Research | American Association for Cancer Research. <https://aacrjournals.org/cancerres/article/63/20/6815/510658/Coexistence-of-High-Levels-of-Apoptotic-Signaling>.
362. Hashimoto, T., Kikkawa, U. & Kamada, S. Contribution of Caspase(s) to the Cell Cycle Regulation at Mitotic Phase. *PLOS ONE* **6**, e18449 (2011).
363. Man, N. *et al.* Caspase-3 controls AML1-ETO-driven leukemogenesis via autophagy modulation in a ULK1-dependent manner. *Blood* **129**, 2782–2792 (2017).
364. Liu, X. *et al.* Caspase-3 Promotes Genetic Instability and Carcinogenesis. *Molecular Cell* **58**, 284–296 (2015).
365. Liu, X. *et al.* Self-inflicted DNA double-strand breaks sustain tumorigenicity and stemness of cancer cells. *Cell Research* *2017 27:6* **27**, 764–783 (2017).
366. Sun, G., Ding, X. A., Argaw, Y., Guo, X. & Montell, D. J. Akt1 and dCIZ1 promote cell survival from apoptotic caspase activation during regeneration and oncogenic overgrowth. *Nature Communications* *2020 11:1* **11**, 1–16 (2020).
367. Fromm, L. & Overbeek, P. A. Inhibition of Cell Death by Lens-Specific Overexpression of bcl-2 in Transgenic Mice. **20**, 276–287 (1997).
368. Wride, M. A., Parker, E. & Sanders, E. J. Members of the bcl-2 and caspase families regulate nuclear degeneration during chick lens fibre differentiation. *Developmental Biology* **213**, 142–156 (1999).



369. Danial, N. N. & Korsmeyer, S. J. Cell Death: Critical Control Points. *Cell* **116**, 205–219 (2004).
370. Kabigting, J. E. T. & Toyama, Y. Interplay between caspase, Yes-associated protein, and mechanics: A possible switch between life and death? *Current Opinion in Cell Biology* vol. 67 141–146 Preprint at <https://doi.org/10.1016/j.ceb.2020.10.010> (2020).
371. Alvarado-Kristensson, M. *et al.* p38-MAPK Signals Survival by Phosphorylation of Caspase-8 and Caspase-3 in Human Neutrophils. *Journal of Experimental Medicine* **199**, 449–458 (2004).
372. Alvarado-Kristensson, M. & Andersson, T. Protein Phosphatase 2A Regulates Apoptosis in Neutrophils by Dephosphorylating Both p38 MAPK and Its Substrate Caspase 3 \*. *Journal of Biological Chemistry* **280**, 6238–6244 (2005).
373. Kuranaga, E. *et al.* Drosophila IKK-Related Kinase Regulates Nonapoptotic Function of Caspases via Degradation of IAPs. *Cell* **126**, 583–596 (2006).
374. Nakhaei, P. *et al.* I $\kappa$ B Kinase  $\epsilon$ -Dependent Phosphorylation and Degradation of X-Linked Inhibitor of Apoptosis Sensitizes Cells to Virus-Induced Apoptosis. *Journal of Virology* **86**, 726 (2012).
375. Zamaraev, A. v., Kopeina, G. S., Prokhorova, E. A., Zhivotovsky, B. & Lavrik, I. N. Post-translational Modification of Caspases: The Other Side of Apoptosis Regulation. *Trends Cell Biol* **27**, 322–339 (2017).
376. Koto, A., Kuranaga, E. & Miura, M. Temporal regulation of Drosophila IAP1 determines caspase functions in sensory organ development. *Journal of Cell Biology* **187**, 219–231 (2009).
377. Kaplan, Y., Gibbs-Bar, L., Kalifa, Y., Feinstein-Rotkopf, Y. & Arama, E. Gradients of a Ubiquitin E3 Ligase Inhibitor and a Caspase Inhibitor Determine Differentiation or Death in Spermatids. *Developmental Cell* **19**, 160–173 (2010).
378. Kang, Y., Neuman, S. D. & Bashirullah, A. Tango7 regulates cortical activity of caspases during reaper-triggered changes in tissue elasticity. *Nature Communications* *2017 8:1* **8**, 1–12 (2017).
379. Kuo, C. T., Zhu, S., Younger, S., Jan, L. Y. & Jan, Y. N. Identification of E2/E3 Ubiquitinating Enzymes and Caspase Activity Regulating Drosophila Sensory Neuron Dendrite Pruning. *Neuron* **51**, 283–290 (2006).
380. Cusack, C. L., Swahari, V., Hampton Henley, W., Michael Ramsey, J. & Deshmukh, M. Distinct pathways mediate axon degeneration during apoptosis and axon-specific pruning. *Nature Communications* *2013 4:1* **4**, 1–11 (2013).
381. Ertürk, A., Wang, Y. & Sheng, M. Local Pruning of Dendrites and Spines by Caspase-3-Dependent and Proteasome-Limited Mechanisms. *Journal of Neuroscience* **34**, 1672–1688 (2014).

382. D'Brot, A. *et al.* Tango7 directs cellular remodeling by the Drosophila apoptosome. *Genes & Development* **27**, 1650 (2013).
383. Sordet, O. *et al.* Mitochondria-targeting drugs arsenic trioxide and lonidamine bypass the resistance of TPA-differentiated leukemic cells to apoptosis. *Blood* **97**, 3931–3940 (2001).
384. Orme, M. H. *et al.* The unconventional myosin CRINKLED and its mammalian orthologue MYO7A regulate caspases in their signalling roles. *Nature Communications* **7**, (2016).
385. Yang, M., Hatton-Ellis, E. & Simpson, P. The kinase Sgg modulates temporal development of macrochaetes in Drosophila by phosphorylation of Scute and Pannier. *Development* **139**, 325–334 (2012).
386. Ding, A. X. *et al.* CasExpress reveals widespread and diverse patterns of cell survival of caspase-3 activation during development in vivo. *Elife* **5**, (2016).
387. Tang, H. L., Tang, H. M., Fung, M. C. & Hardwick, J. M. In vivo CaspaseTracker biosensor system for detecting anastasis and non-apoptotic caspase activity. *Scientific Reports 2015 5:1* **5**, 1–7 (2015).
388. Feinstein-Rotkopf, Y. & Arama, E. Can't live without them, can live with them: Roles of caspases during vital cellular processes. *Apoptosis* **14**, 980–995 (2009).
389. Kong, W. *et al.* Experimental validation of force inference in epithelia from cell to tissue scale. *Scientific Reports 2019 9:1* **9**, 1–12 (2019).
390. Aigouy, B., Cortes, C., Liu, S. & Prud'homme, B. EPySeg: a coding-free solution for automated segmentation of epithelia using deep learning. (2020) doi:10.1242/dev.194589.
391. Rosenblatt, F. THE PERCEPTRON: A PROBABILISTIC MODEL FOR INFORMATION STORAGE AND ORGANIZATION IN THE BRAIN 1. *Psychological Review* **65**, 19–27.
392. Mills, J. C., Lee, V. M. Y. & Pittman, R. N. Activation of a PP2A-like phosphatase and dephosphorylation of tau protein characterize onset of the execution phase of apoptosis. *Journal of Cell Science* **111**, 625–636 (1998).
393. Lane, J. D., Allan, V. J. & Woodman, P. G. Active relocation of chromatin and endoplasmic reticulum into blebs in late apoptotic cells. *Journal of Cell Science* **118**, 4059–4071 (2005).
394. Sproul, L. R., Anderson, D. J., Mackey, A. T., Saunders, W. S. & Gilbert, S. P. Cik1 Targets the Minus-End Kinesin Depolymerase Kar3 to Microtubule Plus Ends. *Curr Biol* **15**, 1420 (2005).
395. Karpova, N., Bobinnec, Y., Fouix, S., Huitorel, P. & Debec, A. Jupiter, a new Drosophila protein associated with microtubules. *Cell Motility and the Cytoskeleton* **63**, 301–312 (2006).
396. Dogterom, M., Kerssemakers, J. W. J., Romet-Lemonne, G. & Janson, M. E. Force generation by dynamic microtubules. *Current Opinion in Cell Biology* **17**, 67–74 (2005).

397. Collins, C. *et al.* Tubulin acetylation promotes penetrative capacity of cells undergoing radial intercalation. *Cell Reports* **36**, (2021).
398. Collins, C., Majekodunmi, A. & Mitchell, B. Centriole Number and the Accumulation of Microtubules Modulate the Timing of Apical Insertion during Radial Intercalation. *Current Biology* **30**, 1958-1964.e3 (2020).
399. Takeda, M., Sami, M. M. & Wang, Y.-C. A homeostatic apical microtubule network shortens cells for epithelial folding via a basal polarity shift. (2017) doi:10.1038/s41556-017-0001-3.
400. Izquierdo, E., Quinkler, T. & de Renzis, S. Guided morphogenesis through optogenetic activation of Rho signalling during early *Drosophila* embryogenesis. *Nature Communications* *2018 9:1* **9**, 1–13 (2018).
401. Ogawa, M., Kawarazaki, Y., Fujita, Y. & Naguro, I. FGF21 Induced by the ASK1-p38 Pathway Promotes Mechanical Cell Competition by Attracting Cells. *Current Biology* **31**, 1048-1057.e5 (2021).
402. Gradeci, D., Bove, A., Lowe, A. R., Banerjee, S. & Charras, G. Distinct modes of cell competition are governed by entropic and energetic properties of mixed cell populations. *bioRxiv* 729731 Preprint at <https://doi.org/10.1101/729731> (2019).
403. Gradeci, D. *et al.* Cell-scale biophysical determinants of cell competition in epithelia. *Elife* **10**, (2021).
404. Shraiman, B. I. Mechanical feedback as a possible regulator of tissue growth. *Proc Natl Acad Sci U S A* **102**, 3318–3323 (2005).
405. Siegrist, S. E. & Doe, C. Q. Microtubule-Induced Pins/G $\alpha$ i Cortical Polarity in *Drosophila* Neuroblasts. *Cell* **123**, 1323–1335 (2005).
406. Igaki, T., Pastor-Pareja, J. C., Aonuma, H., Miura, M. & Xu, T. Intrinsic Tumor Suppression and Epithelial Maintenance by Endocytic Activation of Eiger/TNF Signaling in *Drosophila*. *Developmental Cell* **16**, 458–465 (2009).
407. Manneville, J. B., Jehanno, M. & Etienne-Manneville, S. Dlg1 binds GKAP to control dynein association with microtubules, centrosome positioning, and cell polarity. *Journal of Cell Biology* **191**, 585–598 (2010).
408. Nakamura, M., Zhou, X. Z. & Lu, K. P. Critical role for the EB1 and APC interaction in the regulation of microtubule polymerization. *Current Biology* **11**, 1062–1067 (2001).
409. Etienne-Manneville, S., Manneville, J. B., Nicholls, S., Ferenczi, M. A. & Hall, A. Cdc42 and Par6–PKC $\zeta$  regulate the spatially localized association of Dlg1 and APC to control cell polarization. *Journal of Cell Biology* **170**, 895–901 (2005).
410. Osmani, N., Vitale, N., Borg, J. P. & Etienne-Manneville, S. Scrib Controls Cdc42 Localization and Activity to Promote Cell Polarization during Astrocyte Migration. *Current Biology* **16**, 2395–2405 (2006).

411. Gui, J., Huang, Y. & Shimmi, O. Scribbled Optimizes BMP Signaling through Its Receptor Internalization to the Rab5 Endosome and Promote Robust Epithelial Morphogenesis. *PLoS Genetics* **12**, e1006424 (2016).
412. Shen, J. & Dahmann, C. Extrusion of cells with inappropriate Dpp signaling from *Drosophila* wing disc epithelia. *Science (1979)* **307**, 1789–1790 (2005).
413. Gibson, M. C. & Perrimon, N. Extrusion and death of DPP/BMP-compromised epithelial cells in the developing *Drosophila* wing. *Science (1979)* **307**, 1785–1789 (2005).
414. Zhu, J., Burakov, A., Rodionov, V. & Mogilner, A. Finding the cell center by a balance of dynein and myosin pulling and microtubule pushing: A computational study. *Molecular Biology of the Cell* **21**, 4418–4427 (2010).
415. Tran, P. T., Marsh, L., Doye, V., Inoué, S. & Chang, F. A mechanism for nuclear positioning in fission yeast based on microtubule pushing. *Journal of Cell Biology* **153**, 397–411 (2001).
416. Faivre-Moskalenko, C. & Dogterom, M. Dynamics of microtubule asters in microfabricated chambers: The role of catastrophes. *Proc Natl Acad Sci U S A* **99**, 16788–16793 (2002).
417. Howard, J. & Garzon-Coral, C. Physical Limits on the Precision of Mitotic Spindle Positioning by Microtubule Pushing forces. *BioEssays* **39**, 1700122 (2017).
418. Letort, G., Nedelec, F., Blanchoin, L. & Théry, M. Centrosome centering and decentering by microtubule network rearrangement. *Molecular Biology of the Cell* **27**, 2833–2843 (2016).
419. Wühr, M., Dumont, S., Groen, A. C., Needleman, D. J. & Mitchison, T. J. How does a millimeter-sized cell find its center? *Cell Cycle* **8**, 1115–1121 (2009).
420. Sallé, J. *et al.* Asymmetric division through a reduction of microtubule centering forces. *Journal of Cell Biology* **218**, 771–782 (2019).
421. Röper, K. & Brown, N. H. Maintaining epithelial integrity: A function for gigantic spectraplakins isoforms in adherens junctions. *Journal of Cell Biology* **162**, 1305–1315 (2003).
422. Lacroix, B. *et al.* Microtubule Dynamics Scale with Cell Size to Set Spindle Length and Assembly Timing. *Developmental Cell* **45**, 496–511.e6 (2018).
423. Sedzinski, J., Hannezo, E., Tu, F., Biro, M. & Wallingford, J. B. Emergence of an Apical Epithelial Cell Surface In Vivo. *Developmental Cell* **36**, 24–35 (2016).
424. Werner, M. E. *et al.* Radial intercalation is regulated by the Par complex and the microtubule-stabilizing protein CLAMP/Spf1. *Journal of Cell Biology* **206**, 367–376 (2014).
425. Puthalakath, H., Huang, D. C. S., O'Reilly, L. A., King, S. M. & Strasser, A. The Proapoptotic Activity of the Bcl-2 Family Member Bim Is Regulated by Interaction with the Dynein Motor Complex. *Molecular Cell* **3**, 287–296 (1999).

426. Lane, J. D., Vergnolle, M. A. S., Woodman, P. G. & Allan, V. J. Apoptotic Cleavage of Cytoplasmic Dynein Intermediate Chain and P150GluedStops Dynein-Dependent Membrane Motility. *Journal of Cell Biology* **153**, 1415–1426 (2001).
427. Quintyne, N. J. *et al.* Dynactin Is Required for Microtubule Anchoring at Centrosomes. *Journal of Cell Biology* **147**, 321–334 (1999).
428. Quinn, L. *et al.* Buffy, a Drosophila Bcl-2 protein, has anti-apoptotic and cell cycle inhibitory functions. *The EMBO Journal* **22**, 3568–3579 (2003).
429. Colussi, P. A. *et al.* Debcl, a Proapoptotic Bcl-2 Homologue, Is a Component of the Drosophila melanogaster Cell Death Machinery. *Journal of Cell Biology* **148**, 703–714 (2000).
430. Doumanis, J., Dorstyn, L. & Kumar, S. Molecular determinants of the subcellular localization of the Drosophila Bcl-2 homologues DEBCL and BUFFY. *Cell Death & Differentiation* *2007 14:5* **14**, 907–915 (2007).
431. Krizhevsky, A., Sutskever, I. & Hinton, G. E. ImageNet Classification with Deep Convolutional Neural Networks.
432. Szegedy, C. *et al.* Going deeper with convolutions.
433. Zaritsky, A. *et al.* Interpretable deep learning uncovers cellular properties in label-free live cell images that are predictive of highly metastatic melanoma. *Cell Systems* **12**, 733-747.e6 (2021).



## **Appendix-1: paper supplementary material**

# Supplementary figures

## Microtubule disassembly by caspases is an important rate-limiting step of cell extrusion

Alexis Villars<sup>1,2</sup>, Alexis Matamoro-Vidal<sup>1</sup>, Florence Levillayer<sup>1</sup> and Romain Levayer<sup>1\*</sup>

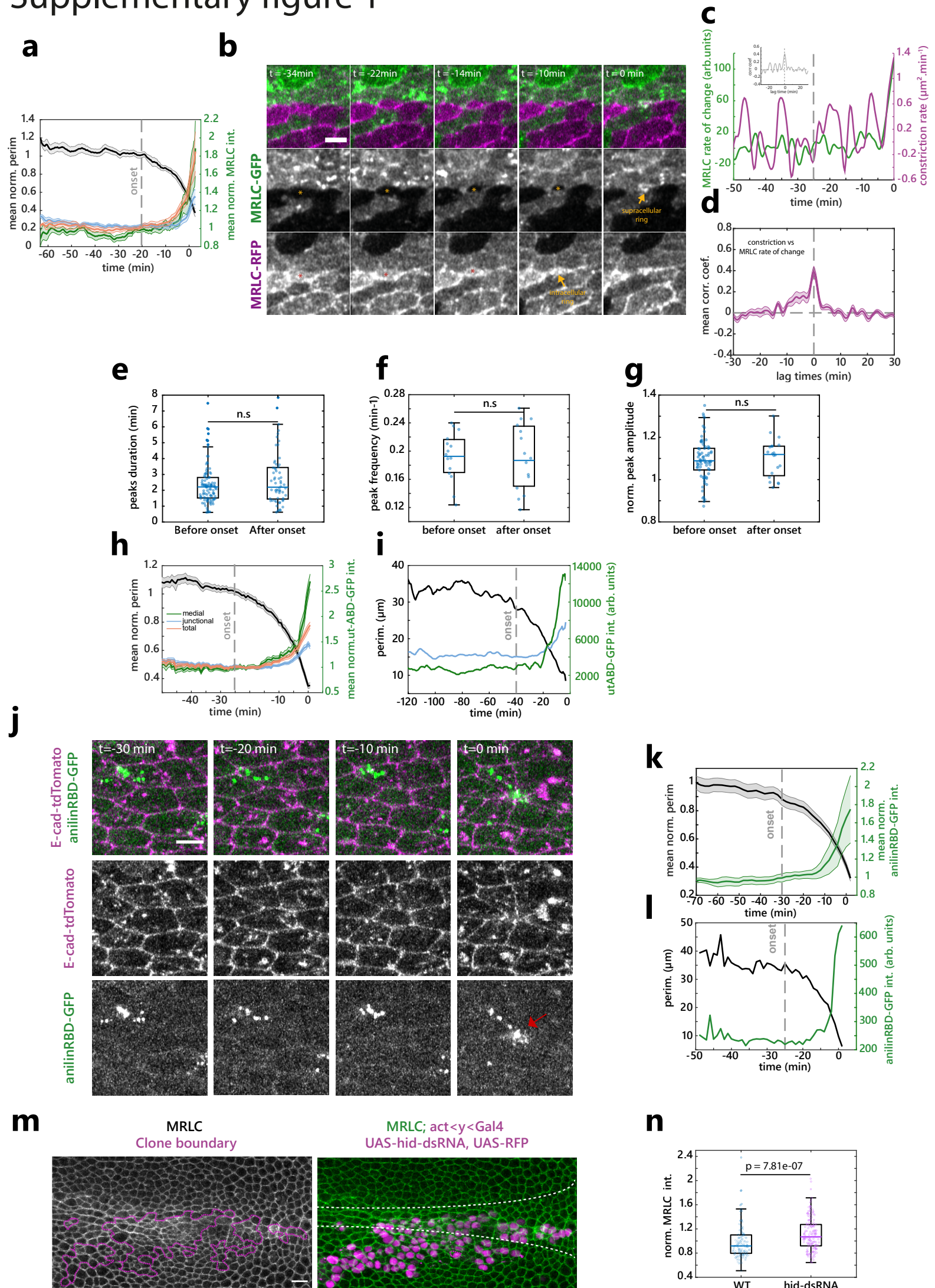
1. Department of Developmental and Stem Cell Biology, Institut Pasteur, Université de Paris Cité, CNRS UMR 3738, 25 rue du Dr. Roux, 75015 Paris, France

2. Sorbonne Université, Collège Doctoral, F75005 Paris, France

\* Correspondance to: [romain.levayer@pasteur.fr](mailto:romain.levayer@pasteur.fr)



# Supplementary figure 1

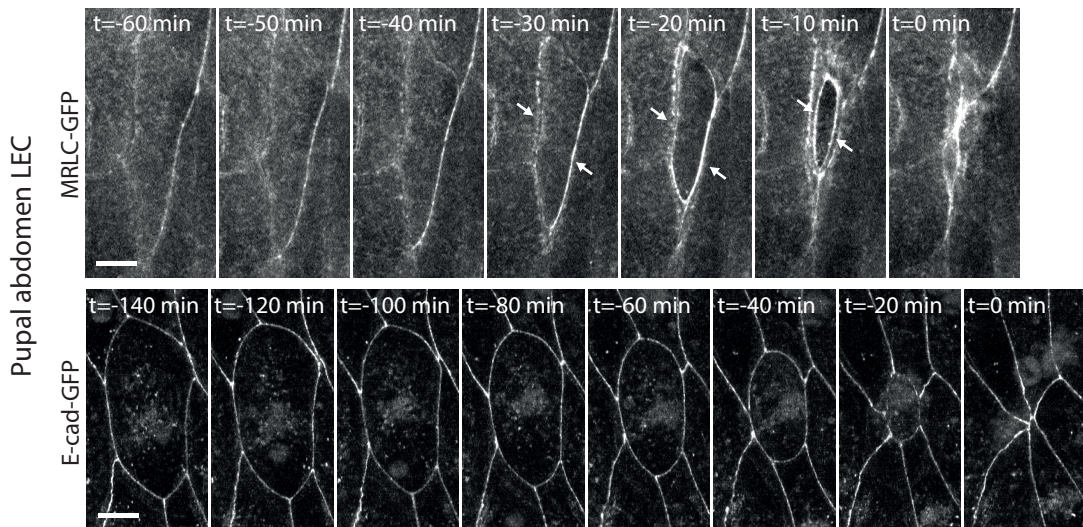


## Supplementary figure 1: Myosin concentration and dynamics do not change at the onset of extrusion

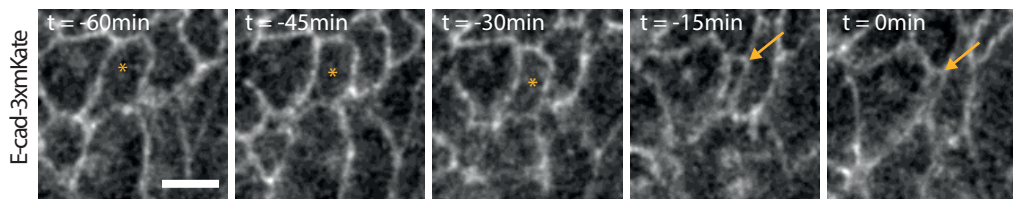
**a** Normalised averaged MRLC intensity (sqh-GFP) in different pools (medial, green, junctional, blue, total, orange) and perimeter (black) in midline extruding cells. Dotted line, onset of extrusion. Light colour areas, S.E.M..  $n=15$  cells. **b** Actomyosin ring marked with mitotic clones expressing either MRLC-GFP, MRLC-RFP or both. Top, overlay, middle, MRLC-GFP, bottom, MRLC-RFP. Orange and red stars, same extruding cell. Arrows, rings formation. Scale bar,  $5\mu\text{m}$ . **c** Representative curve of MRLC-GFP intensity rate of change (green) and perimeter contraction rate (purple) in an extruding cell. Inset, normalised cross-correlation of these curves.  $t_0$ , onset of extrusion (dotted line).  $N=2$ ,  $n>16$  cells. **d** Average normalised cross-correlation of MRLC rate of change and perimeter contraction rate.  $n=15$  cells. Light area, S.E.M.. **e,f,g** Boxplots showing MRLC intensity peaks duration (half-peak width, **e**,  $n=106$  &  $61$  pulses), frequency (**f**,  $n=15$  cells) and normalised amplitude (**g**,  $n>70$  and  $20$  peaks, before or up to  $10$  min after extrusion onset), before and after extrusion onset. n.s.: non-significant. For each boxplot, central line, median value, bottom and top of the box 25th and 75th percentiles. Whiskers, most extreme points not considered outliers. Outliers shown in red. **h** Averaged normalised F-actin intensity (utABD-GFP) in different pools (medial, green, junctional, blue, total, orange) and perimeter (black). Light colour areas, S.E.M.. Grey dotted line, onset of extrusion.  $n=37$  cells. **i** Representative curve of junctional (blue) and medial (green) utABD-GFP intensity and perimeter (black) of an extruding cell. **j** Anillin Rho-Binding-domain-GFP during cell extrusion (green, bottom row) and E-cad-tdTomato (magenta, middle). Red arrow, late Rho accumulation. Scale bar,  $5\mu\text{m}$ . **k** Averaged normalised AnillinRBD-GFP apical signal (green) and perimeter (black) during cell extrusion. Grey dotted line, extrusion onset. Light colour areas, S.E.M..  $N=2$  pupae,  $n=31$  cells. **l** Single representative curve of AnillinRBD-GFP intensity (green) and perimeter (black) of an extruding cell. **m** MRLC-GFP (green, left) with hid-dsRNA clones (magenta, magenta lines, clone borders). White dotted lines, midline. Scalebar,  $10\mu\text{m}$ . **n** Boxplot of MRLC-GFP junctional intensity (one dot per cell) outside or inside hid-dsRNA clones.  $p\text{-value} = 7.8129\text{e-}07$ .  $N=2$  pupae,  $n = 779$  WT and  $155$  clonal cells (only a subset of points shown). All statistical tests: two-sided t-tests. Source data are provided in the source data file.

# Supplementary figure 2

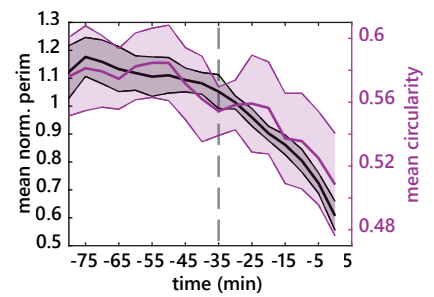
**a**



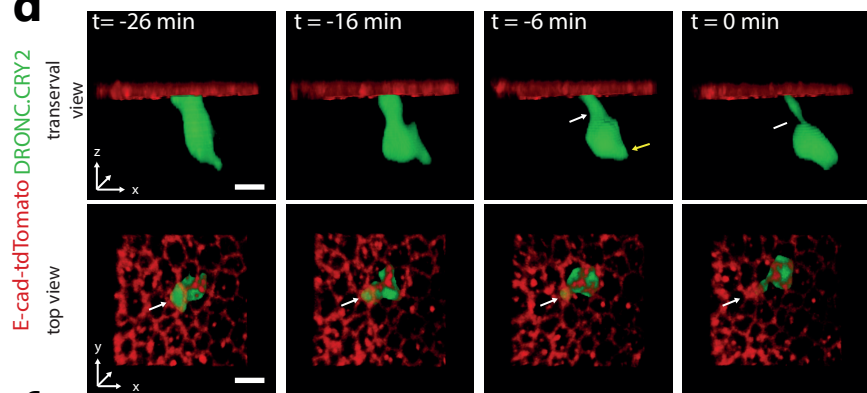
**b**



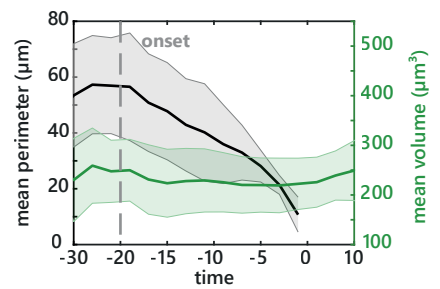
**c**



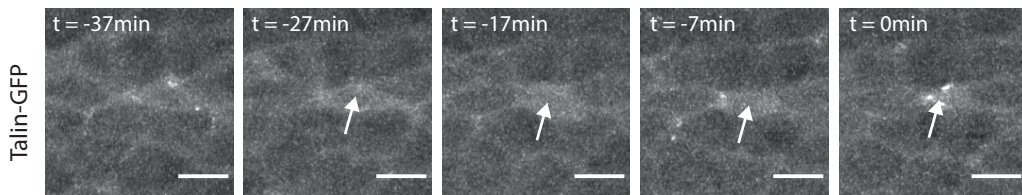
**d**



**e**



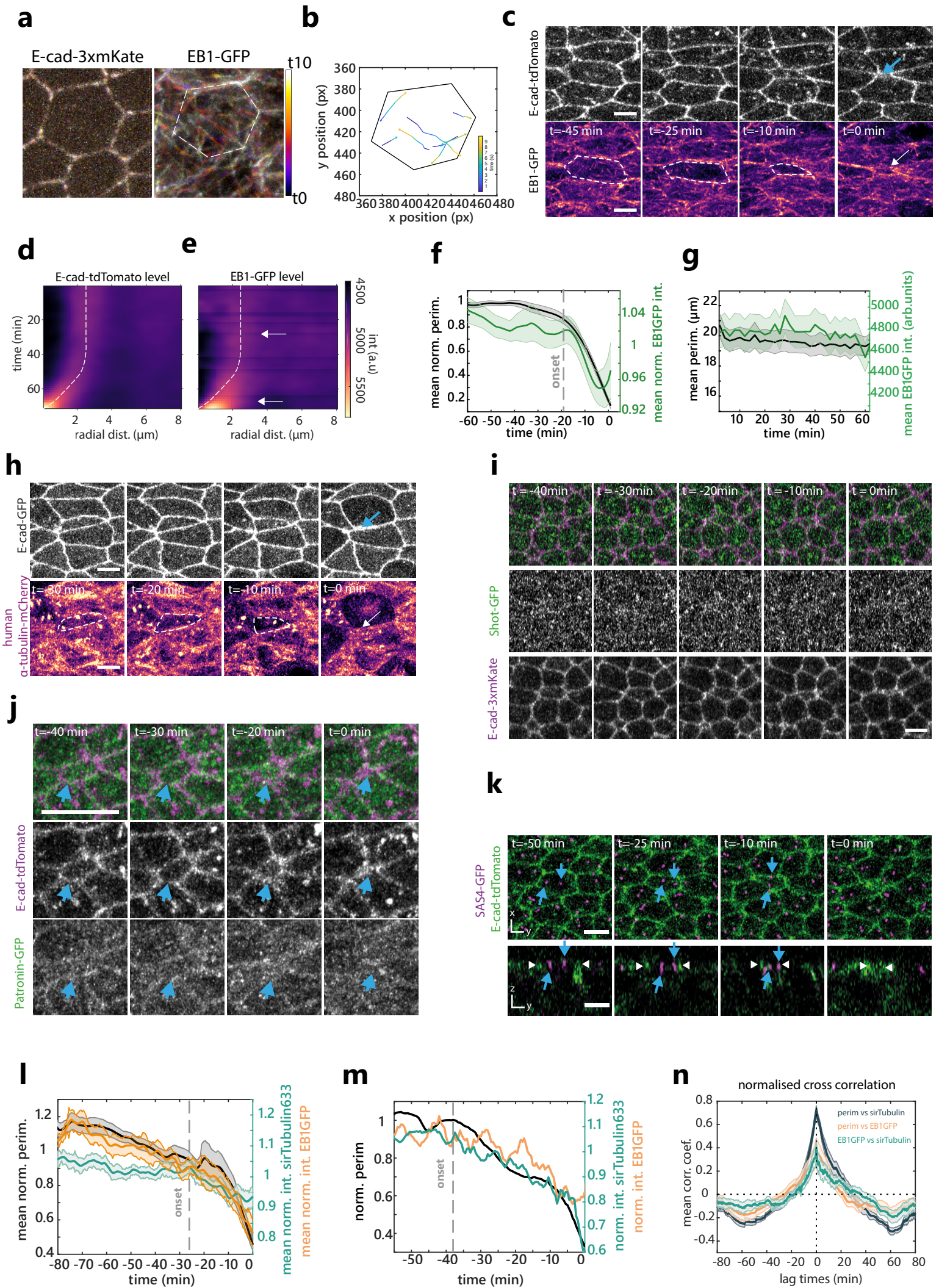
**f**



**Supplementary figure 2: Cell extrusion in the notum is not initiated by an actomyosin ring, nor volume reduction or a modulation of ECM binding**

**a** Snapshots of extruding larval epidermal cells (LEC) from the pupal abdomen. Top shows MRLC (sqh-GFP). N=2, n=27 cells. White arrows, supracellular and intracellular myosin ring. N=1, n=10 cells. Bottom, evolution of cell perimeter visualised with E-cad-GFP which shows cell rounding. Scalebar, 10 $\mu$ m. **b** Snapshots of E-cad-3xmKate during the extrusion of a cell in ROCK-dsRNA (driven by pnr-Gal4). Stars point at the extruding cell. Arrows point at the final stage of cell extrusion where the cell decrease its circularity. Scale bar, 5 $\mu$ m. N=2, n>10 cells. **c** Averaged and normalised perimeter (black) and circularity (purple) during cell extrusion in ROCK-dsRNA context. Dotted line, inflexion point. Shadowed area are S.E.M. n=10 cells. **d** Snapshots of a single extruding cell upon optoDronc activation with 3D rendering (using cytoplasmic GFP signal). Green, segmented cell volume, red, cell contour visualised with E-cad-tdTomato. Top, transversal view, bottom, view from the apical side. White arrows point at apical reduction of volume while yellow arrow shows the basal increase of volume. Scale bars, 5 $\mu$ m. N=2, n=13 cells. **e** Averaged cell volume (green) and perimeter (black) during cell extrusion. Light colour areas are S.E.M.. n=6 cells. **f** Snapshots of Talin-GFP during cell extrusion. t0 is termination of extrusion. White arrows show an extruding cell. Scale bars, 5 $\mu$ m. Source data are provided in the source data file. N=1, n=15 cells.

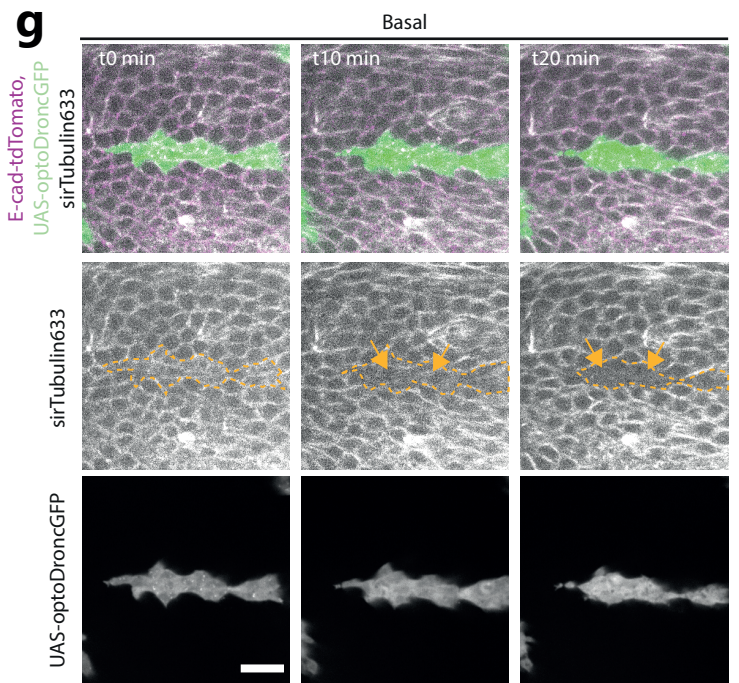
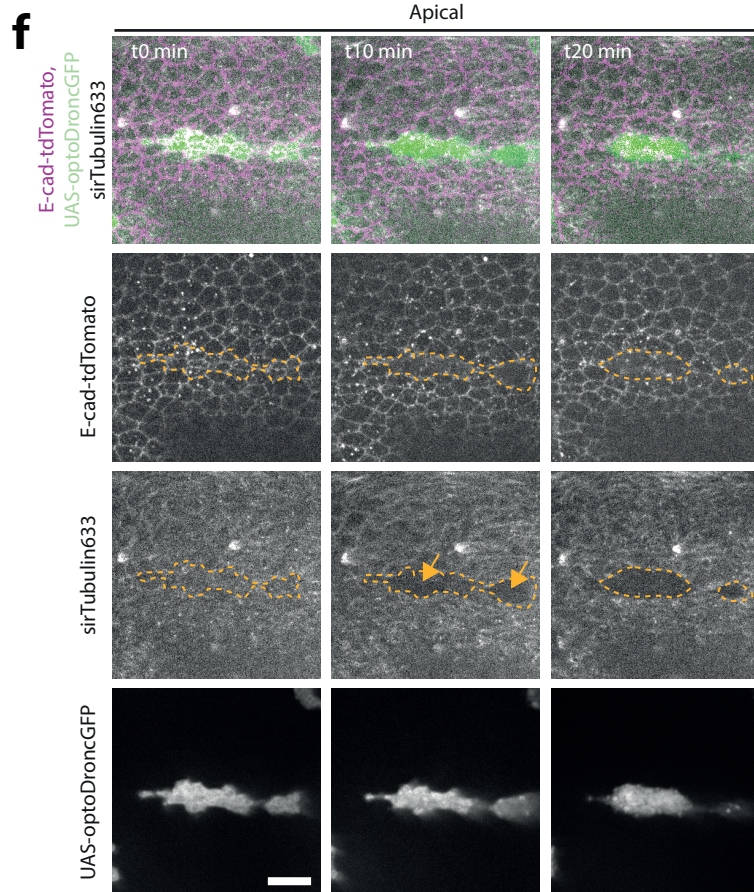
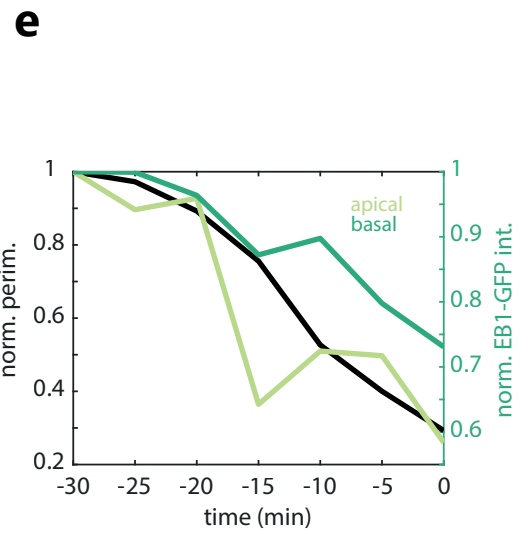
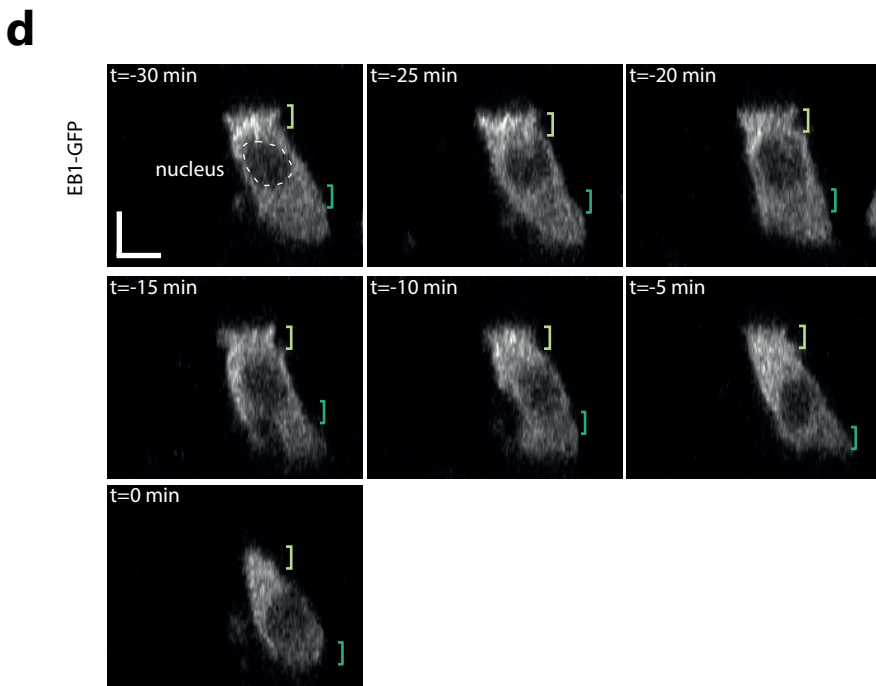
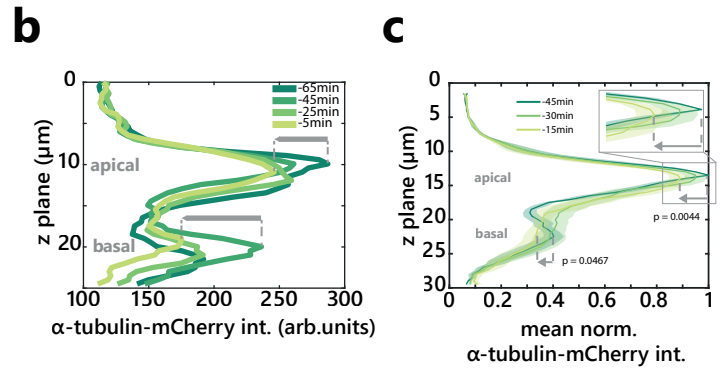
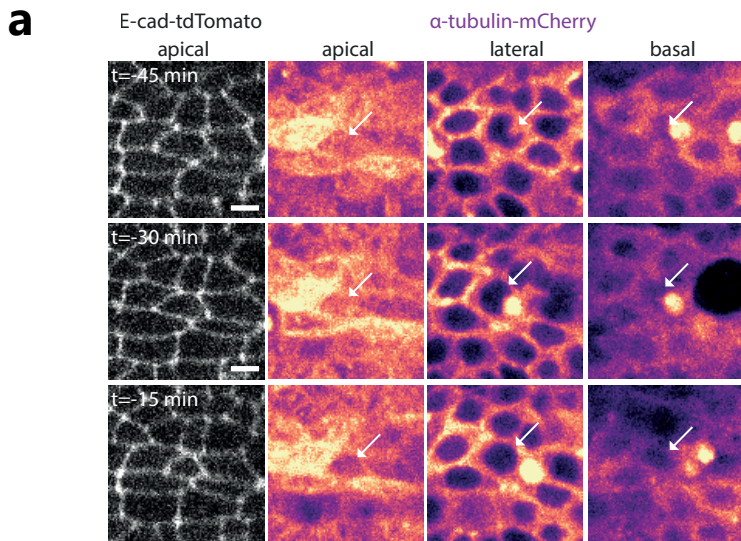
# Supplementary figure 3



### Supplementary figure 3: Visualisation of microtubule depletion using different markers.

**a** Time projection (colour-coded) of E-cad-3xmKate (left) and EB1-GFP (right) over 10s. Dotted white line, cell contour. N=2, n>50 cells. **b** Tracking of EB1 comets over 10s. **c** E-cad-tdTomato (top) and EB1-GFP (bottom, pseudo-colour) during cell extrusion in the midline. Blue arrow, end of extrusion, white arrow, late EB1 accumulation in the neighbours, cell contour, white dotted lines. Scale bar, 5 $\mu$ m. N=2, n=60 cells. **d,e** Radial averaged kymograph (see **Figure 3g-i**) of E-cad-tdTomato (left) and EB1-GFP (right) in pseudo-colour, time on y-axis going downward, x-axis, radial distance from cell center. White dotted lines, average cell contour (detected with the maximum of E-cad signal). Top white arrow, onset of EB1 depletion in the extruding cells, bottom arrow, late EB1-GFP accumulation in the neighbours. n=60 cells. **f,g** Averaged normalised EB1-GFP signal (green) and perimeter (black) in extruding cells (**f**, n=22) and non-extruding cells (**g**, n=27). Grey dotted line, onset of extrusion. Light colour areas, S.E.M.. **h** E-cad-GFP (top) and human  $\alpha$ Tubulin-mCherry (bottom, pseudo-colour) during cell extrusion. Red and white arrows, end of extrusion. White dotted lines, extruding cell contours. Representative of 15 cells. Scale bar, 5 $\mu$ m. **i** Shot-GFP (green, middle panel) and E-cad-tdTomato (magenta, bottom panel) in an extruding cell. t<sub>0</sub>, termination of extrusion. Representative of 20 cells. Scale bar, 5 $\mu$ m. **j** Patronin-GFP (green, bottom) and E-cad-tdTomato (magenta, middle) in an extruding cell (blue arrows). t<sub>0</sub>, termination of cell extrusion. Representative of 20 cells. Scale bar, 10 $\mu$ m. **k** Centrosome position during cell extrusion visualised by SAS4-GFP (magenta) with E-cad-tdTomato (green) top and lateral view. t<sub>0</sub>, termination of cell extrusion. Blue arrows, centrosome positions. White arrows, junctions of the extruding cell. Representative of 15 cells. Scale bar, 5 $\mu$ m. **l** Averaged and normalised perimeter (black), sirTubulin633 intensity (green), EB1-GFP intensity (orange) during extrusion. Grey dotted line, onset of extrusion. Light colour areas, S.E.M.. n=19 cells. **m** Perimeter (black), sirTubulin633 intensity (green) and EB1-GFP intensity (Orange) of an extruding cell. Grey dotted line, onset of extrusion. **n** Averaged and normalised cross-correlation of the perimeter vs sirTubulin633 (black) or vs EB1-GFP (orange) or EB1-GFP vs sirTubulin633 (green). Light colour areas, S.E.M.. Maximum of correlation at t=0min for each curve. n=19 cells. Source data are provided in the source data file.

# Supplementary figure 4



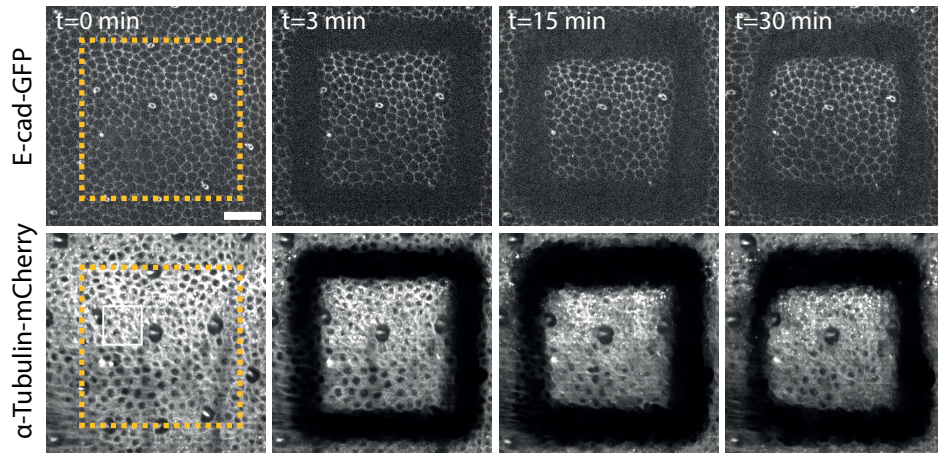
#### Supplementary figure 4: MT depletion occurs throughout the cell.

**a**  $\alpha$ -tubulin-mCherry in different z-planes during cell extrusion (apical, lateral and basal, time from top to bottom, t0, termination of extrusion). Left panels, E-cad-tdTomato in the junction plane. White arrows, extruding cell in every plane. Scale bars, 5 $\mu$ m. N=2, n=11 cells. **b,c** Quantification of apico-basal  $\alpha$ tubulin-mCherry signal during extrusion (y-axis, z-plane, x-axis signal, different colour for each time point, t0 extrusion termination). **b** Single representative quantification for the cells shown in **a**. Grey lines, reduction of signal over time apically and basally. **c** Averaged and normalised quantification of  $\alpha$ tubulin-mCherry apico-basal signal during cell extrusion. Axis are the same as in **b**. The inset highlights apical depletion. Grey arrows, signal reduction in the apical and basal plane. n=11 cells. p-values are pairwise and one-sided t-test. Light colour areas, S.E.M.. **d** Side views of a single-cell clone expressing UAS-EB1-GFP during cell extrusion. Light green bracket, apical plane, darker green, basal plane bellow the nucleus. Nucleus boundary highlighted with the white dotted line. N=2, n=24 cells. **e** Perimeter (black), and EB1-GFP normalised intensity apically (light green) or basally (darker green) of the single extruding cell example shown in **d**. Representative of 10 cells. **f,g** Snapshots of the apical and basal depletion of sirTubulin633 (grey, middle panel) of a clone expressing UAS-optoDronc (green, bottom panel) after blue light exposure (t0 to t20min). N=2, n=12 clones. **f** Snapshots of the apical plane of that clone visualised using Ecad-tdTomato (magenta, top panel). Orange dotted line, border of the clone. Orange arrows, extruding/dying cells where tubulin signal is depleted. **g** Snapshots of a basal plane of that clone. Orange dotted line, border of the clone. Orange arrows, extruding/dying cells where tubulin signal is depleted (the cytoplasm of the cells can be seen with the GFP channel). Scale bars are 10 $\mu$ m. Source data are provided in the source data file.

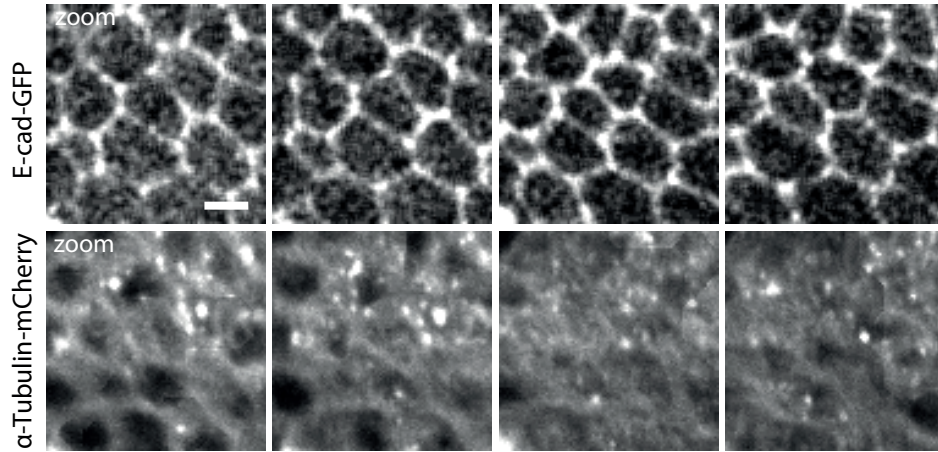


# Supplementary figure 5

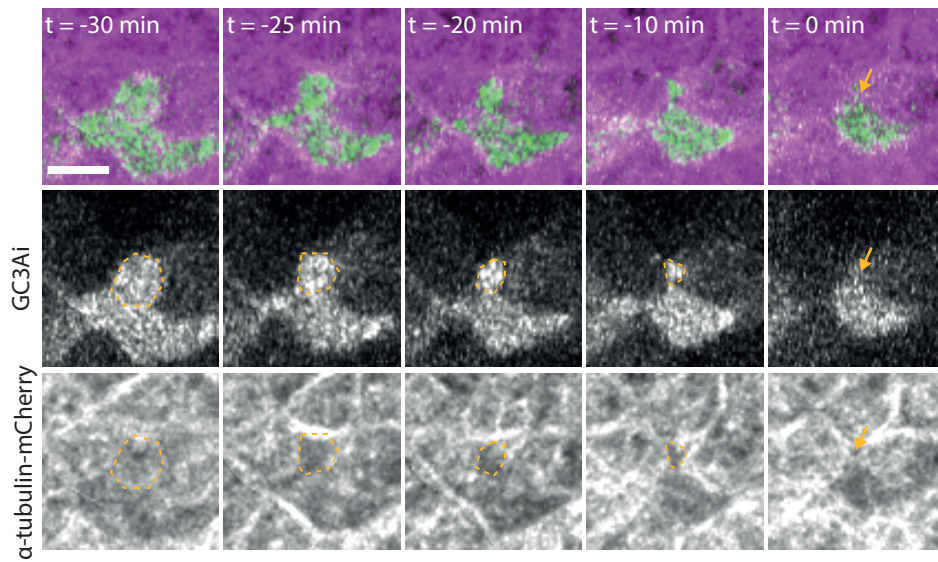
**a**



**b**



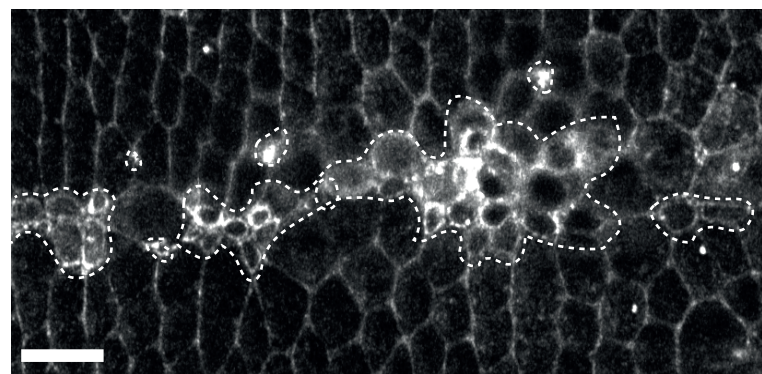
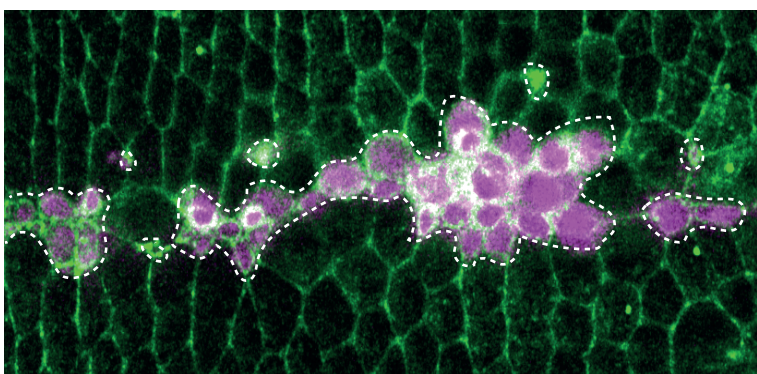
**e**



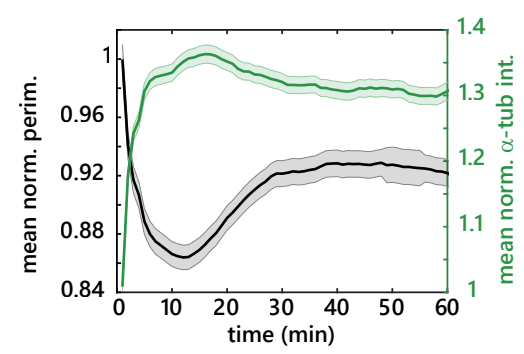
**f**

UAS-optoDronc-GFP ;  
UAS-p35

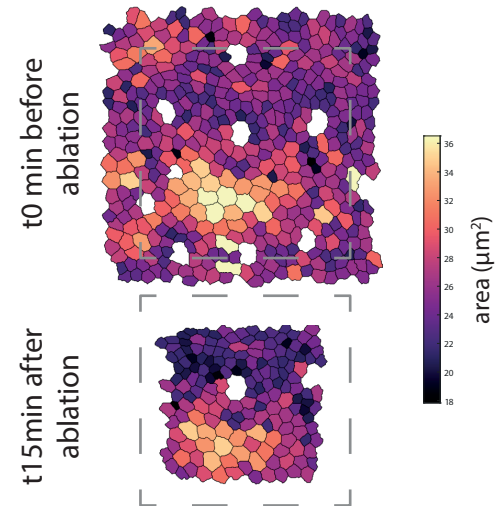
sqh-mKate



**c**



**d**

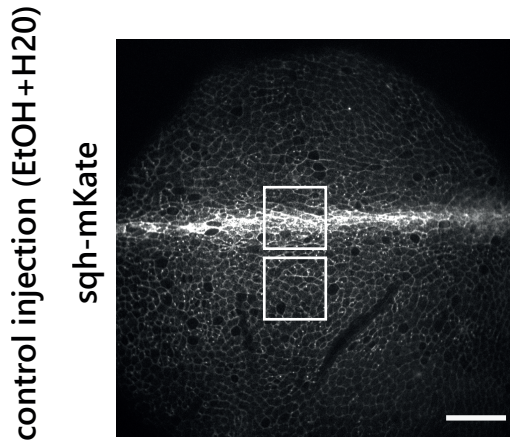


## Supplementary figure 5: The depletion of microtubules is effector caspases dependent

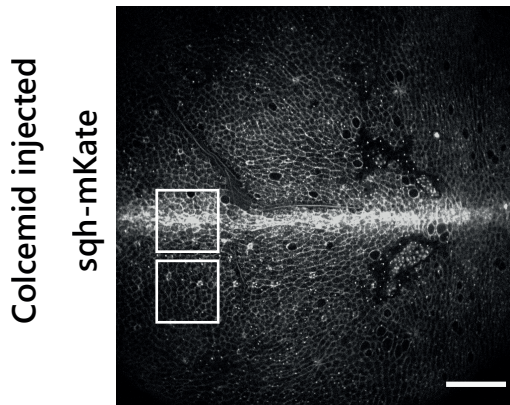
**a,b** Snapshots of a laser ablated pupal notum. **a** Snapshots of the full ablated region (orange dotted square) showing  $\alpha$ -tubulin-mCherry (bottom) and E-cad-GFP (top).  $t_0$  is the last time point before ablation (note the relaxation at  $t=15\text{min}$ ). Scale bar,  $25\mu\text{m}$ .  $N=3$  pupae. **b** Snapshots of a zoom in a sub-region in the ablated region (White Square in **a**) showing  $\alpha$ -tubulin-mCherry (bottom) and E-cad-GFP (top). Scale bar,  $5\mu\text{m}$ . **c** Averaged and normalised  $\alpha$ -tubulin-mCherry signal (green) and cell perimeter (black) in the relaxed square region following ablation. Note the transient increase of Tubulin signal during the transient reduction of cell perimeter. Light colour areas are S.E.M..  $N=3$  pupae,  $n=123$  cells. **d** Snapshots showing the segmentation of the cells in the ablated region and their cell area before ablation ( $t_0\text{min}$ ) or at maximal relaxation ( $t_{15\text{min}}$ ). Grey dotted line shows the ablation region. **e** Snapshots of caspase activation using GC3Ai (green, middle) before microtubule depletion visualised with  $\alpha$ -tubulin-mCherry (magenta, bottom) during cell extrusion. Caspase activation ( $t=-30\text{min}$ ) precedes the beginning of MT depletion ( $t=-25\text{min}$ ). Orange dotted lines, contour of the extruding cell. Orange arrow, termination of extrusion. Representative of 20 cells and 2 movies, scale bar,  $5\mu\text{m}$ . **f** Snapshot of MRLC accumulation (sqh-mKate, green and bottom) in clone expressing UAS-OptoDronc-GFP and UAS-p35 (magenta, contours shown with white dotted lines) after 3hours of blue light exposure. Representative of  $>10$  clones. Scale bar is  $10\mu\text{m}$ .  $N=18$  pupae. Source data are provided in the source data file.

# Supplementary figure 6

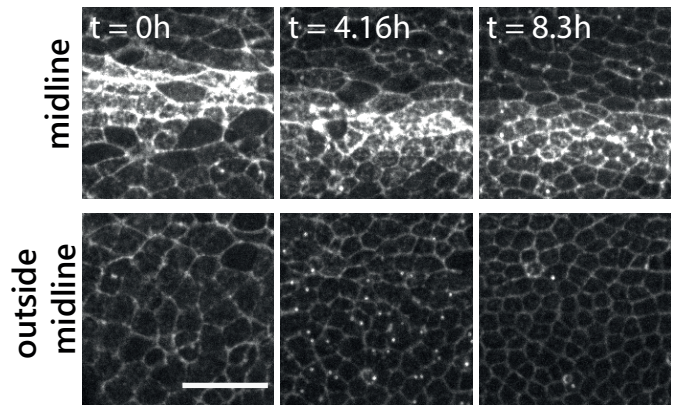
**a**



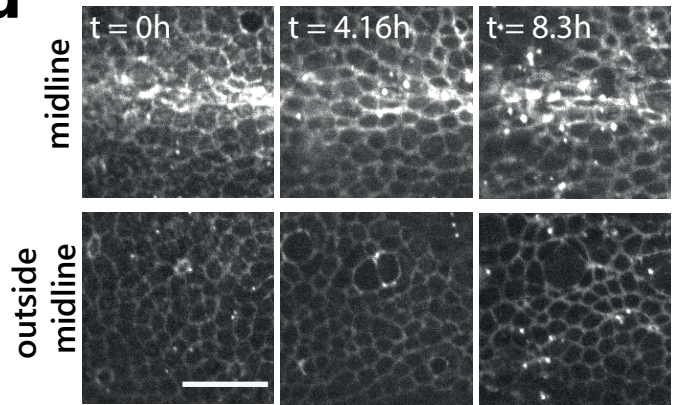
**c**



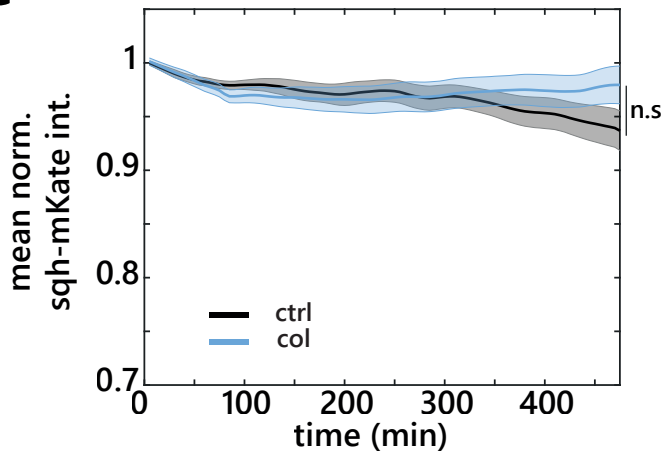
**b**



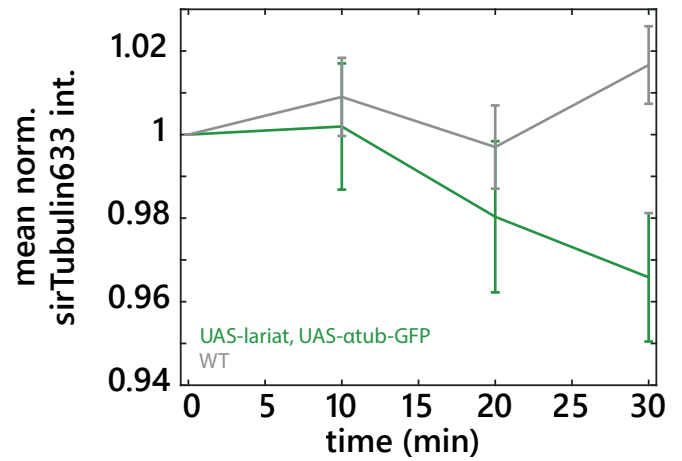
**d**



**e**



**f**

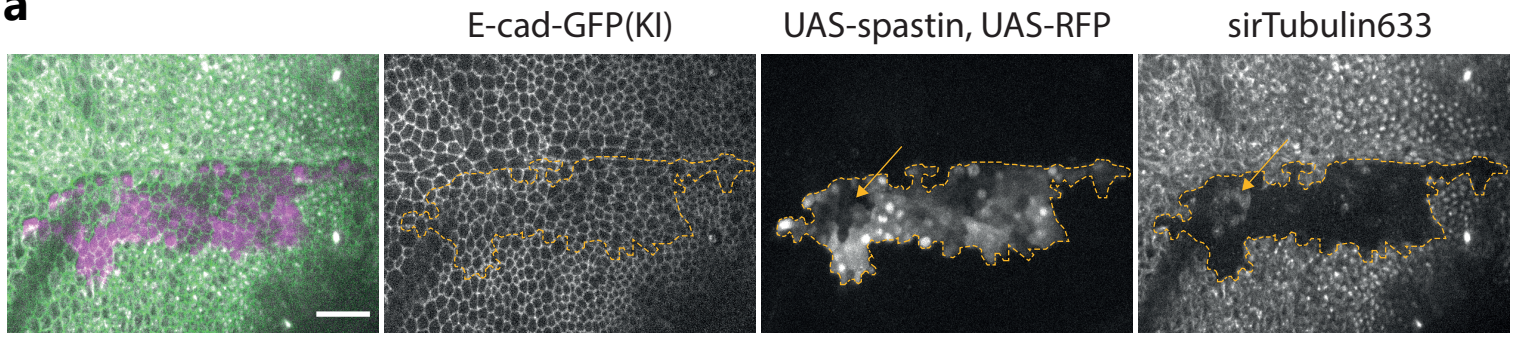


## Supplementary figure 6: Evolution of MRLC levels upon colcemid injection and LARIAT control

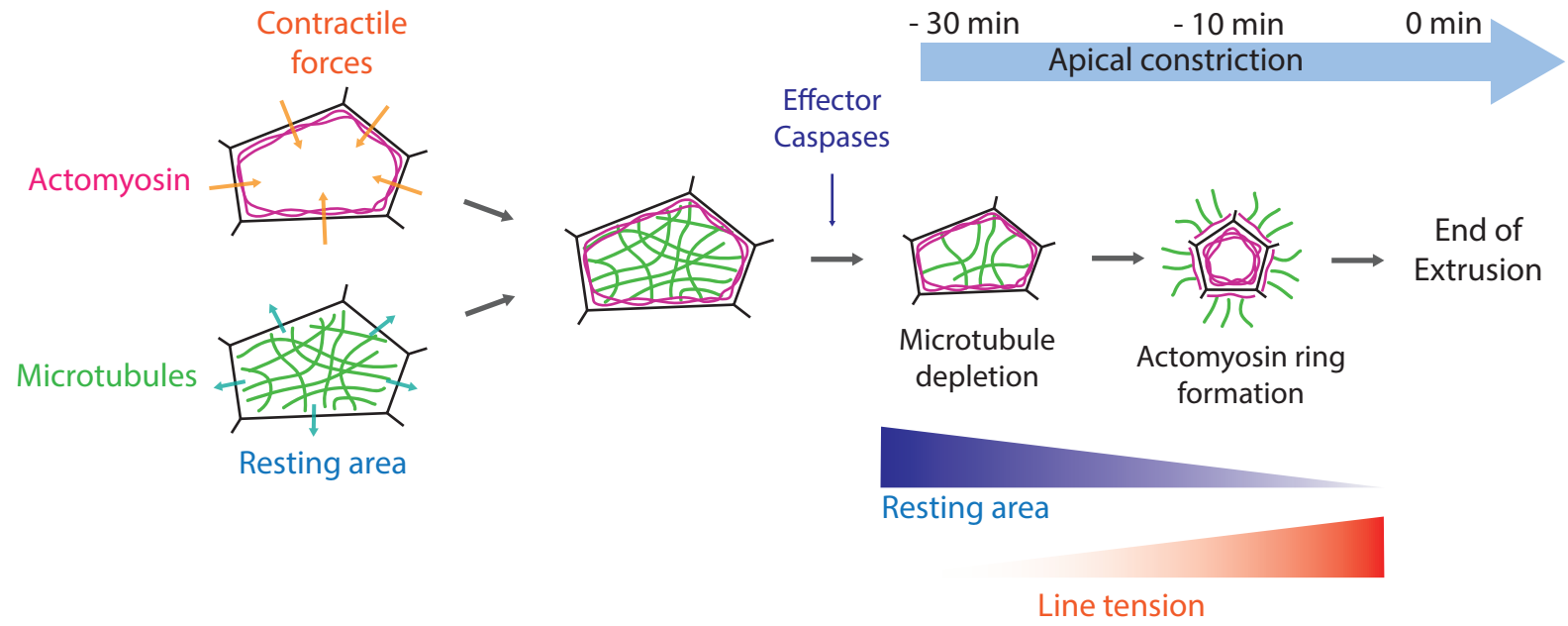
**a-d** Snapshots of local z-projections of live pupal nota of Sqh-mKate (MRCL) levels following mock injection (EtOH+H<sub>2</sub>O) (**a,b**) or colcemid injection (**c,d**) with the same acquisition parameters and contrasts. **a,c** Full nota view right after injection, Scale bars, 50µm. White boxes highlight the midline (top) and out-of-midline (bottom) regions shown in **b** and **d**. **b,d** Snapshots over time after injection. Scale bars, 25µm. **e** Normalised and averaged Sqh-mKate signal from total fluorescence of 3 regions per pupae after injection in colcemid (blue) or control (black) injections. Light colour areas are S.E.M.. N=2 pupa for control and 3 pupa for colcemid. **f** Normalised and averaged sir-tubulin633 levels in cells expressing UAS-Lariat, UAS- $\alpha$ -tubulin-GFP (green) or controls (grey) after blue light exposure. N = 2 nota, n = 20 wt cells, n = 15 clonal cells (UAS-Lariat, UAS- $\alpha$ -tubulin-GFP, green). Error bars are S.E.M.. Source data are provided in the source data file.

# Supplementary figure 7

**a**



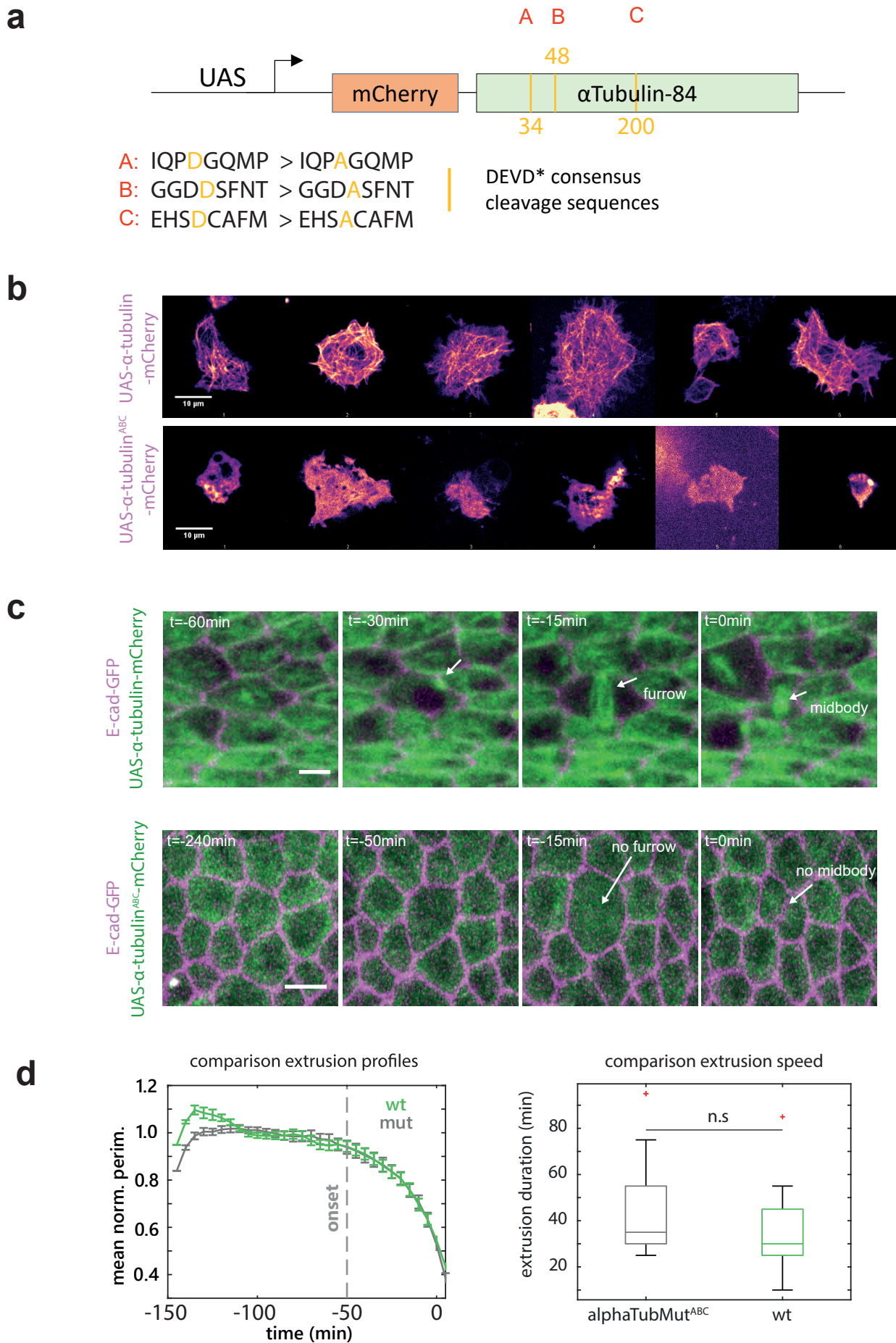
**b**



### **Supplementary figure 7: Spastin depletion of Microtubules and working model**

**a** Snapshots showing sirTubulin633 depletion (grey, right) in clones expressing UAS-Spastin, UAS-RFP (magenta, middle) with tub-Gal80ts in the notum after 6 hours at 29°C (permissive temperature). Cell contour is visualised using E-cad(KI)-GFP (green, left). Orange dotted lines highlight the border of the clone. Orange arrows point at cell expressing less UAS-Spastin, UAS-RFP where the depletion of SirTubulin633 is weaker. Scale bar, 25µm. N=3 pupae. **b** Schematic of the working model. Cell-cell junctions are in black. Actomyosin is in light red and microtubules (MTs) are represented as green lines. Contractile forces are regulated by the junctional actomyosin network. MTs may regulate directly or indirectly the resting area of the cell. At equilibrium the two components are balanced. Upon effector caspases activation, MTs are progressively depleted, hence reducing the resting area of the cell and promoting apical constriction without cell rounding. Later on, actomyosin accumulates in a contractile ring which terminates cell extrusion through an increase of line tension and correlating with an accumulation of MTs in the neighbours. Source data are provided in the source data file.

# Supplementary figure 8



## Supplementary figure 8: Mutation of $\alpha$ Tubulin caspase cleavage sites prevents proper integration in MTs

**a** Schematic representation of the  $\alpha$ -Tubulin-mCherry construct. A,B,C shows the different caspase-cleavage sites at 34, 48 and 200 amino acids respectively. Yellow bars show mutation sites. The sequence of the cleavage site and the introduced mutations are shown below. n=6 cells. **b** Snapshots of different representative S2 cells transfected with the WT  $\alpha$ Tubulin-mCherry construction (top) or the mutated form (labelled  $\alpha$ -Tubulin<sup>ABC</sup>-mCherry, bottom) driven by the UAS promoter. White arrows point at MTs in the WT form. These are absent from the cells expressing the mutant  $\alpha$ -Tubulin<sup>ABC</sup>-mCherry (mostly cytoplasmic signal). n=6 cells. **c** Comparison of the  $\alpha$ -Tubulin-mCherry and  $\alpha$ -Tubulin<sup>ABC</sup>-mCherry localisation in the *Drosophila* pupal notum (UAS promoter, pnr-gal4 driver). Top row shows  $\alpha$ Tubulin-mCherry WT (green) with E-cad-GFP (magenta). White arrows point at one example of division furrow and the persisting midbody after cytokinesis. Bottom row shows mutant  $\alpha$ -Tubulin<sup>ABC</sup>-mCherry. White arrows point at the absence of labelling at the division furrow or the midbody. Scale bars are 5 $\mu$ m. **d** Left panel, Averaged and normalised apical perimeter of extruding cells expressing either WT UAS- $\alpha$ -Tubulin-mCherry (green) or mutant UAS- $\alpha$ -Tubulin<sup>ABC</sup>-mCherry (grey). Error bars are s.e.m.. Grey dotted line shows the onset of extrusion. Cells are aligned by the end of extrusion. n= 30 cells for both conditions. Right panel shows box blot of extrusion duration (between initiation and full apical closure) of cell expressing either UAS- $\alpha$ -Tubulin-mCherry (green) or UAS- $\alpha$ -Tubulin<sup>ABC</sup>-mCherry (grey). The difference is not significant (n.s.). n= 30 cells for both conditions. For each boxplot, the line in the middle represents the median value, the bottom of the box 25th percentiles and the top of the box is the 75th percentiles. The whiskers extend to the most extreme data points not considered outliers. If any, the outliers are plotted in a red marker. Two-sided t-test was performed. Source data are provided in the source data file.



## **Appendix-2: review**



# Collective effects in epithelial cell death and cell extrusion

Alexis Villars<sup>1,2</sup> and Romain Levayer<sup>1</sup>

Programmed cell death, notably apoptosis, is an essential guardian of tissue homeostasis and an active contributor of organ shaping. While the regulation of apoptosis has been mostly analysed in the framework of a cell autonomous process, recent works highlighted important collective effects which can tune cell elimination. This is particularly relevant for epithelial cell death, which requires fine coordination with the neighbours in order to maintain tissue sealing during cell expulsion. In this review, we will focus on the recent advances which outline the complex multicellular communications at play during epithelial cell death and cell extrusion. We will first focus on the new unanticipated functions of neighbouring cells during extrusion, discuss the contribution of distant neighbours, and finally highlight the complex feedbacks generated by cell elimination on neighbouring cell death.

## Addresses

<sup>1</sup> Institut Pasteur, Université de Paris, CNRS UMR3738, Department of Developmental and Stem Cell Biology, F-75015 Paris, France

<sup>2</sup> Sorbonne Université, Collège Doctoral, F75005 Paris, France

Corresponding author: Levayer, Romain ([romain.levayer@pasteur.fr](mailto:romain.levayer@pasteur.fr))

Current Opinion in Genetics & Development 2022, 72:8–14

This review comes from a themed issue on **Developmental mechanisms, patterning and evolution**

Edited by **Magali Suzanne** and **Miguel Torres Sánchez**

For a complete overview see the [Issue](#)

Available online 6th October 2021

<https://doi.org/10.1016/j.gde.2021.09.004>

0959-437X/© 2021 Elsevier Ltd. All rights reserved.

## Introduction

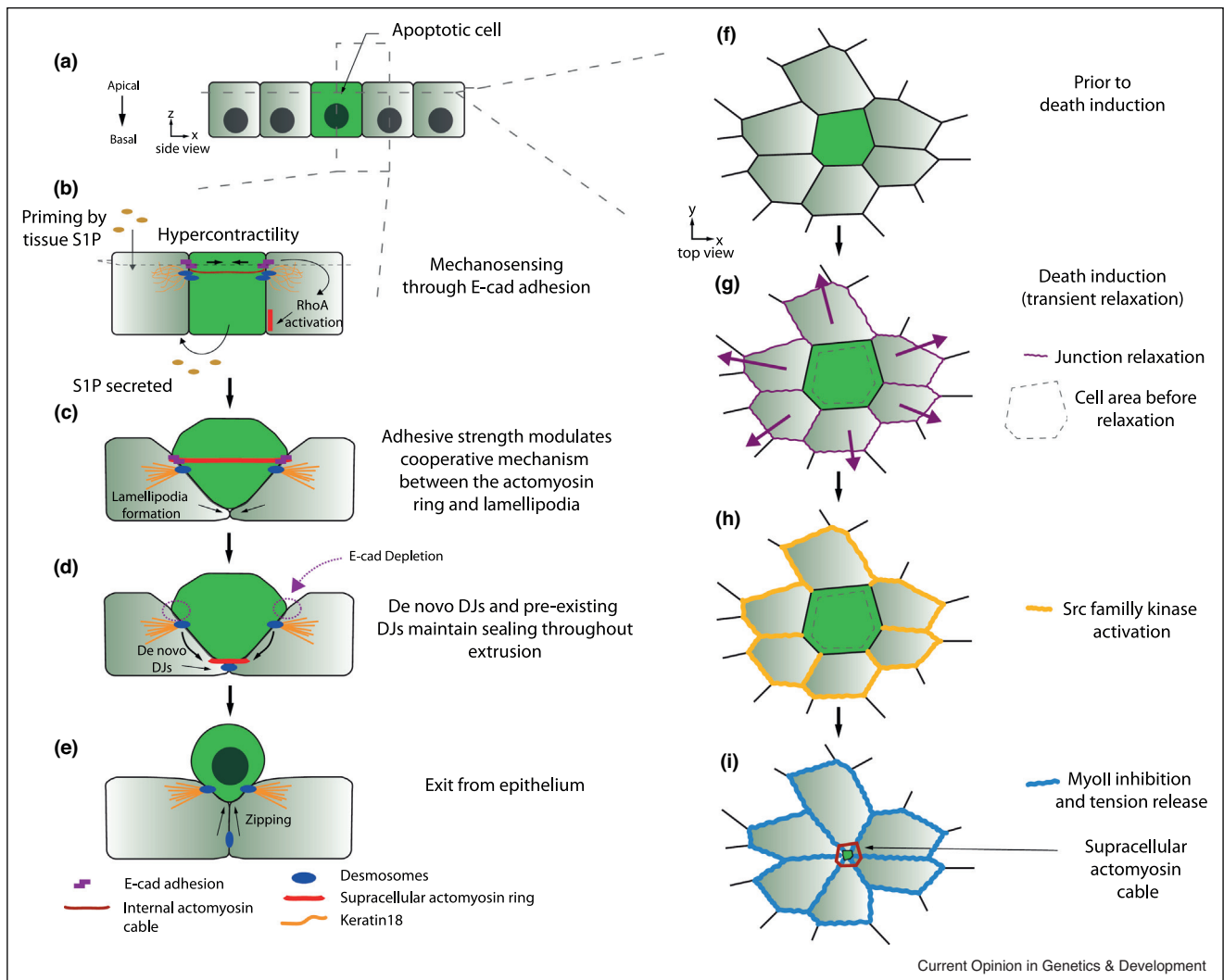
Tissue size regulation and homeostasis rely on the fine balance between cell death and cell proliferation. While we have a very good understanding of the cellular effectors regulating proliferation and apoptosis, how these processes are fine-tuned and coordinated at the tissue level remains quite enigmatic. Apoptosis is the best known programmed-cell death process. It is characterised by cell shrinkage and chromatin condensation followed by membrane blebbing and fragmentation into apoptotic bodies [1]. Apoptosis is orchestrated by caspases, a conserved family of proteases which control

cellular remodeling by cleaving hundreds of proteins [2]. While apoptosis is widespread in tissues during morphogenesis and homeostasis, our understanding of this process is mostly based on isolated cells and was mostly studied in a cell-autonomous framework. However, cell elimination from within a tissue imposes certain constraints and requires a minimal level of coordination. This is particularly true for epithelia, made of tightly adhesive cells forming mechanical and chemical barriers, where tissue sealing must be constantly maintained despite the elimination of cells. This is normally achieved by cell extrusion: a succession of remodeling steps leading to cell expulsion while maintaining tissue sealing [3–5]. Studies over the last twenty years, mostly using MDCK (Madin-Darby Canine Kidney) cells, have provided a good understanding of cell extrusion. It is initiated by the formation of a contractile actomyosin ring in the extruding cell [3,6], followed by the formation of a supracellular ring in the neighbours through secretion from the extruding cell of sphingosine-1-phosphate (S1P) and binding to its S1P2 receptor in the neighbours [7], leading to microtubules reorganisation, Rho activation [8] and the formation of a contractile purse string. Eventually the ring slides basally and expels the extruding cell out of the epithelium while bringing neighbours together [6] (Figure 1a–e). These previous studies outline the concerted actions of the dying cell and its neighbours and demonstrate that cell extrusion is like a miniature morphogenetic process.

Upstream of cell expulsion, the decision to engage in cell death and/or in extrusion is also a complex cell decision making event that is not purely cell-autonomous. For instance, the modulation of local cell density and pressure can trigger cell extrusion [9–12]. Similarly, cell competition, the context-dependent elimination of cells through apoptosis or extrusion, is a perfect illustration of the non-cell autonomous decision to die/extrude [13,14]. This suggests that the engagement in extrusion/apoptosis not only relies on cell-autonomous parameters but also on collective effects.

Here we will review recent literature revealing even more complex cell–cell coordinations at play during cell extrusion and the decision to eliminate a cell. We will first discuss the new roles of neighbouring cells in regulating cell extrusion and the unexpected contribution of distant neighbours. We will then outline recent results illustrating the effects of cell death on the engagement in apoptosis of the neighbouring cells.

Figure 1



### Cell extrusion and coordination with direct neighbours.

**(a)** Side view of an epithelial tissue. Apical side is on top and basal side on the bottom. The green cell represents an apoptotic cell activating caspases. **(b)** Lateral zoom view of the interface of the apoptotic cell with its neighbours. Once it has become apoptotic this cell will become hyper contractile through the formation of an internal actomyosin ring (red line shows the ring, black arrow toward cell centre shows contractility). This will generate forces transmitted to the neighbours by E-cad (purple). This triggers a mechanotransduction pathway in neighbours leading to RhoA activation which requires priming by S1P (brown ellipses). **(c)** Later the neighbours form a supracellular purse string (red line) concomitantly to lamellipodia formation. The two mechanisms contribute to cell extrusion and the balance between both is modulated by adhesion strength (E-cad in purple). Desmosomal Junctions (DJs in blue) remain intact throughout extrusion. They bear forces leading to keratin-18 alignment toward the extruding cells (orange lines). **(d)** The supracellular actomyosin cable is sliding basally while constricting (red line). Newly DJs (blue) are formed at lamellipodia to provide continuous sealing while E-cad is depleted to allow cell expulsion (purple dashed lines). **(e)** The extruding cell is expelled from the epithelium while neighbours are brought together. **(f)** Top view of the epithelium throughout extrusion. **(g)** Following apoptosis induction the extruding cell (green) transiently relaxes (black line = current shape versus dashed line = previous shape). Purple arrows show direction of relaxation. This is concomitant to orthogonal junction transient relaxation (purple curved lines). **(h)** The transient relaxation leads to Src family kinase (SFK) activation at these junctions (yellow curved lines). **(i)** SFK downregulates MyoII specifically at orthogonal junctions further relaxing these junctions. This provides a mechanism to overcome mechanical constraints exerted by the neighbours restricting the constriction of the extruding cell.

Altogether, these recent results illustrate how much epithelial cell death is regulated collectively rather than cell-autonomously. While relevant for the topic, this review will not discuss the non-autonomous effects of

apoptosis on cell proliferation [15] or morphogenesis [16]. We will not discuss either the concept of cell competition as numerous recent reviews have covered the subject [13,14,17].

### The new contributions of direct neighbours to cell extrusion

The removal of epithelial cells through extrusion requires a fine coordination between cell constriction, junction disassembly and formation of new junctions between neighbouring cells. Yet strong mechanical coupling between the extruding and the neighbouring cells is required to maintain tissue cohesion and coordinate cell deformations. Accordingly, E-cad depletion induces extrusion failure and perturb epithelial integrity [18]. Mechanical coupling through E-cad with direct neighbours was previously shown to reorganise actomyosin during extrusion through tension-dependent Coronin1B recruitment and actin reorganisation [19]. A new layer of coordination was recently revealed in MCF7 extruding cells, where E-cad dependent force transmission triggers the tension-dependent recruitment of MyoVI, p114/115 RhoGEF relocalisation and RhoA activation in the neighbours [20,21\*\*] (Figure 1b,c). E-cad coupling not only regulates the actomyosin ring, but also the balance with other active contributors of extrusion. Previously it was shown that basal lamellipodia from the extruding cell neighbours also contribute to cell expulsion, especially in conditions of low cell density [22]. More recently, it was shown that basal protrusions coexist systematically with heterogeneous actomyosin rings and are required to orient the ring and ensure basal sealing [23\*\*] (Figure 1d,e). The robustness and efficiency of extrusion is achieved by the coupling between these two mechanisms (basal protrusions and purse-string) that can compensate each other. The strength of mechanical coupling with the neighbours through E-cad and substrate adhesion modulate the relative contribution of these two actors [23\*\*].

Eventually adherens junctions need to be disassembled between the extruding cell and its neighbours [24,25]. Yet to avoid tissue rupture, cell-cell adhesion must be maintained throughout extrusion. This apparent contradiction may be solved by Desmosomal Junctions (DJs), which were recently shown to be maintained throughout apoptotic extrusion of MDCK cells until new DJs are formed between neighbouring cells [26\*\*] (Figure 1a–e). In addition, DJs are also coupled to the actomyosin ring through their binding to keratin-18. Depleting Desmoplakin (a component of DJs) leads to a reduction of tissue tension, local tissue tearing and extrusion failure, suggesting that DJs maintenance is essential for extrusion and tissue cohesion [26\*\*]. These results argue again for the need of a constant mechanical coupling between the dying cell and its neighbours which relies on diverse adhesive components.

Cell extrusion not only relies on active remodeling of the neighbouring cells but also on the global mechanical state of the tissue that is more or less extrusion-permissive. For instance, a developmental switch which globally changes

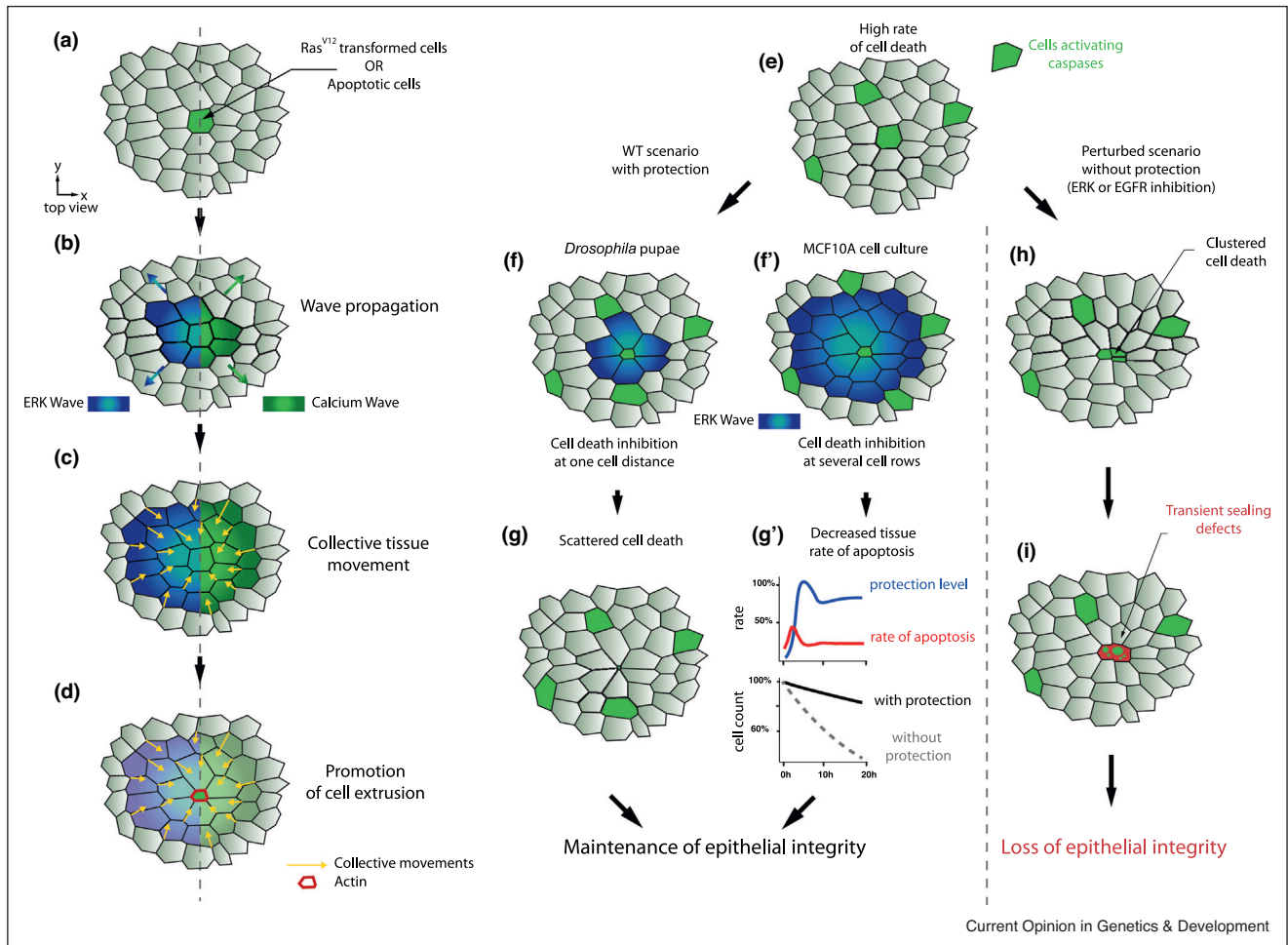
E-cad turnover and tissue tension is essential to modulate the rate of larval cell extrusion in the *Drosophila* pupal abdomen (albeit with contrasted contribution) [27,28]. Similarly, mammalian epithelium also needs to be primed by S1P from the serum to increase mechanosensitive recruitment of p114RhoGEF following initiation of extrusion [20,21\*\*], suggesting that S1P also has a tissue-wide permissive role for extrusion (Figure 1b). Extrusion is also inhibited by high tensile prestress of the tissue and in extruding cell neighbours [29\*,30]. For instance, increased tension through Caveolin1 depletion throughout the tissue or in the extruding cell neighbours prevents the extrusion of oncogenic cells [30]. This illustrates the tug-of-war at play between the contractile extruding cell and the resistance generated by tissue-wide tension. One way to overcome this mechanical constraint is through local relaxation of tension in neighbouring cell junctions which are not shared with the extruding cell (Figure 1f–i). Accordingly, an early release of tension in the apoptotic cell leads to immediate and transient relaxation of the neighbours, which leads to SFK (Src Family protein tyrosine Kinases) activation and MyoII inhibition in the junctions orthogonal to the dying cell [29\*]. This mechanism may restrict the range of action of the forces exerted by the extruding cell, thus preventing the stress to build-up and tissue tearing.

To conclude, these recent results illustrate the complex coupling at play between the extruding cell, its neighbours and the tissue. Constriction and cell protrusions are coordinated through mechanotransduction and mechanical coupling which is maintained through different junctional components (E-cad, DJs). The multiple layers of regulation of tension are at the basis of the self-organised properties of cell extrusion which ensure its robustness and efficiency.

### The contribution of larger collective movements to cell extrusion

Beside the active coordination with close neighbours, recent results revealed larger collective effects also involved in the regulation of cell extrusion. Most of them rely on polarised movements of cells and collective migration toward the extruding cell (Figure 2a–d). For instance, apoptosis initiation or oncogene activation in MDCK cells and zebrafish embryo triggers calcium waves [31\*\*]. These waves propagate from the extruding cells over 3–15 rows of cells through a trigger-wave mechanism combining intracellular calcium storage release, cation channels and gap junctions. They induce actin remodeling in the neighbours which promotes convergent collective cell movements toward the extruding cell and its expulsion (Figure 2a–d). Interestingly, these waves share many similarities with recently described ERK waves induced near oncogenic cells and apoptotic cells [32\*\*]. Sustained ERK activation in MCF10A cells (through B-Raf<sup>V600E</sup>) activates the metalloprotease ADAM17 which

Figure 2



### Large scale coordinations between the extruding cell and the neighbouring tissue.

(a) Top view of an epithelium showing a cell initiating apoptosis or a transformed cell (in green). (b) Initiation of apoptosis or oncogene activation both triggers calcium waves (right side of dashed line in green) or ERK waves (left side of dashed line in blue). Arrows show radial propagation of these waves. (c) These waves travel to several cell rows albeit through different mechanisms (see main text). Both types of waves trigger collective cell movement/migration (yellow arrows) toward the extruding cell. (d) These collective movements promote the extrusion of the apoptotic or transformed cells. (e) High rates of cell death (green cells) can arise for instance in condition of acute stress or during development. (f) In *Drosophila*, the extruding cell triggers ERK pulses in the direct neighbours (blue). This locally and transiently inhibits caspases and cell extrusion. (g) This mechanism alters the spatiotemporal distribution of cell death therefore dispersing cell extrusion in space and time. As a result it maintains epithelial integrity. (f') In MCF10A cell culture, the extruding cell triggers ERK waves travelling up to roughly 3 cell rows (blue). (g') This protective mechanism decreases globally the rate of apoptosis (red curve, top) therefore decreasing the speed of cell elimination (bottom graph, black line). These two mechanisms (f–g') ensure the maintenance of epithelial integrity. (h) and (i) Perturbed scenario without ERK feedbacks. (h) Local clusters of cell death can arise, which prevent proper extrusion and impair transiently epithelial sealing (i). Alternatively, the global increase of the speed of cell elimination may lead to tissue tearing.

releases EGFR ligands and activates ERK over several cell rows. These waves also drive directed cell migration towards the transformed and/or apoptotic cells and promote their extrusion [32\*\*] (Figure 2a–d).

How then can such collective movements promote cell extrusion and cell death? Convergent flow could trigger local topological defects and local increase of pressure which promote cell death and cell extrusion [9–12]. Accordingly, these movements are reminiscent of the

convergent movements of the Wild Type (WT) cells toward *Scribble* mutant cells during mechanical cell competition [14,33,34]. This promotes *Scribble*<sup>KD</sup> cell elimination through their compaction. In this case the collective movements are driven by the secretion of the chemoattractant FGF21 by the *Scribble*<sup>KD</sup> cells [35]. Interestingly, similar movements are also required to expel epithelial cells infected by *Listeria monocytogenes* and are driven by the activation of NF- $\kappa$ B and the relative reduction of stiffness of the infected cells [36].

Taken together, these data highlight unexpected large scale non-autonomous collective effects regulating cell extrusion. These collective movements are observed in a wide range of situations (apoptosis, oncogenic cells, infected cells, mutant cells) and are regulated by different signalling pathways, suggesting that different contexts converged to the same cellular mechanism to expel cells. This unanticipated contribution of distant neighbours to cell extrusion highlights its multiscale regulation.

### Extrusion feedbacks on cell death in the neighbouring cells

So far, we discussed how surrounding cells participate in cell extrusion and regulate apoptosis. Reciprocally, recent studies highlight mechanisms by which cell extrusion/cell death can also feedback on cell death probability of the neighbours.

Recent studies from the group of Olivier Pertz and our group described unanticipated anti-apoptotic effects of cell death on neighbouring cells [37<sup>\*\*</sup>,38<sup>\*\*</sup>]. In MCF10A cells, apoptotic cells trigger ERK/AKT waves which radially propagate over roughly 3 rows of cells. Their propagation is dependent on ADAM17-dependent cleavage of pro-EGF [37<sup>\*\*</sup>] (Figure 2e,f), similar to ERK waves near oncogenic cells [32<sup>\*\*</sup>]. Likewise, we showed in the *Drosophila* pupal notum (a single layer epithelium) that ERK pulses occur in the direct neighbours of extruding cells [38<sup>\*\*</sup>] (Figure 2e,f). Although the range of propagation of these ERK pulses are different in the two cases, both decrease the probability of death in the vicinity of the extruding cell through transient caspase inhibition. Transient caspase inhibition is most likely mediated by the downregulation/inhibition of the pro-apoptotic gene *hid* in the pupal notum [39] (transcriptionally and post-transcriptionally [40,41]), while the pro-survival early transcriptional targets of ERK remained to be identified in MCF10A cells [37<sup>\*\*</sup>]. The transient nature of this inhibition is related to the finite duration of ERK pulses combined with tissue-wide persistent stress (serum/growth factor starvation and cytotoxic treatment in MCF10A cells, expression of *hid* in the posterior region of the notum). These feedbacks have two essential roles for epithelial integrity. On the one hand, they reduce the global rate of apoptosis hence preventing tissue rupture in situation of acute stress [37<sup>\*\*</sup>] (Figure 2g). On the other hand, they also alter the spatiotemporal distribution of cell death by locally and transiently inhibiting caspases, hence scattering cell elimination and preventing the extrusion of cells in clusters [38<sup>\*\*</sup>] (Figure 2g), a very detrimental situation for tissue sealing (Figure 2h,i). These two studies suggest that the rate of cell death/cell extrusion and their distribution in space and time are not purely cell-autonomous, but rather emerging properties of local feedbacks driven by cell extrusion/apoptosis.

Beside these inhibitory feedbacks, apoptosis was also shown to enhance cell death in the surrounding tissue in other situations. For instance caspase activation following acute tissue damages increases globally S1P levels in the zebrafish epidermis and promotes cell extrusion through pulsatile MyoII contractions and reduced tissue tension [42]. Since S1P is also secreted actively by the extruding cell [7], the same mechanism may generate a local positive feedback on extrusion. Alternatively, massive induction of apoptosis in the posterior compartment of the *Drosophila* larval wing disc is sufficient to trigger ectopic cell death in the other compartment [43]. This is driven by the secretion of the TNF orthologue Eiger from the posterior cells which leads to JNK pathway activation across the compartment and ectopic apoptosis. Interestingly, the same TNF-dependent mechanism seems to coordinate hair follicle destruction in mice, suggesting that it is conserved in mammals [43]. Recently, similar propagation effects were observed for alternative modes of cell death in non-epithelial cells [44]. For instance, ferroptosis can propagate in waves in U937 cells through extracellular factors acting upstream of cell swelling [45]. These studies highlight potential positive feedbacks of cell death and extrusion on their neighbours, however they were described only in relatively artificial conditions of acute stress, and it remains unclear whether similar positive feedbacks exist in more physiological contexts.

In summary, these recent studies demonstrate that the probability of cell extrusion/cell death and their distribution are emerging properties of the tissue which are based on non-cell autonomous positive and negative feedbacks on caspases. The negative feedbacks are essential to maintain epithelial sealing in conditions of high rates of elimination by buffering the global rate of elimination and scattering cell death in space and time. Further studies would be required to understand in which conditions positive feedbacks start to dominate and further promote cell elimination.

### Conclusions

While apoptosis was long viewed as a cell-autonomous process, we tried in this review to emphasize the complex multicellular coordinations at play during epithelial extrusion and the regulation of apoptosis itself. Recent studies highlight the diverse contributions of the direct neighbours of extruding cells which allow concerted deformations and maintenance of tissue sealing. The plasticity of the extrusion process reveals self-organised properties which most likely rely on multiple mechanical feedbacks (increase of tension in neighbouring junctions, local relaxation of tension in orthogonal junctions, contribution of basal protrusions). Similarly, global mechanical properties of the tissue and long-range collective movements play respectively a permissive and instructive role in cell extrusion. Upstream of cell expulsion, the activation of caspases also relies on multicellular feedbacks which

include local negative feedbacks near extruding cells, and positive feedbacks upon massive cell death induction. Overall, the probability of a cell to extrude is a complex decision-making process that integrates cell-autonomous factors (e.g. mechanical properties, caspases activity) as well as multiple feedbacks acting on different space-scales, time-scales and layers of regulation. While there is still a long way to go before we will be able to predict when and where an epithelial cell will extrude, the combination of multiplex imaging (including morphological parameters and live-sensors of signalling pathways) with Bayesian approaches will surely help to evaluate the relative contribution of each layer of regulation to the engagement in cell extrusion.

### Conflict of interest statement

Nothing declared.

### Acknowledgements

We thank members of RL lab for critical reading of the manuscript. AV is supported by a PhD grant from the Ecole Doctorale Complexité du Vivant (Sorbonne University) and from an extension grant of La Ligue contre le Cancer (IP/SC-17130), work in RL lab is supported by the Institut Pasteur (G5 starting package), the ERC starting grant CoSpaDD (Competition for Space in Development and Disease, grant number 758457), the Cercle FSER and the CNRS (UMR 3738).

### References and recommended reading

Papers of particular interest, published within the period of review, have been highlighted as:

- of special interest
- of outstanding interest

1. Fuchs Y, Steller H: **Programmed cell death in animal development and disease.** *Cell* 2011, **147**:742-758.
  2. Crawford ED, Wells JA: **Caspase substrates and cellular remodeling.** *Annu Rev Biochem* 2011, **80**:1055-1087.
  3. Rosenblatt J, Raff MC, Cramer LP: **An epithelial cell destined for apoptosis signals its neighbors to extrude it by an actin- and myosin-dependent mechanism.** *Curr Biol* 2001, **11**:1847-1857.
  4. Gudipaty SA, Rosenblatt J: **Epithelial cell extrusion: pathways and pathologies.** *Semin Cell Dev Biol* 2017, **67**:132-140.
  5. Ohsawa S, Vaughen J, Igaki T: **Cell extrusion: a stress-responsive force for good or evil in epithelial homeostasis.** *Dev Cell* 2018, **44**:532.
  6. Kuipers D, Mehonic A, Kajita M, Peter L, Fujita Y, Duke T, Charras G, Gale JE: **Epithelial repair is a two-stage process driven first by dying cells and then by their neighbours.** *J Cell Sci* 2014, **127**:1229-1241.
  7. Gu Y, Forostyan T, Sabbadini R, Rosenblatt J: **Epithelial cell extrusion requires the sphingosine-1-phosphate receptor 2 pathway.** *J Cell Biol* 2011, **193**:667-676.
  8. Slattum G, McGee KM, Rosenblatt J: **P115 RhoGEF and microtubules decide the direction apoptotic cells extrude from an epithelium.** *J Cell Biol* 2009, **186**:693-702.
  9. Eisenhoffer GT, Loftus PD, Yoshigi M, Otsuna H, Chien CB, Morcos PA, Rosenblatt J: **Crowding induces live cell extrusion to maintain homeostatic cell numbers in epithelia.** *Nature* 2012, **484**:546-549.
  10. Marinari E, Mehonic A, Curran S, Gale J, Duke T, Baum B: **Live-cell delamination counterbalances epithelial growth to limit tissue overcrowding.** *Nature* 2012, **484**:542-545.
  11. Levayer R, Dupont C, Moreno E: **Tissue crowding induces caspase-dependent competition for space.** *Curr Biol* 2016, **26**:670-677.
  12. Saw TB, Doostmohammadi A, Nier V, Kocgozlu L, Thampi S, Toyama Y, Marcq P, Lim CT, Yeomans JM, Ladoux B: **Topological defects in epithelia govern cell death and extrusion.** *Nature* 2017, **544**:212-216.
  13. Claveria C, Torres M: **Cell competition: mechanisms and physiological roles.** *Annu Rev Cell Dev Biol* 2016, **32**:411-439.
  14. Matamoro-Vidal A, Levayer R: **Multiple influences of mechanical forces on cell competition.** *Curr Biol* 2019, **29**:R762-R774.
  15. Diwanji N, Bergmann A: **two sides of the same coin - compensatory proliferation in regeneration and cancer.** *Adv Exp Med Biol* 2019, **1167**:65-85.
  16. Ambrosini A, Gracia M, Proag A, Rayer M, Monier B, Suzanne M: **Apoptotic forces in tissue morphogenesis.** *Mech Dev* 2017, **144**:33-42.
  17. Baker NE: **Emerging mechanisms of cell competition.** *Nat Rev Genet* 2020, **21**:683-697.
  18. Lubkov V, Bar-Sagi D: **E-cadherin-mediated cell coupling is required for apoptotic cell extrusion.** *Curr Biol* 2014, **24**:868-874.
  19. Michael M, Meiring JCM, Acharya BR, Matthews DR, Verma S, Han SP, Hill MM, Parton RG, Gomez GA, Yap AS: **Coronin 1B reorganizes the architecture of F-actin networks for contractility at steady-state and apoptotic adherens junctions.** *Dev Cell* 2016, **37**:58-71.
  20. Acharya BR, Nestor-Bergmann A, Liang X, Gupta S, Duszyc K, Gauquelin E, Gomez GA, Budnar S, Marcq P, Jensen OE *et al.*: **A mechanosensitive RhoA pathway that protects epithelia against acute tensile stress.** *Dev Cell* 2018, **47**:439-452.e6.
  21. Duszyc K, Gomez GA, Lagendijk AK, Yau MK, Nanavati BN, Gliddon BL, Hall TE, Verma S, Hogan BM, Pitson SM *et al.*: **Mechanotransduction activates RhoA in the neighbors of apoptotic epithelial cells to engage apical extrusion.** *Curr Biol* 2021, **31**:1326-1336.e5
- This study highlights a new mechanotransduction pathway responsible for actomyosin ring formation through tension-dependent MyoVI recruitment in the neighbours.
22. Kocgozlu L, Saw TB, Le AP, Yow I, Shagirov M, Wong E, Mege RM, Lim CT, Toyama Y, Ladoux B: **Epithelial cell packing induces distinct modes of cell extrusions.** *Curr Biol* 2016, **26**:2942-2950.
  23. Le AP, Rupprecht JF, Mege RM, Toyama Y, Lim CT, Ladoux B: **Adhesion-mediated heterogeneous actin organization governs apoptotic cell extrusion.** *Nat Commun* 2021, **12**:397
- This study highlights the plasticity of extrusion which combines basal protrusions and incomplete actomyosin ring. The two processes can compensate each other and their relative contribution is dictated by cell-cell adhesion and substrate properties.
24. Grieve AG, Rabouille C: **Extracellular cleavage of E-cadherin promotes epithelial cell extrusion.** *J Cell Sci* 2014, **127**:3331-3346.
  25. Teng X, Qin L, Le Borgne R, Toyama Y: **Remodeling of adhesion and modulation of mechanical tensile forces during apoptosis in Drosophila epithelium.** *Development* 2017, **144**:95-105.
  26. Thomas M, Ladoux B, Toyama Y: **Desmosomal junctions govern tissue integrity and actomyosin contractility in apoptotic cell extrusion.** *Curr Biol* 2020, **30**:682-690.e5
- This study describes for the first time the dynamics of DJs and their maintenance throughout cell extrusion as well as their role for cohesion maintenance and extrusion regulation.
27. Michel M, Dahmann C: **Tissue mechanical properties modulate cell extrusion in the Drosophila abdominal epidermis.** *Development* 2020, **147**.
  28. Hoshika S, Sun X, Kuranaga E, Umetsu D: **Reduction of endocytic activity accelerates cell elimination during tissue remodeling of the Drosophila epidermal epithelium.** *Development* 2020, **147**.

29. Teo JL, Tomatis VM, Coburn L, Lagendijk AK, Schouwenaar IM, Budnar S, Hall TE, Verma S, McLachlan RW, Hogan BM *et al.*: **Src kinases relax adherens junctions between the neighbors of apoptotic cells to permit apical extrusion.** *Mol Biol Cell* 2020, **31**:2557-2569

This study suggests that active relaxation of tension in the junctions orthogonal to the extruding cells is required for stress dissipation and extrusion.

30. Teo JL, Gomez GA, Weeratunga S, Davies EM, Noordstra I, Budnar S, Katsuno-Kambe H, McGrath MJ, Verma S, Tomatis V *et al.*: **Caveolae control contractile tension for epithelia to eliminate tumor cells.** *Dev Cell* 2020, **54**:75-91.e7.

31. Takeuchi Y, Narumi R, Akiyama R, Vitiello E, Shirai T, Tanimura N, Kuromiya K, Ishikawa S, Kajita M, Tada M *et al.*: **Calcium wave promotes cell extrusion.** *Curr Biol* 2020

This study highlights unexpected long range waves of calcium propagating from oncogenic and apoptotic cells. These waves trigger collective migration toward the extruding cell and promote cell extrusion.

32. Aikin TJ, Peterson AF, Pokrass MJ, Clark HR, Regot S: **MAPK activity dynamics regulate non-cell autonomous effects of oncogene expression.** *eLife* 2020, **9**

This study characterises long range ERK activation waves in vicinity of groups of oncogenic cells and apoptotic cells. These waves also trigger collective migration toward the oncogenic/apoptotic cells and promote their expulsion.

33. Wagstaff L, Goschorska M, Kozyrsk K, Duclos G, Kucinski I, Chessel A, Hampton-O'Neil L, Bradshaw CR, Allen GE, Rawlins EL *et al.*: **Mechanical cell competition kills cells via induction of lethal p53 levels.** *Nat Commun* 2016, **7**:11373.

34. Bove A, Gradeci D, Fujita Y, Banerjee S, Charras G, Lowe AR: **Local cellular neighborhood controls proliferation in cell competition.** *Mol Biol Cell* 2017, **28**:3215-3228.

35. Ogawa M, Kawarazaki Y, Fujita Y, Naguro I, Ichijo H: **FGF21 induced by the ASK1-p38 pathway promotes mechanical cell competition by attracting cells.** *Curr Biol* 2021, **31**:1048-1057.e5.

36. Bastounis EE, Serrano-Alcalde F, Radhakrishnan P, Engstrom P, Gomez-Benito MJ, Oswald MS, Yeh YT, Smith JG, Welch MD, Garcia-Aznar JM *et al.*: **Mechanical competition triggered by innate immune signaling drives the collective extrusion of**

**bacterially infected epithelial cells.** *Dev Cell* 2021, **56**:443-460.e11.

37. Gagliardi PA, Dobrzyński M, Jacques M-A, Dessauges C, Ender P, Blum Y, Hughes RM, Cohen AR, Pertz O: **Collective ERK/Akt activity waves orchestrate epithelial homeostasis by driving apoptosis-induced survival.** *Dev Cell* 2021, **56**

This study characterises ERK and Akt waves from MCF10A apoptotic cells which inhibit transiently caspases in the neighbours and buffer rate of elimination in the tissue.

38. Valon L, Davidović A, Levillayer F, Villars A, Chouly M, Cerqueira-Campos F, Levayer R: **Robustness of epithelial sealing is an emerging property of local ERK feedback driven by cell elimination.** *Dev Cell* 2021, **56**:1-12

This study characterises local pulses of ERK in the neighbours of extruding cells in the *Drosophila* pupal notum. These pulses are required to scatter cell death in space and time and prevent clusterised eliminations. This mechanism is essential to maintain epithelial sealing.

39. Moreno E, Valon L, Levillayer F, Levayer R: **Competition for space induces cell elimination through compaction-driven ERK downregulation.** *Curr Biol* 2019, **29**:23-34.e8.

40. Bergmann A, Agapite J, McCall K, Steller H: **The *Drosophila* gene *hid* is a direct molecular target of Ras-dependent survival signaling.** *Cell* 1998, **95**:331-341.

41. Kurada P, White K: **Ras promotes cell survival in *Drosophila* by downregulating *hid* expression.** *Cell* 1998, **95**:319-329.

42. Atieh Y, Wyatt T, Zaske AM, Eisenhoffer GT: **Pulsatile contractions promote apoptotic cell extrusion in epithelial tissues.** *Curr Biol* 2021, **31**:1129-1140.e4.

43. Perez-Garijo A, Fuchs Y, Steller H: **Apoptotic cells can induce non-autonomous apoptosis through the TNF pathway.** *eLife* 2013, **2**:e01004.

44. Riegman M, Bradbury MS, Overholtzer M: **Population dynamics in cell death: mechanisms of propagation.** *Trends Cancer* 2019, **5**:558-568.

45. Riegman M, Sagie L, Galed C, Levin T, Steinberg N, Dixon SJ, Wiesner U, Bradbury MS, Niethammer P, Zaritsky A *et al.*: **Ferroptosis occurs through an osmotic mechanism and propagates independently of cell rupture.** *Nat Cell Biol* 2020, **22**:1042-1048.



## **Appendix-3: dispatch**

movements cause our eyes to view different parts of a scene in a short period of time, each potentially containing very different luminance levels [14]. Humans have mechanisms for independently adjusting sensitivity for contrast and luminance [15]. But when instantaneous luminance drops are simulated in lab conditions, human subjects underestimate the contrast of features in a scene [4], highlighting the extreme difficulty of this visual processing challenge. Given the powerful genetic and electrophysiological tools available in the fly visual system, future studies could use the fly as a model for understanding how the brain uses luminance and contrast signals synergistically to improve the robustness of visual behaviours in naturalistic scenarios.

#### REFERENCES

- Barlow, H.B. (1961). The coding of sensory messages. In *Current Problems in Animal Behavior*, W.H. Thorpe, and O.L. Zangwill, eds. (Cambridge: Cambridge University Press), pp. 331–360.
- Ketkar, M.D., Sporar, K., Gür, B., Ramos-Traslosheros, G., Seifert, M., and Silies, M. (2020). Luminance information is required for the accurate estimation of contrast in rapidly changing visual contexts. *Curr. Biol.* 30, 657–669.
- Normann, R.A., and Werblin, F.S. (1974). Control of retinal sensitivity. I. Light and dark adaptation of vertebrate rods and cones. *J. Gen. Physiol.* 63, 37–61.
- Kilpeläinen, M., Nurminen, L., and Donner, K. (2011). Effects of mean luminance changes on human contrast perception: contrast dependence, time-course and spatial specificity. *PLoS One* 6, e17200.
- Reichardt, W., and Wenking, H. (1969). Optical detection and fixation of objects by fixed flying flies. *Naturwissenschaften* 56, 424–425.
- Laughlin, S.B., and Hardie, R.C. (1978). Common strategies for light adaptation in the peripheral visual systems of fly and dragonfly. *J. Comp. Physiol. A* 128, 319–340.
- Fischbach, K., and Dittrich, A. (1989). The optic lobe of *Drosophila melanogaster*. Part I: A Golgi analysis of wild-type structure. *Cell Tiss. Res.* 258, 441–475.
- Joesch, M., Schnell, B., Raghu, S.V., Reiff, D.F., and Borst, A. (2010). ON and OFF pathways in *Drosophila* motion vision. *Nature* 468, 300–304.
- Sanes, J.R., and Zipursky, S.L. (2010). Design principles of insect and vertebrate visual systems. *Neuron* 66, 15–36.
- Shinomiya, K., Karuppudurai, T., Lin, T.-Y., Lu, Z., Lee, C.-H., and Meinertzhagen, I.A. (2014). Candidate neural substrates for off-edge motion detection in *Drosophila*. *Curr. Biol.* 24, 1062–1070.
- Laughlin, S.B., and Hardie, R.C. (1978). Common strategies for light adaptation in the peripheral visual systems of fly and dragonfly. *J. Comp. Physiol. A* 128, 319–340.
- Silies, M., Gohl, D.M., Fisher, Y.E., Freifeld, L., Clark, D.A., and Clandinin, T.R. (2013). Modular use of peripheral input channels tunes motion-detecting circuitry. *Neuron* 79, 111–127.
- Laughlin, S.B., Howard, J., and Blakeslee, B. (1987). Synaptic limitations to contrast coding in the retina of the blowfly *Calliphora*. *Proc. R. Soc. Lond. B* 231, 437–467.
- Mante, V., Frazor, R.A., Bonin, V., Geisler, W.S., and Carandini, M. (2005). Independence of luminance and contrast in natural scenes and in the early visual system. *Nat. Neurosci.* 8, 1690–1697.
- Thomas, M.M., and Lamb, T.D. (1999). Light adaptation and dark adaptation of human rod photoreceptors measured from the a-wave of the electroretinogram. *J. Physiol.* 518 (Pt 2), 479–496.

## Cell Extrusion: Crowd Pushing and Sticky Neighbours

Alexis Villars<sup>1,2</sup> and Romain Levayer<sup>1,\*</sup>

<sup>1</sup>Institut Pasteur, Department of Developmental and Stem Cell Biology, CNRS UMR 3738, Paris, France

<sup>2</sup>Sorbonne Université, Collège Doctoral, F75005 Paris, France

\*Correspondence: [romain.levayer@pasteur.fr](mailto:romain.levayer@pasteur.fr)

<https://doi.org/10.1016/j.cub.2019.12.033>

Cell extrusion is a highly coordinated process allowing the removal of an epithelial cell from the tissue layer without disrupting its integrity. Two new studies shed new light on the complexity of cell–cell coordination at play during cell extrusion.

Epithelia are composed of tightly connected cells and act as mechanical and chemical barriers. These tissues are also incredibly dynamic during morphogenesis and during homeostasis through rapid cell turnover. Accordingly, epithelia can remove cells either during normal homeostatic processes [1] or in order to eliminate aberrant cells through cell competition [2,3]. Yet, these cell removals do not compromise the barrier function of epithelia as they are driven by

cell extrusion — a succession of remodelling steps leading to cell expulsion while maintaining epithelial sealing [4].

Cell extrusion is a highly coordinated multicellular process involving active contraction of the extruding cell and its neighbours [4–7]. Seminal studies in MDCK cells have outlined the two stages of contraction. A contractile actomyosin ring is first formed in the extruding cell [5]. This pulls on cell neighbours and triggers the formation of a supracellular actomyosin

ring in the neighbouring cells [4,5,8]. The ring slides basally and eventually pushes the cell out of the epithelium apically, while bringing neighbours together [5]. The formation of the actomyosin ring is driven by juxtacrine communication between the extruding cell and its neighbours through sphingosine-1-phosphate (S1P) and the S1P2 receptor [9], leading to microtubule reorganisation and Rho activation [10]. The actomyosin ring also relies on strong mechanical coupling between cells



mediated by E-cadherin adhesion [8,11]. Indeed, when E-cadherin is depleted, sealing and extrusion defects appear [11]. This requirement for E-cadherin in extrusion is counterintuitive, given that adherens junctions eventually need to be disassembled to allow cell detachment [12]. Accordingly, a gradual reduction of E-cadherin levels at the interface between the extruding cell and its neighbours has been observed in several systems [6,13]. How the tissue then maintains mechanical coupling and prevents tearing despite the increased contractility has remained a mystery until now.

In this issue of *Current Biology*, two new studies outline the complex cell–cell coordination at play during cell extrusion [14,15]. In the first study, Thomas *et al.* [14] addressed the question of adhesion maintenance during MDCK cell extrusion and characterised for the first time the behaviour of desmosomal junctions (DJs) in this process. Using UV-induced apoptosis to trigger cell extrusion, they first show that, in contrast to adherens junctions, DJs between the extruding cell and its neighbours are maintained throughout extrusion (Figure 1A–D). Moreover, new DJs are formed at the basal side of neighbouring cells prior to the disassembly of old DJs (Figure 1C). Thus, adhesion between the extruding cell and its neighbours is constantly maintained during extrusion through DJs. DJ remodelling involves constant turnover of DJ components (as assessed by fluorescence recovery after photobleaching), and inhibition of DJ turnover prevents cell extrusion.

To dissect the mechanism of DJ remodelling, the authors then focused on intermediate filaments, which are cytoskeletal components that associate with these junctions. Using a photo-convertible version of keratin-18, they could show that new keratin-18 was recruited in the neighbouring cells near interfaces with the extruding cell. More importantly, the keratin filaments progressively realigned toward the extruding cell and bore higher tension (Figure 1C,D). This suggested that the DJs anchored forces during extrusion and could be involved in cell–cell mechanical coupling. The contractile actomyosin cable is a key component of extrusion in MDCK cells. Interestingly, the cable is in close vicinity to DJs at the beginning of

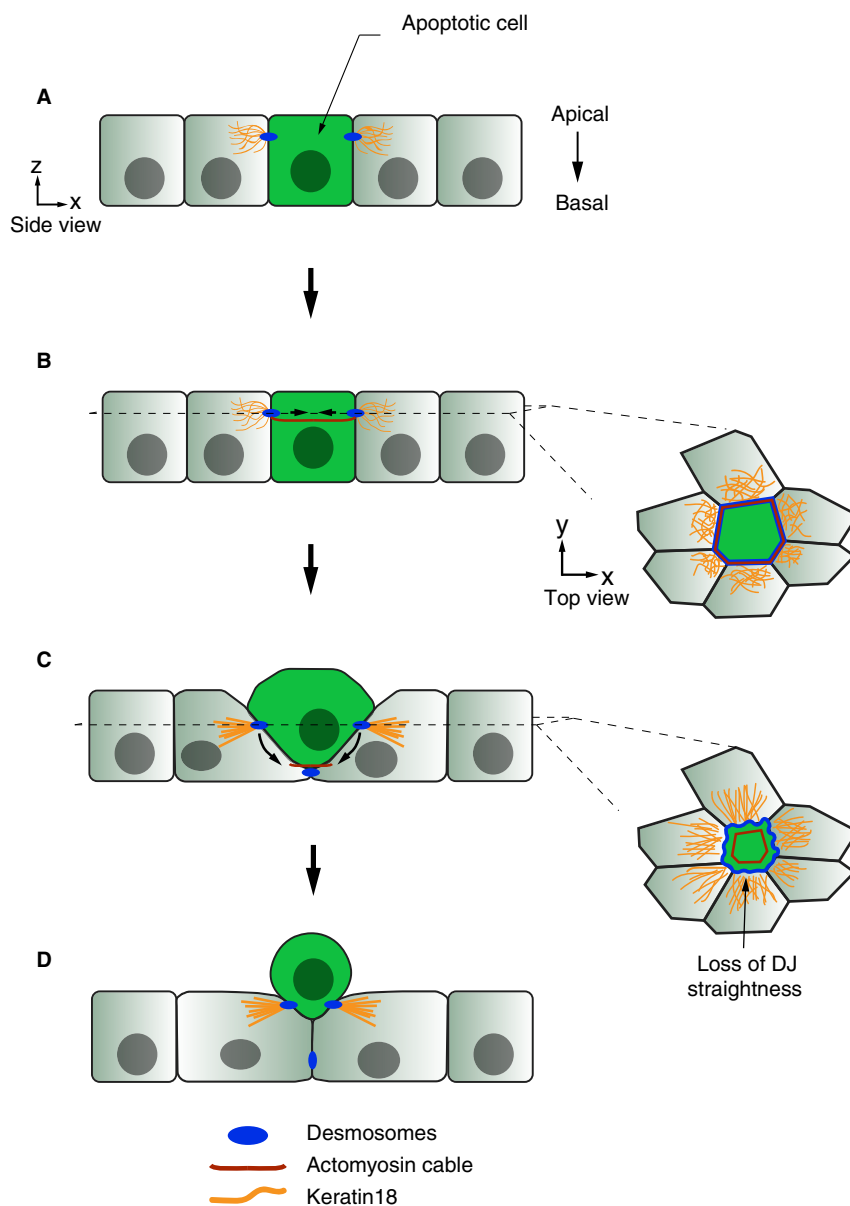


**Figure 1. Dynamics of desmosomal junctions during cell extrusion.**

(A) UV-mediated induction of apoptotic cell extrusion in MDCK cells. (B) Desmosomal junctions (DJs, blue) are dynamic and stay intact during extrusion. An actomyosin ring forms in the vicinity of desmosomes (red). (C) The actomyosin ring detaches from desmosomes and is displaced basally (black arrows). This correlates with loss of DJ straightness (side panel, apical view) and triggers reorientation and accumulation of keratin-18 filaments in neighbours (orange lines). New desmosomes are formed between neighbouring cells beneath the extruding cells. (D) The newly formed desmosomes mature while the cell is being expelled from the layer. The axis shows the direction of view:  $xy$  = top/apical view,  $zx$  = side view. Adapted from [14].

extrusion and becomes detached later (Figure 1B,C). The detachment correlates with a loss of DJ straightness, an indication of tension reduction. These findings suggested that DJs are mechanically coupled to the actomyosin ring and may be required to transmit contractile forces during extrusion.

To test the functional role of DJs during extrusion, the authors either knocked down the DJ component desmoplakin by siRNA or prevented the linkage between keratin and DJs using a dominant-negative form of desmoplakin. Global downregulation of desmoplakin reduced the junctional levels of actin, myosin IIA

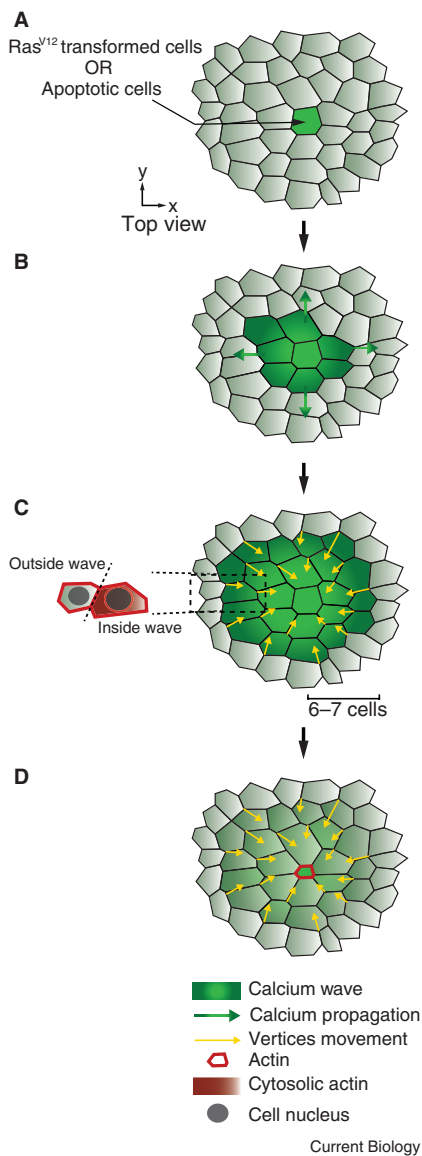


**Figure 2. Calcium wave and collective movements during cell extrusion.**

(A) Cell extrusion is triggered in MDCK cells or zebrafish either by transformed Ras<sup>V12</sup> cells surrounded by wild-type cells (EDAC) or through overexpression of caspase-8. (B) Calcium (Ca<sup>2+</sup>, green) levels increase in the extruding cell and propagate to the neighbours (green arrow), extending between 3 and 16 cells from the extruding cell (C). The wave triggers cytosolic and perinuclear actin relocalisation (in red, side panel). Cells in the wave exhibit polarised movement of their vertices toward the extruding cell (yellow arrows). (D) Coordinated movement of the cell vertices persists after wave termination. Eventually an actomyosin ring is formed around the extruding cell (red), followed by the termination of extrusion. Adapted from [15].

and RhoA as well as tissue tension, and, under this condition, half of the apoptotic cells displayed defective extrusion. Similar

defects were observed upon DJ knockdown either in the extruding cell or in its neighbours. More importantly, these effects could be rescued by RhoA activation, suggesting that the extrusion defects were mostly driven by the downregulation of tension upon DJ knockdown. Last but not least, cell extrusions were also frequently associated with tissue tearing upon DJ knockdown. In conclusion, Thomas *et al.* [14] demonstrated that DJs are essential for extrusion by ensuring mechanical coupling between the extruding cell and its neighbours throughout the process, and that this coupling is required to maintain cell–cell adhesion and generate tension.

In the other study, Takeuchi *et al.* [15] characterised an unexpected contribution of distant cells (between 3 and 16 cells away from the extruding cell) to cell extrusion coordinated by calcium (Ca<sup>2+</sup>) waves originating from the extruding cell. Oncogenic cells (including cells expressing an active form of Ras, Ras<sup>V12</sup>) that are surrounded by wild-type cells are removed from the epithelial layer through apical extrusion (a process called epithelial defence against cancer (EDAC) [2]). By performing live imaging of Ca<sup>2+</sup> after induction of Ras<sup>V12</sup> in a subset of MDCK cells, these authors observed acute bursts of Ca<sup>2+</sup> in oncogenic cells that rapidly propagated to neighbours through a so-called trigger wave mechanism [16] (Figure 2A–C). Inhibition of the inositol-3-phosphate receptor (IP3R), which is responsible for Ca<sup>2+</sup> release from the endoplasmic reticulum, or the Ca<sup>2+</sup> mechanosensitive channel TRPC1 suppressed both the initial Ca<sup>2+</sup> burst in the Ras<sup>V12</sup> cells and the waves, while gap junction inhibition only affected the propagation of these waves. Interestingly, the waves preceded apical extrusion in 70% of the cases, suggesting that they may promote cell extrusion. Accordingly, suppressing the wave via inhibition of IP3R or TRPC1 systematically abolished apical extrusion and also prevented the formation of the actomyosin ring normally associated with cell extrusion.

To investigate the mechanism by which the wave promotes cell extrusion, the authors first looked at neighbouring cell behaviour. Upon Ca<sup>2+</sup> increase, neighbouring cells exhibited polarised movement of their vertices toward the extruding cell (Figure 2C,D). The polarised

movements are concomitant in space and time with a cytosolic and perinuclear accumulation of actin, which is mediated by the formin INF2 (Figure 2C). Inhibition of the Ca<sup>2+</sup> wave through TRPC1 knockdown was sufficient to prevent actin relocalisation and the convergent cell movements. Similarly, INF2 knockdown prevented actin relocalisation and convergent movements and also impaired Ras<sup>V12</sup> cell extrusion. Altogether, these findings suggest that Ca<sup>2+</sup> waves facilitate extrusion by inducing actin reorganisation, which drives a collective convergent movement toward the extruding cell. This movement initiates apical oncogenic cell constriction most likely through pushing forces and precedes actomyosin ring formation. Importantly, the authors suggest that this mechanism may be quite universal. Indeed, similar Ca<sup>2+</sup> waves were reported to precede and be required for Ras<sup>V12</sup> cell extrusion in the zebrafish embryo. Ca<sup>2+</sup> waves were also observed upon apoptosis induction through caspase-8 expression in MDCK cells or following laser-induced apoptosis in zebrafish, with similar actin relocalisation and collective movements. However, in these cases the waves had more of an accessory function and only affected the speed of extrusion.

To conclude, these two studies illustrate in very different ways the complexity of cell–cell coordination during cell extrusion. The work of Thomas *et al.* [14] demonstrates that components from other adhesive complexes, here DJs, are also essential for extrusion. The maintenance of these junctions through late stages of extrusion as well as *de novo* DJ formation are both essential to maintain epithelial sealing and to build up the tension required for cell constriction. This may solve the apparent contradiction between early E-cadherin depletion and the increase in contractility in the extruding cell. So far, most of the studies of extrusion have focused on the role of actomyosin and E-cadherin. This study nicely illustrates the need to explore the role and the dynamics during extrusion of other cytoskeletal and adhesive components (such as extracellular matrix adhesion [17] or tight junctions).

In the other manuscript, Takeuchi *et al.* [15] highlight an unexpected long-range contribution of the surrounding cells to extrusion through collective convergent movements driven by a Ca<sup>2+</sup> wave. The

wave and its contribution to extrusion are conserved from mammalian cells to zebrafish and are observed during both EDAC and apoptotic cell elimination. It is striking that two very different inducers of extrusion (caspases or EDAC) can trigger a similar molecular response. Since the wave is not preceded by any visible morphological changes, the initiator of the first  $\text{Ca}^{2+}$  burst remains unknown. The additional requirement of the stretch-sensitive TRPC1 channel for the first  $\text{Ca}^{2+}$  burst suggests that membrane tension may increase in apoptotic cells or Ras<sup>V12</sup> cells (without obvious changes of cell shape) prior to the initiation of extrusion. The recent development of a live membrane-tension sensor may help to explore this hypothesis [18]. Moreover, it is very difficult at this stage to connect the perinuclear relocalisation of actin with the convergent movement of cells. Interestingly, these waves share many similarities with the recent description of ERK waves observed in the vicinity of apoptotic cells and BRAF-transformed cells [19]. ERK waves also trigger collective movements toward the transformed cells that drive their apical extrusion. Finally, very similar  $\text{Ca}^{2+}$  waves and collective movements have been observed in various models of epithelial wound healing [20]. So it seems that cell extrusion may not be so different from a regular wound healing process.

**REFERENCES**

1. Watson, A.J.M., Duckworth, C.A., Guan, Y.F., and Montrose, M.H. (2009). Mechanisms of epithelial cell shedding in the mammalian intestine and maintenance of barrier function. *Ann. NY Acad. Sci.* 1165, 135–142.
2. Kajita, M., and Fujita, Y. (2015). EDAC: Epithelial defence against cancer–cell competition between normal and transformed epithelial cells in mammals. *J. Biochem.* 158, 15–23.
3. Claveria, C., and Torres, M. (2016). Cell competition: mechanisms and physiological roles. *Annu. Rev. Cell Dev. Biol.* 32, 411–439.
4. Rosenblatt, J., Raff, M.C., and Cramer, L.P. (2001). An epithelial cell destined for apoptosis signals its neighbors to extrude it by an actin- and myosin-dependent mechanism. *Curr. Biol.* 11, 1847–1857.
5. Kuipers, D., Mehonic, A., Kajita, M., Peter, L., Fujita, Y., Duke, T., Charras, G., and Gale, J.E. (2014). Epithelial repair is a two-stage process driven first by dying cells and then by their neighbours. *J. Cell Sci.* 127, 1229–1241.
6. Teng, X., Qin, L., Le Borgne, R., and Toyama, Y. (2017). Remodeling of adhesion and

modulation of mechanical tensile forces during apoptosis in *Drosophila* epithelium. *Development* 144, 95–105.

7. An, Y., Xue, G., Shaobo, Y., Mingxi, D., Zhou, X., Yu, W., Ishibashi, T., Zhang, L., and Yan, Y. (2017). Apical constriction is driven by a pulsatile apical myosin network in delaminating *Drosophila* neuroblasts. *Development* 144, 2153–2164.
8. Michael, M., Meiring, J.C.M., Acharya, B.R., Matthews, D.R., Verma, S., Han, S.P., Hill, M.M., Parton, R.G., Gomez, G.A., and Yap, A.S. (2016). Coronin 1B reorganizes the architecture of F-actin networks for contractility at steady-state and apoptotic adherens junctions. *Dev. Cell* 37, 58–71.
9. Gu, Y., Forostyan, T., Sabbadini, R., and Rosenblatt, J. (2011). Epithelial cell extrusion requires the sphingosine-1-phosphate receptor 2 pathway. *J. Cell Biol.* 193, 667–676.
10. Slattum, G., McGee, K.M., and Rosenblatt, J. (2009). P115 RhoGEF and microtubules decide the direction apoptotic cells extrude from an epithelium. *J. Cell Biol.* 186, 693–702.
11. Lubkov, V., and Bar-Sagi, D. (2014). E-cadherin-mediated cell coupling is required for apoptotic cell extrusion. *Curr. Biol.* 24, 868–874.
12. Grieve, A.G., and Rabouille, C. (2014). Extracellular cleavage of E-cadherin promotes epithelial cell extrusion. *J. Cell Sci.* 127, 3331–3346.
13. Marinari, E., Mehonic, A., Curran, S., Gale, J., Duke, T., and Baum, B. (2012). Live-cell delamination counterbalances epithelial growth to limit tissue overcrowding. *Nature* 484, 542–545.
14. Thomas, M., Ladoux, B., and Toyama, Y. (2020). Desmosomal junctions govern tissue integrity and actomyosin contractility in apoptotic cell extrusion. *Curr. Biol.* 30, 682–690.
15. Takeuchi, Y., Narumi, R., Akiyama, R., Vitiello, E., Shirai, T., Tanimura, N., Kuromiya, K., Ishikawa, S., Kajita, M., Tada, M., *et al.* (2020). Calcium wave promotes cell extrusion. *Curr. Biol.* 30, 670–681.
16. Gelens, L., Anderson, G.A., and Ferrell, J.E., Jr. (2014). Spatial trigger waves: positive feedback gets you a long way. *Mol. Biol. Cell* 25, 3486–3493.
17. Ambrosini, A., Rayer, M., Monier, B., and Suzanne, M. (2019). Mechanical function of the nucleus in force generation during epithelial morphogenesis. *Dev. Cell* 50, 197–211.e195.
18. Colom, A., Derivery, E., Soleimanpour, S., Tomba, C., Molin, M.D., Sakai, N., Gonzalez-Gaitan, M., Matile, S., and Roux, A. (2018). A fluorescent membrane tension probe. *Nat. Chem.* 10, 1118–1125.
19. Aikin, T.J., Peterson, A.F., Pokrass, M.J., Clark, H.R., and Regot, S. (2019). Collective MAPK signaling dynamics coordinates epithelial homeostasis. *bioRxiv*. <https://doi.org/10.1101/826917>.
20. Cordeiro, J.V., and Jacinto, A. (2013). The role of transcription-independent damage signals in the initiation of epithelial wound healing. *Nat. Rev. Mol. Cell Biol.* 14, 249–262.

## Neurobiology: Swimming at the Intersection of Light and Gravity

Sydney Popsuj and Alberto Stolfi\*  
 Georgia Institute of Technology, School of Biological Sciences, Atlanta, GA 30332, USA  
 \*Correspondence: [alberto.stolfi@biosci.gatech.edu](mailto:alberto.stolfi@biosci.gatech.edu)  
<https://doi.org/10.1016/j.cub.2019.12.034>

Many animals use gravity as a spatial reference to help navigate their surroundings, but how they do so is not well understood. A new study reveals that a representative of our closest invertebrate relatives, the tunicate *Ciona*, processes light and gravity cues through a simple neural circuit to decide when and how to swim.

The adaptive value of the nervous system lies in its ability to infer or predict certain aspects of the outside world, in order to plan or accomplish specific tasks [1]. Understanding how external cues and forces are interpreted by the brain to trigger or modify specific animal

behaviors is thus a major goal of the field of neurobiology. Towards this aim, research on neural circuits that sense, perceive, and process cues such as light, sound, or simple chemicals like nutrients or odorants have driven exciting breakthroughs in a wide range of animal



## **General public summary**

Epithelia are tissues covering most of the organs in the human body. Cells are constantly removed from these tissues through cell extrusion: a sequence of remodelling events expelling a cell while bringing its neighbours together to maintain tissue sealing. This process is under the control of death proteases named caspases that cut many proteins. Which cleaved protein leads to cell remodelling is unknown. So far, the study of constriction has focused on the role of contraction proteins such as myosin. However, in the pupal notum epithelium, the initiation of constriction is not associated with myosin changes. Instead, we show that caspases deplete cell structures called microtubules that normally resist compression. Removing microtubules is like removing a beam from a building. It will lead to cell collapse without an increase in cell constriction and is sufficient to bypass the need for caspase. Therefore, microtubule cleavage by caspases is a rate-limiting step for extrusion.

## **Résumé grand public**

Les épithéliums sont des tissus qui recouvrent la plupart des organes du corps humain. Les cellules sont éliminées de ces tissus par extrusion : une séquence de remodelages qui expulse la cellule tout en maintenant l'étanchéité du tissu. Ce processus est contrôlé par des protéases de mort appelées caspases qui coupent de nombreuses protéines. Quelle protéine clivée conduit au remodelage cellulaire ? L'extrusion est normalement dépendante d'une protéine de contraction : la myosine. Cependant, dans l'épithélium du notum pupal de drosophile, l'initiation de l'extrusion a lieu sans changement de myosine. A la place, les caspases déplètent des structures appelées microtubules qui résistent à la compression. Leur élimination est similaire à l'élimination d'une poutre d'un bâtiment. Cela entraîne l'effondrement de la cellule sans augmentation de la contraction et suffit à contourner le besoin de caspase. Ainsi, le clivage des microtubules par les caspases est une étape limitante de l'extrusion.